UNIVERSITY OF STRASBOURG

ECOLE DOCTORALE DES SCIENCES CHIMIQUES

UNIVERSITY OF SOUTHAMPTON

FACULTY OF NATURAL AND ENVIRONMENTAL SCIENCES

CHEMISTRY

DESIGN, SYNTHESIS AND BIOLOGICAL EVALUATION OF NOVEL UNCHARGED BIFUNCTIONAL HYBRID REACTIVATORS FOR ORGANOPHOSPHORUS NERVE AGENT-INHIBITED HUMAN ACETYLCHOLINESTERASE

Julien Alain Albino de Sousa

Thesis for the degree of Doctor of Philosophy

8th December 2015

THESIS SUPERVISORS:

Dr. Rachid Baati	University of Strasbourg
Prof. Richard C. D. Brown	University of Southampton

JURY MEMBERS:

Dr. Agnès Delmas	CBM CNRS	Reviewer
Prof. Bruno Linclau	University of Southampton	Reviewer
Prof. Patrick Pale	University of Strasbourg	Examiner
Dr. Christopher M. Timperley	Dstl	Examiner
Dr. Florian Nachon	IRBA	Examiner
Dr. Emmanuelle Guillot-Combe	DGA	Invited Member

UNIVERSITY OF STRASBOURG

ECOLE DOCTORALE DES SCIENCES CHIMIQUES

UNIVERSITY OF SOUTHAMPTON

FACULTY OF NATURAL AND ENVIRONMENTAL SCIENCES

CHEMISTRY

DESIGN, SYNTHESIS AND BIOLOGICAL EVALUATION OF NOVEL UNCHARGED BIFUNCTIONAL HYBRID REACTIVATORS FOR ORGANOPHOSPHORUS NERVE AGENT-INHIBITED HUMAN ACETYLCHOLINESTERASE

by

Julien Alain Albino de Sousa

Thesis for the degree of Doctor of Philosophy

December 2015

ABSTRACT

Chemistry

Thesis for the degree of Doctor of Philosophy

DESIGN, SYNTHESIS AND BIOLOGICAL EVALUATION OF NOVEL UNCHARGED BIFUNCTIONAL HYBRID REACTIVATORS FOR ORGANOPHOSPHORUS NERVE AGENT-INHIBITED HUMAN ACETYLCHOLINESTERASE

Julien Alain Albino de Sousa

Remediation of both acute and chronic intoxications by organophosphorus nerve agents, both chemical warfare agents and pesticides, continues to be a challenge of paramount importance. These manmade poisons act as covalent and irreversible inhibitors of acetylcholinesterase, a key enzyme mostly located in the nervous system, through phosphylation of its active site. The phosphylated active site residues do not undergo spontaneous hydrolysis. However, hydrolysis can be achieved through the use of strong nucleophiles (also called acetylcholinesterase reactivators) able to enter the buried active site of the protein. Our research is based on the rational design of hybrid structures containing two key elements: a neutral reactivator to restore the enzyme activity, and a peripheral site ligand giving selectivity by targeted binding to a site at the entrance of the enzyme active site gorge. Nine novel reactivators based on acridine, quinoline and original oxoassoanine analogues were synthesised, evaluated and are herein described. Delightfully, most of these hybrids proved to be equally or more potent than the drugs currently in use. Outstandingly, we have discovered the first broad-spectrum reactivator that outperformed all known reactivators (standard and lead compounds) for both chemical warfare agent and pesticide intoxications.

Table of Contents

Declaration of authorship

I, Julien Alain Albino de Sousa

declare that this thesis entitled

Design, synthesis and biological evaluation of novel uncharged bifunctional hybrid reactivators for organophosphorus nerve agent-inhibited human acetylcholinesterase

and the work presented in it are my own and has been generated by me as the result of my own original research. I confirm that:

1. This work was done wholly or mainly while in candidature for a research degree at this University;

2. This thesis has not previously been submitted for a degree or any other qualification at this University or any other institution;

3. This thesis is being presented simultaneously for examination at the University of Strasbourg and the University of Southampton under the terms of a collaborative arrangement;

4. Where I have consulted the published work of others, this is always clearly attributed;

5. Where I have quoted from the work of others, the source is always given. With the exception of such quotations, this thesis is entirely my own work;

6. I have acknowledged all main sources of help;

7. Where the thesis is based on work done by myself jointly with others, I have made clear exactly what was done by others and what I have contributed myself;

8. Parts of this work have been published as:

   European Journal of Organic Chemistry, **2014**, 3468-3474.

   Patents: *WO2015/075082* and *EP15306257*.

Signed: .....

Date: .....

Acknowledgements

I first would like to give a deep thank you to my supervisors Dr. Rachid Baati (Strasbourg) and Prof. Richard Brown (Southampon) for giving me the opportunity to study within their team, supporting me as much as I needed and helping me to build this three years of research as I wanted to. Rachid, thank you for your unconditional trust, as I like to say, “this is just the beginning” … and Richard, thank you for your unwavering support despite your sarcastic sense of humour.

I would like to thank the French Direction Générale de l’Armement (DGA, French Government Defence Procurement and Technology Agency) and the British Defence Science and Technology Laboratory (Dstl) for financial support.

I also would like to thank the members of the jury for accepting to assess this thesis work: Dr. Agnès Delmas (CBM CNRS, Orléans), Prof. Bruno Linclau (University of Southampton), Prof. Patrick Pale (University of Strasbourg), Dr. Christopher M. Timperley (Dstl), Dr. Florian Nachon (IRBA) and Dr. Emmanuelle Guillot-Combe (DGA).

I would like to thank with all my gratitude all the members of each team with whom I have shared the day after day life in the lab: in Strasbourg, Marion, Sasha and Mathias, for helping me so many times when I was “the new guy”, and Emilie and Christine for being part of the survivors; in Southampton, Rob G for sharing with me all these stories, advices and most important the lab 30/3045, Azzam for bringing your exotic happiness, Alex L for sharing this awesome desk space, Lynda for your kind wisdom, Alex P for your jokes, Gareth for supporting the Saints’, Marco for your help out of the lab, and all the other Rob H, Joe, Firas, Victor and Keylla, thank you all for making the lab a great place to work.

I would like to warmly thank all collaborators starting from the biologists Dr. José Dias, Dr. Xavier Brazzolotto and Dr. Guilhem Calas, the structural biologists Dr. Martin Weik, Dr. Gianluca Santoni and Dr. Eugenio De la Mora and the other chemists from Rouen Prof. Pierre-Yves Renard, Dr. Ludovic Jean, Dr. Catherine Gomez, Dr. Julien Renou, Anissa Braiki, Dr. Pierre Warnault and all the other members that I cannot mention due to lack of space.

I also would like to thank the staff from both Universities, Cyril Antheaume, Dr. Patrick Wehrung et Pascale Busine in Strasbourg and Julie Herniman and Dr. Neil Wells in Southampton for services and support.

Special thank to my parents and my sister that have always supported me in my endless education. Thank you for your love and for helping me no matter what. I would not have been able to do it without you.

Last but not least, I would like to thank Irina for making me realise what love can do when it is true. Thank you for always supporting me, especially during the toughest time, and for pretending to understand things that are mostly kept for nerds. Thank you for cheering me up when I needed it and giving me the best gift I could ever expect.

Abbreviations

ACh	Acetylcholine
AChE	Acetylcholinesterase
AcOH	Acetic acid
Ala	Alanine
aq.	Aqueous
BBB	Blood brain barrier
BChE	Butyrylcholinesterase
BINAP	(1,1'-Binaphthalene-2,2'-diyl)bis(diphenylphosphine)
br	Broad
CAS	Catalytic active site
ChE	Cholinesterase(s)
CNS	Central nervous system
CWA	Chemical warfare agent(s)
Da	Dalton(s)
dba	Dibenzylideneacetone
DCE	Dichloroethane
DCC	*N*,*N*'-dicyclohexyl-carbodiimide
DIAD	Di-*iso*-propyl azodicarboxylate
DIBAL-H, DIBAL	Di-*iso*-butyl aluminium hydride
DGA	Direction Générale de l'Armement
DMAP	4-Dimethylaminopyridine
DMF	Dimethylformamide
DMSO	Dimethyl sulfoxide
Dstl	Defence Science and Technology Laboratory

EDC	1-Ethyl-3-(3-dimethyl aminopropyl)-carbodiimide
equiv	Equivalent(s)
ESI^+	Electrospray ionisation (positive ion)
FDA	Food and drug administration
FT	Fourier transform
GABA	Gamma-aminobutyric acid
Gln	Glutamine
Glu	Glutamique acid
Gly	Glycine
*h*AChE	*Human* acetylcholinesterase
His	Histidine
HOBt	Hydroxybenzotriazole
HRMS	High resolution mass spectroscopy
IBS	Institut de biologie structurale
IC_{50}	Half maximal inhibitory concentration
im	Imidazole
IR	Infrared
IRBA	Institut de Recherche Biomédicale des Armées
K_D	Dissociation constant
k_r	Reactivation rate constant
k_{r2}	Second-order rate constant
L	Litre(s)
LRMS	Low resolution mass spectroscopy
m (IR)	medium
m (NMR)	Multiplet
m	Meta

*m*AChE	*Mouse* acetylcholinesterase
mg	Milligram(s)
MHz	Megahertz
MP	Melting point
MW	Molecular weight
OP	Organophosphate(s)
OPCW	Organisation for the Prohibition of Chemical Weapons
OPNA	Organophosphorus nerve agent(s)
PAS	Peripheral aromatic site
Phe	Phenylalanine
PSL	Peripheral site ligand
R*f*	Retardation factor
rt	Room temperature
S_EAr	Electrophilic aromatic substitution
Ser	Serine
sat.	Saturated
T_3P	Propylphosphonic anhydride
TBAF	Tetrabutylammonium fluoride
TBS	*tert*-Butyldimethylsilyl
*Tc*AChE	*Torpedo californica* acetylcholinesterase
TEPP	Tetraethyl pyrophosphate
Tf	Trifluoromethanesulfonyl, Triflate
TFA	Trifluoroacetic acid
THF	Tetrahydrofuran
TLC	Thin-layer chromatography

Trp	Tryptophan
Tyr	Tyrosine
UV	Ultraviolet
viz.	*Videlicet*, namely, that is to say
Val	Valine
WWI (II)	World War I (II)
Δ	Reflux heating
λ	Wavelength(s)
μW	Microwave

Chapter 1: Introduction

1.1 History

1.1.1 Organophosphorus nerve agent as pesticide

Historically, organic chemists had the dangerous habit of tasting new compounds themselves. Hence, it is quite remarkable that the French nobleman and organic chemist Philippe de Clermont did not succumb to tetraethyl pyrophosphate (TEPP, Figure 1.1.1) poisoning when he achieved along with the unrecognized Muscovite Wladimir Petrovich Moschnin the synthesis of the first organophosphate (OP) in 1854.[1–3] As an early pioneer in the field, he failed to recognise the toxicity of this OP as no family record indicated related illness and on the contrary, he even became one of the first generation of organic chemists with a long and prosperous life.[4] It is only eight decades later, in 1932, that a German chemist Willy Lange and his graduate student, Gerda von Krueger, first reported the cholinergic nervous effects of OP by noting a choking sensation and a dimming of vision after exposure to the dimethyl- and diethylphosphorofluoridate.[5]

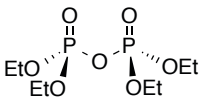

TEPP

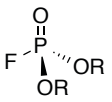

R= Me, dimethyl phosphorofluoridate

R=Et, diethyl phosphorofluoridate

Figure 1.1.1 First organophosphates synthesised.

Inspired by this discovery, the German phytosanitary industry asked Dr. Gerhard Schrader, a chemist at IG Farben to explore these compounds as insecticides.[6] Thus was born with TEPP the first commercialised organophosphorus pesticide in 1944. In the same year the more stable and efficient Parathion was synthesised for the first time. After absorption, Parathion is oxidised into Paraoxon, an extremely toxic form.[7] Therefore, many new OP were developed due to their acute toxicity against insects and animals. Later, their production was even favoured because of the general organochloride insecticide ban in the 1970's.[8,9]

Nowadays, at very low concentration, OPs can be useful products for domestic uses with high therapeutic value in both veterinary and human medicine, for example against lice, etc.

However, most of them are intensively used as pesticides in the plant protection industry and in the farming community (Figure 1.1.2). The use of OPs poses a potentially serious threat to the general public due to their extensive agriculture applications.[10] According to the World Health Organisation (WHO), more than 220,000 fatalities occur annually among a staggering three million acute intoxications estimated (around two million suicidal poisonings and one million serious accidental cases with pesticides) particularly in developing countries.[11–14]

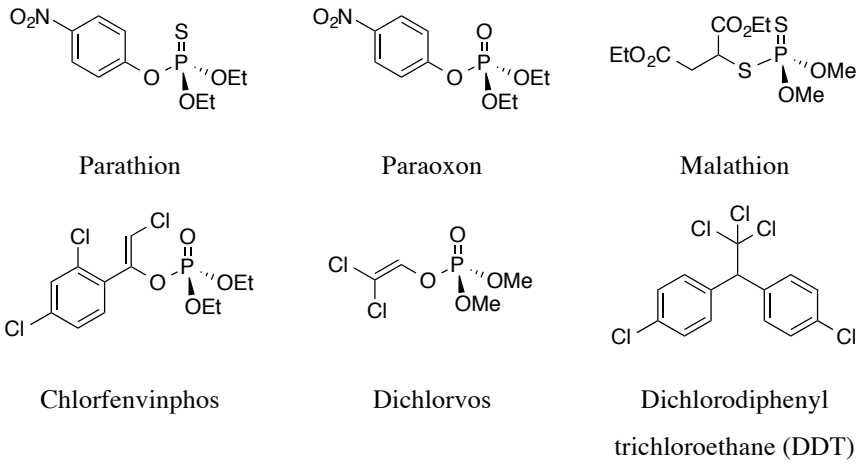

Figure 1.1.2 Examples of pesticides developed during the past century.

Originally investigated for their value as pesticides, the potential use of OP as chemical warfare agents became rapidly apparent.

1.1.2 Chemical warfare agents

While Dr. Gerhard Schrader was developing OPs as pesticides, the Nazi government put him in charge of developing organophosphorus compounds as 'nerve gases'. Therefore, in 1936 he synthesised a highly toxic, colourless and odourless liquid, the (*RS*)-ethyl *N*,*N*-dimethylphosphoramidocyanidate commonly known as Tabun (GA).[15] Three others followed, the (*RS*)-propan-2-yl methylphosphonofluoridate (Sarin, GB)[16] in 1937, the 3,3-dimethylbutan-2-yl methylphosphonofluoridate (Soman, GD)[17] in 1944 and the cyclohexyl methylphoshonofluoridate (Cyclosarin, GF)[18] in 1948. This family of neurotoxic agents was the first generation of organophosphorus nerve agents (OPNAs), also called G-agents (G standing for "German"). They have the property of being liquid with low persistency at rt but volatile, which increases the risk of exposure by inhalation and/or absorption percutaneously. Despite

their acute toxicity, higher than the gas used during WWI (tear gas, mustard gas, phosgene or chlorine for instance),[6] it is interesting to note that there is no confirmation of the use of these weapons in Europe during WWII. This fact is astonishing, since Germany was much more advanced in that area than the Allies, to whom Tabun, Sarin and Soman were completely unknown.[19] The reasons for the non-utilization of these neurotoxic agents by Germany is still a matter of debate: some people argue that Adolph Hitler or German senior officers, themselves victims of chemical warfare agents (CWA) during WWI, would have prohibited the use of chemical weapons. However, the most probable reason was the German fear that the United States and Great Britain possessed equal or similar chemical weapons (which was untrue) and would use them in retaliation.[20]

It was only long after, in 1953, that the allies developed in Great Britain a more perilous OPNA known as VX (ethyl ({2-[bis(propan-2-yl)amino]ethyl}sulfanyl)(methyl)phosphinate) from the insecticide tetram.[21] Subsequent analogues followed in 1963 with Russian-VX (VR, *N*,*N*-diethyl-2-(methyl-(2-methylpropoxy)phosphoryl)sulfanylethanamine) and Chinese-VX (CVX, *O*-*N*-butyl-S-[2-(diethylamino)ethyl]methylphosphonothioate). The V-agents (V standing for "Venomous") exhibit lower volatility and higher persistency in the environment, making them more hazardous than the G-agents because of longer time of exposition (that inscreases the way of penetration) and faster inhibitory potency (Figure 1.1.3).[22]

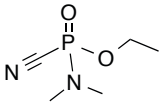
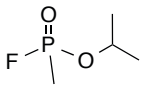
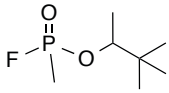
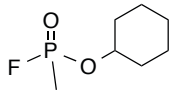

	(±)-Tabun (GA) 1936	**(±)-Sarin (GB) 1937**	**(±)-Soman (GD) 1944**	**(±)-Cyclosarin (GF) 1948**
LD_{50} (mg/kg)	22	28	18	0.35
LCt_{50} (mg/m^3.min)	100-200	70-100	70	n.p.

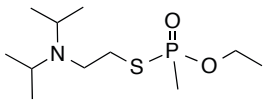
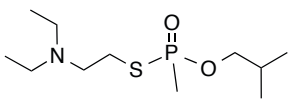
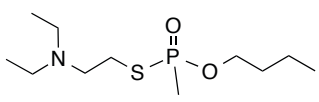

	(±)-VX 1953	**(±)-VR 1963**	**(±)-CVX 1963**
LD_{50} (mg/kg)	0.14	n.p.	n.p.
LCt_{50} (mg/m^3.min)	30-50	10-50	n.p.

Figure 1.1.3 Chemical structures and lethal doses of the most common neurotoxic agents. LD_{50} is the estimated dose required to kill half the tested population of humans after percutaneous intoxication. LCt_{50} is according to time. n.p.: not provided. (Sources: Federation of American Scientists).

Military CWAs are typically classified in several categories, according to their physiological action, the nature of their use and their persistence in the field.[23] They are generally divided in the following classes:

- VESICANTS are substances that cause skin and mucous membrane irritation and inflammation (mainly the lungs). The mustard gases are probably among the most well-known of this group. They usually have only an incapacitating effect, as the victims require one to four months of hospitalisation, for instance, although they can lead to death.
- PULMONARY TOXICANTS are compounds that attack the respiratory tract, causing choking. Phosgene and diphosgene are the most representative of this group.
- CYANIDES are substances that release cyanide ions in the body like cyanogen chloride and hydrogen cyanide.
- INCAPACITATING AGENTS, also called irritating agents, are compounds that produce physiological or mental effects, rendering their victims unable to perform their duties. For instance, the tear gases (like chloroacetophenone, bromoacetone or *o*-chlorobenzylidenemalononitrile, etc.) and the vomiting gases (like chloropicrin) are the most renowned.
- NEUROTOXIC AGENTS, also known as nerve agents or nerve gases, inhibit an enzyme called acetylcholinesterase, causing several deleterious effects, which can lead to death (this part will be fully discussed in section 1.3). As previously mentioned, the main substances belonging to this class are Tabun, Sarin, Soman and VX (Figure 1.1.3).

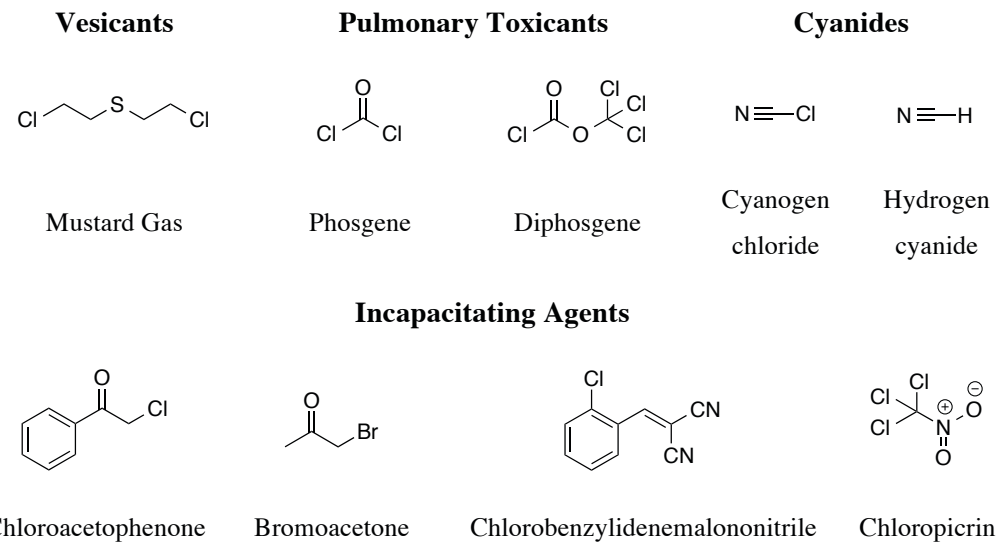

Figure 1.1.4 Most common CWAs that are not acutely neurotoxic.

Despite the fact that the Germans synthesised several thousand of tonnes of G-agents during WWII,[22] the first confirmed use of neurotoxic agents on a large scale came afterwards in the 1980s, during the Iran-Iraq war. The Iraqi regime employed mustard gas and Sarin along with Tabun against Iranian troops in 1983. Five year later, Iraq used CWAs against Kurdish civilians in the village of Birjinni, claiming several thousand lives.[24] VX and Sarin have been used in the terrorist attacks perpetrated by the Aum Shirinkyo sect in the Japanese cities of Matsumoto (1994) and Tokyo (1995).[25–27] The capital subway attack killed 11 people and injured more than 5,000. More recently, the United Nations have confirmed Sarin use during the bombing of Damascus (Syria) on the 21st of August 2013, killing over 1,000 people. Despite all of that, even though the Geneva Protocol prohibited the use of chemical and biological weapons in international armed conflicts since 1925, it is only in 1993 that the intergovernmental Organisation for the Prohibition of Chemical Weapons (OPCW) signed the Chemical Weapons Convention (CWC) (entered into force 1997) prohibiting the use and production of chemical weapons and their precursors, as well as the destruction of all chemical warfare agents.[28] To date, 192 states gave their consent to the treaty. Israel has signed but did not ratify the agreement and four countries have not signed nor accepted the convention (Egypt, North Korea and South Sudan).

In 2010, 60% of the chemical weapons stockpiles were reported destroyed by the Technical Secretariat of the OPCW.[29] Despite all of that, the chemical threat remains. Therefore, the development of effective measures to counteract OPNA poisoning remains a challenging issue to protect and treat both civilian and military populations. Nowadays, studies linked to OPNA are regulated, reported and have to be conducted in specific and qualified laboratories under the control of the government. Thus, in the context of this thesis, all the manipulations (biological assays *in vitro*, *in vivo*, etc), herein described, have been carried out on regulated stocks synthesised by the DGA (Direction Générale de l'Armement) at the Institut de Recherche Biomédicales des Armées (IRBA) recently relocated in Brétigny-sur-Orge (Paris, France) since 2015.

To understand and discuss the toxicity of OPNAs for humans, it essential to describe their biological target, the acetylcholinesterase enzymes.

1.2 OPNA biological targets

1.2.1 The cholinesterases

Since 1940, it has been proven that OPNA target an essential enzyme in mammals, acetylcholinesterase (AChE).[30] AChE [E.C. 3.1.1.7][31] constitutes with butylcholinesterase [BChE, E.C. 3.1.1.8] the group of the cholinesterases (ChEs). As enzymes, they both catalyse the hydrolysis of esters, acetylcholine (ACh) and butyrylcholine, respectively, into acetic acid and choline. The human body has 10 times more BChE than AChE and even if they are different, the two enzymes share 54% of their sequence, their three-dimensional structure and their catalytic mechanism. However, AChE is mainly located in the synapses and neuromuscular junctions, while BChE, synthesised by the liver, is found in large amount in the plasma (5 mg/L)[32] and in numerous tissues such as lung, heart, muscles and intestine.

1.2.2 Butyrylcholinesterase

The physiological function of BChE is not fully understood yet.[33–35] Even if some indications showed its participation in the initial stages of the nervous system development, the enzyme does not appear to be essential to cholinergic transmission.[36] BChE is less selective than AChE hydrolysing efficiently a variety of cholinesters (butyrylcholine, benzoylcholine, succinylcholine, acetylcholine, etc.) due to a difference in the sequences of the enzymes and thus in the size of their active site.[37] BChE is also able to hydrolyse other esters such as aspirin, heroin or cocaine giving it other important biological functions.[38] Some studies have reported BChE as key enzyme during the neurogenesis at the early stage of embryonic development.[39] As BChE is likewise to be rapidly irreversibly inhibited by OPNAs, the concept of “bioscavengers” has been also introduced with the idea of injecting highly purified BChE in the circulatory system to be used as scavenging agent in case of both pre- and post-OP intoxication (*vide infra*, strategy developed in 1.4.1.2).[33,40,41]

1.2.3 Acetylcholinesterase

AChE is a key enzyme of the peripheral and central nervous system (CNS) responsible for regulation of the neurotransmitter acetylcholine (ACh). Located in the cholinergic brain and neuromuscular junctions, the enzyme terminates the synaptic transmission:

The choline acetyltransferase (ChAT) enzyme catalyses first the synthesis of acetylcholine using choline in combination with acetylcoenzyme A (acetyl-CoA) in the axons.[42] ACh is then stored in the synaptic vesicles in about 8,000 to 10,000 molecules of ACh per vesicle in average (Figure 1.2.1).[43] During a nerve impulse, the presynaptic nerve becomes depolarised in response to the action potential (1), opening the membrane to Ca^{2+} ion (2, voltage-gated Ca^{2+} channel), which induces a merging of vesicles with the membrane. Therefore the neurotransmitters diffuse across the synaptic cleft by exocytosis (3). Once released, ACh can bind the postsynaptic cholinergic receptors (4, muscarinic and nicotinic), which controls the entrance of Na^{+} and K^{+} ions into the postsynaptic nerve or the muscular cell (5), among other functions. After this binding, several events occur creating the action potential in the postsynaptic nerve (6) and transmitting the nerve impulse (7). Meanwhile, AChE metabolises ACh into choline and acetic acid (8). Finally, ACh receptor-mediated ion gating finishes and interrupts the transmission of the nerve impulse.[31] Some molecules of ACh can re-enter the presynaptic nerve (9).

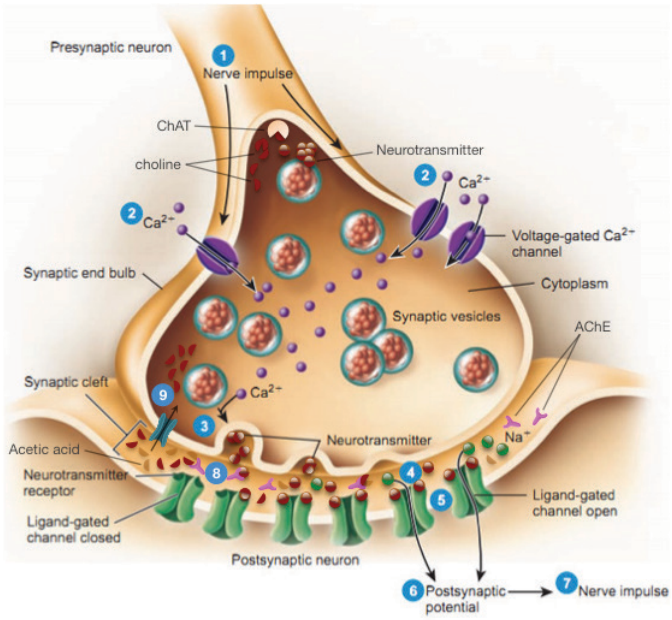

Figure 1.2.1 Synaptic transmission steps.

The neurotransmission process mediated by ACh is a vital process for survival. Its abrupt interruption is lethal, while its gradual reduction is associated to progressive deterioration of the

cognitive and neuromuscular functions, as observed for Alzheimers disease, for instance. Nevertheless, it would be wrong to summarise AChE activity to the cholinergic nervous system only. The enzyme appears to be also involved in other biological processes such as neuritogenesis, cell adhesion, differentiation and amyloid fibre assembly to name a few examples.[44]

1.2.4 Cholinesterase structures

The ChEs are polymorphic enzymes belonging to the α/β-hydrolyse superfamily.[45] They are organised by globular catalytic subunits, each one with a mass of 70-80 kDa. These subunits are usually classified in two categories: the globular and the asymmetric forms. The globular forms are monomers, dimers or tetramers (the latter being formed by monomeric units linked by disulfide bridges). Each monomer is constituted of a β-sheet surrounded by α-helices (Figure 1.2.2) and possesses its own active site. The asymmetric (or elongated) forms are subdivided in three structural subdomains: the catalytic subunit, the collagenous subunit and the noncollagenous subunit. The collagenous subunit is a proteic structure rich in glycine, hydroxyproline and hydroxylysine and comprises generally a triple helix.[46] This subunit ends in three non collagenous proline-rich tail, which interact with four catalytic subunit through proline/tryptophane stacking and disulfide bridge. Despite their structural differences, the catalytic activity is similar.[47]

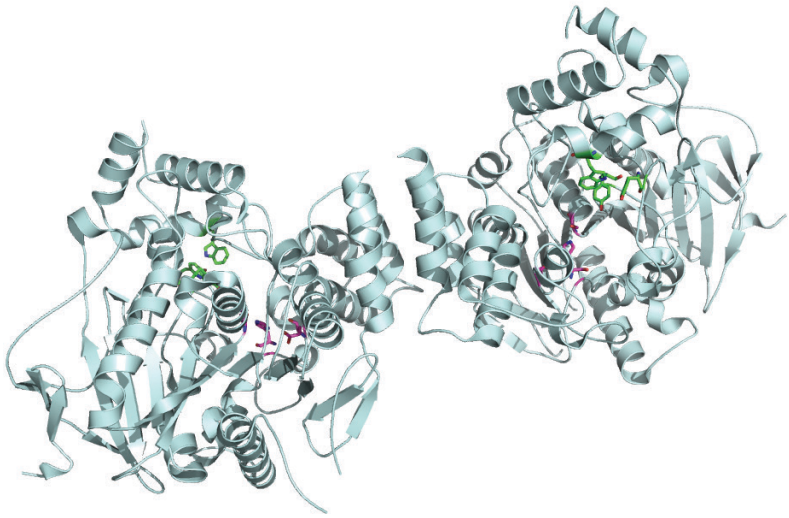

Figure 1.2.2 Dimer structure of AChE (cyan, pdb code 4ey4) showing in each monomer the peripheral anionic site (Tyr72, Tyr124 and Trp286 in green) and the catalytic active site (Ser203, Glu334 and His447 in magenta).

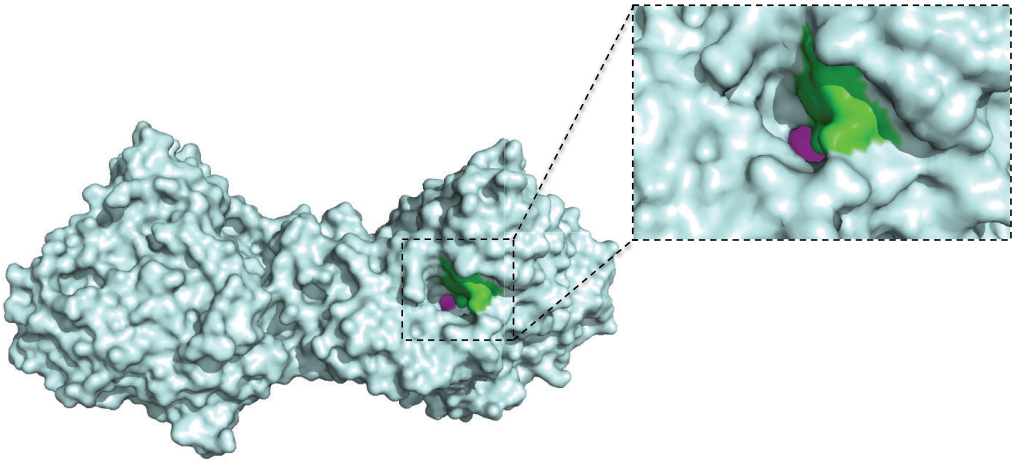

Figure 1.2.3 Dimer structure of AChE (cyan, pdb code 4ey4) showing the surface of the enzyme and the active site gorge on the right monomer (entrance of the gorge in green and the buried catalytic active site in magenta).

The first primary structures determined were the *Torpedo californica* AChE (*Tc*AChE) in 1986,[48] followed by the *human* AChE (*h*AChE).[49] A few years later, the *Tc*AChE three-dimensional crystalline structure was solved by X-Ray diffraction in 1991,[50] followed by *h*AChE in 2000,[51] and BChE in 2003.[52] Meanwhile other crystal structures of AChE were elucidated such as the *mouse* AChE (*m*AChE)[53,54] or the *Drosophila melanogaster* AChE (*Dm*AChE).[55]

Taylor and co-workers[56] determined three subunits of the enzyme that are involved in acetylcholine hydrolysis: (1) the peripheral aromatic site (PAS, in green – Figure 1.2.4), located at the entrance of a deep narrow gorge and the active site (AS, in red), located at the very bottom of the gorge and constituted of (2) the catalytic site (in pink) and (3) the cation-π site (in cyan).

The PAS is mostly comprised by aromatic amino acids such as Tyr72, Tyr124, Trp286 and Tyr341 but also with non-aromatic residue Asp74.[57] Mutagenesis and structural studies have revealed the functional of these aromatic residues at the PAS,[58,59] they guide the substrate towards the enzyme AS by π-stacking or cation-π interactions. Thus, the PAS regulates the catalytic activity by providing a binding locus for an allosteric ligand.[54,60–62] When a molecule of ACh reaches the active site gorge, the trimethylammonium moiety binds first the PAS, predominantly binding to the Asp74. Then, the substrate inserts through the gorge, modifying the position of the residue Trp86 and affecting the relative conformation of the active site.[63] In this way, if the quantity of ACh is too low, the hydrolysis rate increases. On the contrary, if the

concentration is too high, it decreases by inhibition of the excess of substrate at the entrance of the gorge.[54,57,64,65]

The PAS is located at the entrance of a 20 Å deep and 5 Å wide gorge, at the bottom of which is found the active site. The gorge is hydrophobic as mostly constituted of aromatic residues such as tryptophan, tyrosine and phenylalanine, which allow interactions with ammonium moiety.[66]

The active site is constituted of two subunits: the catalytic site (in pink – Figure 1.2.4) where the hydrolysis of ACh itself occurs, while the cation-π site (in cyan – Figure 1.2.4) allows the fixation of the quaternary ammonium ion. The catalytic site is composed of three subunits:[54] the *active pocket* (also called *catalytic triad*), formed by the residues Ser203, Glu334 and His447, is responsible for the hydrolysis of the neurotransmitter ACh (Scheme 1.3.1); the *oxyanion hole*, delineated by the residues Gly121, Gly122 and Ala204, activates the ester by hydrogen bonding and stabilises the carbonyl oxygen of ACh in the transition states for acylation and deacylation;[65,67] and the *acyl pocket*, bordered by the residues Trp236, Phe295 and Phe297, is used to anchor the alkyl group of ACh and stabilises it by van der Waals contacts.

Finally the cation-π site (in cyan Figure 1.2.4), comprised by the residue Trp86, Tyr337 and Phe297, orientates the acyl moiety of ACh towards the catalytic triad by cation-π interactions with the trimethylammonium moiety.[68]

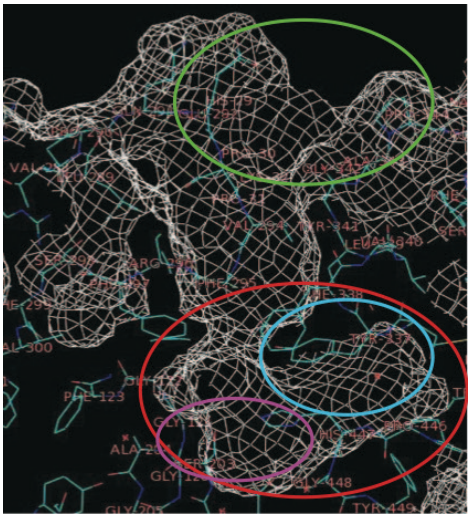

Figure 1.2.4 Representative structure of AChE gorge active site.

The structure of BChE is relatively similar to the AChE. The main difference lies in term of size, as the BChE gorge is about 500 $Å^3$, whereas the AChE is 300 $Å^3$.[35] Besides, the nature of some residues of the PAS and the AS are slightly different. For instance, the small aliphatic residues Ile286 and Val288 replace the large aromatics Phe295 and Phe297 in the acyl pocket. Thus, the pocket is enlarged and is able to accept larger substrates contrary to the AChE acyl pocket, explaining the lower selectivity of the BChE for the substrates.[69] The ligand affinity at the PAS is also weaker as Gln119, Asn68 and Val277 constitute the BChE PAS instead of the aromatic residues of AChE (Tyr72, Tyr124 and Trp286).

1.3 Biological action

1.3.1 Acetylcholine metabolism

AChE is a type B carboxylesterase known as one the nature's fastest enzymes as the protein metabolises the ACh at the astonishing rate close to the diffusion-controlled limit (ca. 2.5 x 10^4 molecules per second and per molecule of AChE).[31,70] The mechanism of the hydrolysis can be described as follows (Scheme 1.3.1):

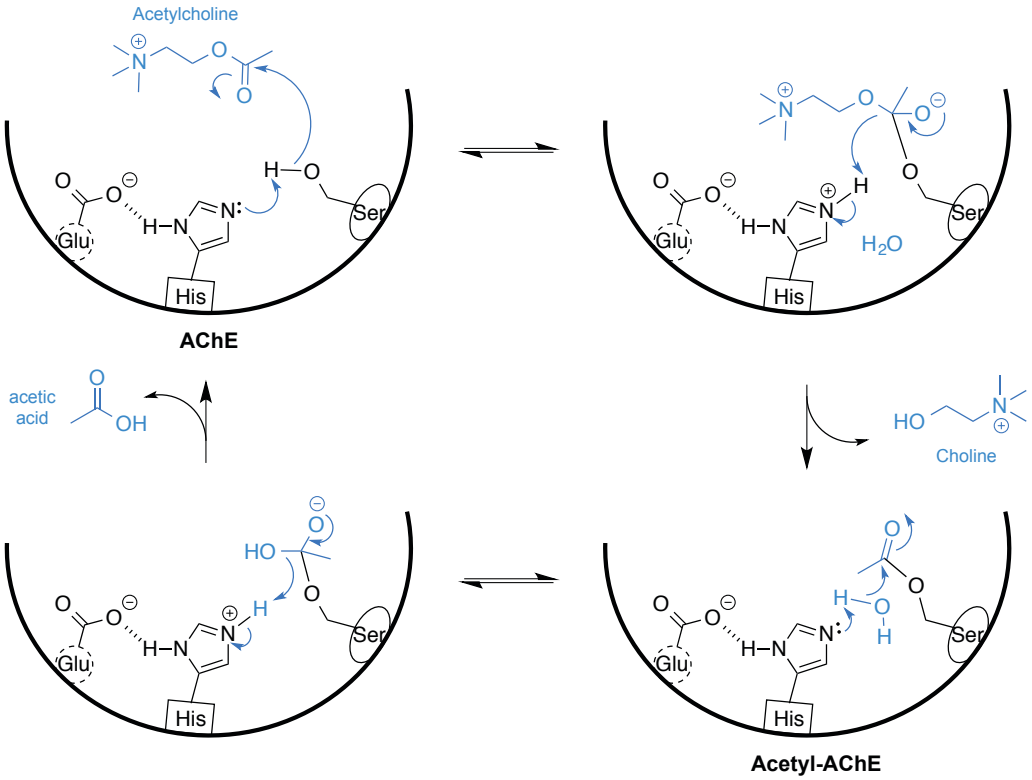

Scheme 1.3.1 Mechanism of ACh hydrolysis by the AChE catalytic triad.

The nucleophilic attack of the substrate carbonyl carbon by the Ser203 hydroxyl generates a transient tetrahedral oxyanion intermediate, which collapses into a short-lived ($t_{1/2}$ = 50 μs) acyl-enzyme (ester) intermediate and a released choline molecule (the tetrahedral intermediate is commonly referred to as a "transition state" in literature).[54] Then, deacylation through hydrolytic attack on the ester carbonyl by a molecule of water, activated by the nearby His447, leads to a second tetrahedral intermediate, which then collapses into a regenerated enzyme and an acetate molecule. It is worthy of note that the rapid rates of substrate association and choline product dissociation contribute to high specific activity and catalytic throughput of AChE. Furthermore, Ser203 is rendered more nucleophilic by the collaboration of the catalytic triad residues Glu334 and His447. Residue Trp86, located at the very base of the active centre gorge, orients the ACh trimethylammonium moiety prior to hydrolysis, whereas the oxyanion hole amide hydrogens from Gly121, Gly122, and Ala204, presumably stabilize the carbonyl oxygen of ACh in the transition states for acylation and deacylation.

1.3.2 OPNA inhibition

OPNA features a phosphorus (V) atom involved in a phosphoryl (P=O) or a thiophosphoryl (P=S) bond. Furthermore, they have an alkoxy group (OR^1), another substituent (R^2) that can be alkyl or also alkoxy and an additional substituent known as "leaving group" (X) more susceptible to be eliminated during hydrolysis or nucleophilic substitution (S_N).

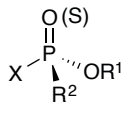

OR^1: alkoxys

R^2: alkoxys, alkyls, aryls, amines, thioalkyls, etc.

X: leaving groups such as F, OR, CN, SR

Figure 1.3.1 General structure of OPNA.

They are really small lipophilic molecules that can easily cross the human natural barriers such as the respiratory, digestive or transcutaneous tracts. It is also noteworthy to mention that before reaching AChE, OPNA may undergo metabolic biotransformation such as oxidative desulfuration, converting a non or low toxic compound into an extremely toxic anticholinesterase agent.[71] In this way phosphorothioates, phosphonothioates or phosphorodithioates are examples of weak AChE inhibitors that can be converted into their

oxidised forms, which are particularly toxic AChE compounds. For instance, after absorption, Parathion is oxidised into Paraoxon, much more toxic for mammals.[7]

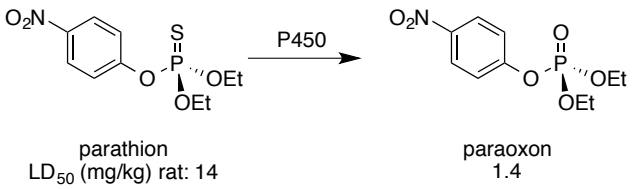

Figure 1.3.2 Metabolic activation of Parathion through reaction of oxidative group transfer by cytochrome P450.

The mechanism of AChE inhibition by OPNA is really similar to the initial step of hydrolysis. After exposure, the OPNA easily crosses the Blood Brain Barrier (BBB)[72] to reach the bottom of the gorge and undergo the nucleophilic attack by the Ser203, generating a bipyrimidal transition state, followed by the formation of a phosphylenzyme after departure of the leaving group.[73] The phosphyl adduct is commonly called the inhibited-enzyme and mimics perfectly the transition step of the hydrolysis initial step. However, His447 cannot activate a molecule of water, in the second step, because it is either forced into a nonproductive conformation (e.g. VX[74] and Tabun[75] conjugates) or shielded from water (e.g. Soman[76] conjugate). Therefore the spontaneous hydrolysis of the phosphylenzyme becomes extremely slow, mostly depending of the R^1 and R^2 groups, as it varies from hours for dimethylphosphoryl conjugates[77] to days for V-agent conjugates.[78]

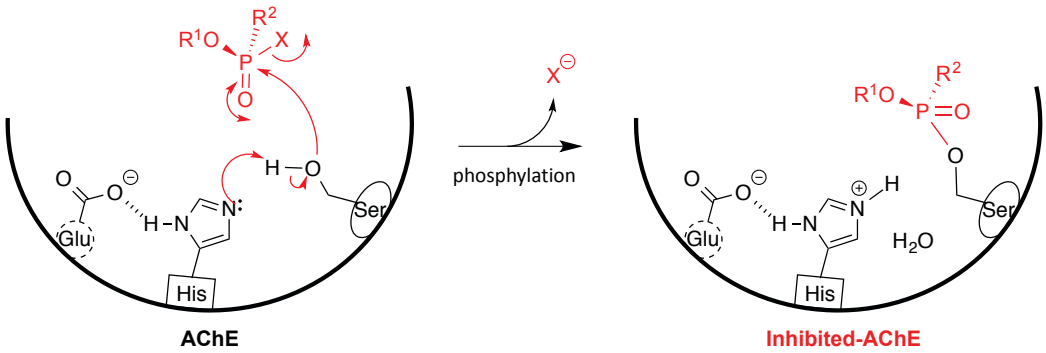

Scheme 1.3.2 OPNA inhibition mechanism of the AChE.

Besides, a time-dependent intramolecular reaction competes with the spontaneous hydrolysis of the conjugate to lead to a more stable form of the complex. The dealkylation of the alkoxy substituent (R^1) yields to a phosphonate adduct or "aged" conjugate.[63,79] Due to the presence of the negative charge on the phosphonic oxyanion, any approach to the phosphorus atom by negatively charged nucleophile is prevented. Consequently, aged phosphyl-AChE conjugates are unreactive towards either hydrolysis or reactivation.

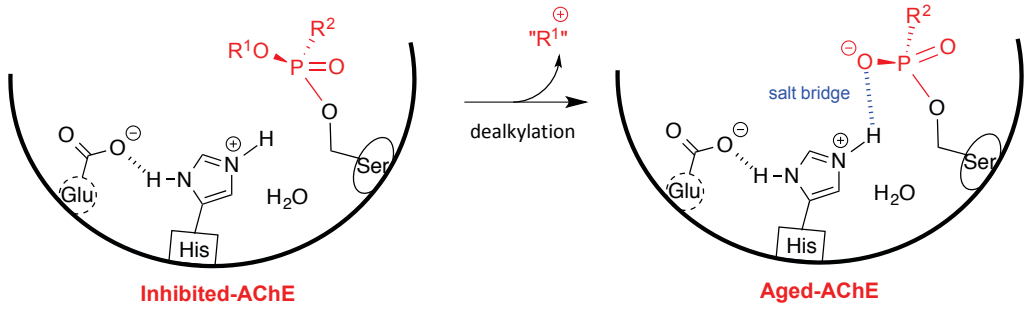

Scheme 1.3.3 Aging phenomenon.

The aging half-time ($t_{1/2}$) is dependent of the substituent group and OPNA stereochemistry. As described Table 1.3.1, the ageing half-time of the Soman conjugate is only about few minutes, whereas it goes up to several hours for Sarin and a few days for Tabun and VX. The formation of a salt bridge between the protonated histidine and the resulting phosphonic oxyanion appears explain increased stability by strongly stabilizing the conjugate complex (Scheme 1.3.3).[75,80]

OPNA	Aging half-life $t_{1/2}$ (h^{-1}) for inhibited-*h*AChE
Tabun (GA)	0.04[81]
Sarin (GB)	0.23[81]
Soman (GD)	9.3[82,83]
VX	0.02[81]
VR	0.04[81]
CVX	0.02[84]

Table 1.3.1 Aging half-life ($t_{1/2}$) for OPNA inhibited-*h*AChE.

Nachon and co-workers proposed an explaination for the difference between the aging rates by comparing VX and Soman-inhibited *Tc*AChE crystalline structures.[76] It was established that the fastest rate was obtained with retention of the catalytic histidine conformation, increasing the stability of the oxyanion formed, viz. with Soman poisoning. Besides, the echothiophate-inhibited *h*BChE crystal structure exposed two plausible mechanisms for the aging reaction.[83] The dealkylation can either occur by cleavage of the C—O or P—O bond after an S_N2-type attack of a nearby molecule of water (Scheme 1.3.4). Mass spectrometry (MALDI-TOF) studies of *h*AChE inhibited with eight different OPNA displayed a classical dealkylation mechanism, whereas only in the case of the isomalathion-inhibited *h*AChE was evidence found for both mechanisms occuring.[85]

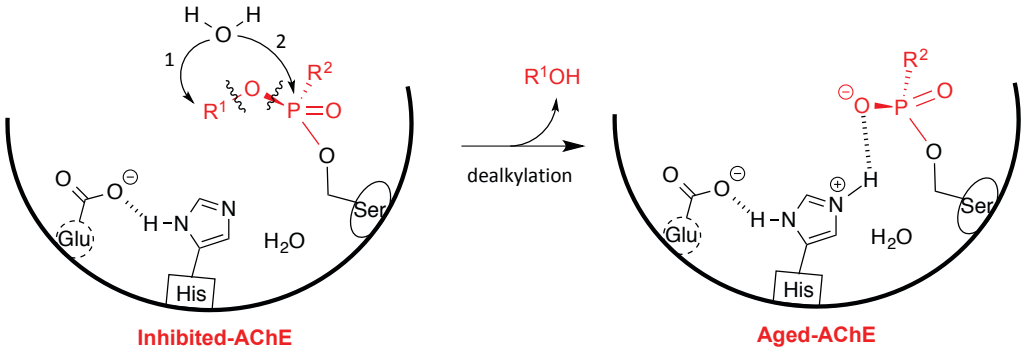

Scheme 1.3.4 Plausible aging reaction mechanisms investigated.

To date, there is no effective treatment against the aged-enzyme. The hypothetic drug should be able to both alkylate the phosphonic oxyanion and selectively hydrolyse the P—O(Ser203) bond to release and reactivate the enzyme. Due to these combined difficulties, over the past decades more emphasis has been placed upon the reactivation of the phosphyl conjugate before aging via hydrolysis of the P—O(Ser203) bond.

1.3.3 OPNA inhibition consequences

OPNAs inhibit AChE, which is responsible for the physiological hydrolysis of ACh. The neurotransmitter is essential in our system as it is involved in cognitive and neuromuscular activity. It is mostly responsible for the transmission of the nerve impulse by binding and activation of cholinergic receptors. Cholinergic receptors can be classified in two types: *nicotinic* receptors are found in autonomic ganglia (ganglionic synapses) and neuromuscular

junctions, and are activated by nicotine, while *muscarinic* receptors are triggered by muscarine and are located on the parasympathetic effector organs and prejunctionally to neuromuscular junctions.[86] After absorption, a small amount of OPNA crosses the BBB and, with a few seconds, halts all cholinesterase activity.[87] This inhibition leads to an accumulation of ACh in the synaptic cleft that generates an overstimulation of the cholinergic receptors before a paralysis of neuromuscular functions (Figure 1.3.3). Depending on the class of OPNA and on the administrated dose, death may occur within a few minutes.

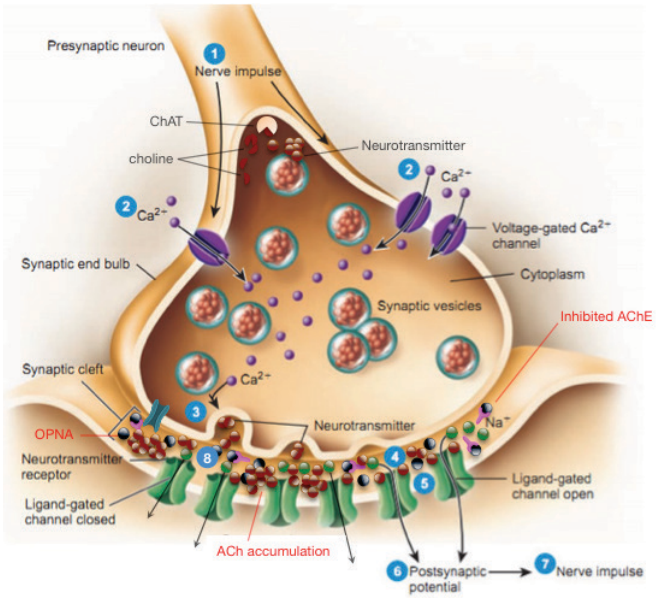

Figure 1.3.3 Synaptic cleft through the inhibition of the AChE.

The “cholinergic” crisis gathers several side effects such as: the *muscarinic syndrome* causes excessive salivation, lacrimation, smooth muscle contraction (miosis and bronchial constriction), increased peristalsis (nausea, vomiting, abdominal pain, diarrhoea), bradycardia and hypotension. The *nicotinic syndrome* that is more related to muscular impairments (asthenia, muscle weakness, uncontrollable movements or paralysis of the respiratory muscles) and heart disorders (tachycardia and enhancement of the blood pressure). Most of the time, these symptoms appear later and express a serious degree of the intoxication. The *central syndrome* is associated to the CNS and produces ataxia, stress, dizziness and headache that can evolve to coma.

Additionally, two long-term syndromes can be observed as the *intermediate syndrome* that occurs 24 to 96 h after the cholinergic crisis but before the *delayed neurotoxic syndrome*.[88] Muscle weakness can affect respiratory muscles, proximal muscles and flexor muscles.[89] These symptoms depend greatly on the OPNA concentration and its kinetics. The *delayed neurotoxic syndrome* or OPIDN (organophosphate induced delay neuropathy) occurs after acute intoxication, mostly related to the inhibition of neuropathytargetesterase (NTE) and causes ataxia and paralysis of the legs that can evolve in spastic hypertonia.[90] The symptoms can appear 2 to 5 weeks after the poisoning and a partial recovery, and sometimes can even be observed after 2 years.[91]

1.4 Medical countermeasures

Since the 1950s finding an effective treatment against OPNA poisoning is a main concern for the international community. Also herein are presented all approaches that have been used to counteract OPNA intoxication over the past decades.

1.4.1 Current pre-treatment of OPNA poisoning

1.4.1.1 Ligand-based strategy

In situations of a potential risk of exposure to OPNAs, pre-treatments can be used to enhance the protection of individuals. The current prophylactic treatment consists in using ligands capable of binding the AChE temporally, masking the active site from OPNA (Figure 1.4.1).

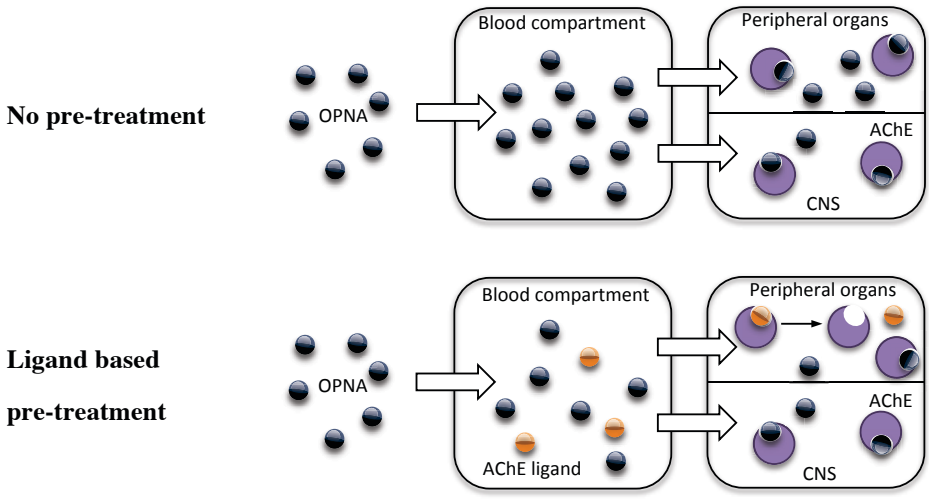

Figure 1.4.1 Ligand-based pre-treatment strategy.

Pyridostigmine (Figure 1.4.2), a carbamate inhibitor, was used during the Persian Gulf War to protect the soldiers before potential exposure to OPNAs.[92] The carbamate binds a certain amount of AChE pseudo-irreversibly by making labile bond with the catalytic site.[93] Then spontaneous decarbamylation releases the AChE. However, with this strategy arise several problems. First, this strategy can be effective only if a sufficient amount of AChE is protected during the exposure time. But, it has been proven that the pseudo-inhibitor is unable to protect the central AChE as the carbamate does not cross the BBB, mainly due to the presence of its permanent charge.[94] Then, this pseudo-inhibition must remain partial in order to preserve some cholinergic activity before the intoxication. Thus, finding the right balance between active/inhibited AChE is a hard challenge in terms of dosage. An ideal occupation rate of 30% of the peripheral AChE was obtained with injection of 30 mg every 8 h. Unfortunately, repeated injection of pyridostigmine appeared to be responsible for several adverse effects (cognitive and muscular) and Gulf War Illness.[92]

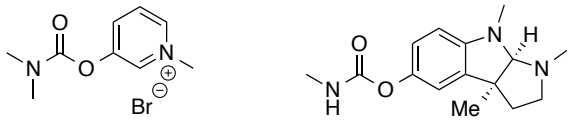

pyridostigmine physostigmine

Figure 1.4.2 Structure of carbamate pseudo-irreversible AChE inhibitors.

Alternatively other covalent and non-covalent reversible AChE inhibitors were investigated as prophylactics for nerve agents. Carbamates that more readily cross the BBB, such as physostigmine, displayed interesting results but exhibited really short life times.[95,96] Candidates with the highest potential were found to be non-covalent AChE inhibitors used to treat neurodegenerative disorders such as Alzheimer disease or Parkinson disease (Figure 1.4.3). For instance, galantamine has been able to counteract the lethality of Soman and Sarin in guinea pigs with no apparent peripheral or central toxicity in the animals, which were also treated with atropine sulphate before poisoning.[97] (–)-Huperzine A, a natural alkaloid used in Chinese traditional medicine, proved to be more potent than pyridostigmine.[98,99] However, at prophylactic doses, it leads to signs of acute toxicity. Administration of a racemic mixture showed lower toxicity and reduced behavioural abnormality against Soman.[100] Analogues of huperzine A have resulted in enhancement of survival of guinea pigs against Soman poisoning and are currently in development.[101]

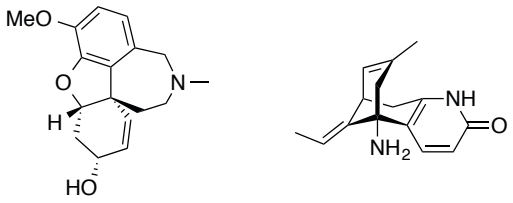

galantamine (–)-huperzine A

Figure 1.4.3 Structure of non-covalent reversible AChE inhibitors.

1.4.1.2 Bioscavenger strategy

An alternative prophylactic treatment is the bioscavenger concept. Bioscavengers consist of biological molecules capable of capturing and deactivating OPNAs in the bloodstream before they reach their physiological target (peripheral and central AChE).[33,102] Three types of bioscavengers have been developed in the last 25 years (Figure 1.4.4).

Stoichiometric bioscavengers are specific molecules that trap OPNAs in a one-to-one ratio before the poison could reach its target. Several studies have been conducted to find a good bioscavengers.[103–105] If exogenous AChE was considered as the candidate of choice, *human* BChE or more precisely recombinant *h*BChE, was rapidly identified due to its better stability in the blood.[106] Really promising results were obtained as this enzyme increases the LD_{50} by 1.5 to 6 times depending on the OPNA used for poisoning.[107] It is important to note that current efforts are underway towards the production of prophylactic doses of *h*BChE, either from plasma,[108] or from transgenic animals (goats, rabbits) or plants.[109,110]

Pseudo-catalytic bioscavengers are stoichiometric bioscavengers combined to a reactivator that helps to regenerate the inhibited scavenger.[41] Kovarik *and coll*. intended to combine *h*BChE with the most efficient mono- and bis-pyridinium aldoximes discovered (*vide infra*, section 1.5.2). However, none of them could efficiently reactivate BChE. Thus they considered a mutant of *m*AChE as bioscavenger.[111,112] Promising results showed that a modification of *m*AChE by mutagenesis combined with a suitable reactivator could potentially be used as pre-treatment for OPNA poisoning.

Catalytic bioscavengers are enzymes, administered in small amounts, that are able to metabolise (hydrolyse) OPNAs. The phosphotriesterases (PTE), also called organophosphorus hydrolases (OPH, EC 8.1.3.1), are probably the best known. They are bacterial enzymes that are extremely effective against insecticides such as Paraoxon.[113,114] There is also an enzyme, human paraoxonase (HPON1), responsible for the circulation of the blood in the human body, which is able to hydrolyse organophosphates.[115] It has been named after its ability to metabolise

Paraoxon. Investigations established its ability to deactivate a broad spectrum of OPNA, albeit only moderately.[116,117] Finally, the organophosphorus acid anhydrolases (OPAA) were investigated. The protein exhibited interesting ability to hydrolyse Soman with mutant *h*BChE. However, more efforts remains for catalytic application of OPAA.[118,119]

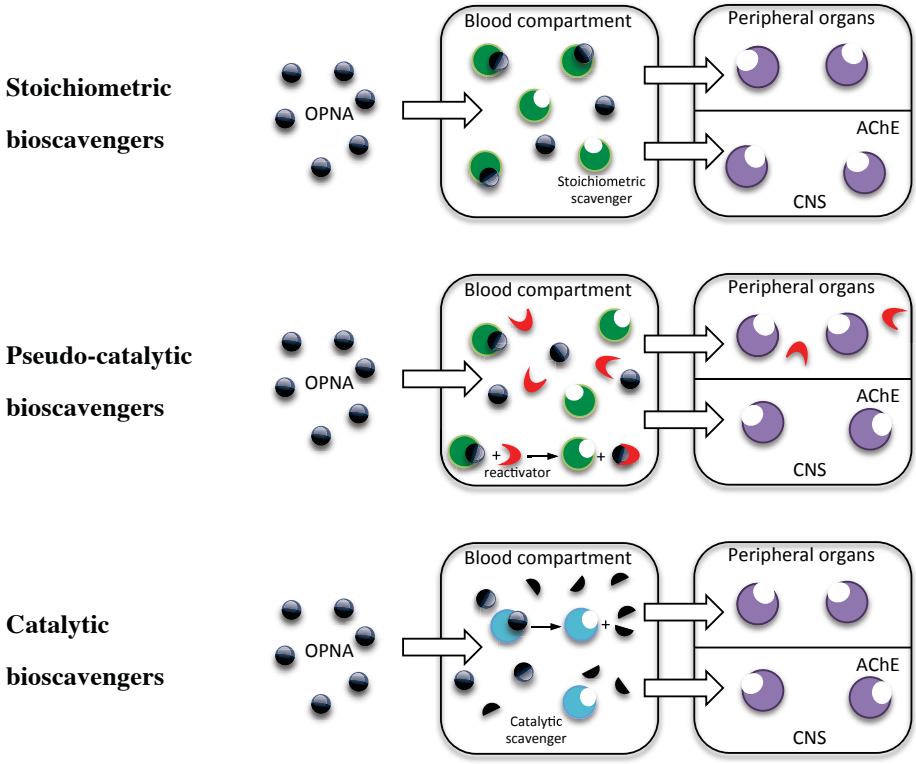

Figure 1.4.4 Bioscavenger pre-treatment strategy.

Despite promising prophylactic pre-treatments against OPNA poisoning, a lack of effective methods remains, and this is without mentioning the ethical issue of producing the desired protein from genetically modified animals. This is why, among the numerous strategies considered to address the problem of OPNA poisoning, we will focus from now on in the development of novel reactivators for ChE, designed to enhance the properties of the current reactivators in the chemostrategy.

1.4.2 Treatment for OPNA poisoning

After exposure to OPNA and depending on the mode of intoxication, a sub-lethal poisoning may be cured by a non-pharmaceutical treatment consisting of providing oxygen supply to the victims. However, this treatment poses major logistical problems in case of mass influx of victims.[120] For instance, on the battlefield, 100 injured soldiers would need 120,000 L of oxygen for 2 h of ventilation, viz. 200 compressed gas bottles and 100 ventilators. Furthermore, in a battle situation, removal of victims of OPNA to appropriate decontamination areas may be a very hard task to accomplish.

In this case, a pharmacological treatment has been developed. This chemostrategy aims to both reduce the effect of ACh excess and reactivate the inhibited AChE. It involves an anticholinergic drug (usually atropine) combined with an anticonvulsant drug (diazepam or derivatives) and a reactivating agent such as an oxime. Using auto-injector syringes, the victim or a colleague can rapidly administer the antidote after the first signs of contamination.[121]

Atropine is a muscarinic antagonist (competing with ACh) that helps against nausea, vomiting symptoms, bronchial hypersecretion and bronchospasm.[122] However, it exhibits limited effects in the CNS and poor efficiency to counteract the nicotinic hyperstimulation effects, viz. it does prevent AChE inhibition and antagonises only the ACh accumulation. Diazepam (or commercially named Valium®) is a benzodiazepine that helps patients suffering from convulsions by modulating the GABA/glutamate receptors, albeit without any curative effect.[123] It also exhibits interesting anxiolytic properties to treat behavioural disorders (central syndromes). A combination of both atropine and diazepam is more effective than a treatment using only atropine or an oxime reactivator.[121,124] The reactivating agent aims to release the phosphoryl group from the inhibited AChE by attacking the phosphorylated Ser203 of the catalytic site. A powerful nucleophile such as an oxime is currently used and will be developed in the following part (*vide supra*, section 1.5.3).

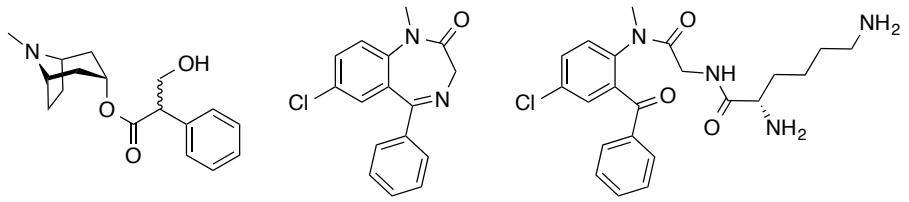

atropine diazepam avizafone

Figure 1.4.5 Structure of atropine, diazepam and its prodrug avizafone.

In France, atropine, avizafone (water-soluble prodrug of diazepam, Figure 1.4.5) and a methanesulfonate salt of 2-pralidoxime (2-pyridinium aldoxime or 2-PAM, Figure 1.5.2) are combined in a subdivided reusable auto-injector (Ineurope®) syringes designed by the Armies Health Service and made by the Central Armed Forces Pharmacy.[125] The drugs are administrated intramuscularly.

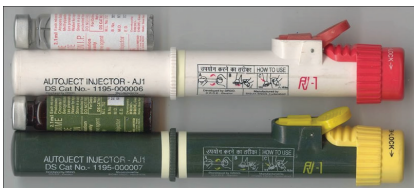

Figure 1.4.6 Example of subdivided reusable auto-injector for OPNA poisoning.

Four different salts of 2-PAM are currently on the market: (1) chloride, used worldwide but mostly employed by the USA; (2) mesylate by France and the UK; (3) methylsulfate and (4) iodide in Australia, India and Japan.[126]

1.5 Reactivating agents

Displacement of the phosphoryl group from the catalytic site Ser203 must be achieved to recover a cholinergic activity and counteract the effect of OPNA poisoning. In this way, powerful nucleophiles, also known as reactivators and mostly oxime-based, have been designed to attack the phosphorus atom and release the reactivated enzyme.

1.5.1 Mechanism of reactivation

The mechanism of action for oxime reactivation of poisoned enzyme has been broadly studied over the past 6 decades (Scheme 1.5.1).[127,128] Once reaching the target, the oximate (Ox, oxime under its physiological pH form) attacks the phosphorus atom of the inhibited enzyme (EP) to form a reactivator/phosphyl-AChE complex (EPOx). This intermediate collapses into a phosphyloxime (POx) and the release of a reactivated enzyme (E).

The reactivation rate constant k_r represents the displacement velocity of the phosphylated residue from the catalytic site by the reactivator, whereas the approximate dissociation constant of the reactivator/phosphyl-AChE complex K_D characterises the affinity of the reactivator towards the enzyme (the lower, the better the affinity is).

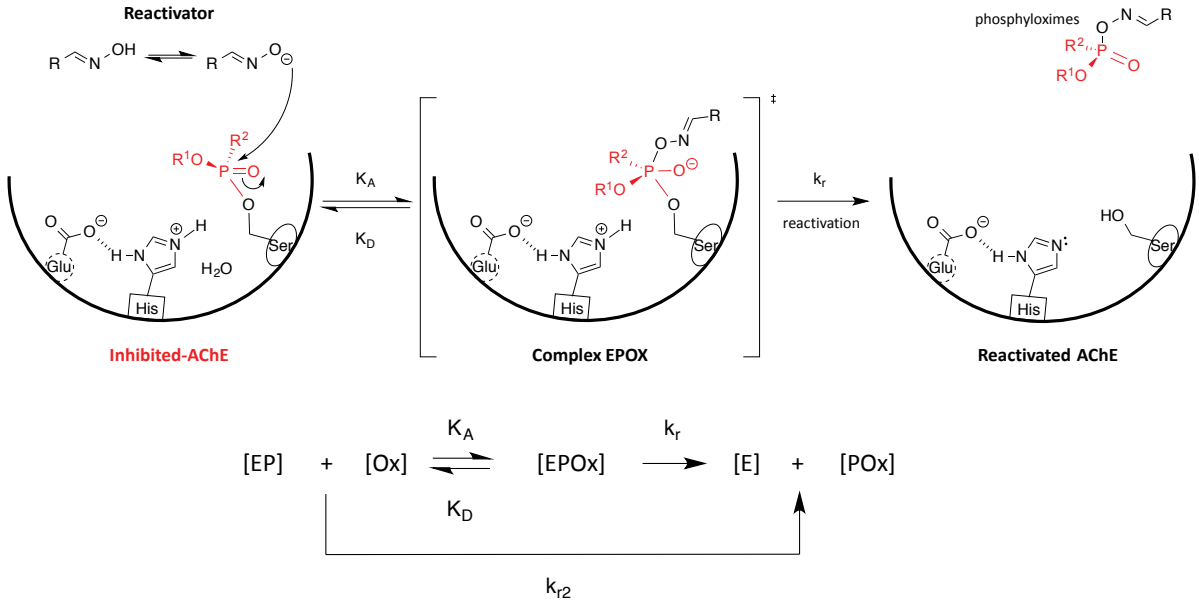

Scheme 1.5.1 Reactivation mechanism and associated kinetic equation.

The reaction order is considered to be 1 for complete reactivation, viz. while the concentration of inhibited enzyme is neglected compared to the concentration of oxime: $[EP]_0 << [Ox]$ In this case, the apparent reactivation rate constant k_{obs} has to be taken into account.[129] It represents the reactivation first-order constant for a specific concentration of oxime and for $[Ox] << K_D$, the second-order rate constant k_{r2} is the ratio of the reactivation rate constant k_r and the approximate dissociation constant of the reactivator/phosphyl-AChE complex K_D.

$$k_{obs} = \frac{k_r.[Ox]}{K_D + [Ox]} \qquad k_{r2} = \frac{k_r}{K_D}$$

Figure 1.5.1 First-order reaction equations.

The efficiency of reactivators can be then estimated using k_{r2}. Furthermore, the three constants (k_r, K_D and k_{r2}) define the potential of a reactivator towards the inhibited enzyme, and they can be used to compare different AChE reactivators and will be used further in this thesis. It is important to keep in mind that values reported in the literature might be slightly different from two different laboratories according to the source of AChE, the exact sequence of the protein (as it may be shortened, or contain more or less glycosylation), the mode of preparation of the enzyme or even its purification. For these reasons, all the *in vitro* and *in vivo* assays in the context of this thesis were carried out in the laboratories of Dr. Florian Nachon at the Institut de Recherche Biomédical des Armées (IRBA). Besides, some literature experiments were repeated to be able to compare our results to those previously reported.

1.5.2 Reactivators: the origins

In the early 1950s, Irwin Wilson was the first scientist to report the use of chemical compounds to reactivate *in vitro* tetraethylpyrophosphate-inhibited AChE using hydroxylamine and nicotinehydroxamic acid.[130,131] In the following years, the good AChE affinity of compounds bearing a quaternary ammonium moiety combined with the efficiency of oxime α-nucleophile led to structurally modified ketoxime and aldoxime reactivators.[132,133] In 1955, Wilson and Ginsburg synthesised pralidoxime (2-pyridinium aldoxime or 2-PAM) for the first time in the USA based on the structural similarity with the neurotransmitter ACh.[134] 2-PAM was a million times more effective than hydroxylamine and was used on humans as an antidote against Parathion poisoning in Japan in 1956.[135] It was thought that the presence of a positive charge at the pyridinium ring enhances its affinity towards the enzyme active site. Hence, Hobbiger and Sadler synthesised two bis-pyridinium aldoximes TMB-4 (trimedoxime) and MMB-4 (methoxime) by chemical modification of 2-PAM with an alkyl chain ligand in the late 1950s.[136,137] Trimedoxime exhibited better reactivation efficacy mostly due to a better affinity towards the enzyme (lower K_D). It was shown to be 'effective' against Tabun poisoning and could protect animals against Sarin and VX intoxications.[138] Unfortunately, trimedoxime is also one of the most toxic reactivators (Table 1.5.2).[139,140]

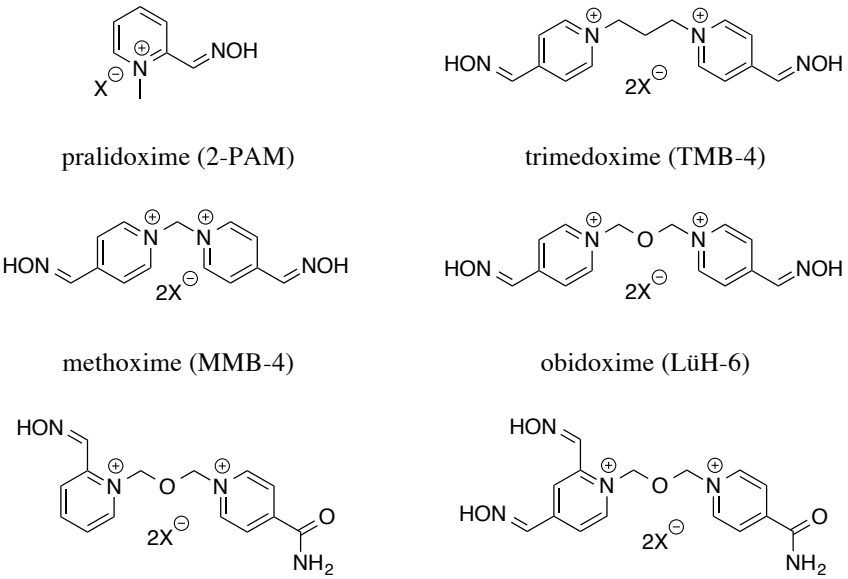

Figure 1.5.2 Structures of common reactivators (counter ion X= halide, mesylate or methylsulfate).

Considering the strong reactivation potency and the structure, analogues of trimedoxime were further synthesised by varying the nature/position of the substituent on the pyridinium rings and/or also the size/nature of the linker. In Germany, in the early 1960s, Obidoxime was synthesised and also named as LüH-6 in honour of Lüttringhaus and Hagedorn.[141] Quite remarkably, obidoxime showed tremendous reactivation potency against Tabun, Sarin and VX but limited efficacy against Soman. This outcome initiated the development of Hi-6[142] (asoxime) in 1966 and HLö-7[143] in 1986. Both reactivators were also named in honour of the researchers that have synthesised them (Hagedorn and Löffler). Hi-6 was quite effective against Soman, Sarin and VX but shows no reactivation at all against Tabun poisoning, whereas HLö was potent against any of the most four perilous OPNAs, including Cyclosarin. Furthermore, research was carried out and more than 1,500 new reactivators were synthesised with various structural advancements and modifications. However, to date, no universal reactivator, capable of reactivating all OPNA effectively, has been found despite tremendous efforts.

1.5.3 Reactivator efficacy

1.5.3.1 Parameters

The potency of each reactivator depends on several parameters such as the affinity of the reactivator towards the enzyme, as well as its reactivity. Herein is described evidence to help understand the potency of these mono- and bis-pyridinium as standard reactivators.

The phosphylated moiety is displaced from the active site by the nucleophilic attack of the oximate anion. Therefore the pK_a of the oxime is very important, as the oxime must remain partially deprotonated in the physiological pH range. Comparison studies have established that the ideal oxime pK_a should be around 8.0 to have a significant amount of deprotonated species.[144]

Crystal structures of enzyme complexed with ligands have showed the importance of the His447 residue orientation in the catalytic site and its influence over the reactivation efficiency (Figure 1.5.3).[145] The strength of the nucleophile can then be enhanced by a rotation of the imidazolium moiety of His447 by creating hydrogen bonding network.

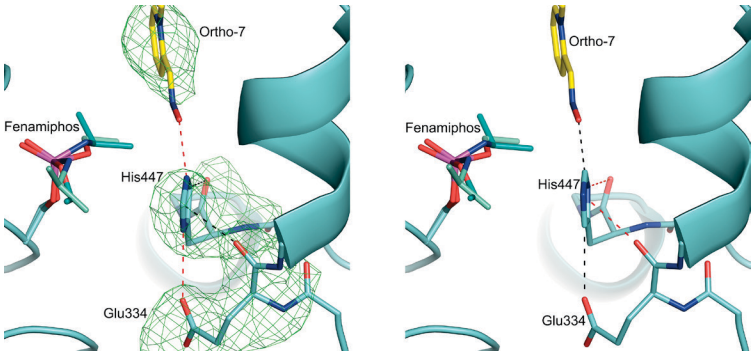

Figure 1.5.3 Oxime-fep-*m*AChE crystal structure showing the formation of hydrogen-bond network between the catalytic site and the oxime.[145]

Cation-π and π-π interactions between the aromatic moieties of the ligand and the PAS residues improve the affinity of the second generation reactivator (bis-pyridinium).[145–147] The amino-pyridinium moiety gets sandwiched by π-π interactions between Trp286 and Tyr124 of the PAS (Figure 1.5.4), while the oxime moiety points towards the catalytic site inside of the gorge and is mostly stabilised by tyrosine residues.[148]

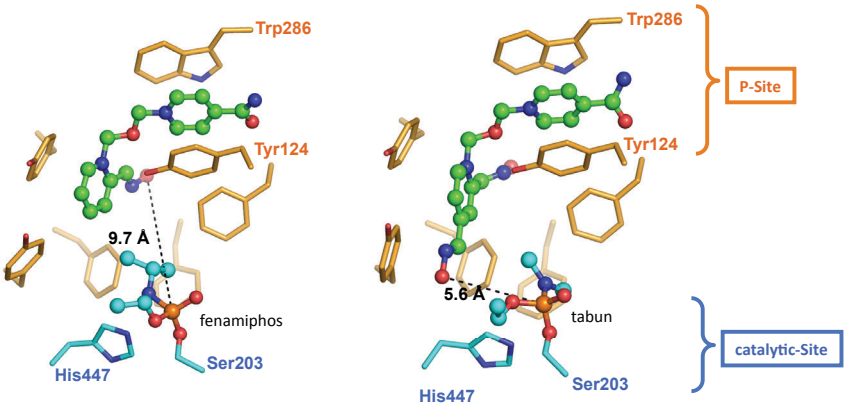

Figure 1.5.4 Crystal structures of Hi-6-fenamiphos-*m*AChE (left) and HLö-7-Tabun-*m*AChE (right) showing interactions between ligand and PAS.

Finally the distance between oxygen and the phosphorus atom is also important for effective reactivation. Improper orientation or larger distance will result in lower reactivation efficiency.

1.5.3.2 Standard reactivator efficacy

To date, the six mono- or bis-pyridinium aldoximes presented in section 1.5.2 are still considered as the most potent *in vitro* and *in vivo* candidates and are used for standardisation and comparison. Here are presented the values of their reactivation constants (K_D, k_r and k_{r2}) collected by Worek and co-workers in the past decades (Table 1.5.1).[128,149]

The *in vitro* results showed 2-PAM to be the less potent drug for OPNA poisoning. Trimedoxime is remarkably the most 'efficient' reactivator for Tabun intoxication but it is also the most toxic.[139,140] Its LD_{50} is 3, 4 and 8 times lower than the ones of obidoxime, 2-PAM and Hi-6, respectively (*vide infra*, section 1.5.4.1). Obidoxime is quite effective against Sarin and VX poisoning and moderately effective against Tabun intoxication. Hi-6 efficiently reactivates most CWA except Tabun against which it shows no activity at all. Finally HLö-7 can be considered as a potential broad spectrum reactivator due to its ability to be effective against most poisoning and even, albeit moderately effective, against Tabun intoxication. Nevertheless, Tabun remains one of the most difficult OPNAs to reactivate due to weak electrophilicity and steric hindrance of the phosphoamidyl-AChE adduct.[150] As discussed in section 1.5.3.1 the enhancement of the affinity of the reactivator towards the inhibited active site enzyme results in better reactivation potency as observed for Hi-6 and HLö-7.

Reactivator	OPNA	K_D (μM)	k_r (min^{-1})	k_{r2} ($mM^{-1}min^{-1}$)
Tabun	2-PAM	706	0.01	0.01
	Trimedoxime	111	0.1	0.9
	Methoxime	1252	0.011	0.008
	Obidoxime	203	0.046	0.23
	Hi-6	n.o.	n.o.	n.o.
	HLö-7	106.5	0.02	0.19
Sarin	2-PAM	27.6	0.25	9.1
	Trimedoxime	n.d.	n.d.	n.d.
	Methoxime	78.4	0.18	2.3
	Obidoxime	31.3	0.937	29.9
	Hi-6	50.1	0.677	13.51
	HLö-7	24.2	0.849	35.1
Cyclosarin	2-PAM	3159	0.182	0.06
	Trimedoxime	343	0.21	0.62
	Methoxime	370.6	0.85	2.29
	Obidoxime	582	0.39	0.68
	Hi-6	123	2.75	22.41
	HLö-7	17.9	1.663	92.9
VX	2-PAM	28.1	0.215	7.7
	Trimedoxime	n.o.	n.o.	n.o.
	Methoxime	241.9	0.328	1.36
	Obidoxime	27.4	0.893	32.6
	Hi-6	11.5	0.242	21.04
	HLö-7	7.8	0.49	62.8
VR	2-PAM	31	0.1	2.0
	Trimedoxime	n.d.	n.d.	n.d.
	Methoxime	574	4.0	7.0
	Obidoxime	106	0.6	5.9
	Hi-6	9	0.7	77.2
	HLö-7	5	0.8	158.5

Table 1.5.1 Reactivation constants for the standard reactivating agents for OPNA-inhibited *h*AChE. (n.d.: not determined. n.o.: reactivation not observed).

In general, the reactivation results *in vivo* match to the results obtained *in vitro*.[151] Hence, on mice and rats, Hi-6 remains better than 2-PAM and obidoxime for both Sarin and VX poisoning,[152] but also remains ineffective against Tabun intoxication.[153] Interestingly, the effectiveness of HLö-7 drops drastically between *in vitro* and *in vivo* assays, explaining why HLö-7 is not among the drugs currently used and commercialised.

Therefore, it appears that the choice of the perfect candidate for an antidote against OPNA intoxication is not based only on its reactivating efficacy results but is counterbalanced by its toxicity and the risks for the victims depending on the situation. In this context, trimedoxime was completely abandoned, 2-PAM and obidoxime are the only ones on the market (*vide supra*, section 1.4.2). However, very recently, French and British governments found in Hi-6 a better compromise (despite no notable activity against Tabun poisoning) and have asked for a full market approval to further replace 2-PAM in the auto-injector syringes.

1.5.3.3 Pharmacological effects of standard reactivating agents

Interestingly, pharmacological studies showed that oximes also present other therapeutic properties.[154] Survival improvement has been observed on monkeys after being exposed to Tabun and treated with Hi-6 (in combination with atropine and diazepam), even if Hi-6 does not reactivate Tabun-inhibited *h*AChE.[155]

Besides, it was found that if the oxime was administrated before poisoning, a decrease of the intoxication was observed.[156,157] The oximes appeared to have a direct pharmacological effect on the nicotinic receptors located in the ganglions, muscles and CNS by inhibition of pre-synaptic ACh production.

1.5.4 Drawbacks of the standard reactivators

Some standard reactivators, such as 2-PAM and obidoxime, are already commercialised and used by different armies for OPNA intoxication. However, none of them can claim to be broad spectrum reactivator effective against all types of OPNA poisoning. Besides, they are unable to regenerate the aged form of the enzyme and other weaknesses, highlighted herein, reduce their capacity towards the inhibited enzyme.

1.5.4.1 Inhibition and Toxicity

The toxicity of a compound is vital in the evaluation and the development of a potential drug. *In vivo* studies on mice have displayed the LD_{50} of the standard reactivators administrated intramuscularly.[139,140]

Reactivators	LD_{50} (mg kg^{-1})
2-PAM	263.6
trimedoxime	150.5
obidoxime	188.4
Hi-6	671.3

Table 1.5.2 LD_{50} of the standard reactivators on mice after intramuscular administration.

As noted previously (*vide supra*, section 1.5.3.2), trimedoxime cannot be used as antidote as it is the most toxic reactivating agent with a LD_{50} of 150.5 mg kg^{-1}. According to the quantities used, oxime can provoke intoxications with symptoms including convulsions and respiratory failures.[158] Therefore, the toxicity of the reactivator has to be taken into account when defining the optimum dose. Besides, there is always a thin line between affinity and inhibition. Also if the reactivator has a good affinity towards the inhibited enzyme active site, it has to be slightly lower for the free enzyme after release. Otherwise, the oxime becomes a competitive inhibitor.

1.5.4.2 Blood brain barrier problem

The BBB is an impermeable lipoidal membrane, comprised of endothelial cells, that resides between the peripheral and CNS. Due to the presence of tight junctions between the endothelial cells, the BBB prevents entry to bacteria, viruses, proteins and polar molecules.[72,159] However, small lipophilic compounds such as OPNA manage to pass by diffusion and are therefore able to inhibit central AChE. However, hydrophilic oximes based on quaternary ammonium ions, suffered from an inability to cross the BBB due to the presence of their permanent positive charge.[159]

Many *in vivo* reports stated inefficacy of the treatment with the standard drugs mostly due to a lack of activity in the CNS.[160] As evidence, central symptoms or respiratory failure were reported as being the main causes of death after acute intoxication. Thus, several approaches were taken to try to improve the reactivation of central AChE and BBB penetration of the drugs: the first method involved the measurement of the oxime concentration inside of the brain by radioactive tracers, spectrophotometry or HPLC (High Performance Liquid Chromatography).

The second technique relies on the evaluation of the biological effects of the oxime by measuring the activity of inhibited AChE inside the brains of animals after treatment with a reactivator. The third method consists in knowing if the oxime can counteract the biological effects of the intoxication in the CNS by observing any modification in EGG test (electroencephalogram) and in the animal survival rate or by analysing the speed of breath.[159] Therefore, the percentage of penetration for the standard reactivators was determined: the penetration of 2-PAM in the brain has been estimated to be about 10% by *in vivo* rat brain microdialysis technique with HPLC/UV compared to 2-PAM in the plasma.[160] The penetration of obidoxime varies between 3% and 5%, while with Hi-6 it goes up to 18%. Interestingly, when the enzyme is exposed to Soman, the BBB penetration efficacy drops to 9%,[161] which contradicts a recent report that OPNA exposure increases permeabilisation of the BBB allowing a better oxime penetration.[162] It is important to note that reactivator penetration in the CNS can also vary with additional factors, such as dose, as larger administrated amount of oxime results in enhancement of the BBB penetration.[161] Worek and co-workers reported on guinea pigs that Hi-6 and HLö-7 show different levels of partial reactivation of the central enzyme depending on the region of CNS.[163]

1.5.4.3 Recapture phenomenon

During the reactivation process, the oxime attacks the phosphylated enzyme generating the formation a phosphyloxime and the release of the reactivated enzyme. However, the phosphyloxime adduct formed is also a reactive species depending on the OPNA used, which can undergo the reverse reaction with the hydroxyl group of Ser203 (Scheme 1.5.2). Wilson and Ginsburg reported this process known as "recapture phenomenon" in 1955,[134] which creates an equilibrium that decreases the efficacy of the reactivation.

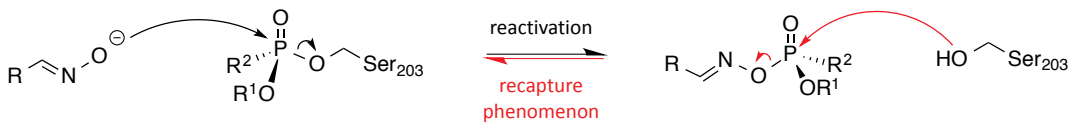

Scheme 1.5.2 Recapture phenomenon.

Subsequently, *in vitro* studies showed that the phosphyloxime adduct could even be more toxic than the poison itself.[164] Thus, their persistence in the active site has to be as short as possible and their affinity towards the native enzyme has to be as low as possible. To reduce this

phenomenon, it has been shown that the phosphyloxime adduct can undergo a rearrangement *in situ* if the reactivator is a pyridinium aldoxime.[165] Also, it is important to mention that the recapture phenomenon is not a major drawback in further *in vivo* investigations due to the overall concentration and low probability of the phosphyloxime re-entering the enzyme gorge.

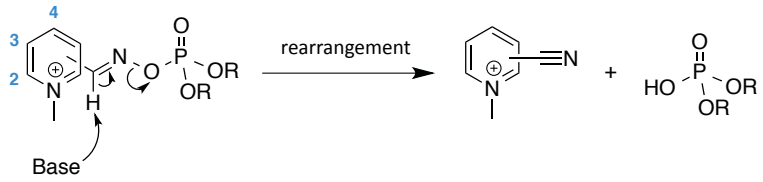

Scheme 1.5.3 Pyridinium phosphyloxime adduct degradation by rearrangement.

The stability of the phosphyloxime adduct depends on the position of the oxime in the pyridinium ring. The degradation (or rearrangement) of the adduct is faster with an oxime in position 2 than in position 3 or 4.[166] The different rates are due to the distance between the nitrogen atom of the pyridinium ring and the phosphyloxime moiety. The shorter, the more acidic the α-proton is and the faster the rearrangement. Thus, reactivators bearing 3- or 4-pyridinium aldoxime moiety have higher risk of recapture phenomenon.[167] Interestingly, AChE reactivation kinetics can be enhanced by adding to the oxime an enzyme capable of hydrolysing the phosphyloxime adduct such as paraoxonase or phosphoesterase.[168–170] This additional protein cleaves the intermediate adduct to regenerate the pyridinium aldoxime.

In response to the main drawbacks observed, substantial efforts have been made over the last decades to design and develop more effective reactivators with less disadvantages and a broader spectrum of application.

1.6 Structural modifications of oxime reactivators

Since the discovery of 2-PAM as a reactivator of poisoned AChE, the search for better reactivating agents leads to various structural modifications considering its reactivation potency, spectrum of activity, hydrophobicity, binding affinity, etc. More than 1500 novel oximes were synthesised and vary from 2-PAM structure by number and position of the oxime moiety, number and types of rings, structure and position of a connecting linker, quaternary or uncharged oximes and/or structure and position of a side chain ligand.[127,171] This part of the thesis describes the most significant advances in the evolution of reactivators, particularly the ones that lead to the discovery of the current standard reactivators, up to the most recent promising hybrid reactivator strategy that will be developed in the following chapters.

1.6.1 Mono-pyridinium aldoxime

Structural modification of mono-pyridinium aldoximes, such as 2-PAM can address the position of the oxime moiety, the nature of the quaternary ammonium substituent (R) and/or the presence/type of substituent R^2 in the aromatic ring (Figure 1.6.1).

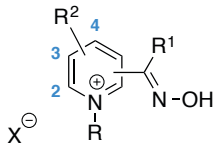

Figure 1.6.1 General structural modifications of mono-pyridinium aldoximes.

1.6.1.1 Influence of the oxime moiety position

The investigation on the influence of the oxime moiety position started in the early 1960s.[172] The molecule bearing the aldoxime function in position 2 (2-PAM) exhibited better reactivation efficacy compared to its isomers 3-PAM and 4-PAM (Table 1.6.1). This difference can be explained by a variation of pK_a of the oxime according to its position in the pyridinium ring (3-PAM compared to 2-PAM and 4-PAM). Additionally, as described in section 1.5.4.3, the position of the oxime moiety can favour the recapture phenomenon and consequent decrease the reactivation efficiency.

Reactivators	Reactivation efficacy (%)
2-PAM	19.54
3-PAM	3.42
4-PAM	9.19

Table 1.6.1 Percentage of reactivation 20 min after treatment ([oxime] = 0.5 mg mL^{-1}).[173]

Analogues of 2-PAM have been synthesised to improve their affinity and ability to cross the BBB. The structural modifications oriented towards the alkyl group (R) linked to the quaternary nitrogen atom, aimed to increase the lipophilicity of the reactivators (Figure 1.6.1).[174,175] Unfortunately, variation of the chain (alkyl, alkene and phenyl derivatives) did not show any improvement. Most of the reactivation efficacies were inferior compared to 2-PAM. Furthermore, replacement of the side chain with heterocyclic systems such as furan, isoxasole or thiophene resulted in reactivators that were no better than the standard oxime.[176] More recently, ether substituents were introduced (alkyloxy and benzyloxy) in order to enhance the affinity with the gorge residues and guide the oxime moiety towards the catalytic site.[177] While the alkyloxy derivatives exhibited lower potency, two benzyloxy analogues showed interesting equipotent reactivation efficacy compared to 2-PAM and obidoxime for VX and DFP (diisopropyl fluorophosphate) inhibited AChE (Table 1.6.2). However, in case of Sarin poisoning, none of them was potent.

Reactivators	VX	DFP
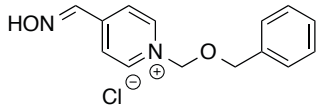	54%	52%
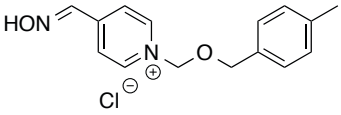	41%	42%
2-PAM	52%	46%
Obidoxime	45%	35%

Table 1.6.2 Percentage of reactivation at 10^{-3} M after 10 min of OPNA-inhibited rat-AChE.

Recently, another promising reactivator has been synthesised based on the same approach.[178] The phenyloxyalkyl analogue exhibits a reactivation potency of 25% *in vivo* (rat) in 30 min

(Figure 1.6.2), whereas the standard reactivators do not (0%) for Sarin surrogate NIMP (nitrophenyl isopropyl methylphosphonate) poisoning. Besides, it is 60-fold more lipophilic than 2-PAM by measurement of the partition-coefficient log P.

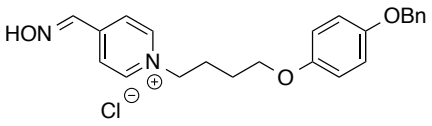

Figure 1.6.2 Phenyloxyalkyl analogue of 4-PAM.

Therefore this type of oxime has a potential as brain-protecting therapeutics but more investigations are required.

1.6.1.2 Influence of functionalisation

Wilson and Ginsburg briefly investigated the functionalization of 2-, 3- and 4-PAM in the late 1950s.[179] They reported the synthesis of different analogues without any further information relating to their reactivation efficiencies (Figure 1.6.3). To date these compounds remain unevaluated.

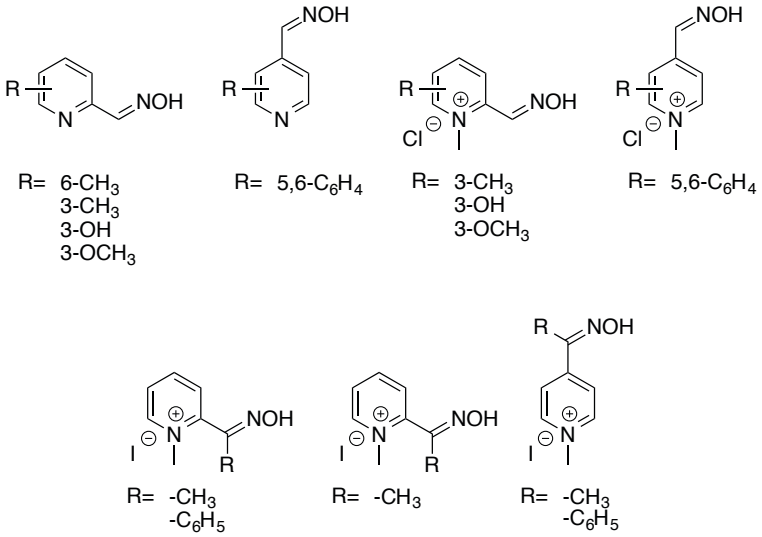

Figure 1.6.3 Structure of 2-, 3- and 4-PAM analogues.

Kuča and co-workers designed, synthesised and evaluated ketoximes analogues of 2-PAM.[180] Unfortunately, the best candidates exhibited very limited potency compared to 2-PAM (Figure 1.6.4). Salvador and co-workers have synthesised similar trifluoromethylketoxime analogues in order to study the influence on the oxime pK_a.[181] The idea is to use a powerful electron withdrawing group in the α-position to enhance the nucleophilic strength of the oxime by increasing the proportion of the oximate at physiological pH. Besides, the presence of fluorine atoms could help to increase its lipophilicity and enhance BBB crossing. However, none of the synthesised compounds was found to be better than 2-PAM.

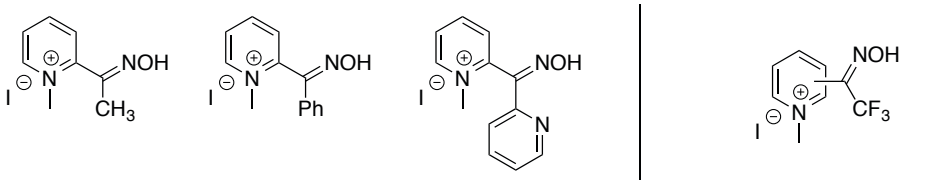

Kuča *and coll.* Salvadore *and coll.*

Figure 1.6.4 Structure of ketoxime analogues.

1.6.1.3 Imidazolium substitution

Imidazolium derivatives attracted interest in the 1980s due to the structural similarity with the pyridinium ring.[182–184] Several tens of compounds were synthesised and evaluated mostly with an oxime function in position 2 and both imidazole nitrogen atoms substituted (alkyl, aryl, unsaturated side chain, etc.) to mimic the pyridinium reactivator. However none of the synthesised compounds exhibited higher potency than 2-PAM. One of the explanations for such low reactivity was the high value of the imidazolium oxime pK_a (~8.5).

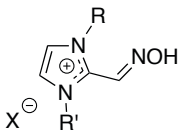

Scheme 1.6.1 General structure of the imidazolium aldoxime analogues.

1.6.2 Bis-pyridinium aldoximes

After the discovery of the reactivity enhancement with the bis-pyridinium trimedoxime and methoxime in the late 1950s (*vide supra*, section 1.5.2), several groups studied the influence of structural modifications such as the length and the nature of the connecting linker or the position of the oxime moiety.

1.6.2.1 Bis-pyridinium reactivators with alkyl linker

Musilek and co-workers synthesised several bis-pyridinium mono-aldoximes substituted by different groups or heterocyclic rings such as pyridinium, pyridazinium, quinolinium or isoquinolinium on the other end of the side alkyl chain.[185] Despite the ability to moderately reactivate Paraoxon and DFP poisoning, none of these compounds satisfactorily reactivated Tabun-inhibited AChE.

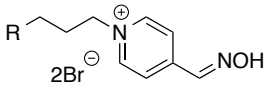

R= 1-pyridinium
R= 1-pyridazinium
R= 1-quinolinium
R= 1-isoquinolinium

Figure 1.6.5 Examples of bis-pyridinium mono-oxime reactivators.

The influence of the oxime moiety position has also been broadly studied by synthesising analogues of trimedoxime (Figure 1.6.6).[185–187] *In vitro* assays revealed a greater potency of reactivation for the analogues bearing the oxime moiety in position 4. However, despite an ability to reactivate Paraoxon intoxication, these compounds displayed limited potency towards Tabun poisoning and all of them were less potent than trimedoxime and obidoxime.

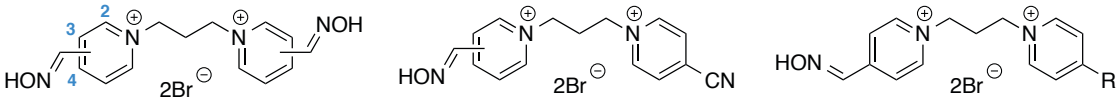

R= Me, *t*Bu, Ph, CH_2OH, COMe, CO_2H, CO_2Et, $C(NH_2)NOH$, 3,4-$CONH_2$

Figure 1.6.6 Examples of bis-pyridinium analogues.

Chennamaneni Rao and co-workers have explored the influence of the linker length on the bis-pyridinium mono-oxime analogues (Figure 1.6.7).[188,189] The most potent candidates were the compounds bearing 3 to 5 carbon atoms in the connecting linker and the amide substituent in the *meta* position.

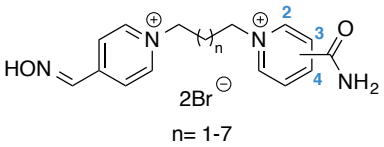

Figure 1.6.7 General structure of bis-pyridinium mono-oxime analogues.

Independently, Kuča and co-workers confirmed this outcome by testing another series of homologues.[190] Quite remarkably, the 4-carbon linker analogue exhibited better reactivation potency *in vitro* than the standard reactivators (Table 1.6.3), but in this case, the amide was in the *para* position.

Reactivators	k_{r2} (mM^{-1} min^{-1})
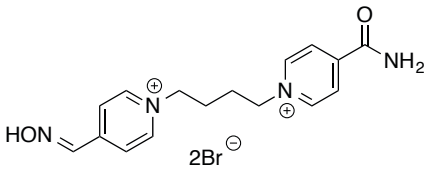	0.239
Trimedoxime	0.050
Hi-6	n.o.
Obidoxime	0.239

Table 1.6.3 *In vitro* reactivation efficiency measured for Tabun-inhibited AChE by Kuča and co-workers. (n.o.: reactivation not observed)

The best results of Tabun-inhibited rat-AChE reactivation were obtained with the compounds containing 3 or 4 carbon connecting linkers.[191] However, Pang and co-workers demonstrated that the connecting linker length was directly related to the position of the oximes in the pyridinium rings if the molecule was symmetrical.[192] In case of *ortho* substitution, the ideal length was from 6 to 9 carbons while for *para* substitution, it was from 2 to 5. For instance, ortho-7 (Figure 1.6.8) exhibited better reactivation efficacy than 2-PAM or trimedoxime for echothiophate-inhibited *m*AChE. Crystal structures of *m*AChE with ortho-7 showed that the length of the connecting linker was able to compensate the position of the oxime (*ortho* instead

of *para*, which is usually more effective) by small distortions (possible due to the high number of carbon atoms in the linker) during structural rearrangement of the catalytic site (Figure 1.6.9).[148]

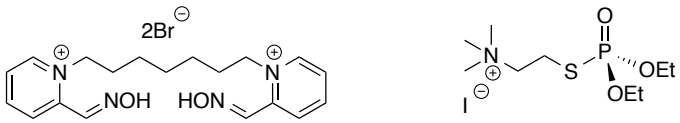

ortho-7 echothiophate

Figure 1.6.8 Structure of ortho-7 and echothiophate.

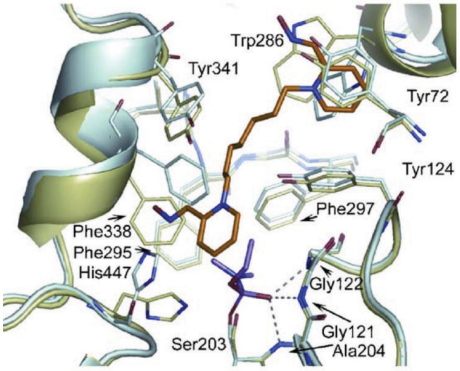

Figure 1.6.9 Structure alignment Tabun *m*AChE (cyan) with crystal structure of *m*AChE-ortho-7 (green). Reactivator and OPNA are in orange and magenta, respectively.

1.6.2.2 Bis-pyridinium reactivators containing heteroatoms in the linker chain

Hi-6 and obidoxime demonstrate the efficacy of bis-pyridinium reactivators with heteroatoms in the linker chain. The standard reactivators are among the most potent molecules for treating Sarin and VX intoxications (*vide supra*, section 1.5.3.2). Thus, molecules with a heteroatom in the bridging linker have received great interest in order to improve the general low reactivity towards Tabun poisoning, and the quest for broad spectrum reactivators. Several groups have independently designed homologues series of bis-pyridinium aldoximes bearing heteroatoms in the linker in order to enhance the interaction with residues of the enzyme gorge. Ekström and co-workers showed the presence of hydrogen bonding between the hetero atom and the tyrosine residues of the enzyme gorge.[148]

Kuča and co-workers reported series of bis-pyridinium bis-oximes and mono-oxime analogues bearing an oxygen atom in the linker.[193] Among the synthesised reactivators, only one analogue (Figure 1.6.10) was found to be twice as effective as trimedoxime for Tabun-*h*AChE but also less potent than HLö-7.[194]

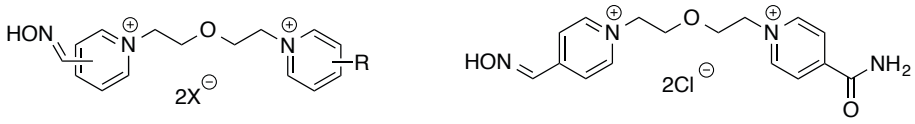

Figure 1.6.10 General structure of bis-pyridinium reactivators with heteroatoms in the connecting linker investigated by Kuča and co-workers (left) and most potent compound (right).

More recently, Worek and co-workers have explored the kinetic effect and reactivity of bis-pyridinium mono-oximes substituted by a ketone in the second ring.[195] The influence of the alkyl group (R) chain length was investigated (from methyl to 12 carbon chain), but unfortunately, the synthesised compounds exhibited lower reactivation potency towards Cyclosarin inhibition.

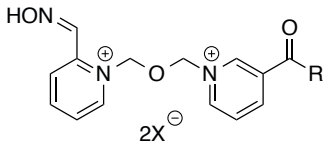

Figure 1.6.11 General structure of bis-pyridinium mono-oxime analogues.
(R= alkyl chain from 1 to 12 carbon atoms).

Acharya and co-workers explored the development of bis-pyridinium bis-oximes with longer aliphatic linker (bearing two oxygen atoms) and evaluated their potency against VX and Sarin poisoning.[196] Surprisingly, only one molecule was found to be more effective than 2-PAM for Sarin-inhibited *h*AChE and as effective as Hi-6 for VX-inhibited *h*AChE.

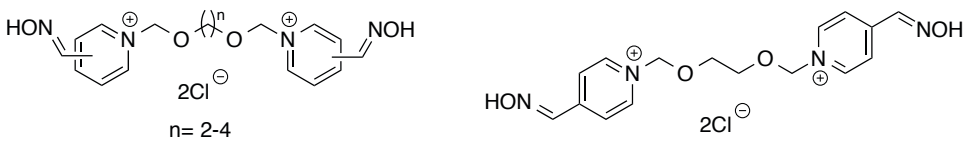

Figure 1.6.12 General structure of bis-pyridinium with two heteroatoms in the linker investigated by Worek and co-workers (left) and most potent compound (right).

1.6.2.3 Bis-pyridinium reactivators with rigid connecting linker

Recently, xylene linked bis-pyridinium oximes have received great interest.[197] The evidence of cation-π and π-π interactions of xylene linked oximes with the active site of AChE are generated by docking studies and believed to be responsible for an enhanced activity.[140] Musilek and co-workers reported a series of various analogues bearing a xylene linker. However, they exhibited lower potency than trimedoxime. Independently, Acharya and co-workers extended their investigation with a series of analogues having a xylene bridging linker and studied their *in vitro* potency against VX and Sarin poisoning.[198] Unfortunately, the most potent molecules remained less effective than 2-PAM and obidoxime.

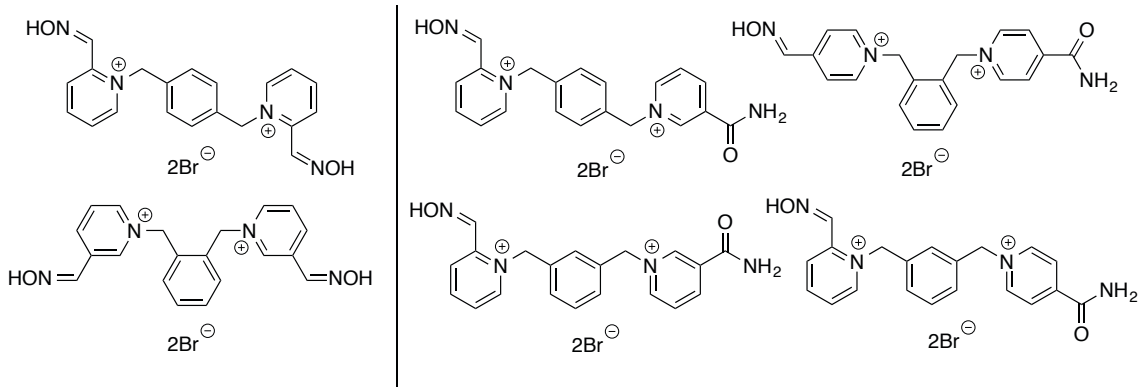

Musilek and co-workers Acharya and co-workers

Figure 1.6.13 Most potent bis-pyridinium oximes bearing a xylene linker.

Believing in the design concept of bis-pyridinium oximes with a xylene linker, Acharya and co-workers recently explored another feature with the addition of an amide group between the pyridinium ring and the oxime moiety.[199] The amide function simultaneously can function as hydrogen bond donor (-NH-) and hydrogen bond acceptor (C=O), which may result in better binding interactions within the enzyme gorge. Besides, it may reduce the dissociation constant (K_D) of oximes.

Reactivators		k_{r2} (mM^{-1} min^{-1})	
		Sarin	VX
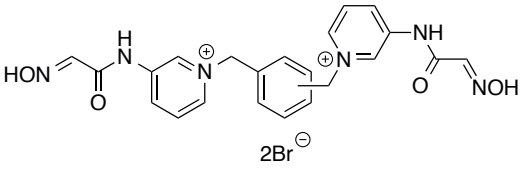	1,2-phenylene	2.24	3.47
	1,4-phenylene	10.85	5.04
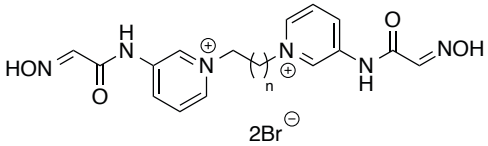	n= 0	1.25	4.17
	n= 4	1.50	3.76
	n= 5	2.16	3.97
2-PAM		2.23	3.59
Obidoxime		8.03	8.31

Figure 1.6.14 Bis-pyridinium bis-oximes featuring an amide function.

Kuča and Musilek have also explored broadly the bis-pyridinium oximes having an unsaturated double bond in the connecting linker in order to make the structure more rigid and enhance the affinity to the inhibited enzyme (by decreasing K_D). The biological evaluation on Tabun-inhibited rat-AChE has shown several trends: superior reactivation potency was observed with an oxime moiety in position 4 of the pyridinium ring if the reactivator contains an aliphatic linker.[200] Then the presence of a carbamoyl moiety in position 4' in the second pyridinium ring increases the reactivation potency by hydrogen bond interactions with the PAS residue Ser298.[140,201] Finally, reactivators containing an (*E*) olefinic linker were generally better than (*Z*).[202–204] Quite remarkably, the analogue K203 among the synthesised reactivators was more effective than the standard reactivators (2-PAM, Hi-6 and obidoxime) for Tabun- and Soman-poisoning in rat brain and also as potent in treating Sarin poisoning (Table 1.6.4). However, it is important to note that the percentage of reactivation to Tabun intoxication remains generally low.

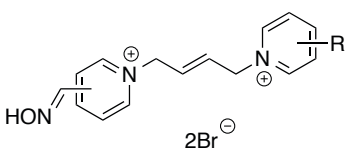

R= CHNOH, $CONH_2$, 4'-Me, 4'-Ph, 4'-Bn, 4'-CH_2OH, 4'-CO_2H, 4'-COMe, 4'-CO_2Et, 4'-CN, 4'-CH_2CO_2H, 4'-$C(NH_2)NOH$

Figure 1.6.15 General structure of bis-pyridinium oximes bearing a butene linker.

Reactivator associated to atropine	Reactivation (%)		
	Tabun[205]	Sarin[152]	Soman[206]
Trimedoxime	14.2	36.4	42.9
Hi-6	9.4	52.5	43.7
Obidoxime	11.1	33.4	44.4
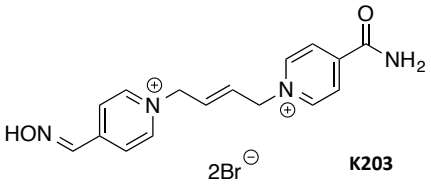 K203	14.5	31.4	49.7

Table 1.6.4 percentage of *in vivo* reactivation of AChE in rat brain intoxicated by Tabun, Sarin and Soman, respectively.

Docking studies were performed to explain the efficiency of K203 and rationalise possible interactions with the inhibited adduct (Figure 1.6.16).[140] The molecular docking showed mostly aromatic interaction in the PAS, sandwiching π-stacking between Trp286 (3.6 Å) and Tyr124 (3.8 Å). Additionally, the carbamoyl moiety forms hydrogen bonds with Trp286 (3.4 Å) and Glu285 (2.9 Å). Potentially, the π-electrons of the unsaturated double bond in the bridging linker displayed possible interactions with Phe297 (3.7 Å) and Phe338 (3.7 Å). Consequently, the improved reactivation ability can be attributed to these favoured interactions and orientation of the oxime moiety (extremely similar compared to obidoxime).

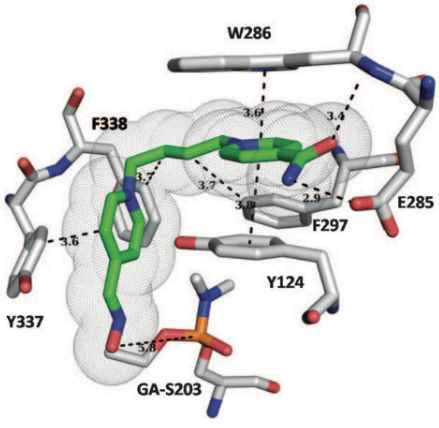

Figure 1.6.16 Molecular docking of the most potent reactivator K203 (green) bearing a butene linker in Tabun-inhibited *m*AChE (grey).

1.6.2.4 Combination of oximes

Kassa and co-workers pronounced recently the idea of using a mixture of oximes with defined proportions and compared the effect of Hi-6 with trimedoxime and Hi-6 with K203.[207,208] The antidotal treatment was improved compared to application of single oxime. Furthermore, *in vivo* assays reported better protection of laboratory animals (mice and rats) for blood and tissue AChE against Cyclosarin intoxication.

Despite lots of effort to find good reactivators, all the charged oximes (mono- and bis-) were found to be effective but mostly only in the peripheral system. The limitations of pyridinium oximes to be active in CNS compelled researchers to adopt other strategies to protect the CNS from OPNA intoxications.

1.6.3 Blood Brain Barrier: strategy for penetration

Lots of effort has been completed in the past six decades to understand the structure-activity relationship between the enzyme and the standard reactivators. Most structural modifications were then made on mono- and bis-pyridinium scaffolds but the presence of permanent positive charge restricts their ability to cross the BBB.[159,209] Also very recently novel strategies have been developed in order to solve this major problem of penetration. These approaches rely on the enhancement of the lipophilicity of the scaffold, drug delivery using nanoparticles and synthesis of novel reactivating function as well as uncharged molecules.

1.6.3.1 Drug delivery using nanoparticles

Significant achievements have been made in crossing the BBB with targeted nanoparticle drug delivery.[210] This idea is to combine oximes with biodegradable nanoparticles made from human serum albumin. The apolipoproteins (protein that binds lipids) on the surface of the nanoparticules will help to improve BBB passage and further the oxime delivery in the CNS. Promising attempts reported that obidoxime and Hi-6 were able to cross through the *in vitro* BBB model (ethyl paraoxon-inhibited porcine-AChE) compared to normal diffusion.[211] Additionally, cell viability studies confirmed the non-toxicity of the nanoparticles. Therefore, this promising method seems to have a real potential but *in vivo* investigations must be completed to clearly define the real potential of nanoparticle drug delivery reactivation.

1.6.3.2 Fluorinated reactivators

In the frame of structural modifications, the potential of incorporating fluorine in the pyridinium ring (mono and bis) was investigated to increase the liphophilicity and enhance the diffusion across the BBB. Jeong and co-workers used computational calculations to show that fluorinated analogues were indeed more lipophilic than their non-fluorinated parent compounds.[212,213] The predictions were confirmed by reactivation experiments and by assessment of BBB permeability using the parallel artificial membrane permeation assay (PAMPA) method.[213] Timperley and co-workers have screened the potential of uncharged fluoroheterocyclic pyridinaldoximes as therapeutic agents (Figure 1.6.17).[214] The synthesised compounds exhibited lipophilic enhancement but pK_a measurement showed insufficient values to obtain valuable reactivators (lower than 2-PAM).

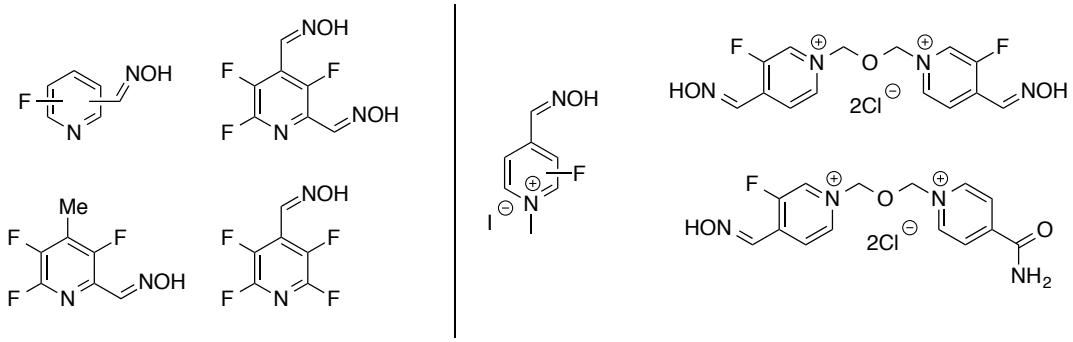

Timperley *and coll.* Jeong *and coll.*

Figure 1.6.17 Structure of fluoroheterocyclic aldoxime analogues.

1.6.3.3 Glycoconjugated oxime reactivators

Heldman and co-workers were the first to suggest that sugar oximes might be able to cross the BBB due to the recognition of sugar moiety by membrane transport mechanisms.[215] Therefore, one pyridinium aldoxime nucleus was replaced by a sugar moiety. Garcia and co-workers continued along these lines a few years later and synthesised several glycoconjugated mono-pyridinium oximes (Figure 1.6.18).[216] *In vitro* investigations on DFP and Paraoxon inhibited *h*AChE showed that only one compound (8-carbon linker and aldoxime in position 2 of the pyridinium moiety) displayed equal reactivation potency compared to that of 2-PAM. The same observation was made with Sarin and VX poisoning.[217]

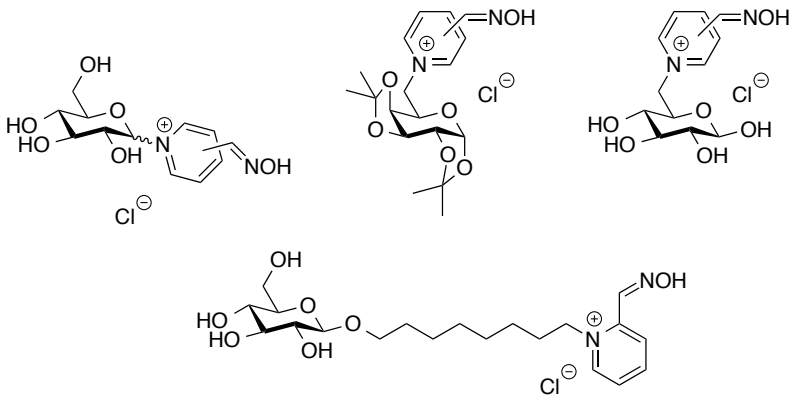

Figure 1.6.18 General structure of glycoconjugated mono-pyridinium oxime analogues.

Despite the fact that these compounds generally displayed lower toxicity than trimedoxime in several animals (mice and guinea pigs), strong evidence for enhanced BBB crossing efficiency has not been provided and further investigations must be made. Furthermore Odžak and co-workers have extended this work by synthesising and evaluating the potency of heterocyclic glycoconjugates such as imidazolium and quinuclidinium with no significant breakthrough (Figure 1.6.19).[218,219]

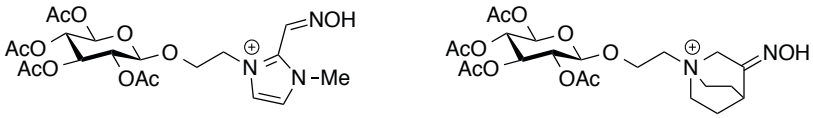

Figure 1.6.19 Other glycoconjugated oximes investigated.

1.6.3.4 Prodrug-type reactivators

Bodor and co-corkers have investigated an interesting prodrug approach using pro-2-PAM as a precursor to the reactivator 2-PAM.[220] The method was based on chemical modification of the reactivator in order to increase its liphophilicity to cross the BBB and then once in the brain, using the presence of coenzymes, such as oxydoreductases, to reform the active species *in situ* and reactivate central AChE (Scheme 1.6.2).[221,222]

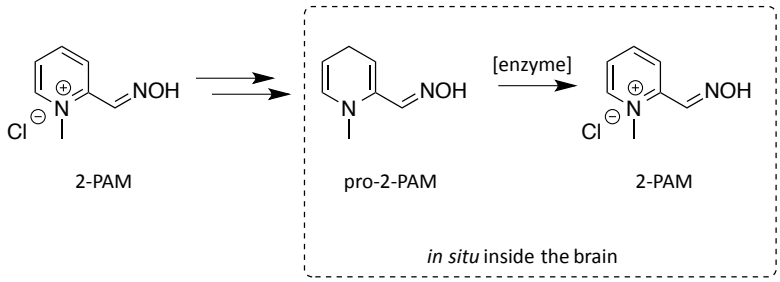

Scheme 1.6.2 Approach of reactivation using a prodrug of 2-PAM.

Quite remarkably, *in vivo* assays on guinea pigs showed that pro-2-PAM is able to reactivate the inhibited enzyme located in the CNS thanks to a better passage across the BBB, contrary to 2-PAM.[223] However, it is unlikely that such compound could be used as treatment due to its challenging synthesis and low stability due to autoxidation.

1.6.3.5 Novel reactivating function

Another strategy used to improve the BBB permeability is the synthesis of uncharged reactivators. Childs and co-workers started investigations in 1955 with the α-oxo-oxime function.[133] One of the advantages of this type of compound is that the carbonyl moiety increases the oxime nucleophilicity. Besides, ketoaldoxime such as the famous monoisonitrosoacetone (MINA) are reported to cross the BBB. But unfortunately, *in vitro* evaluation exhibited poor reactivation potency towards OPNA-inhibited AChE compared to the standard oximes.[224–227] *In vivo* investigations on guinea pigs have shown that despite a protective effect on the animal, MINA is also readily able to reactivate central AChE compared to 2-PAM.[227] But its low affinity towards the inhibited enzyme (confirmed *in vitro* by the very high values of K_D) requires large administrated doses to achieve only a moderate reactivation.

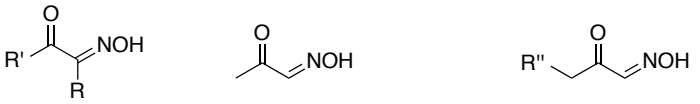

α-oxo-oxime MINA R"= -SMe, -SOMe, $-SO_2Me$, $-S^+Me_2$

Figure 1.6.20 α-oxo-oxime general structure, MINA and its thioanalogues.

In the late 1980s, Degorre and co-workers synthesised analogues of MINA, introducing a sulfur atom (Figure 1.6.20).[228] These analogues were less toxic than MINA and *in vivo* evaluation on Sarin, VX and Paraoxon-inhibited electric eel-AChE displayed lower potency than 2-PAM but with a reactivation rate 1.2 to 2.6 fold faster than MINA. Unfortunately, they also exhibited weak affinity towards the inhibited enzyme, which limits their potency.

More recently, Radić and co-workers have developed uncharged reactivators bearing an amide function and another nucleus with a second nitrogen atom readily to protonate under physiological pH.[229,230] These scaffolds exhibit three major advantages: they are uncharged to enhance BBB penetration; the amide function may interact with the enzyme active site through hydrogen bonding; at physiological pH the amine may be protonated enabling cation-π interaction in the active site.

Figure 1.6.21 General structure of iminoacetamide (left) and most potent candidate (right).

Interestingly, Radić and co-workers justified the choice of iminoacetamides by an easy access compared to their ketoaldoxime analogue, as the acetamide decreases the nucleophilic strength of the oxime and thus its pK_a. Only one candidate was more potent than MINA (Figure 1.6.21) with a fast reactivation rate. However, it remained less effective than 2-PAM for almost all OPNAs tested.

Analogues of this candidate have been made and explored (introduction of heteroatom, methyl group or fluorine, Figure 1.6.22). Unfortunately, none of the synthesised analogues showed any improvement.[231]

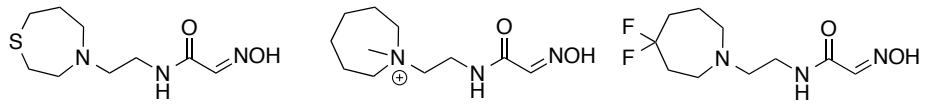

Figure 1.6.22 Structure of iminoacetamide analogues of the most potent candidate.

Amidine-oximes were introduced by Kalisiak and co-workers to also improve the passage across the BBB (Figure 1.6.23).[232] Based on the 2-PAM design, these molecules display advantages such as low toxicity, good aqueous solubility, hydrogen bond acceptor potential. Furthermore, they are already used in drugs (e.g. anticoagulant dabigatran, antiinfective diminazen or antimicrobial pentamidine). Besides, the basic group readily undergoes protonation under physiological conditions to form a positively charged centre, similar to the 2-PAM pyridinium quaternary nitrogen (Figure 1.6.23), which may then favour the binding affinity through cation-π interactions with aromatic residues of the enzyme active site. In this case, these compounds work as hybrids where the amidine moiety is responsible for efficient binding to phosphylated active site, while the proximal oxime group functions as nucleophile responsible for reactivation of the inhibited enzyme.

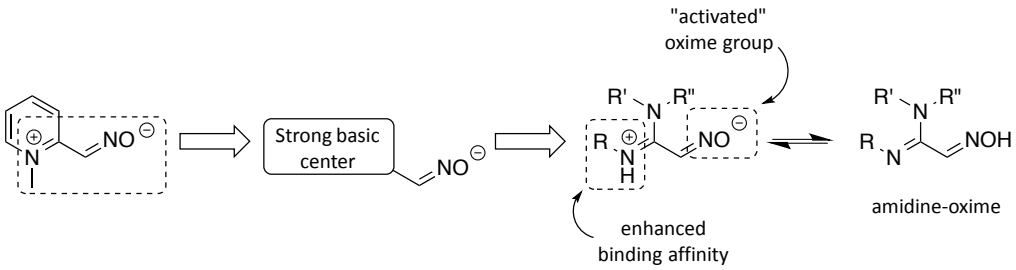

Figure 1.6.23 Retrostructural analysis of amidine-oxime proposed by Kalisiak and co-workers.

In addition, the electron-withdrawing character of the protonated amidine group enhances the ionization of the oxime group and increases the concentration of the functionally active nucleophilic oxime anion. In the ethyl substituted amidine analogue (R= ethyl, Figure 1.6.24), the pK_a of the oxime moiety is 8.0 ± 0.1 and the amidine group is 12.1 ± 0.1 providing

approximately 25% of deprotonated oxime at physiological pH, according to Henderson-Hasselbalch equation, an improvement compared to 12% for MINA.[233]

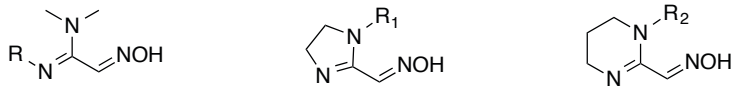

R= alkyl, aryl, alkoxy, cycloalkane | R_1= alkyl, aryl | R_2= alkyl, aryl

Figure 1.6.24 General structure of amidine oximes.

Despite better reactivation results compared to MINA, these compounds were found to be less potent than 2-PAM *in vitro*.[234] However, two compounds (R= ethyl and propyl, Figure 1.6.24) were effective *in vivo* and were found to protect from CNS toxicity in animal models mostly due to higher lipophilic properties. Therefore, these compounds could be an interesting alternative to oximes containing permanently charged quaternary nitrogens. However, their binding affinities remain a major issue to improve.

Recently, uncharged heterocyclic compounds have also been investigated based on 2-pyridine aldoxime (initially explored in the 1950s with very low potency).[235] *In vitro* investigation against Paraoxon poisoning showed good potency of the thiophene derivative. However, optimisation of the scaffold remains to improve its reactivation properties (decrease K_D and increase k_r).

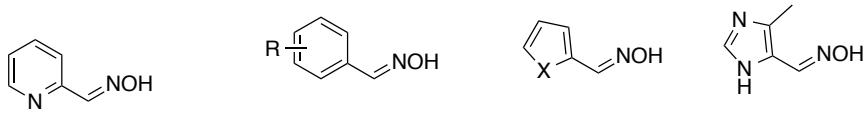

2-pyridine aldoxime | R= 2-Me, 2-OH, 3-NH_2, 4-OMe, 4-NMe_2 | X= S, O, NH

Figure 1.6.25 Example of uncharged heterocyclic reactivators.

Independently, Kovarik and co-workers have explored the efficiency of imidazole-based uncharged reactivators.[236] One of the synthesised compounds was highlighted as a promising reactivator for Tabun intoxication. Its good binding affinity (K_D 3-fold smaller than 2-PAM) balanced with its slower reactivation rate (smaller k_r). However, the reactivation potency remains moderate compared to the bis-pyridinium standard reactivators.

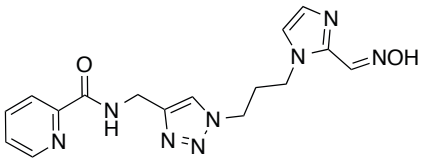

Figure 1.6.26 Most potent imidazole-based uncharged reactivator for Tabun poisoning.

1.6.3.6 Peripheral site ligand and bifunctional uncharged hybrid theory

Novel uncharged reactivating functions showed promising results for targeting the passage across the BBB. However, all compounds reported displayed slow reactivation rates and low binding affinities towards the phosphylated-enzyme decreasing their reactivation potency. Therefore several research groups, including our one (*vide infra*, chapter 2), developed a novel strategy consisting in the association an uncharged oxime moiety and a ligand, also called peripheral site ligand (PSL), which exhibits good affinity with the PAS and thus may enhance the interactions between the reactivator hybrid and the inhibited enzyme.

De Koning and co-workers proposed linking the reactivating α-ketaldoxime function to piperidine derivatives that have good binding affinities with the PAS.[237] Despite being ineffective against Tabun and exhibiting lower reactivation potency than Hi-6 for Sarin and VX intoxications, these compounds displayed significant improvement in terms of their affinity and potency compared to the reactivator alone and the mono-pyridinium standard reactivators.

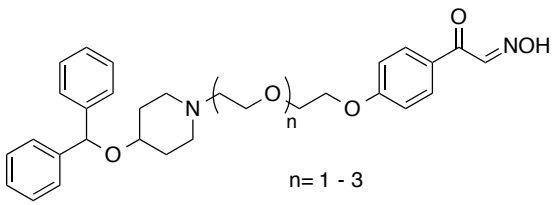

Figure 1.6.27 Bifunctional uncharged hybrids synthesised by de Koning and co-workers.

This strategy offers promising hope in the design of novel hybrids that exhibit potential for efficient passage across the BBB. However, it is important to mention that the PSL must be carefully selected, as a ligand with too high binding affinity with the native enzyme will result in competitive inhibition and will slow the reactivation process and cause toxic effect.

1.7 Conclusion

Since the discovery of mono- and bis-pyridinium oximes as reactivators for OPNA-inhibited AChE, hundreds of variations have been designed, synthesised and undergone biological assays over the past six decades. Unfortunately, all of these compounds exhibit three major drawbacks: (1) the presence of permanent positive charge prevents them from efficiently crossing the BBB to reactivate AChE located in the CNS; (2) they showed unequal reactivation abilities against different types of OPNA poisoning; and finally, (3) they are ineffective at reactivating "aged" enzyme. Recently, new research has uncovered efficient uncharged reactivators that are able to cross the BBB. However, further investigation is necessary to discover a reactivator able to reactivate all types of OPNA-poisoned AChE. None of existing pyridinium oximes can claim to be true broad spectrum reactivators. Regarding the "aged" AChE, further research remains, as none of the existing reactivators is able to reactivate it. For a better protection of civilians and soldiers against poisoning by OPNAs used in both pest control and chemical warfare, further investigation is necessary.

Chapter 2: Design and synthesis of novel uncharged bifunctional hybrid reactivators based on tacrine and analogues

2.1 Introduction

Research conducted over the past six decades has culminated in the discovery of mono- and bis-pyridinium aldoximes that exhibit good ability to reactivate OPNA-inhibited AChE. However, their lack of binding affinity and the presence of a permanent positive charge cause substantial issues for *in vivo* investigations. Their therapeutic efficacy is considerably reduced by the fact that they are not able to reactivate central AChE. Consequently, the poor CNS activity of known reactivators compelled the researchers to adopt other strategies to target CNS OPNA-inhibited AChE.

2.1.1 Preliminary results

The basis of the research described in this thesis originates from a study (*Saint-André*, thesis, 2009, University of Strasbourg) and a collaboration in the frame of a postdoctoral grant (ANR 06 BLAN 0163 NEURODETOX), involving chemists from the University of Strasbourg supervised by Dr. Rachid Baati and the University of Rouen supervised by Prof. Pierre-Yves Renard, and biologists from IRBA supervised by Dr. Florian Nachon. The investigations centred on the discovery of novel biocompatible scavengers able to detoxify OPNA before reaching their target (*vide supra*, section 1.4.1.2). They developed a high-throughput screening (HTS) assay using pro-fluorescent probes to detect nucleophilic functionality able to efficiently break down a P–S bond (as the main focus was on VX and derivatives).[238] The mechanistic strategy can be described as nucleophilic substitution at the phosphorus atom by a S_N2P mechanism, cleaving the P–S alkyl bond (VX mimic) and leading to a thiolate species that spontaneously decomposes into the corresponding highly fluorescent 7-hydroxycoumarin and thiirane (Figure 2.1.1). Ethylene can also be formed by β-elimination, but the reaction mechanism has not been fully proven.

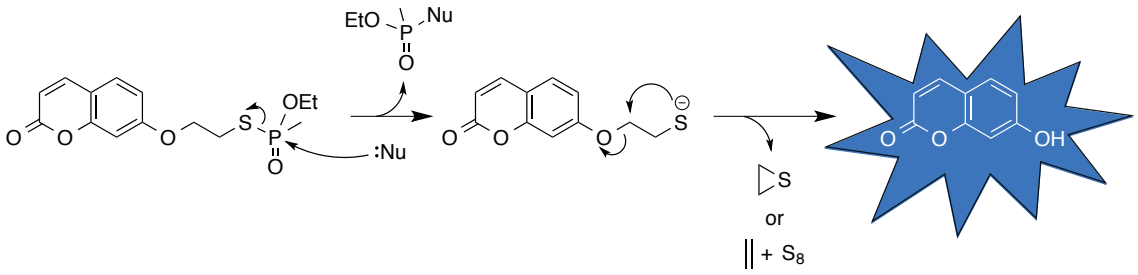

Figure 2.1.1 High-throughput fluorescence assay for the detection of OPNA scavengers.

From several hundred candidates, the best compounds were then screened to study their potency in degradation of an analogue of VX with reduced toxicity (PhX, Figure 2.1.2) monitored by NMR. Only two uncharged α-nucleophiles, the 3-hydroxy2-pyridinaldoxime **2.1** and amidoxime **2.2**, stood out in the screening and exhibited better hydrolytic properties towards PhX with similar reaction rates to 2-PAM.[239] Furthermore, these candidates were evaluated *in vitro* for VX-inhibited *h*AChE and their reactivation constants were determined (Table 2.1.1).

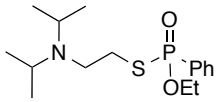

Figure 2.1.2 PhX, an analogue of VX with reduced toxicity.

Reactivator	K_D (μM)	k_r (min^{-1})	k_{r2} (mM^{-1} min^{-1})
2-PAM	215 ± 75	0.06 ± 0.01	0.28
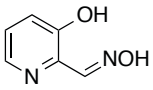 **2.1**	30,000 ± 10,000	0.5 ± 0.1	0.016
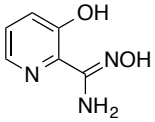 **2.2**	30,000 ± 20,000	0.08 ± 0.1	0.0026

Table 2.1.1 Reactivation constants of reactivators **2.1** and **2.2** for VX-inhibited *h*AChE.

Despite its low binding affinity (140-fold lower than 2-PAM), 3-hydroxy-2-pyridine aldoxime (**2.1**) exhibited interesting reactivation rate (8-fold faster than 2-PAM). Besides, **2.1** has two major advantages compared to the conventional reactivator: (1) it is uncharged, thus it is more likely to cross the BBB; and (2) the hydroxyl group in position 3 has the ability to both increase the oxime pK_a,[240] and reduce the "recapture phenomenon" (*vide supra*, section 1.5.4.3) by taking part in the formation of an isoxazole via a subsequent intramolecular reaction. This irreversible reaction increases significantly the OPNA hydrolysis rate.

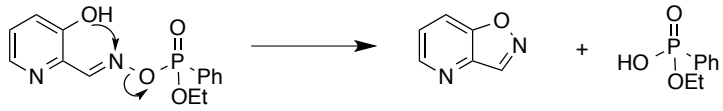

phosphyloxime isoxazole

Scheme 2.1.1 Intramolecular reaction leading to the irreversible formation of isoxazole.[239]

2.1.2 Bifunctional hybrid reactivator strategy

A solution to improve the lack of affinity of the reactivator towards the active site of AChE is to conjugate the nucleophile **2.1** to a ligand capable of interactions with the PAS. The cation-π and π-π interactions at the PAS should enhance the binding affinity of the hybrid with the phosphylated enzyme, orientate the reactivating moiety inside the gorge and improve the reactivation potency. The reactivator warhead and the peripheral binding site ligand would be linked through a suitable alkyl or heteroalkyl chain fitting the AChE gorge, constituting the so-called bifunctional hybrid strategy. However, it is important to keep in mind that the choice of the ligand might greatly influence the reactivation potency of the hybrid; a ligand with too high affinity for the native enzyme will reduce the efficacy by functioning as an inhibitor of AChE.

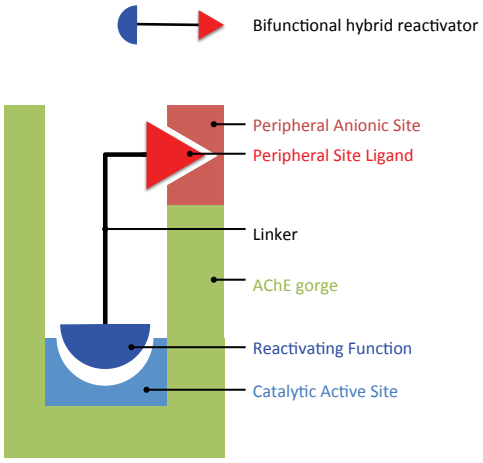

Figure 2.1.3 Schematic representation of the bifunctional hybrid reactivator strategy.

Many hybrid reactivator candidates were synthesised by the chemists in our consortium (Figure 2.1.4). While Renard and co-workers mainly focused on reactivators bearing phenyl-tetrahydroisoquinoline (PIQ) or tryptoline moieties,[241–244] Baati and co-workers investigated reactivators containing a tacrine peripheral site ligand.[245]

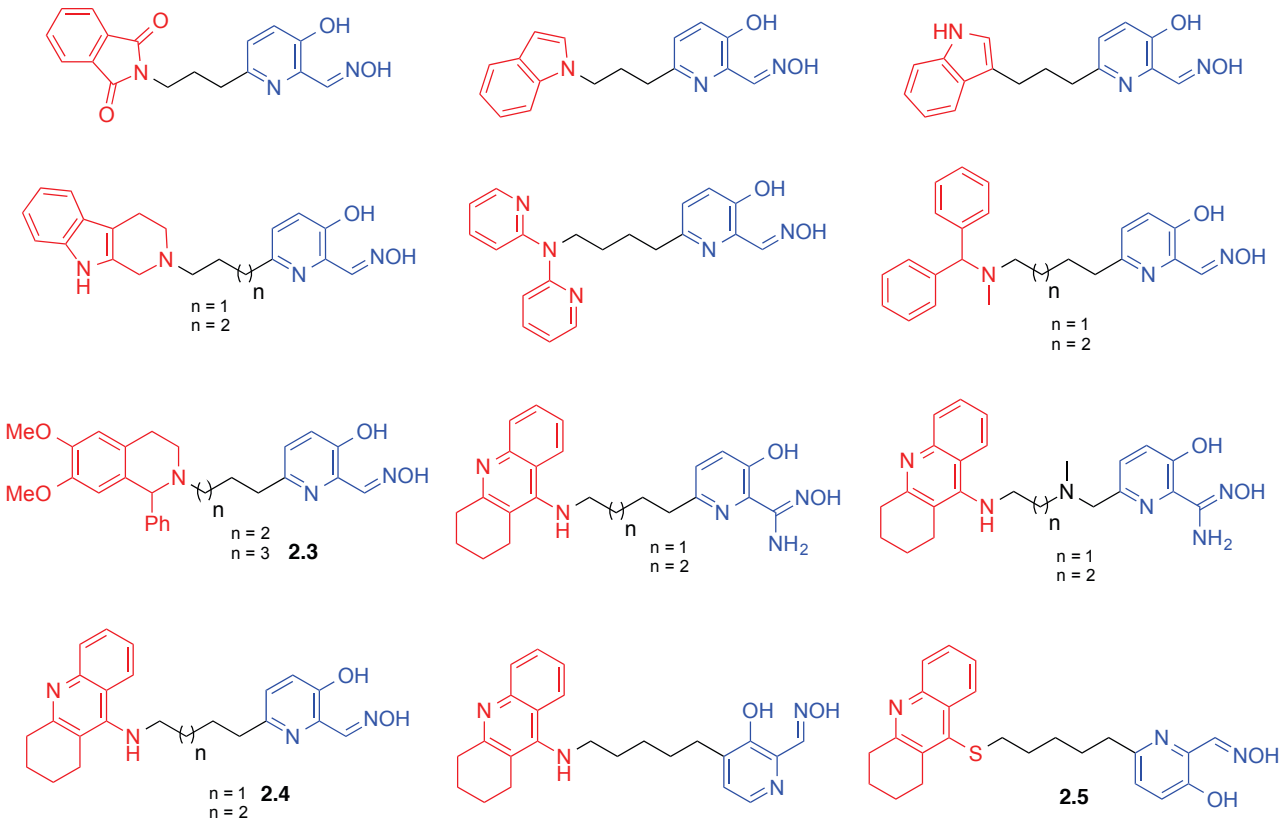

Figure 2.1.4 Examples of hybrids synthesised by our consortium over the last 5 years.

All these hybrids have been evaluated *in vitro* for VX- Tabun- and Paraoxon-inhibited *h*AChE and their reactivation constants were determined. Quite remarkably, hybrids **2.3** and **2.4** were reported to have higher affinity towards the phosphylated-enzyme and enhanced reactivation for VX and Tabun intoxication (Table 2.1.2).[242,245] The reactivation rates equalled and even exceeded those of HI-6, obidoxime, and HLö-7. Surprisingly, hybrid **2.4** proved to be 79 x, 2 x, 44 x and 2.5 x more efficient than 2-PAM, obidoxime, trimedoxime, and HI-6, respectively, in reactivating VX-inhibited *h*AChE. Significantly, **2.3** and **2.4** were respectively 5 x and 4 x more effective than trimedoxime at reactivating Tabun-inhibited *h*AChE, which is currently known as the best bis-pyridinium oxime reactivator for Tabun intoxication.

	VX-*h*AChE			Tabun-*h*AChE		
Reactivator	K_D (μM)	k_r (min^{-1})	k_{r2} (mM^{-1} min^{-1})	K_D (μM)	k_r (min^{-1})	k_{r2} (mM^{-1} min^{-1})
2-PAM	215 ± 75	0.06 ± 0.01	0.28	706 ± 76	0.010 ± 0.0005	0.01
Trimedoxime	n.d.[a]	n.d.[a]	0.50	27 ± 4	0.085 ± 0.005	0.6
Obidoxime	54 ± 12	0.60 ± 0.05	11	250 ± 110	0.040 ± 0.006	0.16
Hi-6	50 ± 26	0.44 ± 15	9	n.r.[b]	n.r.[b]	n.r.[b]
HLö-7[129]	7.8	0.49	63	106 ± 15	0.020 ± 0.0007	0.19
2.3	17.3 ± 6.4	0.44 ± 0.05	26	0.06 ± 0.01	0.015 ± 0.001	2.7
2.4	31 ± 6	0.72 ± 0.07	22	7.1 ± 1.5	0.021 ± 0.001	3.0

Table 2.1.2 Reactivation constants of hybrid reactivators **2.3** and **2.4** for VX- and Tabun-inhibited *h*AChE. ([a]not determined if [Ox] << K_D, then there is a linear dependence between k_{obs} and [Ox]: $k_{obs}= (k_r/K_D)[Ox]$. In this case, k_r and K_D cannot be determined, but $k_{r2}= k_r/K_D$ is the slope of the line; [b]no reactivation observed until [Ox]= 5 mM).

With these tremendous *in vitro* results, our consortium seemed to be in a good position to discover the broad spectrum reactivator that was missing for so many years. While hybrid **2.3** shows an IC_{50} higher than 100 μM, **2.4** actually displays a strong inhibition activity (0.25 ± 0.02 μM)[245] towards the native enzyme (enzyme after reactivation) becoming a competitive inhibitor. Only reactivators with IC_{50} values greater than 100 μM exhibit lower binding affinity towards the native enzyme than towards the phosphylated enzyme. Consequently, hybrid **2.4** represents an interesting new starting point for further improvement. Particularly, since it neither bears a permanent charge nor a tertiary amine, it should show improved BBB penetration efficiency.

2.1.3 Objectives

As part of continuing efforts towards the discovery of efficient reactivators of OPNA-inhibited *h*AChE, the main objective in this chapter was to design and synthesise new bifunctional uncharged reactivators based on our more potent lead compound **2.4**, and deliver further improvements of its properties and converge on the goal of developing a new drug.

In the context of this international PhD founded in a joint-program by the French Direction Générale de l'Armement (DGA) and the Defence Science and Technology Laboratory (Dstl), its important to mention that the synthesis described here was carried out jointly within the laboratories of Dr. Rachid Baati at the University of Strasbourg (ICPEES, UMR CNRS 7515) and Prof. Richard C. D. Brown at the University of Southampton; the biological evaluation (*in silico*, *in vitro* and *in vivo*) for all synthesised reactivators were made within the laboratories of Dr. Florian Nachon at the Institut de Recherche Biomédicales des Armées (IRBA) recently relocated from La Tonche (Grenoble, France) to Brétigny-sur-Orge (Paris region, France); and the crystal structure studies were investigated within the laboratories of Dr. Martin Weik at the Institut de Biologie Structurale (IBS, Grenoble, France).

2.2 Rational design of bifunctional tacrine-based hybrid reactivators

2.2.1 Tacrine scaffold

Tacrine was not a random choice as Peripheral Site Ligand (PSL). Indeed, tacrine (9-amino-1,2,3,4-tetrahydroacridine, THA, **2.6** - Figure 2.2.1) was known to possess a good affinity for AChE.[246] In fact, THA also commercially named Cognex®, was one of the first discovered AChE inhibitors (AChEI), and was also found to be an effective drug approved by the Food and Drug Administration (FDA) agency in 1993 for symptomatic treatment of Alzheimer's disease.[247] However, despite its very good pharmacokinetic properties (e.g. BBB penetration and inhibition of AChE at nM concentration),[248,249] THA was hampered by its low therapeutic index, short half-life and liver toxicity during clinical trials.[250]

Several structure-activity relationship (SAR) studies with THA analogues were carried out and reported to understand, modulate and improve its biological effect towards AChE.[251–257] General trends emerged: it appeared that a substituent such as chlorine in position 6 of the THA nucleus

strongly increases the inhibitory potency of the tacrine while a substitution in position 7 decreases it (Figure 2.2.1).[246,251,252,258] Computational and theoretical calculations supported that an electron-withdrawing group (EWG) in position 6 tends to reduce the electronic density on the tacrine aromatic rings favouring further π-electron interactions with nearby residues Phe330 and Trp84 of the enzyme active site. Conversely, steric hindrance drives THA behaviour when substituted in position 7.

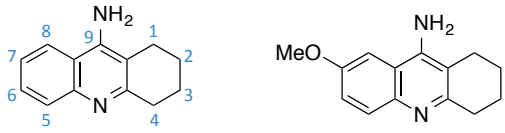

tacrine, THA, Cognex® **2.6**

7-MeOTA **2.7**

Figure 2.2.1 Structure of tacrine and its analogue 7-MeOTA.

More recently, Kuča and co-workers focused on 7-MeOTA **2.7** derivative corresponding to the analogue of THA **2.6** bearing a methoxy group in position 7 (Figure 2.2.1), along with some *N*-alkyl analogues.[254–257,259,260] **2.7** was found to be equally active pharmacologically but less toxic compared to THA.[249,250] In fact, 7-hydroxytacrine undergoes metabolism by *O*-demethylation and subsequent conjugation with glucuronic acid leading to excretion in urine. The *N*-alkyl analogues did not demonstrate any significant improvement. However, from a synthetic perspective, it is interesting to note that the low nucleophilicity of the NH_2 resulted in low yields of *N*-alkyl derivatives (20% average for 1 or 2 steps).

Consequently, based on the pharmacological properties of tacrines and on our existing data for hybrid **2.4**, we designed a series of novel uncharged bifunctional AChE reactivators (Figure 2.2.2). The structural modifications investigated can be summarised as follows: (1) addition of a substituent (R) in the A ring (e.g. 7-chloro or 7-methoxy); (2) modification of the saturated ring size in the PSL nucleus (from 5 to 7 membered); (3) variation of the alkyl linker length. These three main modifications would help to decrease the binding affinity of the PSL towards the native enzyme and thus may also enhance its reactivation potency.

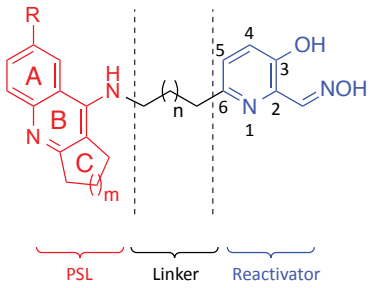

R= -Cl, -OMe, -H
m= 1, 2, 3
n= 1, 2

Figure 2.2.2 General structure of novel hybrid reactivators.

Noteably, another modification considered during the design of the new hybrids was the nature of the atom or functionality connecting the PSL moiety to the linker: methylene, ether oxygen or amide function instead of the nitrogen atom. However, the *in vitro* evaluation of hybrid **2.5** (Figure 2.1.4), thioanalogue of hybrid **2.4**, displayed a complete loss of reactivation potency. This result may be explained by the ability of the C9 amino group to form interactions with the gorge residues that are not possible with soft non-basic sulfur atom. Consequently, the amine function at position 9 of the scaffold was conserved in the compounds described below. Additionally, various positions to connect the linker to the reactivating moiety were previously investigated and reported by our group:[245] it was found that linking through position 6 of the pyridine nucleus gave the best reactivation results. Therefore, we decided to strictly conserve the linkage to the reactivator at position 6 (Figure 2.2.2). Separately, we conducted a brief study of alternative new heterocyclic reactivators, which are described in Appendix.

2.2.2 Structure-based *in silico* screening

As the basis for the development of an *in silico* model, the X-ray crystal structure of *Torpedo californica* (*Tc*)AChE complexed with a bis-tacrine inhibitor was used to predict how the tacrine moiety would bind to the PAS.[261] The length of the linker was then optimized so that the oxime moiety could approach the catalytic site phosphylated serine, whilst retaining the ligand binding with the PAS to maximise the reactivation potency of the bifunctional hybrids. Molecular dynamics simulations were used in the flexible docking experiments to optimise structures for the novel hybrids. As reported by our group last year,[245] ternary complexes involving the reactivator, the OPNA VX and the enzyme AChE were simulated.

The linker length was optimised by analysing the distributions of distances between the aldoxime oxygen atom and the VX-AChE phosphorus atom. The molecular dynamic

simulations were performed for 5 ns at 300 K. The shorter the distance, the higher the probability to form a covalent bond between the oxygen atom and the phosphorus atom, hopefully leading to faster the reactivation. The simulations indicated that a saturated 4-carbon linker between the PSL moiety and the pyridinaldoxime reactivator was as optimum length, but that 3- and 5-carbon linker should be also considered.[245] Our group previously reported the synthesis and evaluation of the analogue hybrid bearing a 5-carbon linker.[245] As this longer linker hybrid was found to be ineffective against VX intoxication, we decided to focus on the analogues bearing 3 and 4 methylene groups. Besides, as we faced synthetic issues (*vide infra*, section 2.3.1) to access derivatives substituted with a 7-methoxy group (R = OMe, Figure 2.2.2), we primarily focused on analogues with and without the 7-chloro substituent (R = H or Cl, Figure 2.2.2).

In the flexible docking experiments, the key residues of the active site gorge (Tyr72, Asp74, Trp86, Tyr124, Ser125, Trp286, Tyr337, Phe338 and Tyr341 along with the ethyl group of VX) were allowed to wander from their native position. In all docking experiments, modification of the Trp286 conformation was observed in the PAS (Figure 2.2.3), reproducing the crystallographic observation from the bis-tacrine/*Tc*AChE complex (pdb code 2ceK).[261] This transformation is mostly due to a π-π sandwiching interaction of the tacrine moiety between the aromatic residues Tyr72 and Trp286.

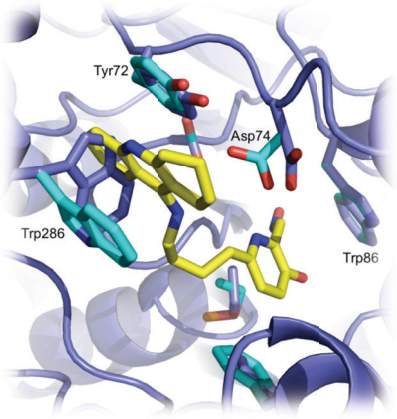

Figure 2.2.3 Docked conformation of hybrid **2.4** at the PAS of VX-inhibited *h*AChE. The flexible residues are in cyan while the native conformation (pdb code 1b41) is in purple.

The scoring function of the docking algorithm yielded the binding energies or affinities (Table 2.2.1), which represent the energy of interaction calculated between the molecule and the

catalytic active site. It allows prediction and identification of undesired interactions that can lead to rejection of the molecule from the active site.

Entry	R	Linker length (CH_2)	Saturated ring size (C)	Binding Energy (kcal mol^{-1})
1	Cl	3	5	–11.7
2	H	3	5	–11.2
3	Cl	3	6	–12.5
4	H	3	6	–11.7
5	Cl	3	7	–10.3
6	H	3	7	–11.3
7	Cl	4	5	–11.7
8	H	4	5	–11.5
9	Cl	4	6	–11.4
10	H	4	6	–11.7[245]
11	Cl	4	7	–11.6
12	H	4	7	–11.5

Table 2.2.1 Flexible docking scores for potential novel hybrid reactivators.

The potential dissociation constant K_D can be determined from the Gibbs free energy equation as followed:

$$\Delta G = -RTln(K_D)$$

$$\text{thus, } K_D = e^{(-\frac{\Delta G}{RT})}$$

As the stability of the enzyme-substrate complex is correlated to the docking score, the lower the value, the better. As a general guide, hybrids with high affinity are potentially a good reactivators. All molecules exhibited a score lower than –9 kcal mol^{-1}, indicating that the linker is sufficiently long to prevent unproductive binding of the reactivators in the gorge of the inhibited enzyme. These calculated binding energies values predict a range of micro to nano molar inhibitors. Examples of dockings are shown in the experimental part (section A.5).

2.3 Synthesis of the first chlorinated hybrid analogue

Prior to embarking on the synthesis of a series of novel hybrid reactivators, we chose first to focus on the synthesis of the hybrid **2.8** (**Error! Reference source not found.**), the chlorinated analogue of the recently reported hybrid **2.4**, which is described below.[245]

2.3.1 Preliminary investigation towards the hybrid synthesis

Our initial strategy relied on direct *N*-alkylation of the 7-chloro-9-aminotacrine **2.12** with an activated butyne linker followed by Sonogashira cross-coupling reaction with the methyl 3-(benzyloxy)-6-bromopicolinate (**2.10**) as precursor to the reactivating functionality (Scheme 2.3.1).

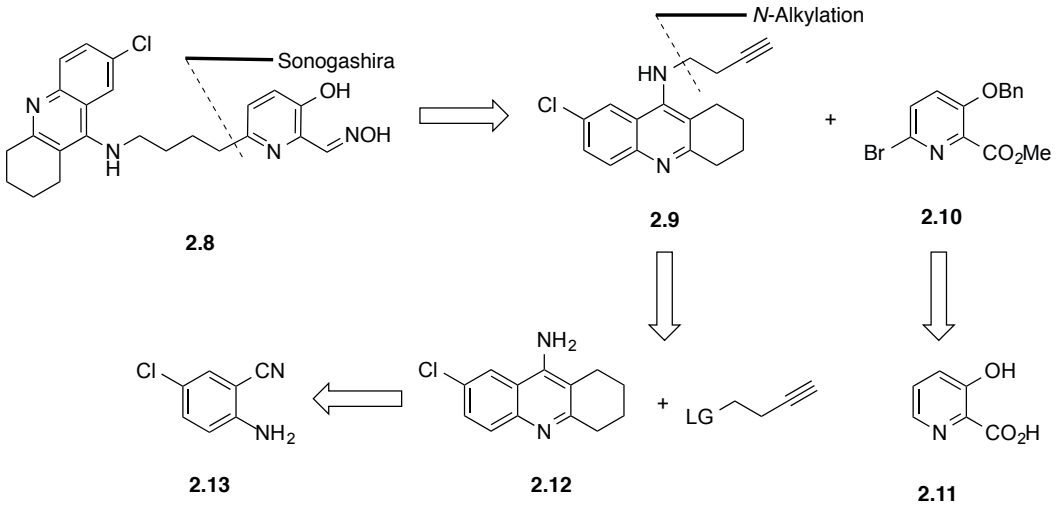

Scheme 2.3.1 Retrosynthetic plan 1 for hybrid **2.8**.

The reactivator precursor **2.10** was prepared as previously reported (Scheme 2.3.2).[238,262] Commercially available 3-hydroxypicolinic acid (**2.11**) was first successfully esterified (**2.14**, 82%) using concentrated sulphuric acid in MeOH. Then, bromine was introduced selectively at the 6-position of the pyridine ring by electrophilic aromatic substitution (S_EAr) yielding to the mono-brominated pyridine **2.15** in excellent yield (87%). While the hydroxyl substituent is *ortho*/*para*-directing and strongly activating, the carboxymethyl is *meta*-directing and moderately deactivating. Therefore the stronger resonance donating effect of the hydroxyl group guides the substitution in position 6. Finally, Williamson ether synthesis was employed to protect the phenolic position and afford the desired benzyl ether **2.10** in an excellent overall yield for the three steps (71%).

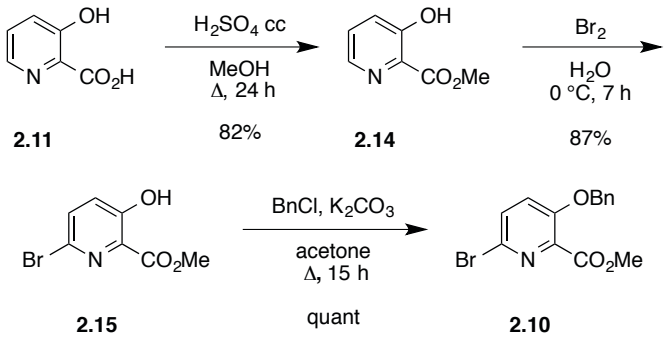

Scheme 2.3.2 Synthesis of the reactivator precursor **2.10**.

Meanwhile, a Lewis acid mediated intermolecular cyclodehydration reaction between commercially available 2-amino-5-chlorobenzonitrile (**2.13**) and cyclohexanone gave the desired 7-chloro-9-aminotacrine (**2.12**) in moderate yield (40%, Scheme 2.3.3).

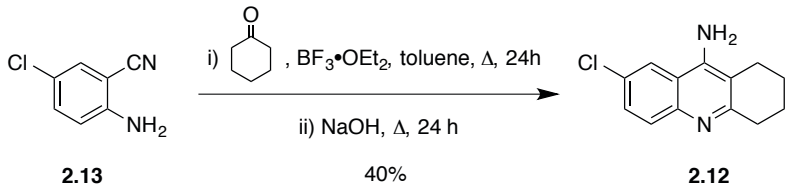

Scheme 2.3.3 Synthesis of 7-chloro-9-aminotetrahydroacridine (**2.12**).

In parallel, the 3-butyn-1-ol (**2.16**) was activated by tosylation to afford the desired tosylate **2.17** in quantitative yield (Scheme 2.3.4).

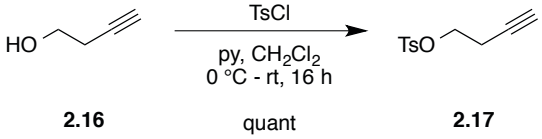

Scheme 2.3.4 Synthesis of *p*-toluenesulfonyl alkyne **2.17**.

A brief investigation towards direct *N*-alkylation was then explored to form the desired C-N bond (Table 2.3.1). Unfortunately, the starting material **2.12** did not react with the alkyne **2.17**, leading mostly to degradation of the linker by elimination to butenyne. This result is not entirely unexpected as noted in section 2.2.1, and could be ascribed to the poor reactivity of the 9-amino substituent. The low reactivity of 9-aminotacrine was already observed and reported by Kuča and co-workers with the analogue 7-MeOTA **2.7**.[255] Under harsh conditions (Table 2.3.1, entry 1), the 7-MeOTA **2.7** was alkylated in only 6% yield.

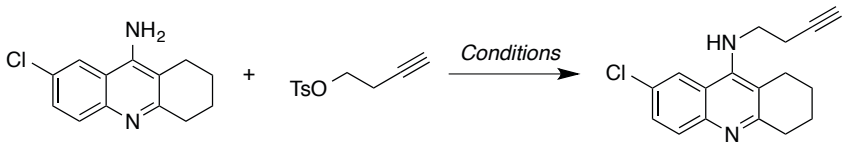

2.12 **2.17** **2.9**

Entry	Conditions	Solvent	Time	Temperature	Yield
1	KOH	DMSO	48 h	60 °C	-
2	i/ NaH ii/ KI, linker	DMF	i/ 1 h ii/ 48 h	i/ 60 °C ii/ Δ	-
3	Et_3N	CH_3CN	48 h	60 °C	-
4	Et_3N	DMSO	48 h	60 °C	-

Table 2.3.1 Attempted *N*-alkylation of 7-chloro-9-aminotacrine (**2.12**).

As described in the literature, 7-MeOTA (**2.7**) was synthesised in 4 steps starting from the commercially available 5-hydroxy-2-nitrobenzaldehyde (**2.18**, Scheme 2.3.5).[263] The methyl ether **2.19** was isolated in quantitative yield after treating the starting material **2.18** with dimethyl sulfate in 30% aqueous NaOH solution. Then treatment of the methyl ether **2.19** with hydroxylamine hydrochloride under acidic conditions afforded rapidly and quantitatively the corresponding nitrile **2.20** by alkylation and subsequent *in situ* dehydration.[264] Hydrogenation (1 atm) in presence of 10% Pd/C catalyst yielded the amine **2.21**. Finally, a Lewis acid mediated intermolecular cyclodehydration gave the desired 7-methoxy-9-aminotacrine (**2.7**) in excellent overall yield (85%).

Further attempts to alkylate the analogue **2.7** were also briefly investigated using the conditions described (Table 2.3.1, entry 1), but remained unsuccessful as no conversion was observed.

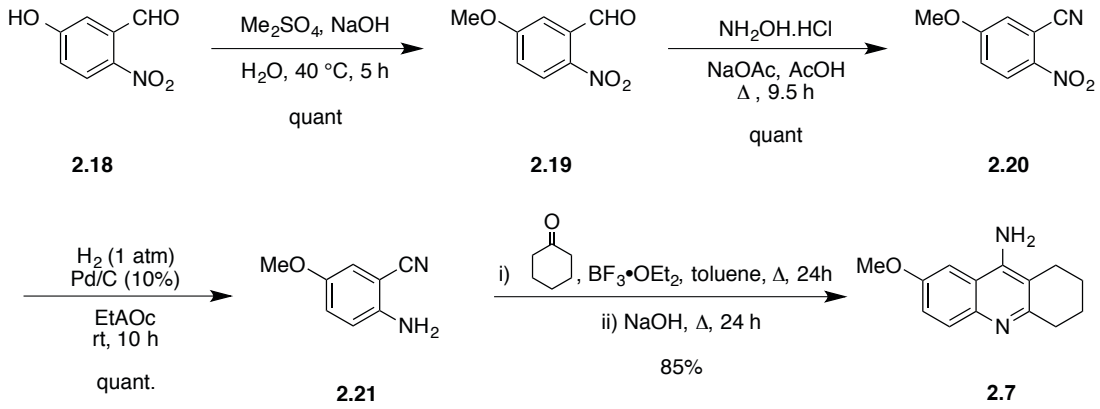

Scheme 2.3.5 Synthesis of the 7-MeOTA **2.7**.

Therefore, the formation of amide bond linkage was explored (Scheme 2.3.6). Unfortunately, following several reported classical conditions,[265–267] the formation of the corresponding amides was not achieved.

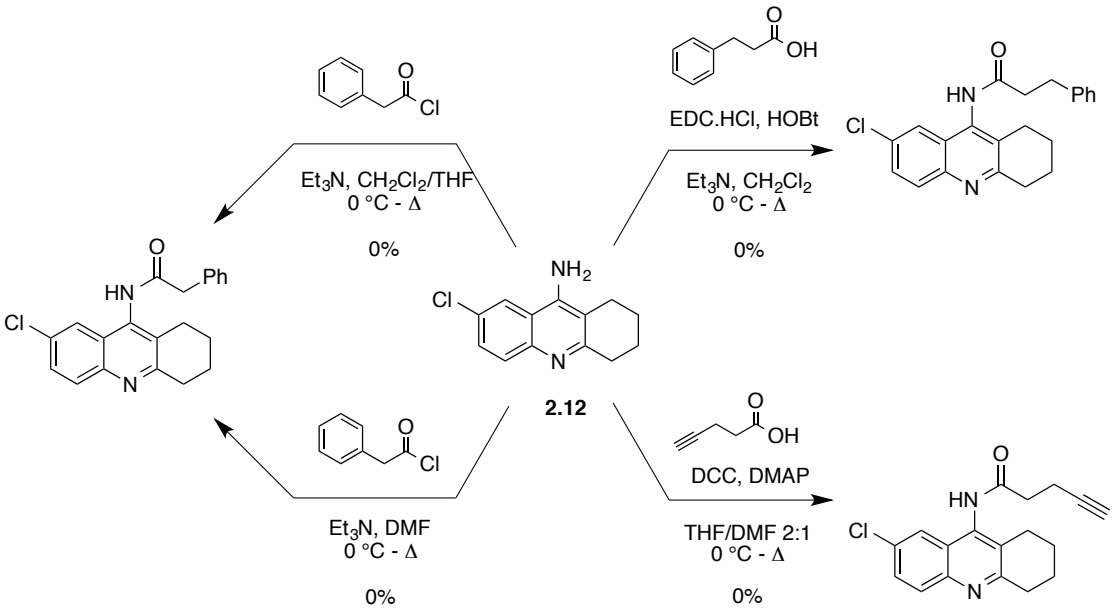

Scheme 2.3.6 *N*-Acylation of 7-chloro-9-amino-tacrine (**2.12**).

Finally, a reductive amination reaction was also attempted on the 7-chloro-9-aminotacrine (**2.12**) using a procedure reported for tacrine derivatives (Scheme 2.3.7).[268] Unfortunately, none of the desired amine was observed and the starting tacrine **2.12** was recovered.

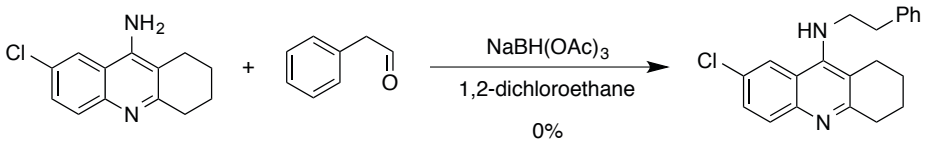

2.12

Scheme 2.3.7 Attempted reductive amination of 7-chloro-9-aminotacrine (**2.12**).

In the face of the problem of low reactivity of the amino function towards alkylation and amidation, a new approach was considered for the formation of the key C–N bond. This involved investigating reactive electrophilic tetrahydroacridines such as **2.22** (X= electrophile, Scheme 2.3.8) that is able to undergo either S_NAr amination or Pd-catalysed cross-coupling (Buchwald-Hartwig Amination, BHA). Significantly, one added advantage of using such an electronically inverted strategy is the ability to access the chemical synthesis of several potential tetrahydroacridine surrogates by replacing the nitrogen atom by an oxygen or carbon linker.

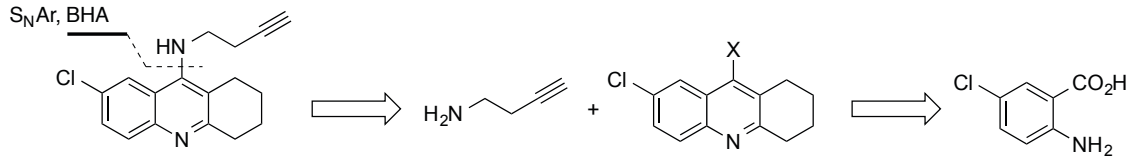

2.9 **2.22** **2.23**

Scheme 2.3.8 Retrosynthetic plan 2 for the alkyne intermediate **2.9**.

Several electrophiles were investigated: halides (Cl, Br and I), trifluoromethanesulfonate and nosylate. The 7,9-dichloro-1,2,3,4-tetrahydroacridine (**2.22.1**) and the 9-bromo-7-chloro-1,2,3,4-tetrahydroacridine (**2.22.2**) were converted by condensation of the commercially available 5-chloroanthranilic acid (**2.23**) with cyclohexanone in presence of phosphorus oxychloride (quantitative) and phosphorus oxybromide (23%), respectively (Scheme 2.3.9).

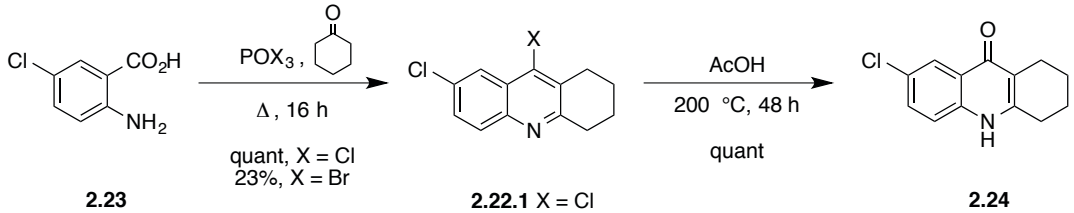

2.23 **2.22.1** X = Cl **2.22.2** X = Br **2.24**

Scheme 2.3.9 Synthesis of 9-halo-7-chloro-1,2,3,4-tetrahydroacridines **2.22.1** and **2.22.2**.

Condensation of the starting 5-chloroanthranilic acid (**2.23**) with cyclohexanone initially formed an imine that tautomerised to a conjugated enamine (Scheme 2.3.10). Cyclisation can then occur by addition of the enamine to the activated carboxylic acid derivative (acid chloride). Conversion to the chloro derivative **2.22.1** probably proceeds by *O*-phosphorylation of the vinylogous amide to create a leaving group, followed by nucleophilic aromatic substitution by displacement with the chlorine anion generated *in situ*.

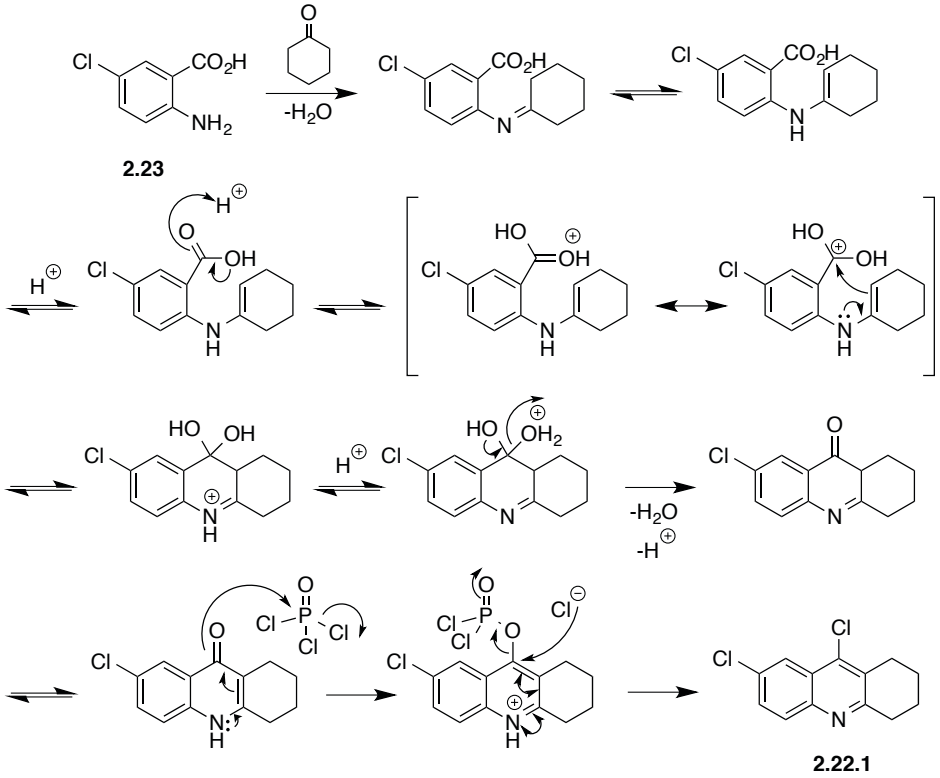

Scheme 2.3.10 Proposed mechanism for the formation of 7,9-chloro-1,2,3,4-tetrahydroacridine (**2.22.1**).

Hydrolysis of the dichloride **2.22.1** in glacial acetic acid at 200 °C afforded the 7-chloro-1,2,3,4-tetrahydroacrid-9(10*H*)-one (**2.24**) in quantitative yield. Subsequent triflation of the intermediate **2.22** with triflic anhydride yielded to the highly electrophilic 7-chloro-1,2,3,4-tetrathydroacridin-9-yl trifluoromethanesulfonate (**2.22.3)** in excellent yield as a stable white crystalline solid (Scheme 2.3.11). These three steps have been conducted on a multigram scale with an excellent 90% yield over three steps.

To extend our family of electrophilic coupling partners, attempts to convert the intermediate **2.24** into nosylate **2.22.4** were investigated using nosyl chloride and DIPEA at rt and 40 °C as recently reported on coumarin derivatives (Scheme 2.3.11).[269] Unfortunately, almost no conversion of **2.24** was obtained and only traces of **2.22.4** were observed by LCMS.

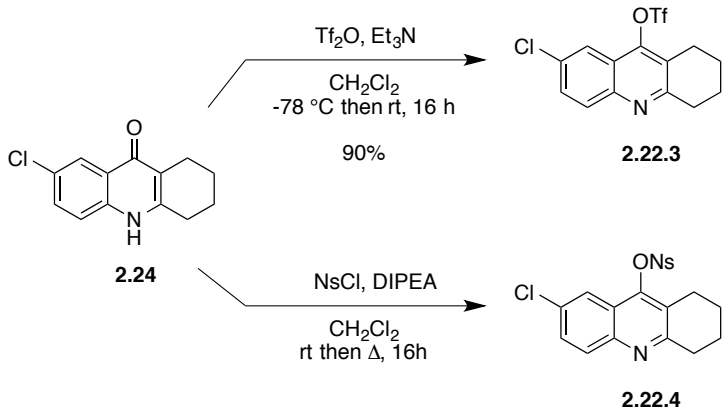

Scheme 2.3.11 Synthesis of electrophiles **2.22.3** and **2.22.4**.

Finally, treatment of the 7-chloro-9-aminotetrahydroacridine (**2.12**) with isoamyl nitrite, iodine and copper iodide in 1,2-diiodomethane at 85 °C afforded, through the formation of a diazoamino-intermediate, the desired 9-iodo-7-chloro-1,2,3,4-tetrahydroacridine (**2.22.5**) in moderate 43% yield using a procedure reported for pyridine derivatives (Scheme 2.3.12).[270]

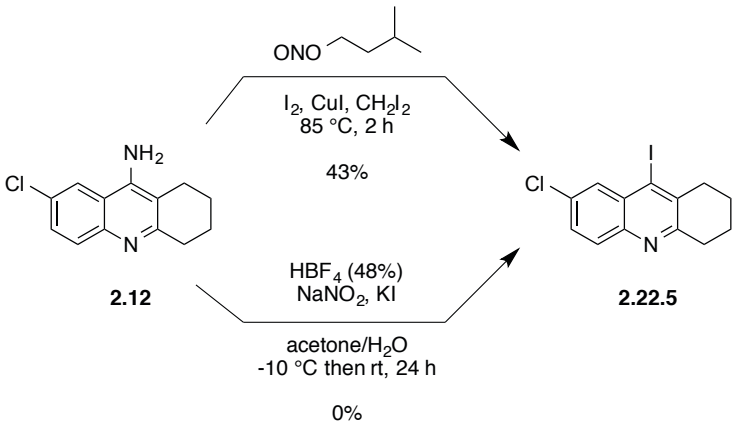

Scheme 2.3.12 Synthesis of electrophile **2.22.5**.

Smith and co-workers proposed a mechanism involving the formation of radical species (Scheme 2.3.13).[270] Initially, the amine rapidly reacted with isoamyl nitrite to form a

diazoamino derivative followed by another molecule of amine to form a triazole species. Subsequent addition of a second equivalent of isoamyl nitrite lead to the rapid formation of the iodo adduct that can be explain by thermal decomposition of the triazene intermediate to form a highly reactive radical species that can react with iodine.

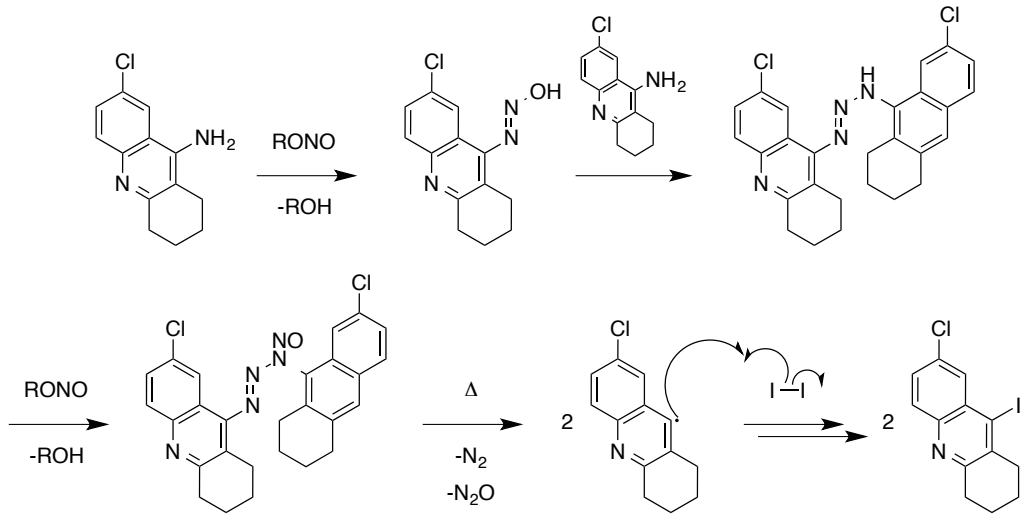

Scheme 2.3.13 Proposed mechanism for the formation of the electrophile **2.22.5**.

However, the literature describes this process as not being compatible with large-scale reactions. Several attempts on modest 250 mg scales proved to be unfruitful. Besides, as the 1,2-diiodomethane, used here as a solvent, is quite expensive and not very attractive on environmental grounds Therefore, an alternative protocol proceeding through the more conventionally recognised diazonium salt formation for pyridine derivatives was investigated in a Sandmeyer-type reaction (Scheme 2.3.12).[271,272] Unfortunately, the reaction did not proceed with our substrate.

It is noteworthy that efforts have also been made towards the synthesis of the 7-methoxy-9-chloro-1,2,3,4-tetrahydroacrines (**2.26**, Scheme 2.3.14). However, **2.26** was obtained only in about 30% yield on each attempt, while the chlorinated analogue **2.22.1** was formed quantitatively. For this reason, further investigations were carried out with chlorinated derivatives.

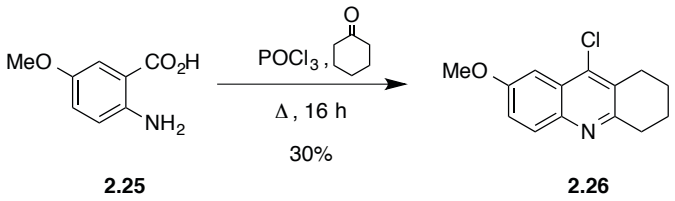

Scheme 2.3.14 Synthesis of electrophile **2.26**.

The first attempts towards the synthesis of PSL-linker scaffold explored nucleophilic aromatic substitution (S_NAr) to introduce the linker onto the tetrahydroacridine derivative. Commonly described in literature,[273] S_NAr reactions on 9-chloro-tetrahydroacrine were reported with radically varying efficiencies. Conditions were tested on the dichloride derivative **2.22.1** with 1-amino-3-butyne with and without base (Et_3N) at reflux in pentanol (Scheme 2.3.15). However, no conversion was observed even after several days of reaction.

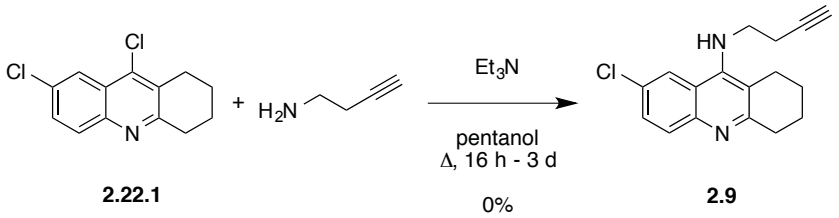

Scheme 2.3.15 Attempted nucleophilic aromatic substitution reaction.

Given the widespread success of Buchwald-Hartwig protocols to effect amination of aryl halides and triflates,[274–276] our attention turned to Pd-catalysis. Furthermore, the emergence of microwave technology as a convenient tool to increasing reaction rates was extremely appealing.[277] Reactions that previously required hours to run to completion can be finished within minutes in some cases. We therefore explored the feasibility of our previously synthesised electrophiles **2.22** in Buchwald-Hartwig Amination (BHA) reactions assisted by microwave irradiation, for which results are described Table 2.3.2. There are only a few publications on the synthesis of *N*-alkyltacrines and their analogues using Pd-catalysis.[278–280] However, our approach was inspired by Renard and co-workers who have recently reported a study in which they investigated the effects of various palladium sources, ligands, bases and solvents to find optimum conditions for the preparation of *N*-alkylated tacrine analogues.[280]

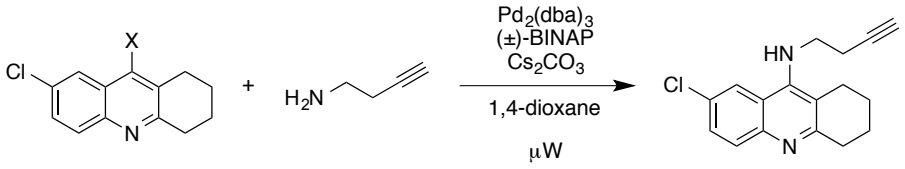

2.22 **2.9**

Entr	SM	X	Irradiation time	T (°C)	SM conversion	Isolated Yield
1	**2.22.1**	Cl	2 x 1 h	150	60%	27%
2	**2.22.1**	Cl	1 h + 2 x 30 min	150	40%	degradation
3	**2.22.1**	Cl	1 h 30	150	50%	30%
4	**2.22.2**	Br	1 h	150	>99%	92%
5	**2.22.5**	I	1 h	150	>99%	40%
6	**2.22.3**	OTf	1 h 30	150	>99%	32%
7	**2.22.3**	OTf	1 h	130	>99%	85%
8	**2.22.3**	OTf	1 h	100	>99%	80%

Table 2.3.2 Reactivity of electrophiles **2.22** under microwave-assisted Pd-catalysed BHA.

In this investigation, 1.5 equiv of amine and 2.5 equiv of base were used along with the catalyst precursor (6 mol %) and the ligand (12 mol %). The conversion of the starting material (SM) was determined by analysing the crude reaction mixtures using ^{1}H NMR spectroscopy. While the use of chloride **2.22.1** only exhibited moderate conversion (40 to 60%, entries 1 to 3), we were pleased to observe that the analogous **2.22.2** (entry 4), **2.22.3** (entries 6 to 8), and **2.22.5** (entry 5) underwent complete conversion. This difference of reactivity is not surprising as despite improvements, this transformation has long been proficient with aryl bromides or iodides whereas aryl chlorides react more slowly.[277,281] Isolation of the cross-coupled product by column chromatography on silica gel required some optimisation (due to the acidity of the silica), explaining a noticeable difference between the conversion of SM and isolated yield (entries 5 and 6 for instance). Unusual eluent system of Et_2O and MeOH was found to be much more effective than treating silica gel with Et_3N.

Given the high yield realised for this BHA, and more general pharmacological interest of substituted tacrines, the optimised conditions were used to explore the generality of this Pd-catalysed amination of the triflate **2.22.3** with various amines. This methodology investigation is described in the following section.

2.3.2 Buchwald-Hartwig Amination (BHA) approach to the synthesis of functionalized 1,2,3,4-tetrahydroacridine derivatives

Nitrogen-containing heterocyles are key functional components of many drugs and other biologically active molecules. For instance, tacrine (**2.6**) is arguably a key structural motif in bioorganic chemistry, medicinal chemistry and drug discovery.[282–285] Besides, the chemical modification of tacrine is of great interest for the development of multipotent drugs prepared by conjugation of the THA scaffold with other medicinally relevant groups.[286] Thus, the development of the multi-target-directed ligand strategy requires reliable and selective synthetic methods possessing broad substrate scope to assemble tacrines, and more broadly, 1,2,3,4-tetrahydroacridines.[287,288]

In view of the promising preliminary results, demonstrating the high reactivity of triflate **2.22.3** combined with its ease of preparation, the scope of the BHA reaction was evaluated using additional selected amines (Scheme 2.3.16).

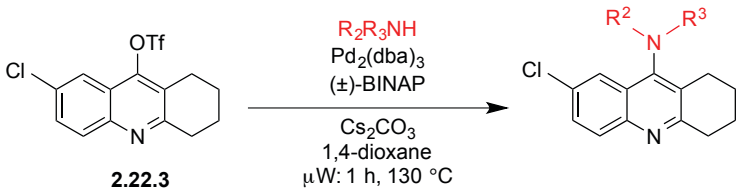

Scheme 2.3.16 Buchwald-Hartwig amination approach to the synthesis of tacrines.

The reaction of the aryl triflate **2.22.3** and 1-amino-3-butyne was initially used to rapidly screen suitable microwave reaction conditions (Table 2.3.2). Tris(dibenzylideneacetone)di-palladium(0), $Pd_2(dba)_3$, was the catalyst of choice to form *in situ* Pd(0) complexes with suitable ligands through substitution of the dba moieties.[289–291] Dioxane was used as solvent as it is commonly applied in Pd-catalysed C–N bond-forming reactions using microwave irradiation.[292,293] The highly polar solvent is efficiently heated under microwave irradiation and has a suitably high boiling point allowing the screening of high temperatures. The catalyst system includes an electron-rich bidentate (±)-BINAP ligand, which is superior compared to monodentate ligands by inhibiting competing β-hydrogen elimination during the process.[290,291] As second-generation catalysts, the combination of $Pd_2(dba)_3$ and BINAP in the presence of a base constitutes a superior catalyst system for the cross-coupling of amines.[275] Finally the use of insoluble weak inorganic base, such as Cs_2CO_3, has also improved the substrate scope with respect to base-sensitive functional groups.[276,293]

The mechanism of this amination follows the classical steps of palladium-catalysed reactions (Scheme 2.3.17). Starting from the oxidative addition of the trifluoromethanesulfonate species to Pd(0), introduction of the amine proceeds by ligand exchange before formation of the desired product by reductive elimination. It was found that an unproductive side reaction can compete with the reductive elimination step wherein the amine moiety undergoes a β-hydride elimination yielding an imine derivative and reduction of the aryl triflate.[274]

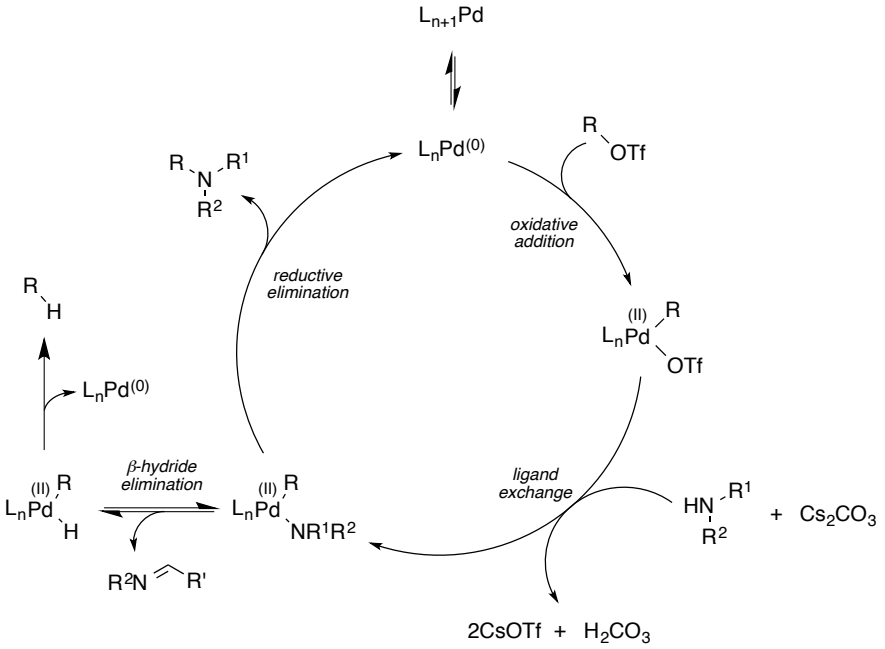

Scheme 2.3.17 Buchwald-Hartwig amination reaction mechanism.

Exposure of primary amines such as, benzylamine, *n*-butyl amine, aniline, and the bulky 1-aminopyrene resulted in the formation of the corresponding *N*-substituted tacrines **2.27**–**2.29** in good to excellent isolated yields (Figure 2.3.1), which constituted substantial improvement in comparison to previous reports that used the aryl chloride (9-chlorotacrine analogue).[278–280]

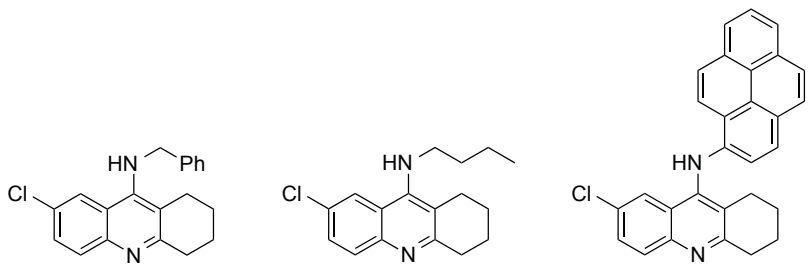

2.27 100% **2.28** 71% **2.29** 96%

Figure 2.3.1 BHA reaction products from primary amines.

To our delight, the by-product from the potential β-hydride elimination of benzylamine was not observed (Figure 2.3.2).

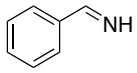

Figure 2.3.2 By-product from β-hydride elimination of benzylamine.

Significantly, this method was compatible with both electron-rich and electron-poor anilines bearing a variety of synthetically valuable functional groups (Figure 2.3.3). 4-Bromoaniline was successfully cross-coupled (91%) in adduct **2.31**, highlighting the high reactivity of triflate **2.22.3** in BHA reactions. Electron-rich anilines such as *p*-anisidine also exhibited good reactivity to afford **2.32** in 65% yield.

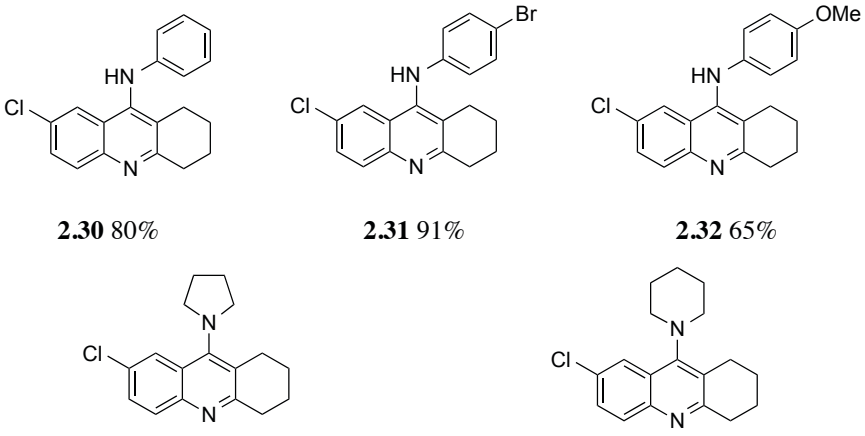

2.30 80% **2.31** 91% **2.32** 65%

2.33 87% **2.34** 54%

Figure 2.3.3 BHA reaction with aniline derivatives and secondary amines.

Secondary cyclic amines such as pyrrolidine and piperidine underwent coupling in 87% (for **2.33**) and 54% (for **2.34**), respectively (Figure 2.3.3). These results suggest that the cross-coupling of **2.22.3** with secondary amines is less sensitive to steric hindrance in contrast to previous reports using 6,9-dichlorotetrahydroacridine, where cyclic secondary amines were poor cross-coupling partners.[280] Attempts to further expand the reaction scope to include allylamine and propargylamine were fruitful and the corresponding adducts **2.35** and **2.36** were isolated in chemical yields of 64% and 90% respectively. Notably, the use of 3-aminopyridine as an electron-deficient heteroaromatic nucleophile also led to the *N*-arylated product **2.37**, in good isolated yield (81%).

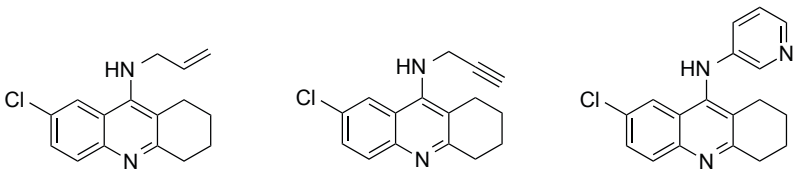

2.35 64% **2.36** 90% **2.37** 81%

Figure 2.3.4 BHA reactions of **2.22.3** with bifunctional and heteroaromatic amines.

Other nitrogen nucleophiles such as *tert*-butylsulfinamide, benzamide and diethyl phosphoramidate also successfully engaged in BHA reactions under our optimised conditions (Figure 2.3.5). To our delight, the reactions displayed, not only total conversion of the triflate **2.22.3** but also a high chemical efficiency. The sulfinylated **2.38**, acylated **2.39** and phosphorylated **2.40** tacrines were obtained in good to excellent isolated yields of 67%, 76% and 87% respectively.

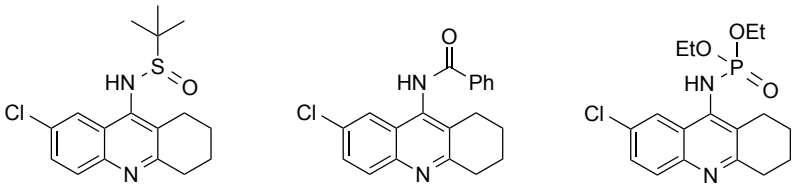

2.37 67% **2.38** 76% **2.40** 87%

Figure 2.3.5 BHA reactions with other nitrogen species.

Amine substrates containing additional functional groups, such as 2-(2-aminothoxy)ethanol and glycine ethyl ester, were also subjected to our conditions and gave the aminated adducts **2.41** and **2.42** with excellent yields (96% and 92%, respectively).

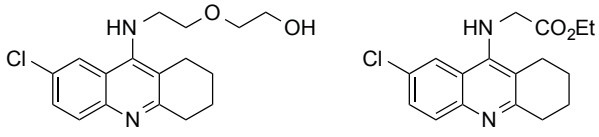

2.41 96% **2.42** 92%

Figure 2.3.6 BHA reaction with bifunctional amines.

It is noteworthy that total conversion of triflates **2.22.3** was observed for the majority of the reactions, with significantly reduced reaction times and lower temperature compared to 9-

chlorotacrine analogue. The reduced byproducts were not observed to any significant extent under our conditions. Besides these features, a wide range of functionality was tolerated, including unprotected alkynes, free alcohols, olefins, bromo- and chloroarenes, ethers and ester groups. Additionally, in the cross-couplings, complete chemoselectivity for the triflate group versus the chloro substituent was observed. Consequently, this method provides efficient access to new tacrine derivatives containing functionality suitable for further potential ligation to a variety of other valuable building blocks via Pd-cross coupling (**2.9**, **2.31**, **2.35**, **2.36**), click chemistry (**2.9**, **2.36**), metathesis (**2.35**), thiol-ene reaction (**2.9**, **2.35**, **2.36**), or ester- and amide-bond formation (**2.41**, **2.42**).

Finally, to extend the scope of the cross-coupling methodology to other 1,2,3,4-tetrahydroacridines, the application of triflate **2.22.3** was explored in synthetically useful Pd-catalyzed C–C bond forming reactions such as Sonogashira, Suzuki, and cyanation cross-couplings (Scheme 2.3.18). Sonogashira reaction with phenyl acetylene afforded the corresponding product **2.43** in excellent isolated yield (98%). Furthermore, it was also possible to access 9-phenyl-1,2,3,4-tetrahydroacridine derivative (**2.44a**) in 71% yield under Suzuki cross-coupling conditions,[294] with a minor bisarylated product (**2.44b**, 28%) resulting from a secondary arylation of the chlorine substituent in position 7. A synthetically valuable nitrile analogue **2.45a** was obtained in 75% yield through cyanation of the triflate **2.22.3** using $Zn(CN)_2$ under Pd-catalysis in dry DMF, along with a minor amount of the biscyanated product (**2.45b**, 25%). Finally, we explored C–S and C–O bond-forming reactions using thiophenol and benzyl alcohol respectively. Gratifyingly, the 9-mercapto-1,2,3,4-tetrahydroacridine (**2.46**) and 9-benzyloxy-1,2,3,4-tetrahydroacridine (**2.47**) were formed after 1 h under our optimised microwave conditions in 83% and 60% yields respectively.

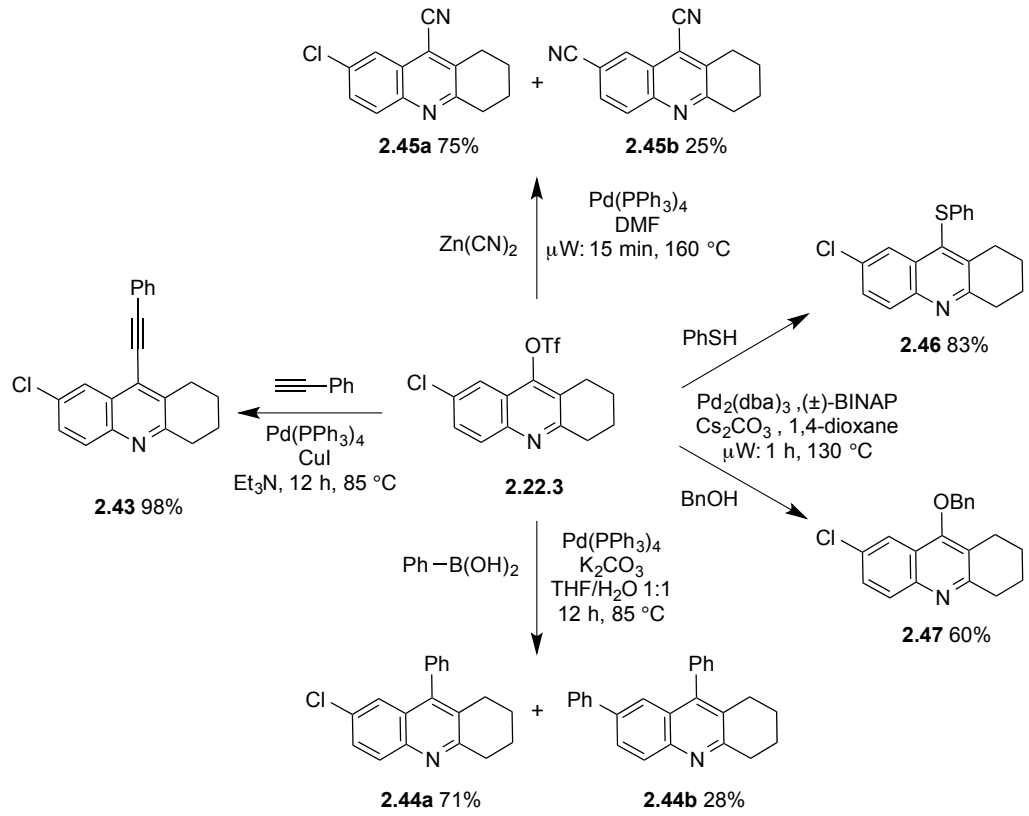

Scheme 2.3.18 Application of the triflate **2.22.3** in C-C, C-S and C-O bond-forming reactions.

In summary, we have demonstrated 1,2,3,4-tetrahydroacridin-9-yl trifluoromethanesulphonate **2.22.3** to be a superior substrate in Buchwald-Hartwig amination reactions, and to display broader substrate scope and applicability, in comparison to previously employed 9-chloro-derivatives. A variety of amines (alkyl amines, anilines, heteroaryl amines) were shown to react smoothly under microwave conditions to give the corresponding *N*-alkylated tacrines in reasonable to excellent yields. Even secondary amines and other poorly nucleophilic nitrogen species such as *tert*-butylsulfinamide, benzamide and diethyl phosphoramidate were shown to react efficiently. Functional groups including terminal alkynes, alcohols, bromo- and chloro-arenes, ethers, esters, and olefins were tolerated. Investigation of other Pd-catalyzed C–C, C–O and C–S bond-forming reactions also showed promise for the development of practical routes to 9-substituted 1,2,3,4-tetrahydroacridines, and extend the application of this heterocycle in drug design.

This work has been published by the *European Journal of Organic Chemistry*, **2014**, 3468-3474, DOI: 10.1002/ejoc.201402122.

2.3.3 Synthesis of hybrid 2.8

Following the outlined synthetic strategy towards the hybrid reactivator **2.8**, a Sonogashira cross-coupling of the methyl 6-bromo-3-hydroxypicolinate (**2.15**) with the terminal alkyne intermediate **2.9** was explored. The advantage of this reaction was to gain 2 steps compared to the synthesis of hybrids described in the literature by avoiding protection/deprotection of the phenolic function.[242–245,262] A procedure using dichlorobis(triphenylphosphine)palladium(II) described on aryl derivatives that was shown to be compatible with free phenol function was applied,[295] but only the homodimer **2.48** was obtained (Scheme 2.3.19).

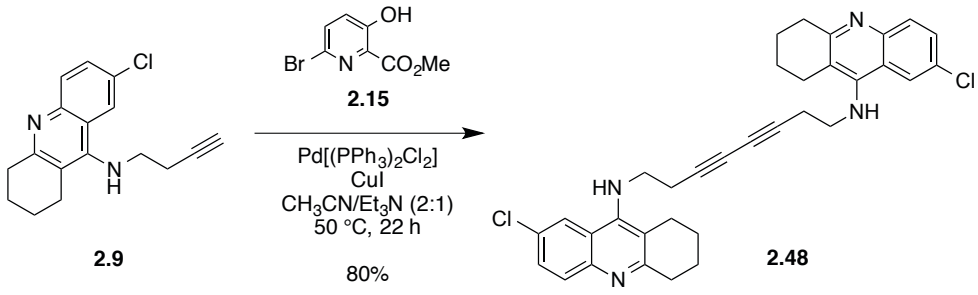

Scheme 2.3.19 Attempted Sonogashira cross-coupling reaction using the pyridine derivative **2.15**.

Therefore, established Sonogashira cross-coupling conditions using tetrakis(triphenylphosphine)palladium(0) optimised for hybrid synthesis were explored.[245] The reaction between the methyl 3-(benzyloxy)-6-bromopicolinate (**2.10**) and the terminal alkyne **2.9** afforded the desired product **2.49** in 66% isolated yield.

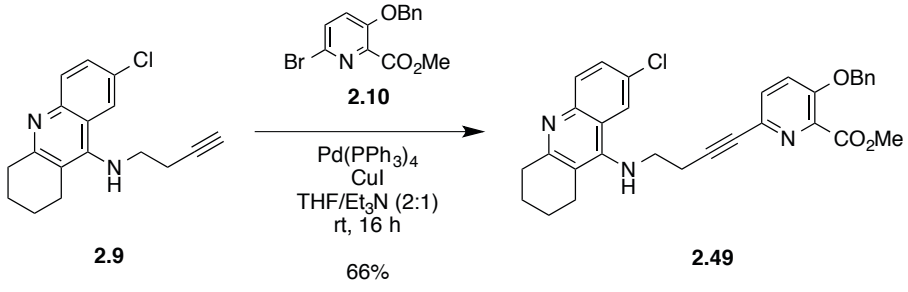

Scheme 2.3.20 Sonogashira cross-coupling reaction of **2.9** and **2.10**.

The reaction mechanism has not been fully elucidated but to date most researcher groups agree that it follows the familiar pathways of Pd(0) catalysis (Scheme 2.3.21). Starting from the oxidative addition of the aryl bromide **2.10** to Pd(0), the copper acetylide undergoes transmetalation before forming the desired product by reductive elimination. A *trans-cis* isomerisation may occur to favour the ligand orientation for subsequent reductive elimination. The copper(I) co-catalyst is used to activated the terminal alkyne species (copper cycle, Scheme 2.3.21). Also, the presence of a suitable base, such as Et_3N, results in the formation of π-complex, increasing the acidity of the terminal alkyne proton to lead to the formation of a copper acetylide species involved in the transmetalation step.

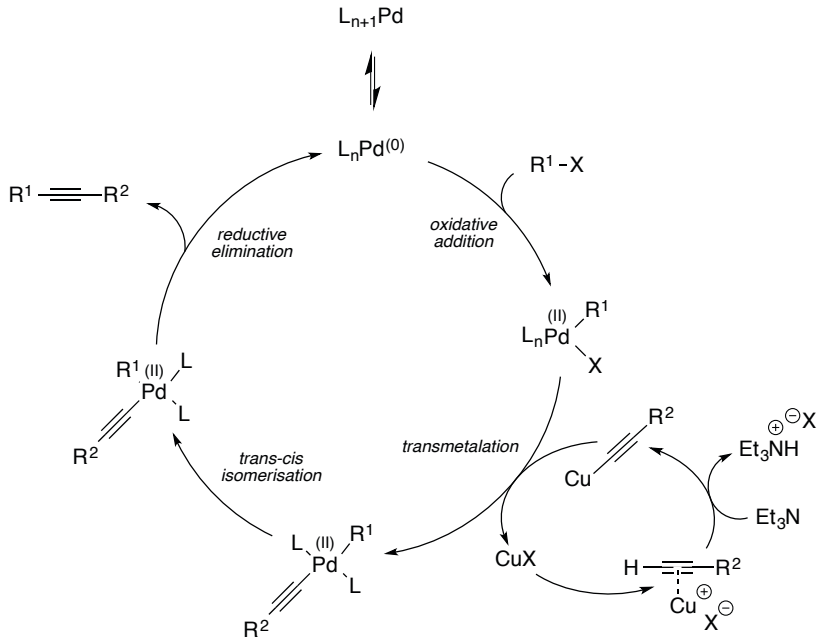

Scheme 2.3.21 Proposed mechanism for Sonogashira cross-coupling reaction.

Afterwards, a "one-pot" alkyne reduction and *O*-debenzylation was investigated to afforded the adduct **2.50**.

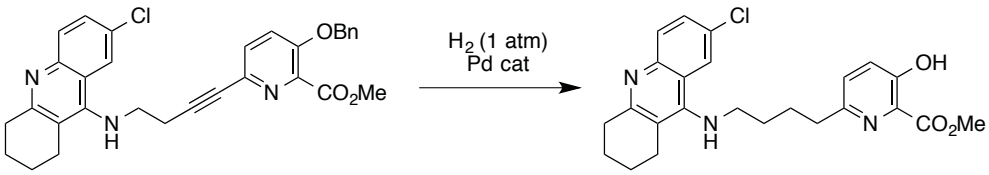

2.49 **2.50**

Scheme 2.3.22 "One-pot" alkyne reduction and *O*-debenzylation.

Due to the array of functionalities present within alkyne **2.49** that can potentially react under hydrogenation conditions, 4 products can be envisaged (Figure 2.3.7).

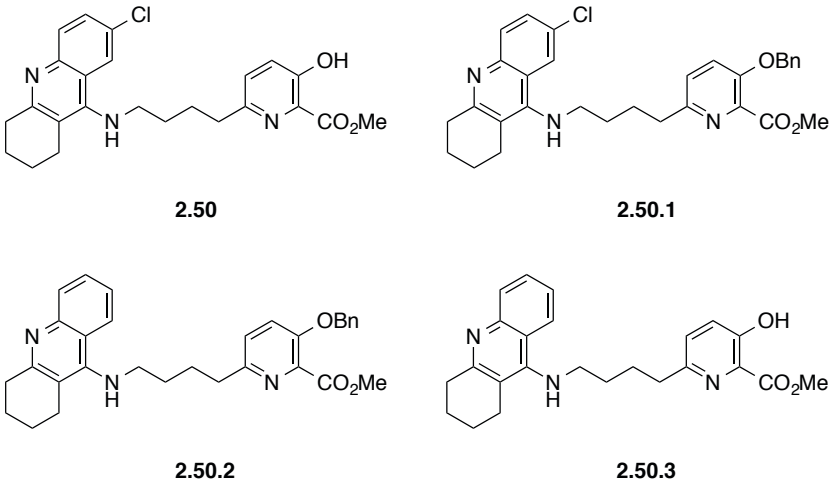

2.50 **2.50.1**

2.50.2 **2.50.3**

Figure 2.3.7 Possible products from exposure of **2.49** to hydrogenation/hydrogenolysis conditions.

Various conditions were explored (palladium source, catalyst loading, solvent and reaction time) and the results are described in Table 2.3.3. Reactions in MeOH were relatively fast and quantitative after 16 h, but afforded the corresponding dehalogenated phenol **2.50.3** (Entries 1 and 2). On the contrary, reactions in EtOAc were slower: 2-3 h to fully reduce the alkyne and convert the starting material **2.49** into **2.50.1**, with 16-40 h needed to deprotect the benzyl

group, yielding a mixture of compounds (Entries 3, 4 and 10). However if the reaction was left longer under H_2 atmosphere (30-72 h), degradation of the products was observed by LCMS.

The desired product **2.50** has been isolated as main product only twice: (1) in presence of Pearlman's catalyst ($Pd(OH)_2/C$) in EtOAc at rt for 7 h (entry 5); and (2) using a combination of palladium catalysed reactions (entry 10): (i) the triple bond was reduced into alkane **2.50.1** in 2 h using Pearlman's catalyst in EtOAc, then after filtrating and evaporating the solvent, (ii) the residue was subjected to *O*-debenzylation using "Pd black" (a Pd/C with bigger contact surface) in MeOH and 1,4-cyclohexadiene as source of hydrogen.[296] Unfortunately, and despite several attempts, this result could not be reproduced.

Entry	Catalyst	Pd equiv	Solvent	Time	Product
1	$Pd(OH)_2/C$ (Pearlman, 20 wt.%)	0.2	MeOH	16-22 h	**2.50.3**
2	$Pd(OH)_2/C$	0.1	MeOH	4 h	**2.49**/**2.50.1** 1 : 1
3	$Pd(OH)_2/C$	0.2	EtOAc	2 h	**2.49**/**2.50.1**/**2.50**/**2.50.3** 2 : 29 : 1 : 2
4	$Pd(OH)_2/C$	0.2	EtOAc	16 h	**2.50**/**2.50.3** 1 : 1
5	$Pd(OH)_2/C$	0.2	EtOAc	7 h	**2.50** (80%)[a]
6	PtO_2 (Adam)	0.2	EtOAc	2 h	**2.50.1**
7	Pd/C (10 wt.%)	0.1	EtOAc	16 h	**2.50.1**
8	Pd/Al_2O_3 (5 wt.%)	0.1	EtOAc	16 h	**2.49**
9	$Pd/CaCO_3.PbO_2$ (Lindlar, 5 wt.%)	0.1	EtOAc	16 h	**2.49**
10	i) $Pd(OH)_2/C$ ii) Pd black + 1,4-cyclohexadiene	i) 0.2 ii) 0.2	i) EtOAc ii) MeOH	i) 2 h ii) 2 h	i) **2.50.1** ii) **2.50** (65%)
11	Pd black + 1,4-cyclohexadiene	0.2	MeOH	7 - 24 h	**2.49**
12	Pd/C (Degussa type E101 NE/W, 10 wt.%)	0.2	EtOAc	4 h	**2.49**
13	Degussa E101 + Pearlman	0.2 + 0.2	EtOAc	2 h	**2.50**/**2.50.3** 1 : 2

Table 2.3.3 Hydrogenation conditions investigated to afford the adduct **2.50**.

[a] This results was only obtained on one occasion and could not be reproduced.

Attempts using 1,4-cyclohexadiene as source of hydrogen was explored (entry 11) but did not show any conversion of the starting material **2.49** even after 24 h. Pd/C (Degussa Type E101 NE/W) was shown to be selective for deprotection of benzyl groups in the literature.[297] Unfortunately, these conditions were found to be ineffective for substrate **2.49** (entry 12), and a combination with Pearlman's catalyst (1:1 by wt.) resulted substantially in the cleavage of the aryl-chlorine bond (entry 13). In this investigation it appeared that the triple bond can be selectively and rapidly reduced into the corresponding alkane, but the phenolic deprotection and the halide cleavage displayed similar kinetics under all conditions screened.

Facing the difficulty of forming the product **2.50** without cleavage of the chlorinated-aryl bond, another approach was considered and investigated (Scheme 2.3.23). Contrasting with the retrosynthetic pathway 2, this strategy relied first on the coupling between the amino-linker and the reactivator precursor **2.10** before being reduced into the corresponding alkane and furthermore involved in BHA reaction with triflate **2.22.3**.

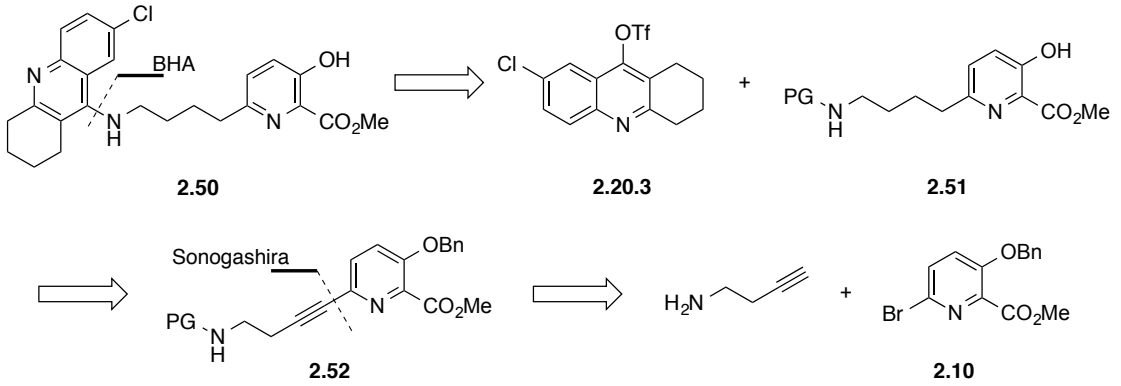

Scheme 2.3.23 Retrosynthetic pathway 3 to afford the intermediate product **2.50**.

Prior to embarking, this novel approach has been investigated with 3 different starting amines: propargyl amine, 1-amino-3-butyne and pent-4-yn-1-amine. Due to the atmospheric degradation potential of these amines,[298] the first step consisted in the protection of the amine function with di-*tert*-butyl dicarbonate (Scheme 2.3.24) at 0 °C for 1 h. The corresponding boc-protected amines **2.53.1**, **2.53.2** and **2.53.3** were obtained in excellent yields (95%, 96% and 97%, respectively). Subsequent Sonogashira cross-coupling, under the same conditions used for the isolation of alkyne **2.49**, afforded the corresponding alkynes **2.52.1**, **2.52.2** and **2.52.3** in excellent yields (84%, 91% and 97%, respectively).

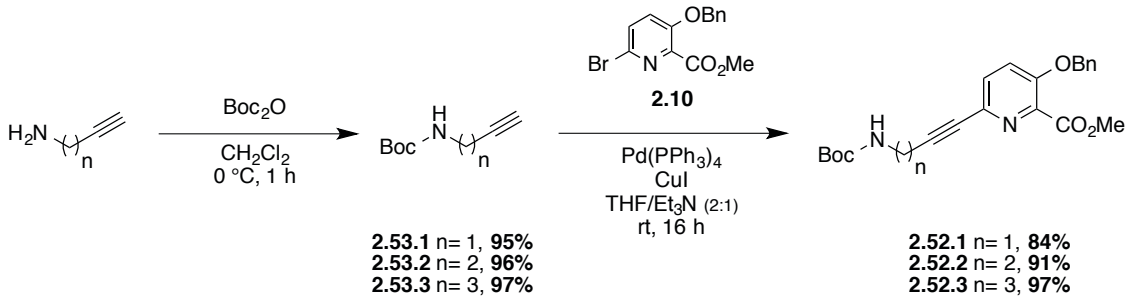

Scheme 2.3.24 Synthesis of the intermediate products **2.52**.

As part of attempts to circumvent the selective reduction/debenzylation, hydrogenation, BHA and Boc deprotection reactions were tested on the intermediate products **2.52** (Scheme 2.3.25). Unfortunately, all attempts, independently or combining reactions, remained unfruitful probably due to the instability of the primary amines.

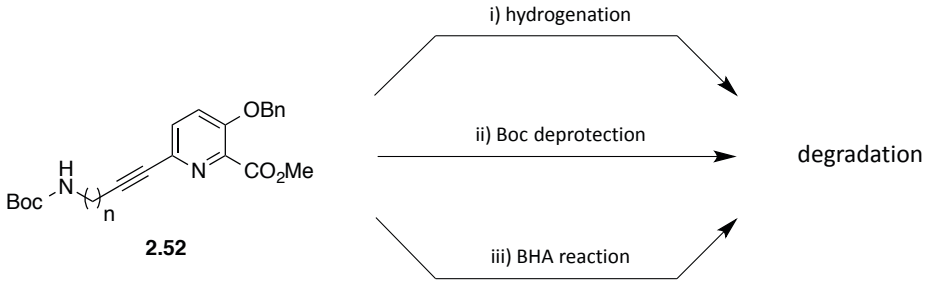

Scheme 2.3.25 Different attempts to convert the intermediates **2.52** to primary amines.

However, the amount of the product **2.50** previously isolated (Table 2.3.3) was sufficient and could be used to complete the synthesis of hybrid reactivator **2.8** in sufficient quantity to permit preliminary bioassays. The ester **2.50** was converted into aldehyde **2.54** in good yield (55%) using a three-step sequence including: (a) TBS protection of the phenol function; (b) reduction of methyl ester into the corresponding aldehyde using DIBAL-H; (c) subsequent deprotection of the silylether using TBAF.

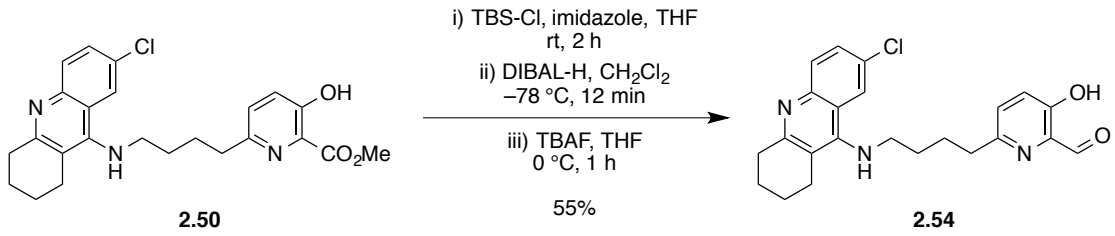

Scheme 2.3.26 Three-step ester to aldehyde conversion.

Ultimately, the desired hybrid **2.8** was isolated by condensation of hydroxylamine onto the aldehyde **2.54** in presence of anhydrous sodium acetate (Scheme 2.3.27). The desired aldoxime **2.8** was recovered in moderate 34% yield after purification by column chromatography.

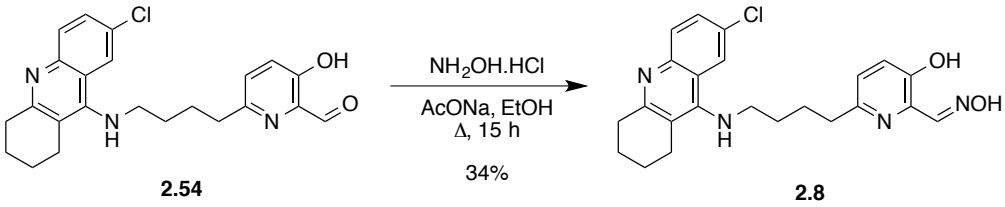

Scheme 2.3.27 Oxime formation reaction to afford the hybrid reactivator **2.8**.

Hence, the final hybrid reactivator **2.8** was obtained in 10-steps with a non-optimised overall yield of 7%. Subsequent biological evaluation was undertaken at IRBA and IBS in the groups of Dr. Florian Nachon and Dr. Martin Weik, respectively, and is discussed in chapter 4.

2.4 Synthesis of uncharged bifunctional hybrid reactivator analogues

The objectives for this part are to improve our knowledge concerning the importance of the linker length and the aliphatic ring (C ring, Figure 2.2.2) in the AChE active site. Different hindered cycles may influence the π-stacking interactions at the PAS and thus the affinity of the reactivator towards the enzyme. Therefore, analogues of hybrid **2.8** were investigated and are herein described.

2.4.1 New trifluoromethanesulfonate scaffolds

Following the route previously established (section 2.3), a novel family of electrophilic trifluoromethanesulfonates were synthesised (Scheme 2.4.1). Starting from the commercially available 5-chloroanthranilic acid, the dichloro-analogues **2.55** and **2.56** were obtained by Lewis Acid–mediated intermolecular cyclodehydration with the corresponding cyclic ketone (cyclopentanone and cycloheptanone, respectively) in good yield (81% and 80%, respectively). These intermediates were subsequently hydrolysed using acetic acid in a sealed tube at 200 °C. The two–step synthetic sequence proved to be superior over the more frequently reported direct condensation reactions of anthranilic acids and cycloalkanone via azeotropic distillation of water.[299] Subsequent triflate formation afforded the desired 5- and 7-membered ring trifluoromethanesulfonates **2.59** and **2.60** in excellent overall yields (Scheme 2.4.1).

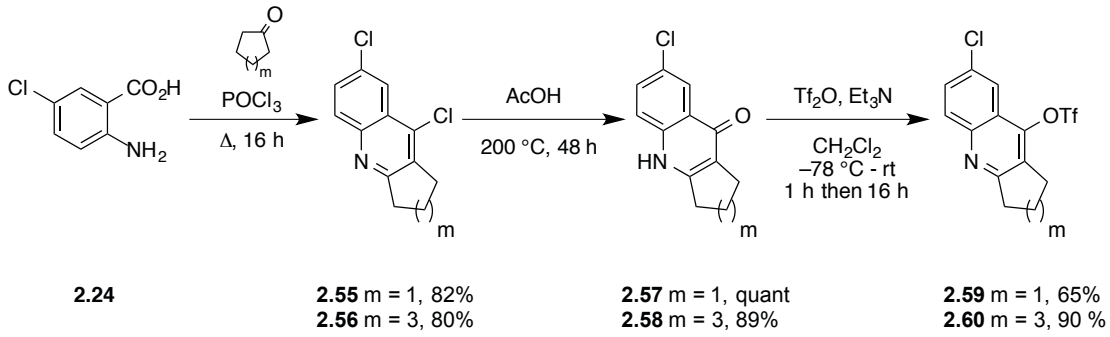

2.24

2.55 m = 1, 82%
2.56 m = 3, 80%

2.57 m = 1, quant
2.58 m = 3, 89%

2.59 m = 1, 65%
2.60 m = 3, 90 %

Scheme 2.4.1 Synthesis of triflate **2.59** and **2.60**.

Under the same conditions, the triflate **2.62** was obtained in one step from commercially available 1,2,3,4-tetrahydro-9-acridanone (**2.61)** in excellent yield (85%).

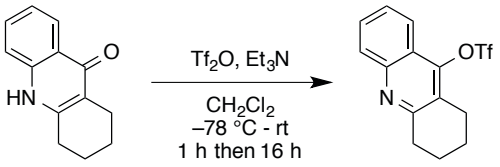

85%

2.61 **2.62**

Scheme 2.4.2 Synthesis of triflate **2.62**.

2.4.2 5-Membered ring hybrids

Focusing on the hybrids containing 5-carbon aliphatic C rings, introduction of the linker on the 7-chloro-2,3-dihydro-1*H*-cyclopenta[*b*]quinolin-9-yl trifluoromethanesulfonate (**2.59**) was achieved with the unprotected propargyl amine and 1-amino-3-butyne, respectively, using our optimised microwave assisted Pd-catalysed BHA procedure[300] to afford the desired terminal alkynes **2.63** and **2.64** in excellent yields (90% and 85% respectively, Scheme 2.4.3).

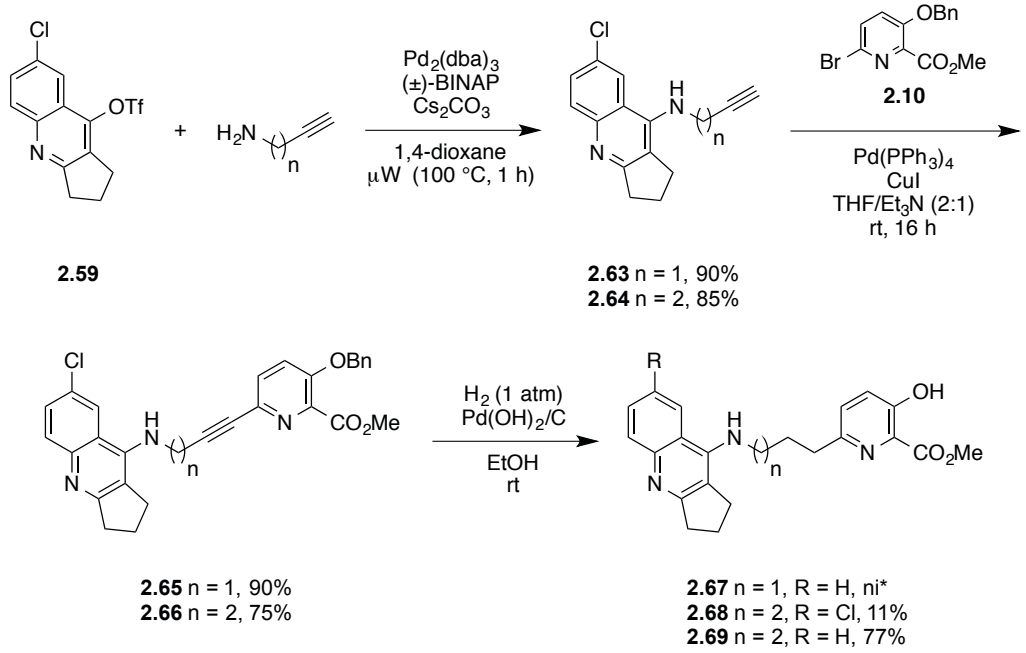

Scheme 2.4.3 Synthesis of intermediate **2.67**, **2.68** and **2.69**. (*ni: non isolated).

Subsequent Sonogashira cross-coupling with the methyl 3-benzyloxy-6-bromopicolinate (**2.10**) proceeded efficiently, isolating the corresponding hybrid precursors **2.65** and **2.66**, respectively. Then, a *one-pot* alkyne reduction and *O*-debenzylation was performed under an atmosphere of hydrogen in the presence of Pearlman's catalyst. Curiously the two structurally similar substrates exhibited quite different reactivities. While the intermediate **2.65** was completely converted into a dechlorinated derivative **2.67** in 3 hours, the alkyne **2.66** gave the two 3-hydroxypyridines **2.68** and **2.69** in high yield (88%) in a ratio 1:8 after 8 hours (Scheme 2.4.3). Experimentally, it was observed that the presence of the chlorine on the scaffold significantly effects the polarity of the intermediates **2.68** and **2.69** and allows isolation of both products by chromatography.

Following the route previously established (section 2.3), the three methyl esters **2.67**, **2.68** and **2.69** were converted into the pyridinaldoximes **2.70**, **2.71** and **2.72** respectively using the three-step sequence involving: (a) TBS protection of the phenol function using TBSOTf and 2,6-lutidine; (b) a reduction of the methyl ester into the corresponding aldehyde using DIBAL-H; (c) subsequent oximation reaction using hydroxylamine chloride and anhydrous sodium acetate in ethanol. We were pleased to isolate three new hybrids **2.70**, **2.71** and **2.72** in good yields over three steps (57%, 79% and 67% respectively) after chromatography and crystallisation.

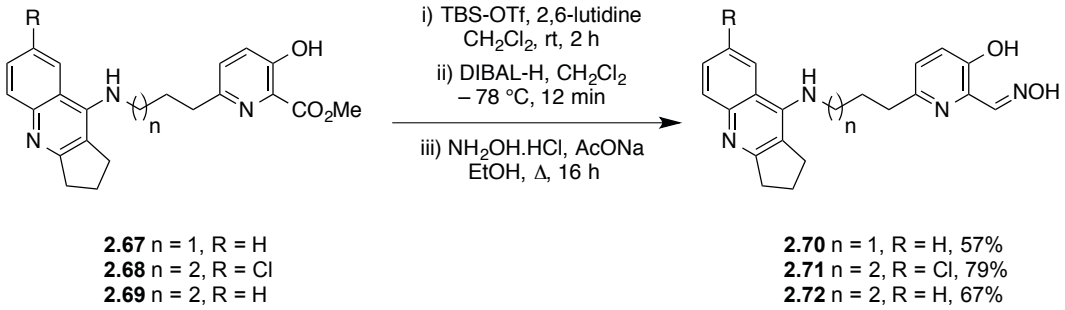

2.67 n = 1, R = H
2.68 n = 2, R = Cl
2.69 n = 2, R = H

2.70 n = 1, R = H, 57%
2.71 n = 2, R = Cl, 79%
2.72 n = 2, R = H, 67%

Scheme 2.4.4 Three-step sequence to afford the hybrid reactivators **2.70**, **2.71**, **2.72**.

Hence, the final hybrid reactivators **2.70**, **2.71** and **2.72** were obtained over 9-steps with non-optimised yields of 24%, 4% and 21%, respectively. Subsequent biological evaluations were undertaken at IRBA and IBS in the groups of Dr. Florian Nachon and Dr. Martin Weik, respectively, and are discussed in chapter 4.

Quite remarkably, in the synthesis of previous hybrids, deprotection of the relatively labile phenolic silylether was carried out as a separate step.[245] However, the low electron density of the heterocyclic ring in hydroxypyridine derivatives leads to a weakening of the Si-O bond, which offered an opportunity to induce cleavage under modified work-up conditions. Thus, it was found that a work-up using an aqueous solution of NaOH (1 M) was sufficient to deprotect the silylether and avoid the use of potentially hazardous fluoride sources in the synthesis. This problem of lability was also observed during the silylether formation step using TBSCl and imidazole, where subsequent work-up to remove the imidazole lead mostly to a deprotected product.

As an aside, an interesting observation was made in the ^{1}H NMR spectra concerning the signals of the pyridine H_A and H_B protons the final hybrids. Theoretically, H_A and H_B are supposed to

form an AB system, typically two doublets. However, in the ^{1}H NMR spectra of hybrid **2.70** (Figure 2.4.2), H_A and H_B form a closely spaced AB quartet. The pattern can be clearly recognized but has to be confirmed by the calculation of the shifts (it is the case when $\frac{\nu_{AB}}{J_{AB}} < 4$).

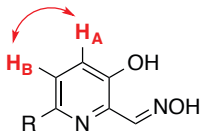

Figure 2.4.1 General structure of final hybrid pyridine moiety.

We have, $|J_{AB}| = (\nu_1 - \nu_4) = (\nu_2 - \nu_3) = (2884.54 - 2860.33) = 8.0\ Hz$

And $\nu_{AB} = \sqrt{(\nu_1 - \nu_4)(\nu_2 - \nu_3)} = \sqrt{(2884.54 - 2860.33)(2875.99 - 2868.77)} = 13.2\ Hz$

Thus, $\frac{\nu_{AB}}{J_{AB}} = \frac{8.0}{13.2} = 0.6 < 4$

Consequently the signal won't appear as 2 doublets but as an AB quartet system (Figure 2.4.2).

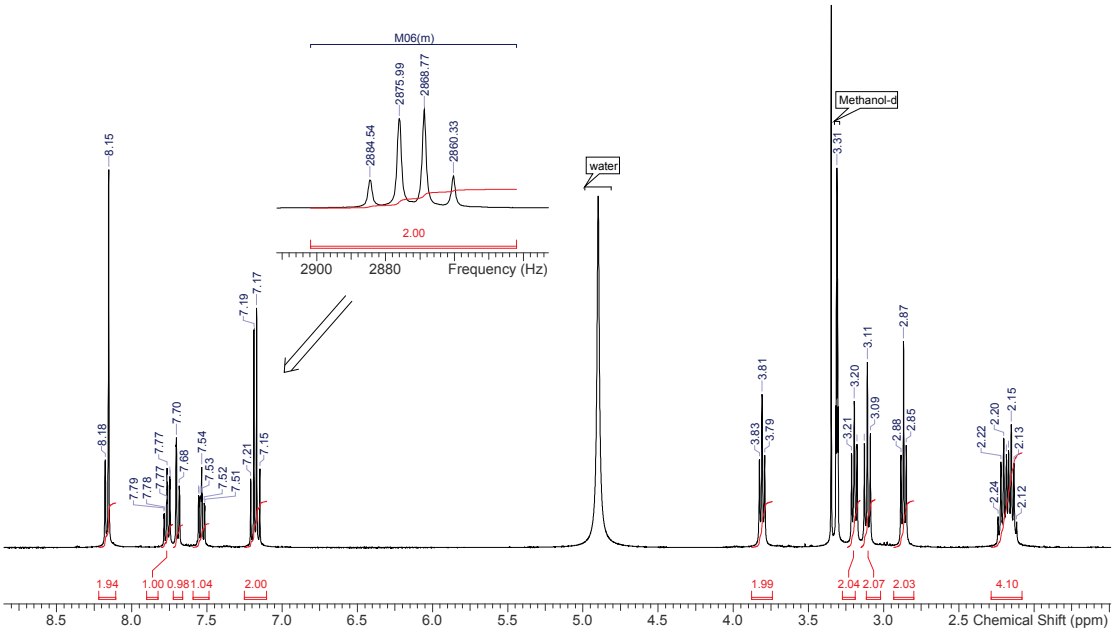

Figure 2.4.2 ^{1}H NMR spectra of hybrid **2.70** showing an AB quartet signal for the pyridine ring protons (Frequency: 400 MHz, Solvent: Methanol-d4).

Therefore, the description of the corresponding molecule in the experimental part requires the determination of other parameter as $\Delta\delta_{AB}$:

- $\nu_{center} = \frac{1}{2}(\nu_2 + \nu_3) = \frac{1}{2}(2875.99 + 2868.77) = 2872.38\ Hz$
- $\nu_A = \nu_{center} + \frac{1}{2}\nu_{AB} = 2872.38 + \frac{1}{2}\times 13.22 = 2878.99\ Hz$
- $\nu_B = \nu_{center} - \frac{1}{2}\nu_{AB} = 2872.38 - \frac{1}{2}\times 13.22 = 2865.77\ Hz$
- $\delta_A = \frac{\nu_A}{400\ MHz} = \frac{2878.99}{400} = 7.20\ ppm$
- $\delta_B = \frac{\nu_B}{400\ MHz} = \frac{2865.77}{400} = 7.16\ ppm$
- $\Delta\delta_{AB} = |\delta_A - \delta_B| = 7.20 - 7.16 = 0.04\ ppm$

Thus, the quartet signal can be described as followed: 7.18 ppm (ABq, $\Delta\delta_{AB}$ = 0.04, *J* = 8.0 Hz, 2H, $H_A + H_B$)

NB: When the ratio $\frac{\nu_{AB}}{J_{AB}} > 4$, the pattern has to be treated as first order, i.e., as two doublets.

2.4.3 6-Membered ring hybrids

Despite the synthesis of hybrid **2.8** (section 2.3), the reactivator bearing 3-carbon atoms in the connecting linker was investigated. Starting from the previously synthesised 1,2,3,4-tetrahydroacridin-9-yl trifluoromethanesulfonate (**2.62**), BHA reaction with propargyl amine afforded the corresponding terminal alkyne **2.73** in excellent yield (90%, Scheme 2.4.5). Sonogashira coupling with the methyl 3-benzyloxy-6-bromopicolinate **2.10** delivered the corresponding hybrid precursor **2.75** in excellent yield (94%).

Subsequent *one-pot* alkyne reduction and *O*-debenzylation under an atmosphere of hydrogen in the presence of Pearlman's catalyst yielded the corresponding adduct **2.75**. While the reaction in EtOAc was slow and gave the desired product in modest yield (37%), the reduction in MeOH was twice faster and afforded it in excellent yield (97%).

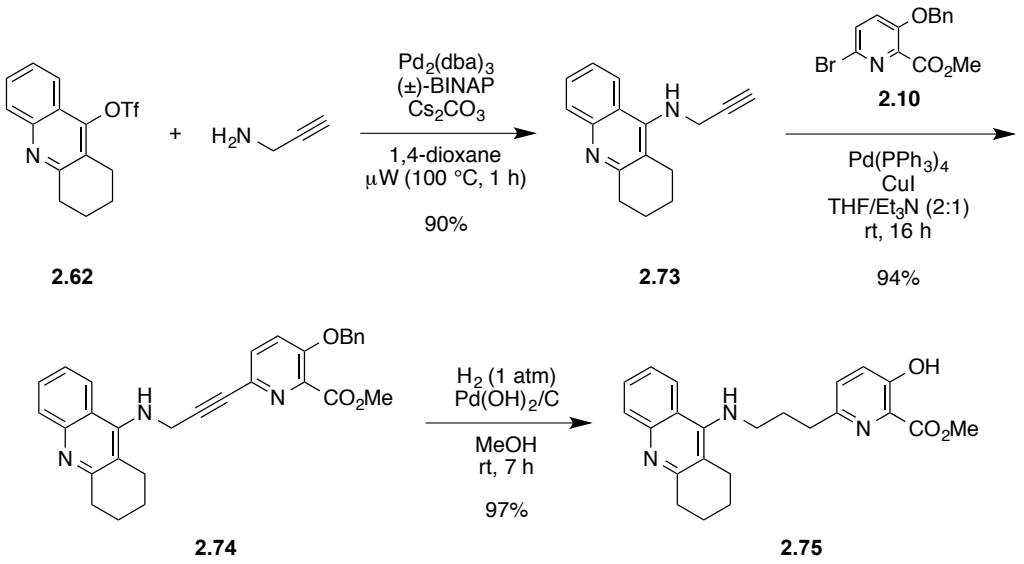

Scheme 2.4.5 Synthesis of the intermediate **2.75** starting from triflate **2.62**.

In parallel, the synthetic route involving the 7-chlorotriflate **2.22.3** was carried out and lead to the same reduced adduct **2.75**, due to reductive dehalogenation in good yield over 3 steps (61%, Scheme 2.4.6).

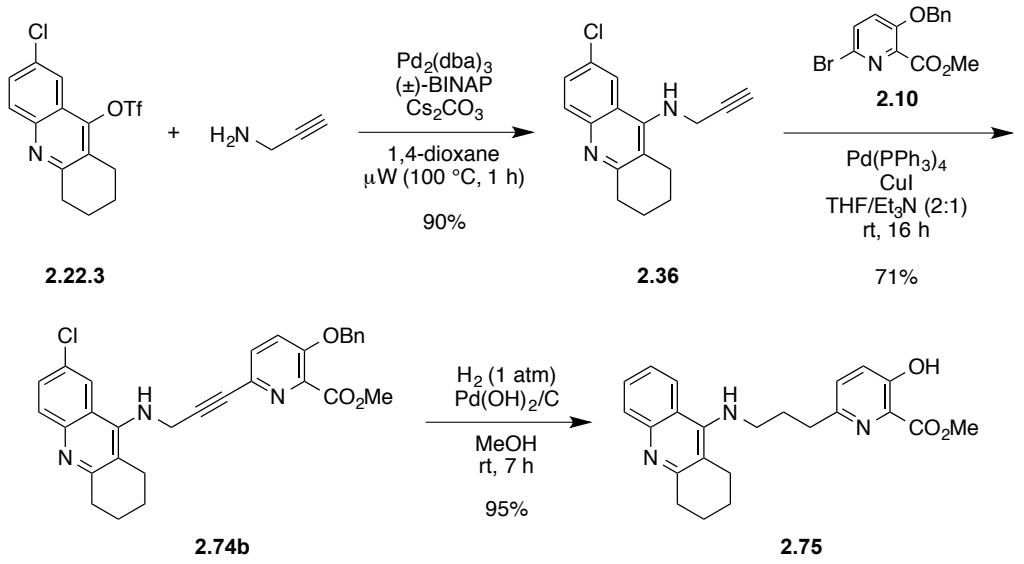

Scheme 2.4.6 Synthesis of the intermediate **2.75** starting from triflate **2.22.3**.

Then the methyl ester **2.75** was converted into the pyridinaldoximes **2.76** using the proven three-step sequence (Scheme 2.4.7). We were pleased to isolate the new hybrid **2.76** albeit in modest yield (27% after 3 steps). As previously discussed, the modest yield is largely due to the stability of the TBS ether during the successive work-up, and was not optimised for this substrate.

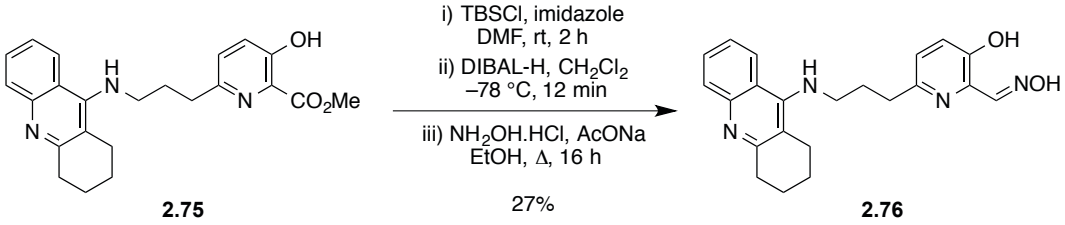

Scheme 2.4.7 Three-step sequence to afford the hybrid reactivator **2.76**.

Consequently, the final hybrid reactivator **2.76** was obtained over 7-steps with a non-optimised 19% overall yield. Subsequent biological evaluation was undertaken at IRBA and IBS in the groups of Dr. Florian Nachon and Dr. Martin Weik, respectively, and is discussed in chapter 4.

2.4.4 7-Membered ring hybrids

Focusing now on hybrids containing 7-carbon aliphatic C rings, introduction of the linker on the trifluoromethanesulfonate **2.60** was accomplished with the unprotected propargyl amine and 1-amino-3-butyne, respectively, using Pd-catalysed BHA[300] to afford the desired terminal alkynes **2.77** and **2.78** in excellent yields (84% and 93% respectively, Scheme 2.4.8).

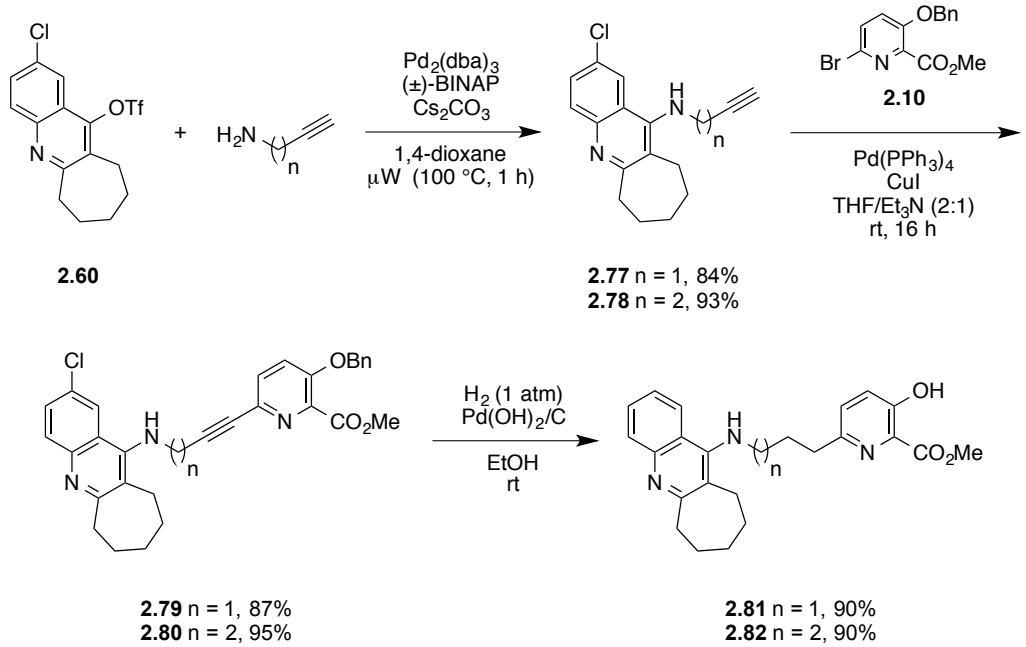

Scheme 2.4.8 Synthesis of the intermediates **2.81** and **2.82**.

Subsequent Sonogashira cross-coupling with the methyl 3-benzyloxy-6-bromopicolinate (**2.10**) afforded the corresponding alkynes **2.79** and **2.80** in excellent yields (87% and 95%, respectively). Then, *one-pot* alkyne reduction and *O*-debenzylation yielded the corresponding hybrid precursors **2.81** and **2.82** in excellent yields (90% both). As observed previously, dechlorination of the 7-chloro substituent was an undesired side reaction, although the products were still useful for the preparation of novel hybrids. The two methyl esters were converted into the corresponding aldehydes **2.83** and **2.84** respectively (Scheme 2.4.9) before, oximation yielded the desired hybrids **2.85** and **2.86** in excellent yields (87% and 73% respectively).

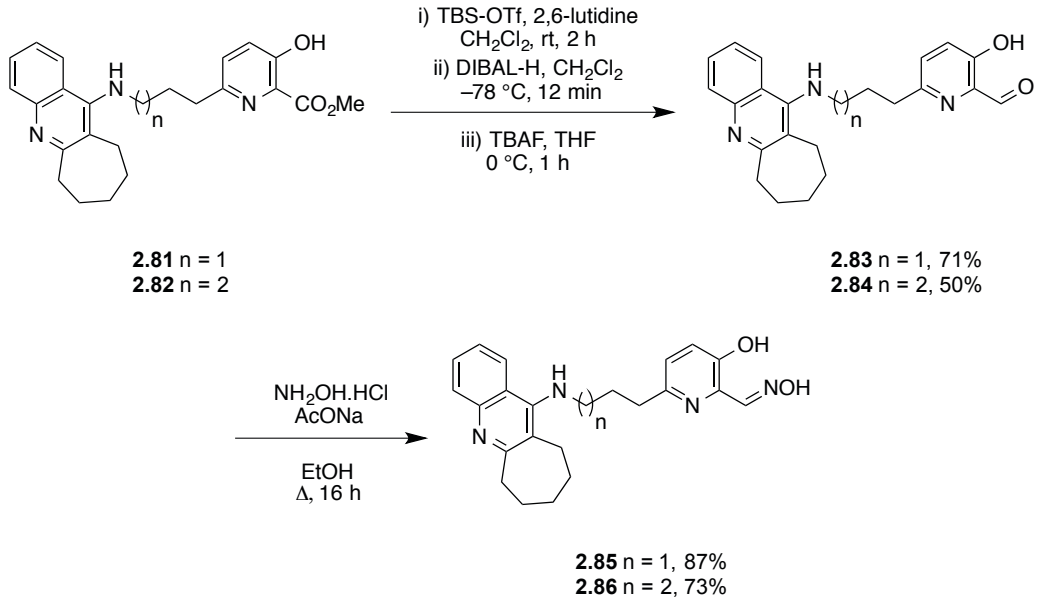

2.81 n = 1
2.82 n = 2

2.83 n = 1, 71%
2.84 n = 2, 50%

2.85 n = 1, 87%
2.86 n = 2, 73%

Scheme 2.4.9 Synthesis of the new hybrid reactivators **2.85** and **2.86**.

Hence, the final hybrid reactivators **2.85** and **2.86** were obtained over 10-steps with non-optimised 26% and 19% overall yields, respectively. Subsequent biological evaluations were undertaken at IRBA and IBS in the groups of Dr. Florian Nachon and Dr. Martin Weik, respectively, and are discussed in chapter 4.

2.5 Conclusion

The first objective of this chapter was to design and synthesise novel uncharged bifunctional reactivator analogues of the most potent hybrid **2.4** discovered by our group, with the objective of reducing binding affinity towards the enzyme active site. For this reason, a first hybrid **2.8** bearing a chlorine substituent at C7 was synthesised.

Then a family of hybrid analogues (Figure 2.5.1) was synthesised to try to understand the requirement and purpose of the aliphatic ring of the PSL moiety along with its interactions with the PAS in the enzyme gorge. In this regard, structural biology studies would provide valuable insight (Chapter 4). Although the initial efforts focussed on a family of chlorinated derivatives, the key *one-pot* hydrogenation step exhibited a lack of selectivity leading to dechlorination competing with debenzylation due to similar reaction rates. Nonetheless, the syntheses with the dechlorinated substrates were completed, as variation in the linker length and C-ring size would still improve our structure based knowledge and bring new biological evaluation data.

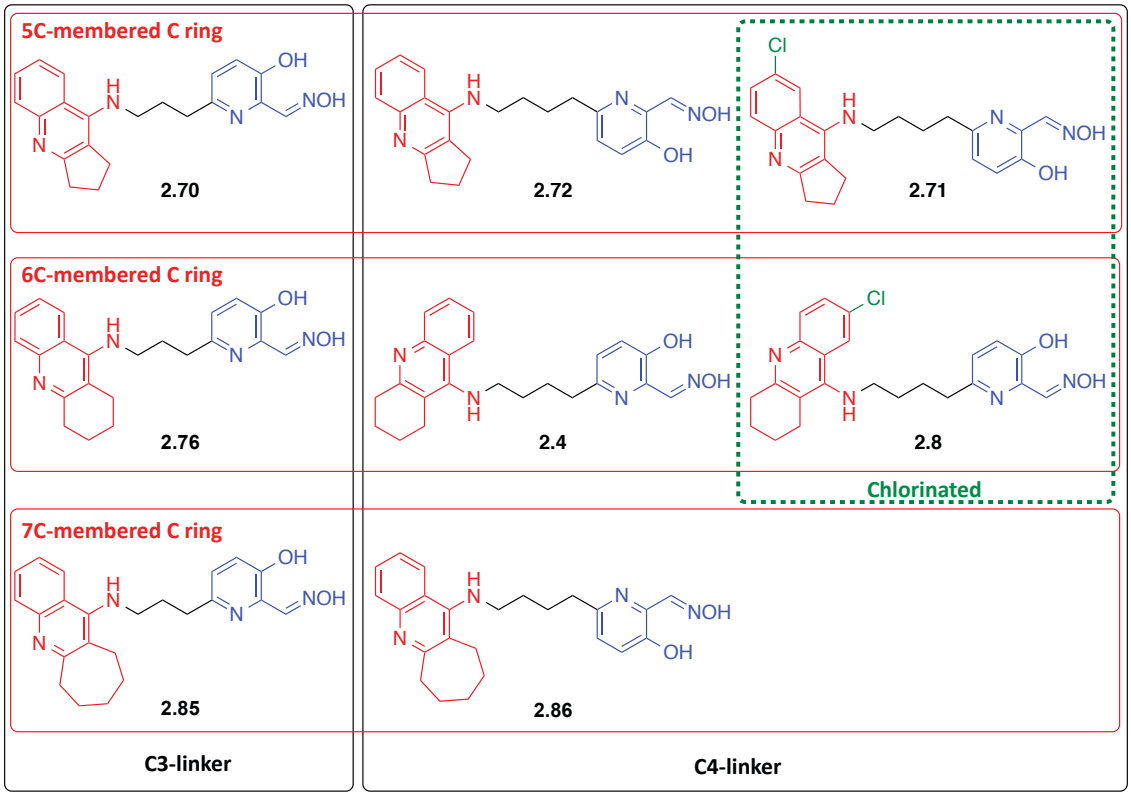

Figure 2.5.1 Novel hybrid reactivators synthesised.

In addition, an improvement to the synthetic route was achieved by exploiting the properties of the molecule (e.g. TBAF deprotection step removed).

Diverse protecting groups of the phenolic position such as acetate, acetal, TMS, methyl, MOM and MEM were also tried but are not described in this thesis because either the desired product was not observed nor showed to be compatible with Sonogashira cross-coupling.

Finally, the optimisation of the synthetic pathway allowed the discovery of novel trifluoromethanesulfonate derivatives that enable valuable C–N, C–C, C–O and C–S bond-forming reactions allowing the rapid access to functionalised *N*-alkylated tacrines, key scaffolds, for medicinal chemistry.

Chapter 3: Novel uncharged bifunctional hybrid reactivators

3.1 Quinoline- and pyridine-based hybrid reactivators

Molecular simplification represents a drug design strategy to shorten synthetic routes while keeping or enhancing the biological activity of any given natural or synthetic template. Initially, this concept was applied empirically to natural products with complex structures in order to obtain simplified active derivatives. Classical examples of molecular simplification are the natural alkaloids morphine and quinine, which led to several drugs currently used in therapy.

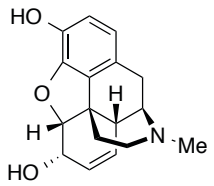

morphine

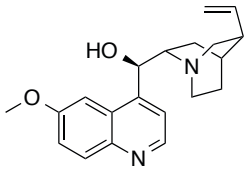

quinine

Figure 3.1.1 Examples of natural alkaloids that have been the subject of molecular simplification strategies.

3.1.1 *In silico* design.

New hybrids were investigated to fully confirm and understand the impact/necessity of the aliphatic C ring (Figure 3.1.2) on the interactions with the PAS located at the entrance of the enzyme gorge active site. For this reason, the molecular simplification strategy was used to consider new PSL scaffolds. In fact, removing the aliphatic C ring from the tacrine led to the quinoline structure (Figure 3.1.2). Then further simplification, retaining only the essential part and removing the aromatic A ring reduced down to the pyridine nucleus.

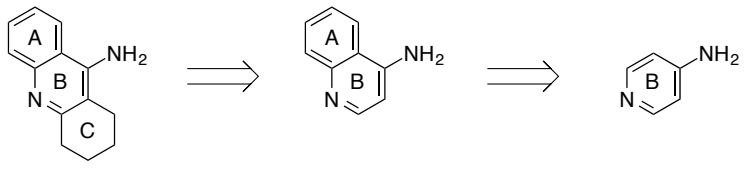

tacrine quinoline pyridine

Figure 3.1.2 Molecular simplification strategy.

The molecular dynamic simulations previously investigated (chapter 2, section 2.2.2) identified an optimum length linker containing 4 methylenes units. Thus flexible docking experiments were explored using the same model described above (chapter 2, section 2.2.2) on quinoline **3.1** and pyridine **3.2** (Figure 3.1.3). The docking scores are presented in Table 3.1.1.

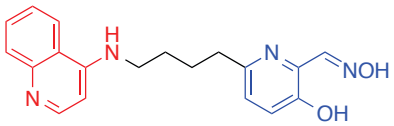

3.1

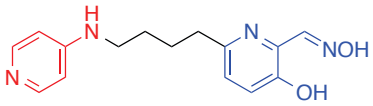

3.2

Figure 3.1.3 Hybrid reactivators **3.1** and **3.2**.

Entry	Hybrid	Linker length (CH_2)	Affinity (kcal mol^{-1})
1	**3.1**	4	–10.9
2	**3.2**	4	–9.4

Table 3.1.1 Flexible docking scores for hybrid reactivators **3.1** and **3.2**.

The quinoline hybrid **3.1** exhibited a binding affinity score lower than –9 kcal mol^{-1}, indicating that the linker is sufficiently long to prevent unproductive binding of the reactivators in the gorge of the inhibited enzyme. Hybrid **3.2** displayed a score of –9.4 kcal mol^{-1} corresponding to the limit defining potential good reactivator. This results can be explained by the fact that the PSL got smaller than reactivating moiety in terms of size, creating potential folding or artefact. For instance, such hybrid (**3.2**) can go "upside-down" in the gorge favouring interactions between the reactivating moiety of the hybrid and the PAS of the gorge (Figure 3.1.4).

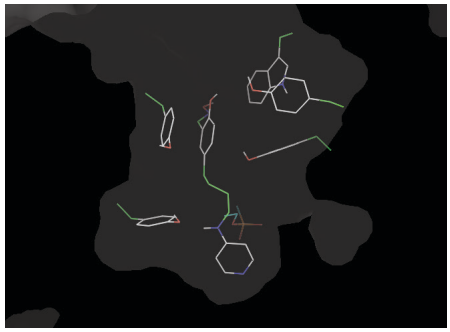

Figure 3.1.4 Example of docking when hybrid **3.2** interacts "upside-down" in the gorge.

Therefore, the syntheses of two new hybrid reactivators bearing PSL structures based on quinoline and pyridine were undertaken (Figure 3.1.3). Interestingly, using the 4-aminopyridine as PSL generates a neutral hybrid that is a close analogue of the standard bis-pyridinium oxime reactivators.

3.1.2 Quinoline-based hybrid reactivator

Following the synthetic route previously established (Chapter 2, section 2.4), the commercially available 4-quinolinol (**3.3**) was converted in the corresponding trifluoromethansulfonate derivative **3.4** in modest yield (Scheme 3.1.1). Then, introduction of the linker was achieved with the unprotected 1-amino-3-butyne using the BHA procedure to afford the desired terminal alkyne **3.5** in modest yield.

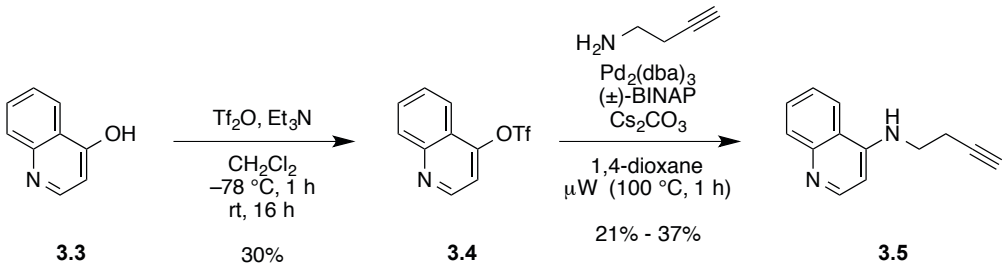

3.3 30% **3.4** **3.5**

Scheme 3.1.1 Synthesis of the terminal alkyne **3.5** from 4-quinolinol.

Experimentally, triflate **3.4** proved to be quite unstable and difficult to purify. Thus another synthetic pathway was considered starting from the commercially available 4-bromoquinoline (**3.6**, Scheme 3.1.2). The BHA reaction was carried out with 1-amino-3-butyne to afford **3.5**. The terminal alkyne **3.5** was subsequently linked to the methyl 3-benzyloxy-6-bromopicolinate (**2.10**) by Sonogashira cross-coupling yielding to the intermediate alkyne **3.7** in good yield after two steps (60%).

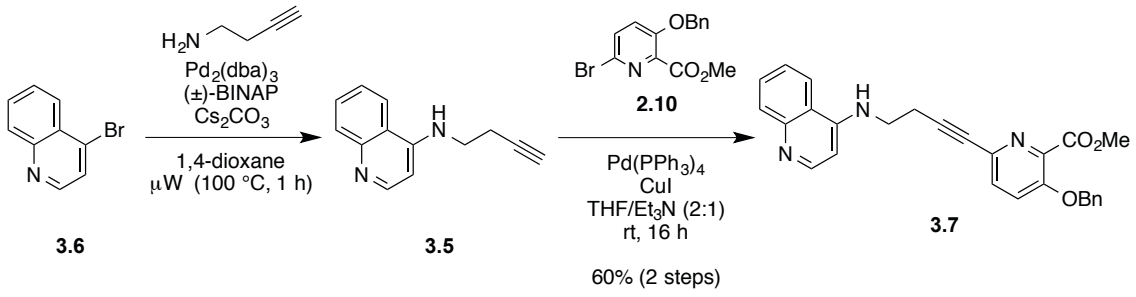

3.6 **3.5** **3.7**

Scheme 3.1.2 Synthesis of the alkyne **3.7**.

The aldehyde **3.8** was obtained in good yield (69%) using the established three-step hydrogenation, protection, reduction/deprotection sequence from ester **3.7**. Finally, the oxime **3.1** was isolated by condensation of hydroxylamine with the aldehyde **3.8** in the presence of anhydrous sodium acetate (Scheme 3.1.3). The desired hybrid **3.1** was recovered in 54% yield after purification by column chromatography and subsequent crystallisation.

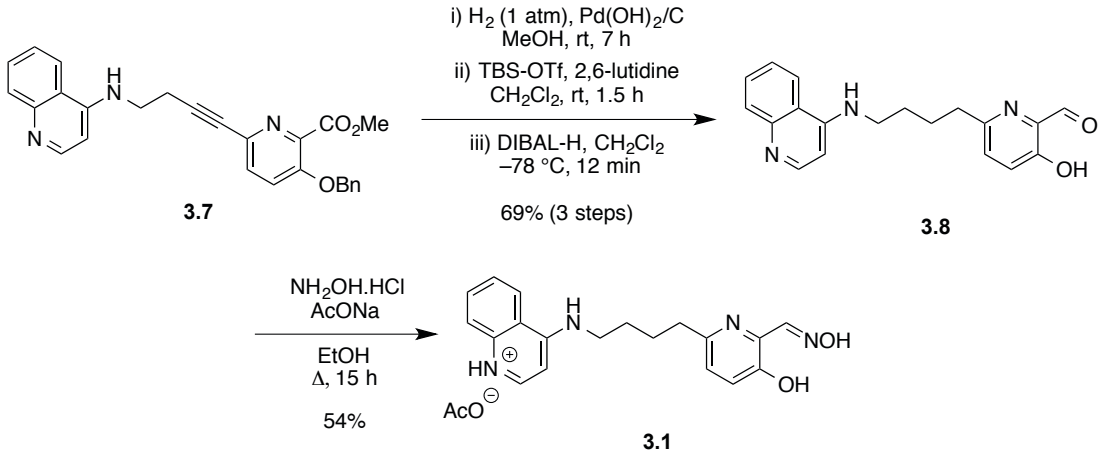

Scheme 3.1.3 Synthetic of the quinoline hybrid **3.1**.

Hence, the final hybrid reactivator **3.1** was obtained over 6-steps with a satisfying non-optimised overall yield of 22%. Subsequent biological evaluation was undertaken at IRBA and IBS in the groups of Dr. Florian Nachon and Dr. Martin Weik, respectively, and is discussed in chapter 4.

Interestingly, after the oxime formation step, the hybrid was isolated as mono-acetate salt, in contrast to all previously synthesised hybrids. Therefore, in view of requests from the biologists to provide them salt forms of the reactivators to improve their aqueous solubilities, we submitted hybrid **3.1** under its mono-acetate form. In addition, di-acetate salt of hybrid **3.1** was prepared by dissolving it into glacial acetic acid before removing the excess acid. The formation of the di-acetate salt was confirmed by ^{1}H NMR analysis in CD_3OD.

3.1.3 Pyridine-based hybrid reactivator

Following the synthetic route previously established, several attempts were carried out to convert the commercially available 4-hydroxypyridine (**3.9**) into the corresponding triflate **3.10** (Scheme 3.1.4). However, even though evidence for moderate conversion was obtained from the crude by LRMS, the triflate **3.10** apeared to be unstable and decomposed during the purification process or in direct use in subsequent coupling attempts.

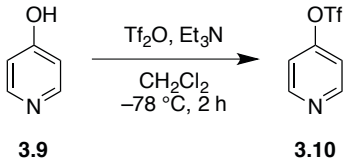

Scheme 3.1.4 Triflate formation reaction from 4-hydroxypyridine (**3.9**).

Thus, the terminal alkyne **3.12** was obtained by S_N2 type reaction with commercially available 4-bromopyridine (**3.11**) and 1-amino-3-butyne in 1-pentanol under reflux in the presence of Et_3N (Scheme 3.1.5). The 4-bromopyridine was obtained as its hydrochloride form, reducing its nucleophilicity. None the less, S_N2 reaction in the absence of Et_3N did still proceed but with slower rates and corresponding lower conversion. Additionally, several attempts were explored using the 4-bromopyridine (**3.11**) in the BHA reaction, but unfortunately, only degradation and evidence of pyridine dimer formation was observed (LRMS).

Due to the high polarity of the terminal alkyne **3.12**, a quick filtration on neutral alumina was used to remove most of the pentanol and then the crude material was subjected to the subsequent Sonogashira cross-coupling. Thereby, the alkyne **3.13** was isolated in excellent yield (83%, Scheme 3.1.5).

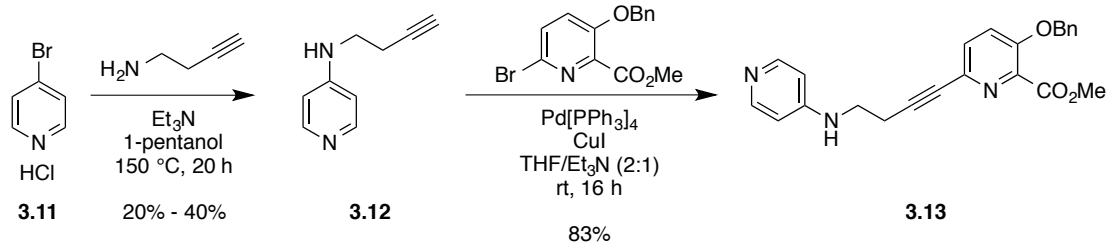

Scheme 3.1.5 Synthesis of alkyne **3.13**.

Reduction and *O*-debenzylation over Pearlman's catalyst in MeOH afforded the intermediate phenol **3.14**, which was used as a crude product in the next step. Pyridinaldehyde **3.15** was

obtained from the ester **3.15** using a two-step sequence involving TBS protection of the phenolic group and a reduction of the methyl ester into the corresponding aldehyde using DIBAL-H (Scheme 3.1.6).

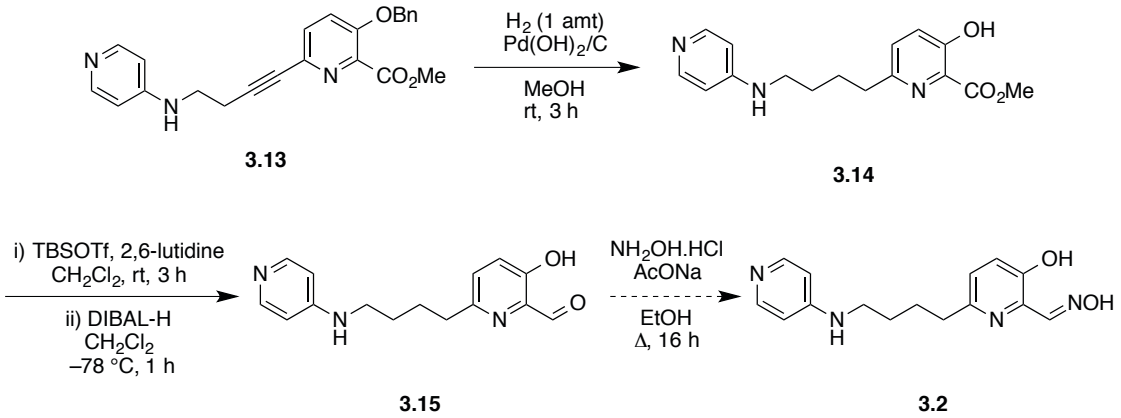

Scheme 3.1.6 Synthetic route towards the hybrid reactivator **3.2**.

It is important to note that the main difficulty encountered during the synthesis of the pyridine hybrid remains the work-up conditions. The TBS protection was carried out in presence of 2,6-lutidine, and consequently a washing with saturated aqueous $CuSO_4$ solution was employed as an efficient way to remove pyridine and derivatives such as 2,6-lutidine. Unfortunately, this aqueous solution was sufficiently acidic (2,6-lutidinium chloride from the silylation) to protonate the bis-pyridine ring product. Furthermore, the desired product also extracted into the aqueous solution by coordinating the metal. Subsequent attempts of extractions and basification of the solution revealed to be unfruitful to recover the product. Hence it was decided to set up the methyl ester reduction on the crude material after removing the solvent under reduced pressure. Once the reaction completed and quenched with MeOH at –78 °C, the reaction mixture was washed with a solution of NaOH (0.5 M). Here again, the desired di-pyridine intermediate remained in the aqueous phase and extractions were unsuccessful. At each step, the presence of the silylether and aldehyde **3.15** was supported by LRMS. Finally, attempts to obtain the desired product **3.2** by oximation were explored, but unfortunately the desired hybrid **3.2** has not been isolated or even observed in the crude reaction. Unfortunately, due to a lack of material and time, no further investigation towards the hybrid **3.2** was possible.

Careful reconsideration of the reaction condition and work-up (if any) will be required to give the best chance to isolate the desired. An excess of sodium acetate in the oxime formation will help to deprotect the phenolic position and form the desired product. Reverse-phase purification should also be considered in future efforts towards pyridine PSL-containing targets.

3.2 Alkaloid-based hybrid reactivators

In the frame of the development of a broad-spectrum hybrid reactivator, alternative PSLs have also been considered and will be discussed within the design and synthesis of hybrids based on phenanthridinoid alkaloids from Amaryllidaceae. Some of these alkaloids are known competitive inhibitors of AChE, and can provide inspiration for new PSLs for reactivators hybrid design.

3.2.1 The Amaryllidaceae family

The Amaryllidaceae is a widely spread monocotyledonous family of plants found across many areas, composed of more than 800 species and grouped into 59 genera.[301] Their biodiversity results from the fact that these plants are able to live in different habitats. The major diversity is located in South America and South Africa with 80% of the genera, followed by the Mediterranean region (14%) and Australia (5%).

Figure 3.2.1 Example of a plant from the Amaryllidaceae family (*Hippeastrum Psittacinum*).[2]

Plants of the Amaryllidaceae family are known for the production of a group of alkaloids, generally addressed as "Amaryllidaceae alkaloids" which are isolated from plants of all genera of this family. Depending on their structures, the Amaryllidaceae alkaloids are classified into eight backbone types (Figure 3.2.2).[302] Among these alkaloids, galanthamine appears to be the most famous as fully recognised and FDA approved drug in the treatment of Alzheimer disease as a long acting, selective, reversible and competitive AChE inhibitor.[303–305] Designing a novel hybrid reactivator based on galanthamine would have certainly been interesting and definitely challenging. However, its inhibitory activity (IC_{50} = 0.33 μM) towards AChE revealed a binding affinity that is too high for the native enzyme. Thus the potential reactivator will remain in the

[2] http://www.plantsystematics.org/imgs/shimizu/r/Amaryllidaceae_Hippeastrum_psittacinum_36420.html

gorge active site after reactivation, functioning as a powerful competitive inhibitor. None the less, it is possible that structurally simplified galanthamine derivatives might serve as useful PSLs with reduced binding affinities.

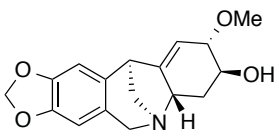

montanine

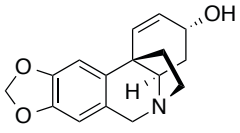

crinine

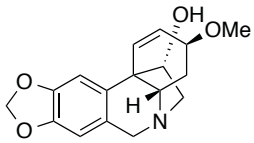

haemanthamine

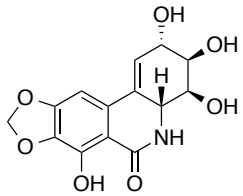

narciclasine

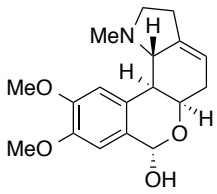

lycorenine

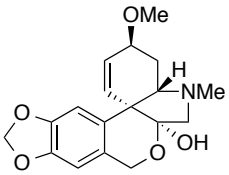

tazettine

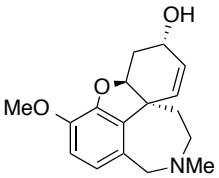

galanthamine

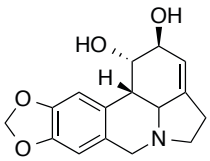

lycorine

Figure 3.2.2 Sub-structures of Amaryllidaceae alkaloids.

However, assoanine and oxoassoanine (Figure 3.2.3), other Amaryllidaceae alkaloids belonging to the lycorine skeleton type, exhibited interesting inhibitory activity (IC_{50} = 3.87 and 47.21 μM, respectively),[306] with potential value as PSL. Thus, a collaborative project was explored including the Brown group (Southampton) due to its interest in alkaloids from Amaryllidaceae.

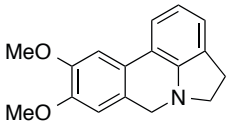

assoanine

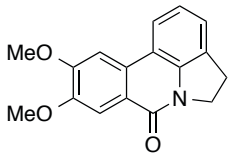

oxoassoanine

Figure 3.2.3 Phenanthridinoid alkaloids assoanine and oxoassoanine.

3.2.2 *In silico* design

A preliminary docking study was investigated by Dr. Florian Nanchon to understand the interactions between the assoanine **3.16** and its more air-stable analogue **3.17** with the PAS (Figure 3.2.5). The results clearly indicated that those compounds had the potential to act as PSL, interacting through sandwich π-stacking between Trp286 and Tyr124 (affinity estimated to –9.4 kcal mol^{-1}). Besides, it is interesting to highlight the fact that the methoxy substituent 1 points in the direction of the gorge. Thus a linker/reactivator bind on this position will be optimum to favour the reactivation.

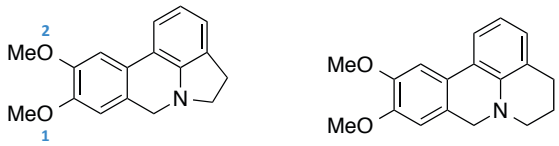

3.16 **3.17**

Figure 3.2.4 Assoanine **3.16** and its 6-membered ring analogue **3.17**.

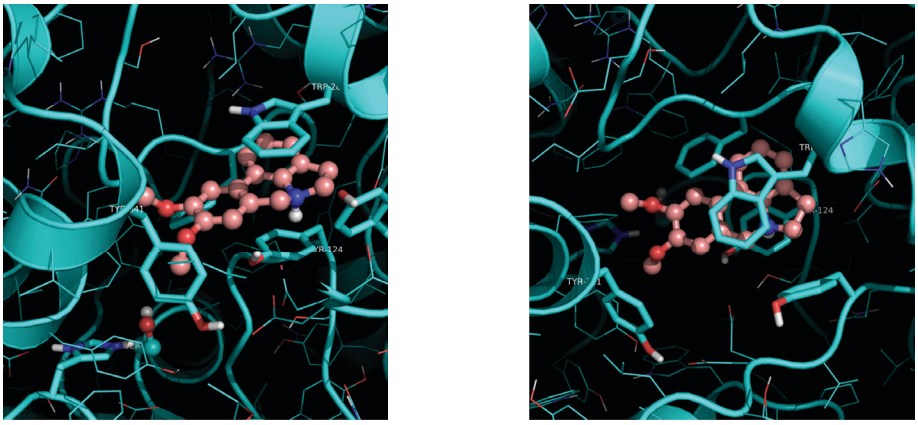

(a) (b)

Figure 3.2.5 Dockings of assoanine in AChE gorge showing the sandwich π-stacking between Trp286 and Tyr124 from side (a) and top (b) views.

The 6-membered-ring analogue **3.17** showed similar results. Consequently, the Brown group started to investigated the syntheses of both scaffolds (**3.16** and **3.17**) involving a C-H activation/cyclisation step.[307] As an *ortho*-directing group (e.g. amide) is usually required for the formation of the organopalladium intermediate which can subsequently undergo cross-coupling or intramolecular cyclisation,[308] intermediates **3.19** and **3.20** were considered (Scheme 3.2.1). Treatment of 3,4-dimethoxybenzoic acid (**3.18)** with tetrahydroquinoline and indoline in the

presence of propylphosphonic anhydride ($T_3P^{®}$) afforded the corresponding amide **3.19** and **3.20** in excellent yields (98% and 96%, respectively).

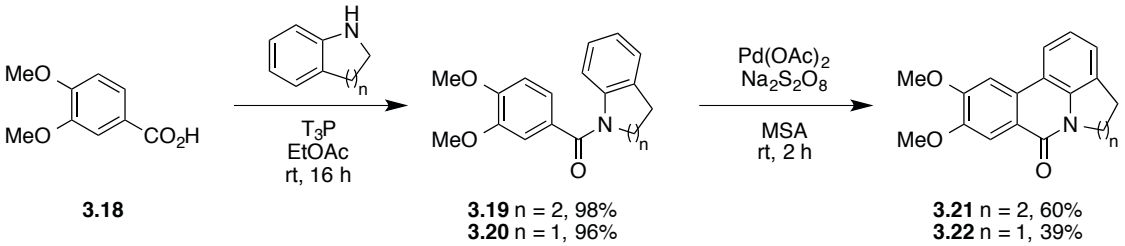

Scheme 3.2.1 C-H activation-cyclisation step to afford analogues **3.21** and **3.22**.

Then an improved protocol for C-H activation/cyclisation modified from a literature method,[309] was employed using neat methanesulfonic acid (MSA), $Pd(OAc)_2$ and $Na_2S_2O_8$. While the desired cyclised product **3.21** was isolated in reasonable yield (60%), oxoassoanine **3.22** was obtained with rather poor efficiency (39% yield). This result can be explained by the instability of indoline derivatives **3.20** towards oxidation and form the less reactive intermediate **3.23** (Scheme 3.2.3).[310]

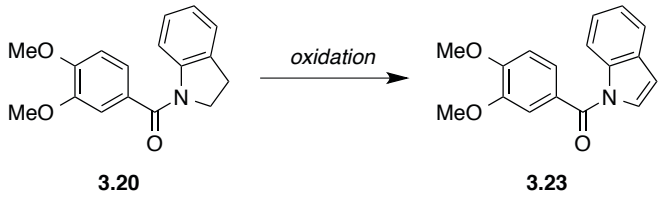

Scheme 3.2.2 Oxidation of the indole amide intermediate **3.20**.

Based on these results combined with the fact that the oxoassoanine is a 10-fold less potent inhibitor than assoanine, a novel hybrid reactivator **3.24** was designed and investigated (Scheme 3.2.3).

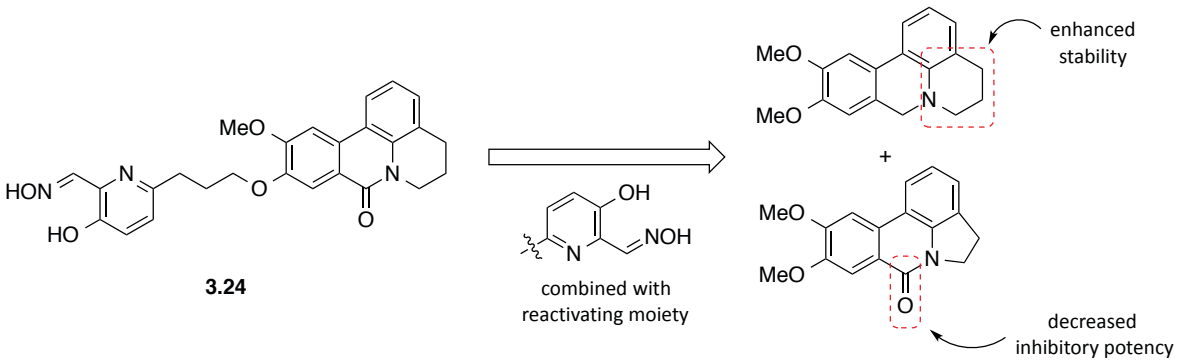

Scheme 3.2.3 General strategy to design the hybrid reactivator **3.24**.

The *in silico* model displayed an interesting affinity of –13 kcal mol^{-1} predicting a potential good reactivator. Besides, the dockings showed the interactions of the PSL at the PAS through π-stacking between Trp286 and Tyr124 and the reactivating moiety points in the direction of the gorge towards the VX-phosphylated serine.

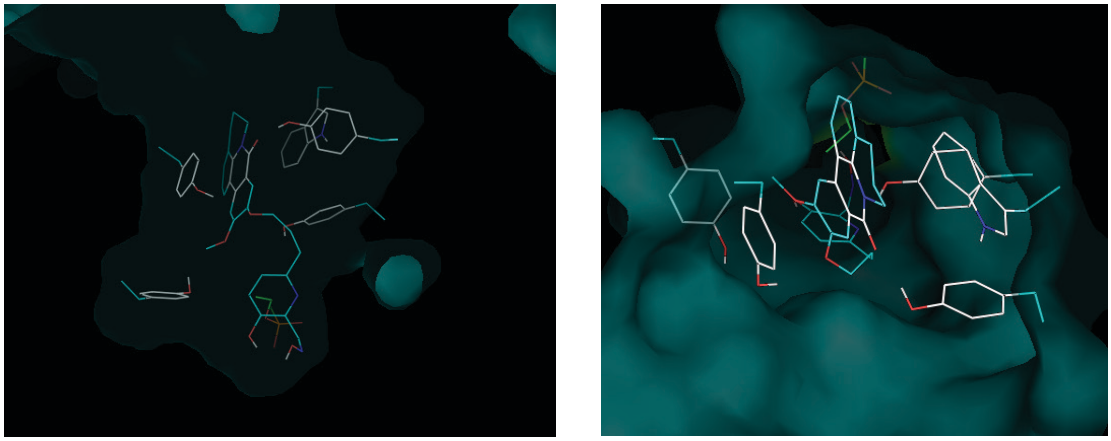

(a) (b)

Figure 3.2.6 Dockings of hybrid **3.24** in VX-AChE gorge showing the sandwich π–stacking at the PAS from side (a) and top (b) views.

Consequently, our initial strategy relied on the synthesis of the phenanthridinoid alkaloid fragment **3.26** that can be subsequently attached to the linker **3.25** by Mitsunobu reaction or nucleophilic substitution. Sonogashira cross-coupling reaction can be employed for the connection with the reactivator precursor **2.10** (Scheme 3.2.4). Fragment **3.26** can be isolated in just a few steps from isovanillin (**3.27**).

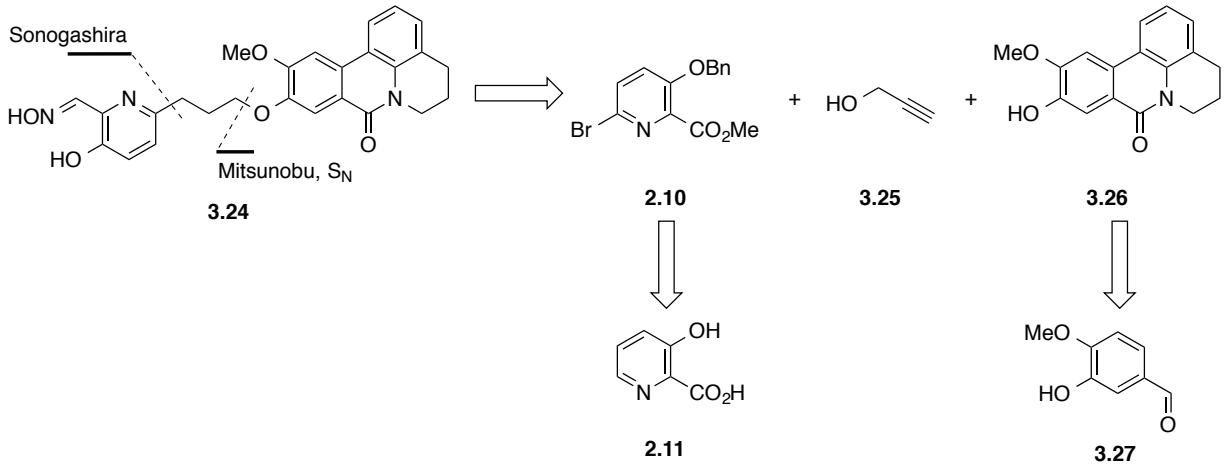

Scheme 3.2.4 Retrosynthetic pathway to afford the desired hybrid reactivator **3.24**.

3.2.3 Synthesis of the alkaloid fragment 3.26

Initial efforts were made to apply the previously explored chemistry, employing a key C-H activation/cyclisation step. The synthesis started from isovanillin (**3.27**) with the *O*-protection of the phenolic group via mesylation (Scheme 3.2.5). Subsequent Pinnick oxidation afforded the acid **3.29** analogue of 3,4-dimethoxybenzoic acid previously investigated. Coupling with tetrahydroquinoline in the presence of propylphosphonic anhydride ($T_3P^{®}$) in EtOAc provided amide **3.30**, which under basic conditions was deprotected yielding cyclisation precursor **3.31**. Such deprotection was revealed to be necessary since attempts to cyclise **3.30** under the developed reaction conditions resulted in complex reaction mixtures. Unfortunately, it was also true for the phenolic compound **3.31**, which ultimately cyclised to product **3.26** in rather low yield (27%, Scheme 3.2.5), following a literature protocol.[310]

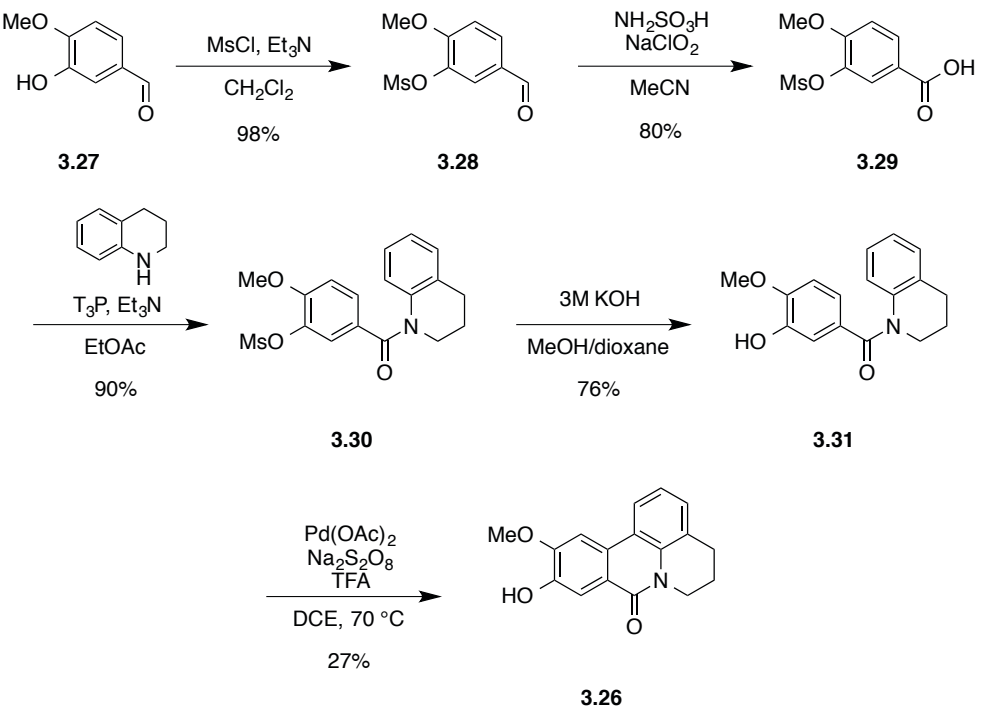

Scheme 3.2.5 Synthesis of phenanthridinoid alkaloid scaffold **3.26** via C-H activation.[3]

However, no regioselective control was imposed upon this last step, partially explaining the low yield and the difficulty to reproduce the results. It was believed that the absence of a directing group on the aromatic ring of the cyclisation position affects the efficiency and the

[3] Acknowledgment: Dr. Lynda J. Brown and Dr. Valerio Isoni for investigating the synthesis of phenanthridinoid alkaloid scaffold **3.26** as described in Scheme 3.2.5**.**

regioselectivity of the double C-H activation-cyclisation process via Pd^{II}/Pd^{IV} catalytic pathway leading to the formation of a by-product **3.26b** (Scheme 3.2.6).

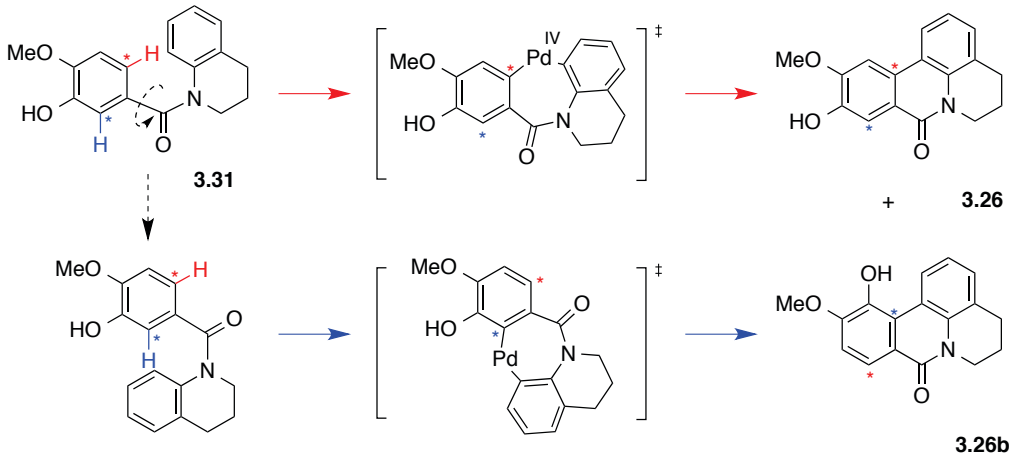

Scheme 3.2.6 Two plausible *ortho*-positions for the C-H activation/cyclisation process.

Thus, subsequent investigations centred on introduction of a directing group (e.g. halide) on the aromatic ring of the cyclisation position in order to enhance the efficiency and the regioselectivity of the subsequent cyclisation *via* palladium-catalysed Heck-type reaction.[4] Starting from isovanillin **3.27**, Williamson reaction was used to protect the active phenolic group forming the isopropyl ether **3.32** (Scheme 3.2.7). A weak inorganic base, such as K_2CO_3, was enough to deprotonate the phenolic group (due to its high acidity, pK_a 9.2) and neutralise the reaction by-product, hydrogen bromide (HBr).

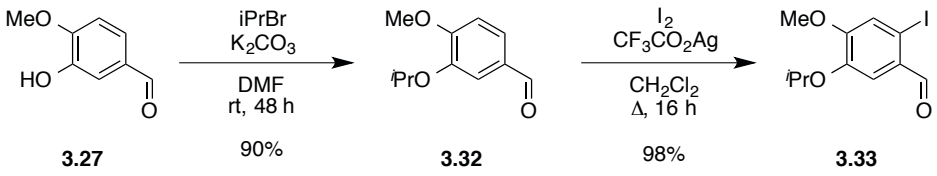

Scheme 3.2.7 Synthesis of intermediates **3.32** and **3.33**.

[4] Acknowledgment: Dr. Lynda J. Brown and Ming Long Tse (BSc) for investigating the synthesis of phenanthridinoid alkaloid scaffold **3.26** introducing a directing group.

An iodine atom was then introduced in the aromatic ring by S_EAr in presence of a soft Lewis acid (Scheme 3.2.7).[311] Both ether groups are *ortho*/*para*-directing and strongly activating, while the aldehyde is *meta*-directing and moderately deactivating. Therefore the stronger resonance donating effect of the isopropyl ether (compared to methyl ether) guides the substitution in *para*-position. Interestingly, silver trifluoroacetate was able to play a dual function: i) Lewis acid catalyst, and ii) halide scavenger. The reaction generates hydrogen iodide (HI) as by-product that was scavenged as a yellow precipitate of AgI due to the presence of silver ion.

Pinnick oxidation of aldehyde **3.33** yielded to the corresponding carboxylic acid **3.34** in excellent yield (95%, Scheme 3.2.8). Several advantages of this reaction can be highlighted: i) the tolerance towards iodine functional group,[312] ii) the presence of ClO_2^- and $H_2PO_4^-$ ions that help to generate the active oxidant ($HClO_2$), iii) the oxidant species is regenerated *in situ* due to the presence of hydrogen peroxide, and iv) no side reactions with hypochlorous acid.[313]

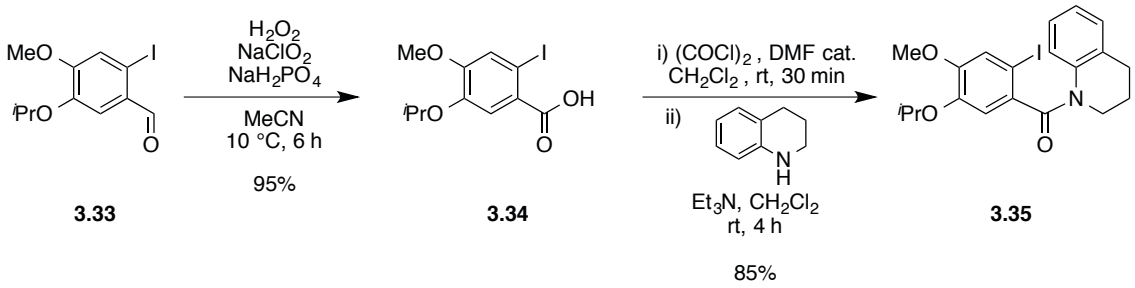

Scheme 3.2.8 Pinnick oxidation and amide formation.

Attempts to afford the amide **3.35** *via* the procedure previously investigated (involving $T_3P^®$) were unsuccessful. A plausible explanation may lie on the presence of the iodine substituent that hindered the approach of the coupling reagent. Therefore, even though wide range of amide coupling reagents is available (e.g. HATU, HBTU or EDCl), an alternative route described by Harayama and co-workers involving an acyl chloride intermediate was performed (Scheme 3.2.8).[314] In the first step, a catalytic amount of DMF reacts with the oxalyl chloride to form the Vilsmeier-Haack iminium intermediate, more reactive than oxalyl chloride, which subsequently reacts with the acid **3.34** to form *in situ* the corresponding acyl chloride intermediate. Then, after removal of the excess of oxalyl chloride *in vacuo*, nucleophilic substitution with tetrahydroquinoline afforded the corresponding amide **3.35** in excellent yield (85%) in multi-gram scale.

Interestingly, the ^{1}H NMR spectra of amide **3.35** showed broad signals due to restricted rotation. Thus, high temperature NMR (80 °C) was needed to visualise an average signal arisen by the spin active nuclei by speeding up the transformation between the two conformational isomeric forms (rotamers).

Further intramolecular Heck cyclisation reaction was conducted following a procedure from Harayama and co-workers on similar bis-aryl substrates.[315] After a few attempts to perform the reaction under reflux using classical thermal conditions, the reaction mixture was irradiated using a microwave apparatus at 100 °C for 1 h to isolate the desired cyclised product **3.36** in excellent yield (87%, Scheme 3.2.9).

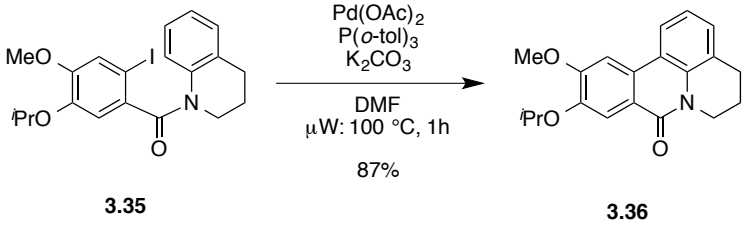

3.35 **3.36**

Scheme 3.2.9 Heck cross-coupling reaction.

Classical Heck reactions require $Pd(OAc)_2$ and bulky phosphine ligands in order to generate *in situ* the active Pd(0) species. Harayama and co-workers obtained interesting results involving tri(*o*-tolyl)phosphine ($P(o\text{-tol})_3$). Amatore and co-workers proposed an interesting mechanism *via* an anionic pathway (Scheme 3.2.10).[316] After generating the active Pd(0) species from $Pd(OAc)_2$, the first step is an oxidative addition of amide **3.35**. Then, elimination of iodide takes place to provide a vacant site on the metal facilitating coordination of the tetrahydroquinoline π-system. Subsequent, *syn*-addition leads to a thermodynamically favoured 6-*exo-trig* ring closure product upon β-hydride elimination. The Pd(II) species underwent further reductive elimination and regenerated the active Pd(0) species in order to complete the catalytic cycle. The coordination and the *syn*-addition steps are also known as "carbopalladation".[317]

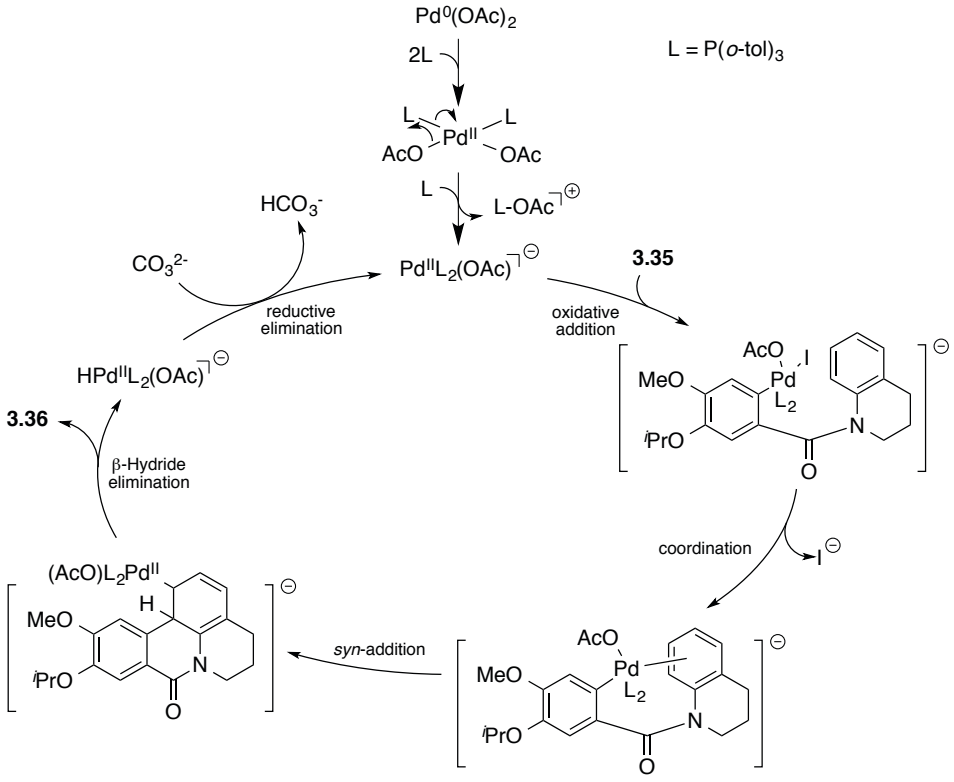

Scheme 3.2.10 Proposed mechanism for the Heck intramolecular cyclisation.

Spectroscopic data obtained were consistent with the desired structure and the monoclinic crystalline structure was confirmed by X-ray crystallography (Figure 3.2.7).

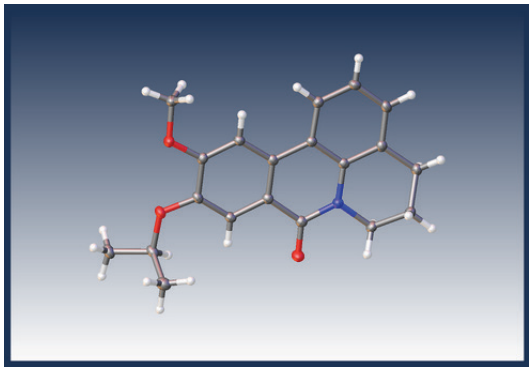

Figure 3.2.7 X-ray crystal structure of oxoassoanine analogue **3.36**.

Finally, the selective deprotection of the isopropyl ether yielded the desired alkaloid fragment **3.26** (Scheme 3.2.11). Despite a wide range of Lewis acid available for ether deprotection, relatively mild and selective conditions suggested by Banwell and co-workers were applied using $AlCl_3$.[318] The ether cleavage mechanism follows a S_N1-type mechanism. However, on the first attempts, a by-product was observed in the reaction mixture suggesting a possible *in situ* intermolecular side reaction (LRMS, m/z 324.0 $[M+H]^+$).

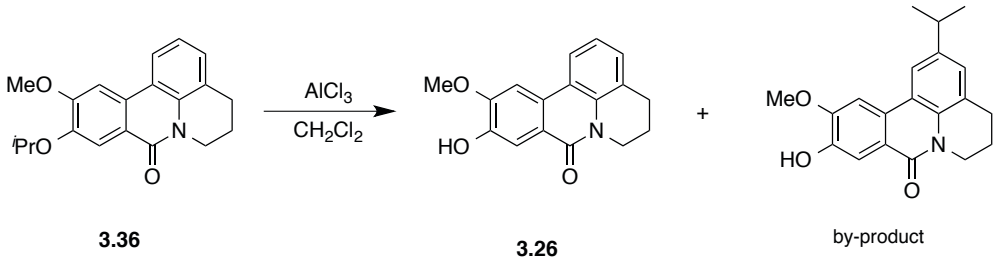

3.36 **3.26** by-product

Scheme 3.2.11 Isopropyl ether deprotection leading to the desired product **3.26** and by-product.

In fact, it was found that the aromatic ring of the product **3.26** was highly activated to undergo a Friedel-Crafts alkylation with isopropyl cation (by-product formed *in situ*) in the presence of a Lewis acidic catalyst $AlCl_3$ *via* S_EAr (Scheme 3.2.12).

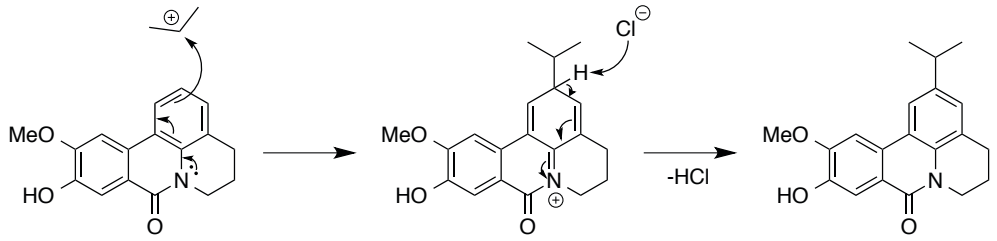

3.26

Scheme 3.2.12 Formation of the observed byproduct by *in situ* Friedel-Crafts alkylation.

Consequently, a cationic scavenger such as ethane thiol was added to trap the isopropyl cation formed *in situ*.[319] Following implementation of this modification, selective deprotection afforded the desired alkaloid fragment **3.26** in excellent yield (83%, Scheme 3.2.13). The synthesis of fragment **3.26** was brought to multigram scale, setting the stage for the hybrid synthesis.

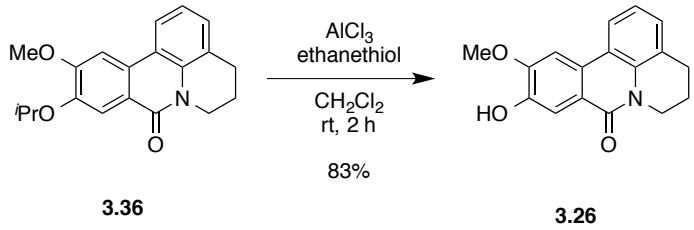

3.36 **3.26**

Scheme 3.2.13 Isopropyl ether deprotection reaction to afford the alkaloid analogue **3.26**.

Interestingly, comparison of the spectroscopic data (^{1}H NMR) between the compound isolated **3.26** and a sample of the previously investigated route (*vide supra*, synthesis of compound **3.26** *via* C-H activation route) confirmed the formation of the product **3.26b** as major product in the double C-H activation/cyclisation route. In theory, two distinct singlet signals should be observed in **3.26** due to different chemical environments. In practice, the two signals were observed almost overlapping at 7.73 and 7.72 ppm (Top Spectrum, Figure 3.2.8) corresponding to the product of the double C-H activation/cyclisation reaction **3.26b**, whereas signals shifted at 7.80 and 7.68 ppm (Bottom Spectrum, Figure 3.2.8) for the desired product **3.26**. The halide introduced control in the cyclisation position in the Heck reaction. Further confirmation of the regioselectivity was obtained from X-ray crystallography of the intermediate **3.36** (Figure 3.2.7).

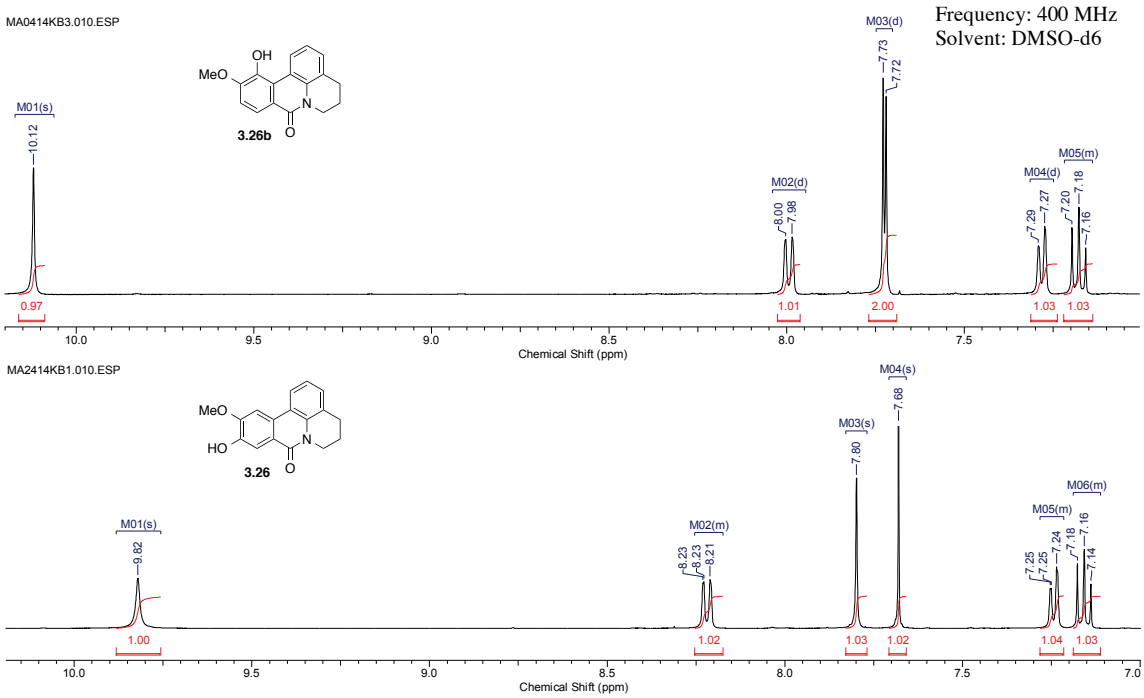

Figure 3.2.8 Comparison of the ^{1}H NMR aromatic regions of both products **3.26** (bottom spectra) and **3.26b** (top spectra).

3.2.4 Synthesis of hybrid reactivator 3.24

The first strategy considered to reach the desired hybrid reactivator **3.24** relied a convergent retrosynthetic pathway (Scheme 3.2.14): the target can be obtained after few transformations by Mitsunobu reaction between the alkaloid fragment **3.26** and the intermediate **3.37** which can be synthesised by Sonogashira cross-coupling of the reactivator precursor **2.10** and propargyl alcohol **3.25**.

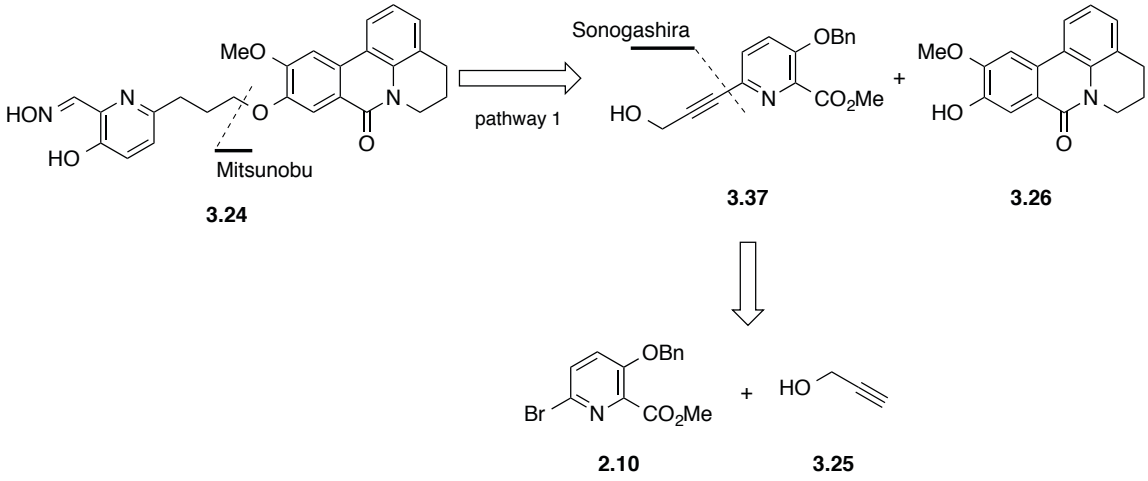

Scheme 3.2.14 Retrosynthetic pathway 1 to afford the hybrid ractivator **3.24**.

Propargyl alcohol (**3.25**) was linked to the methyl 3-benzyloxy-6-bromopicolinate (**2.10**) by Sonogashira cross-coupling yielding to the intermediate alkyne **3.37** in excellent yield (94%, Scheme 3.2.15). Subsequently, to form the hybrid precursor, Mitsunobu reaction with phenol **3.26** in presence of PPh_3 and diisopropyl azodicarboxylate (DIAD) proceeded in moderate yield (51%) to afford ether **3.38**.

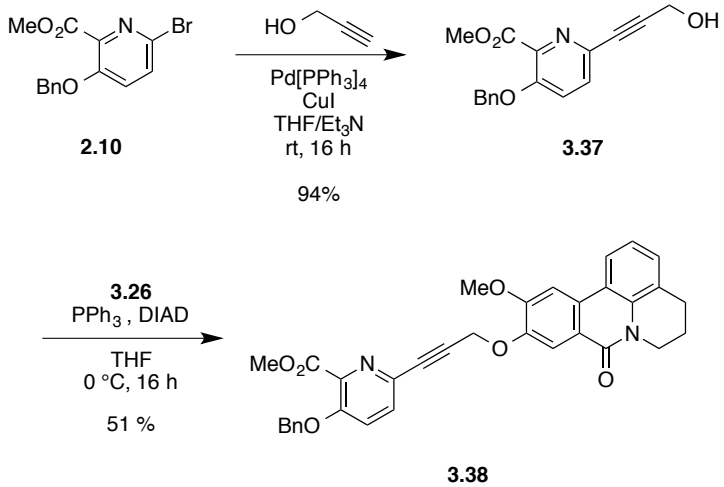

Scheme 3.2.15 Successive Sonogashira and Mitsunobu reactions to afford ether **3.38**.

Surprisingly, the Mitsunobu coupling was not readily amenable to scale-up. While the reaction proceeded in moderate yield on small scale (50 mg), no conversion was observed for any scaled-up reactions (100 to 250 mg). The analogous synthetic route using 3-butyn-1-ol instead of propargyl alcohol (Scheme 3.2.16), gave only highly conjugated by-product **3.40** by dehydration of **3.39** under the conditions of the Mitsunobu reaction. Such activated propargylic systems often suffer from elimination.

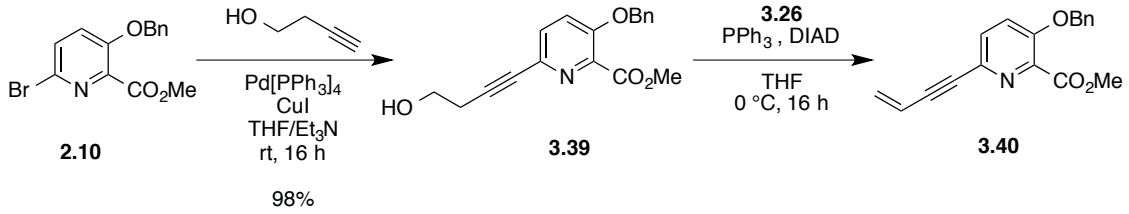

Scheme 3.2.16 Successive Sonogashira and Mitsunobu reactions with 4 carbon linker.

Rather than screen lots of conditions for the ether formation, design of an alternative pathway was considered to be a better option: the desired hybrid reactivator **3.24** can be obtained through an iterative retrosynthetic pathway (Scheme 3.2.17): the hybrid precursor **3.38** can be obtained by Sonogashira cross-coupling of the reactivator precursor **2.10** and the alkyne intermediate **3.41**, which can be synthesised by well-established Williamson reaction with fragment **3.26** and propargyl bromide (**3.42**).

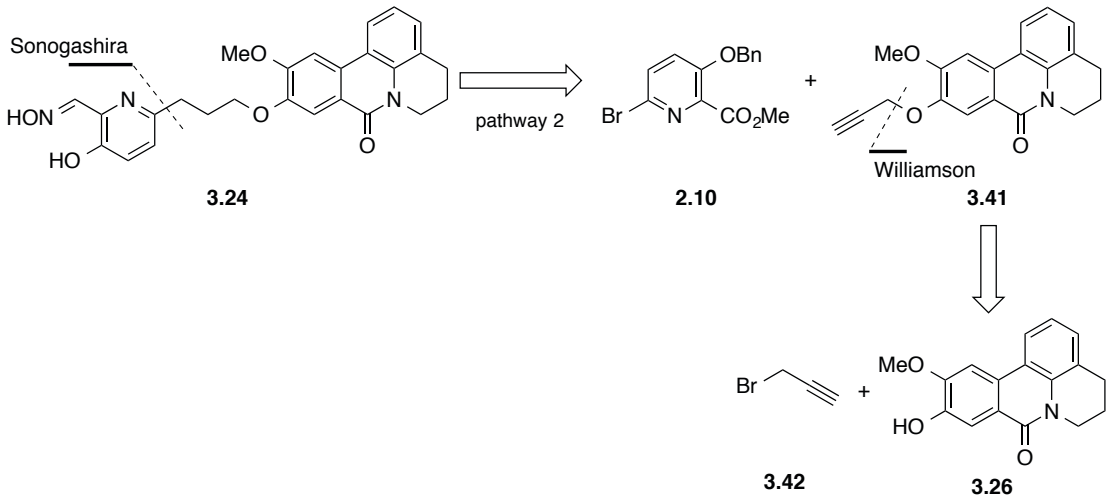

Scheme 3.2.17 Retrosynthetic pathway 2 to afford the hybrid **3.24**.

The phenol ether **3.41** was first afforded by Williamson reaction with propargyl bromide in good yield (82%, Scheme 3.2.18). Furthermore, the reaction was effective on a gram scale. Subsequent Sonogashira cross-coupling using the bromopyridine **2.10** gave the alkyne **3.38** in excellent yield (96%). It was found that presence of DMF was required to improve the solubility of the starting material and drive the reaction to form the product.

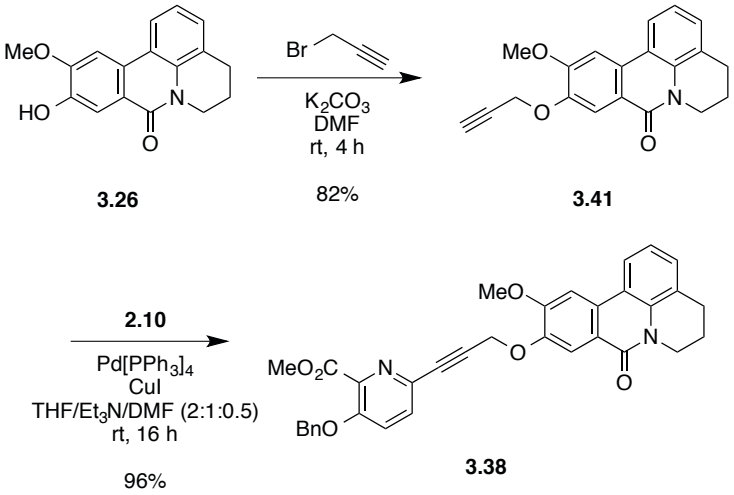

Scheme 3.2.18 Successive Williamson and Sonogashira reactions to afford alkyne **3.38**.

One-pot alkyne reduction and *O*-debenzylation was then performed under an atmosphere of hydrogen in presence of Pearlman's catalyst to afford the phenol **3.43** (Scheme 3.2.19). The alkyne **3.38** was found to be poorly soluble, so an investigation was carried out to determine a suitable solvent for the reduction step (Table 3.2.1).

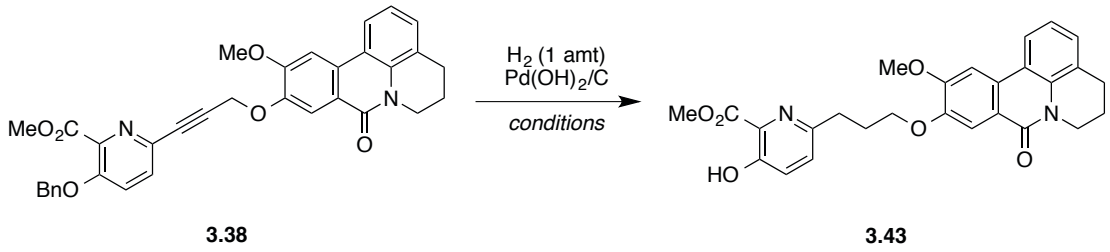

Scheme 3.2.19 One-pot alkyne reduction and *O*-debenzylation to afford the phenol **3.43**.

Entry	Solvent	Temperature	time	product (ratio)[a]
1	MeOH	rt	15 h 32 h	**3.38** / **3.43** (2:1) **3.43** (>90% on crude)
2	EtOH	rt	16 h 44 h	**3.38** / **3.43** (85:15) **3.43** / **3.44** (2:1)
3	EtOAc	rt then 50 °C	48 h	**3.38**
4	EtOAc/DMF	rt	24 h	**3.38** / **3.45** (4:1)
5	DMF	rt then 50 °C	72h	mixture of products including (**3.38**, **3.43**, benzylated alkene and alkane intermediate)
6	THF	rt	48 h	**3.38**
7	AcOH	rt	20 h	**3.38** / **3.45** (1.5:1)

Table 3.2.1 Hydrogenation conditions investigated to afford the adduct **3.43**.
[a]determined by ^{1}H NMR and/or LRMS.

While the desired phenol **3.43** was the major product obtained in MeOH after 32 h (entry 1), the pyridine **3.44** (Figure 3.2.9) was observed by LRMS as a product of degradation with EtOH when the reaction proceeded for longer periods (entry 2). No reaction was observed in EtOAc or THF (entries 3 and 6), while a mixture of EtOAc/DMF (5:1) lead to partial degradation of the starting material **3.38** into the pyridine **3.45** (Figure 3.2.9). A similar observation was made for reaction in glacial acetic acid (entry 7).

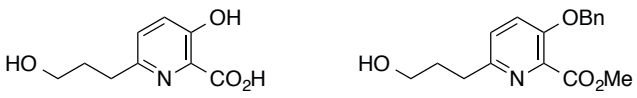

3.44 **3.45**

Figure 3.2.9 Two products of degradation observed by LRMS during the hydrogenation.

Nevertheless, sufficient crude product **3.43** from the extended reaction in MeOH (Table 3.2.1, entry 1) was available to be used in the three-step sequence for converting the methyl ester to the corresponding oxime hybrid reactivator **3.24** in non-optimised yield (4% after 4 steps, Scheme 3.2.20). Due to a lack of time, only a few milligrams were submitted for biological evaluation. Significantly, the feasibility of accessing the pyridinaldoxime **3.24** was proven and some preliminary biological evaluation was enabled.

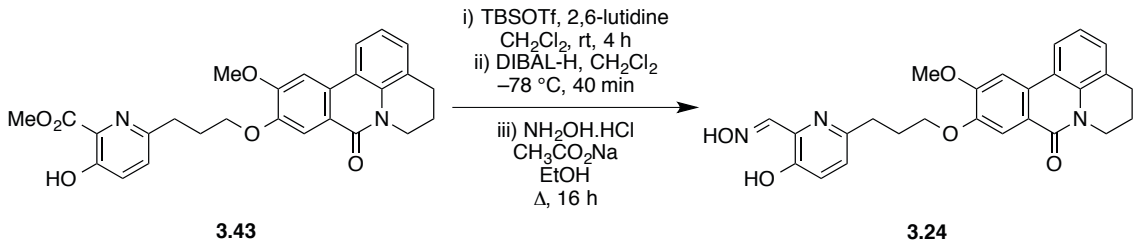

Scheme 3.2.20 Three-step sequence to afford the hybrid reactivator **3.24**.

Hence, the final hybrid reactivator **3.24** was obtained in 13-steps from isovanillin. Subsequent biological investigation was undertaken at IRBA and IBS in the groups of Dr. Florian Nachon and Dr. Martin Weik, respectively, and is discussed in chapter 4.

3.3 Conclusion

The objectives detailed within this chapter were to design and synthesise novel uncharged bifunctional reactivators with structurally different and original PSL moieties in order to potentially discover new powerful and effective reactivators of poisoned AChE. Towards this aim, the first hybrid reactivator **3.1** bearing a quinoline scaffold was designed using molecular simplification and synthesised. Then hybrid **3.24** bearing an alkaloid scaffold based on a natural product was prepared. Unfortunately, the synthesis of pyridine PSL hybrid **3.2** was interrupted due to a lack of time and material. Nonetheless, it is undoubtedly an interesting scaffold that needs to be further evaluated due to its promising in silico screening results and simplified structure.

While the quinoline hybrid **3.1** was attractive in terms of length of synthetic route compared to the previously synthesised reactivators (chapter 2), the synthesis of hybrid **3.24** was really exciting and challenging from diverse points of view (different scaffold, varied chemistry, multi gram scale synthesis until the very last step). The synthetic availability of the hybrids containing novel PSLs is an important achievement, and enabled subsequent biological investigation in the context of reactivation of poisoned AChE.

Chapter 4: Biological evaluation of hybrid reactivators

4.1 *In vitro* assays

Due to the high risk of hazard involved in OPNA manipulation, *in vitro* assays were carried out in authorised army laboratories at the Institut de Recherche Biomédicale des Armées, (IRBA, Brétigny-sur-Orge, France) under the supervision of Dr. Florian Nachon.[5]

4.1.1 Protocol

The reactivators are characterised by 3 constants that are k_r (reactivation rate constant), K_D (dissociation constant) and k_{r2} (reactivation efficacy) that have been previously defined in section 1.5.1. The reactivation rate constant k_r represents the displacement velocity of the phosphylated residue from the catalytic site by the reactivator, whereas the approximate dissociation constant of the reactivator/phosphyl-AChE complex K_D characterises the affinity of the reactivator towards the enzyme (the lower, the better the affinity is).

These constants are determined by monitoring the acetylcholinesterase reactivation activity using the Ellman assay (Scheme 4.1.2).[320,321]

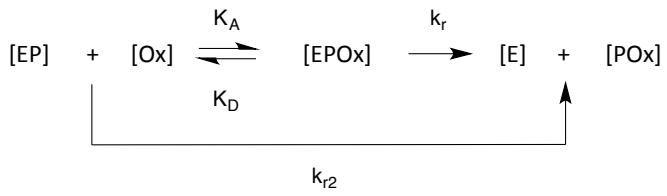

Scheme 4.1.1 Reactivation mechanism and associated kinetic description.

First, the enzyme is inhibited using a large excess of the desired nerve agent (10 equiv) until no AChE activity remains, resulting in the inhibited complex (EP, Scheme 4.1.2). At this point, excess of OPNA is removed by desalting on a gel filtration column. Then, the oxime (Ox - hybrid reactivator) is added at a certain concentration ([Ox]) and reacts with the inhibited

[5] Acknowledgment to Dr. José Dias and co-workers for conducing the *in vitro* assays.

enzyme. The percentage of reactivated enzyme ($\%E_{react}$) can be measured by spectrophotometry as the ratio of the percentage of activity recovered (%Activity) and the activity in the control. This measurement is facilitated using Ellman's reagent (5,5'-dithiobis-[2-nitrobenzoic acid], also called DTNB) that reacts with the thiolate species generated *in situ* after reaction of the recovered enzyme with acetylthiocholine (ATC) to form a subsequent disulfide species and releases the dianion TNB^{2-}. The latter has a bright yellow colour that can be quantified by measuring the absorbance of visible light at 412 nm.

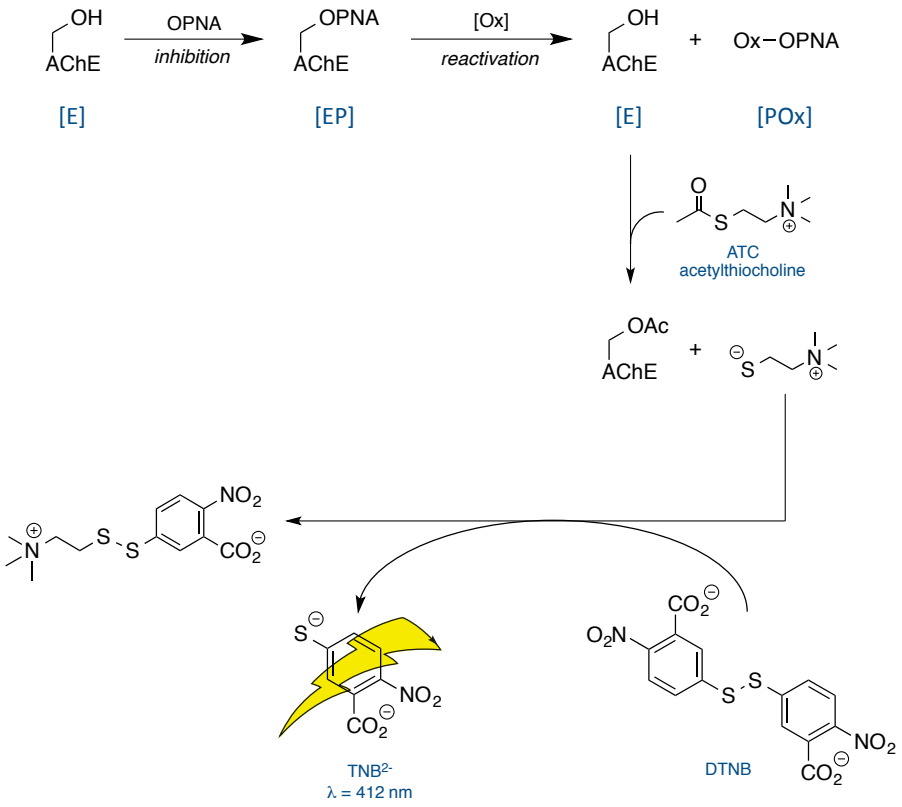

Scheme 4.1.2 Principle of Ellman assay.

The curve %Activity as a function of time can be plotted as shown (Figure 4.1.1, one measurement corresponding to one curve). Then, when the test is repeated at different concentrations, various curves are obtained (plot (a) Figure 4.1.1). The reaction order is considered to be 1 for complete reactivation, while the concentration of inhibited enzyme is negligible compared to the concentration of oxime: $[EP]_0 << [Ox]$. In this case, the apparent reactivation rate constant k_{obs} has to be taken into account.[129] It represents the first-order reactivation constant for a specific concentration of oxime and for $[OX] << K_D$, the second-order rate constant k_{r2} is the ratio of the reactivation rate constant k_r and the approximate

dissociation constant of the reactivator/phosphyl-AChE complex K_D. Graphically speaking, k_r represents the top value reached for curves obtained by plotting k_{obs} according to the concentration of oxime and K_D the concentration corresponding to 50% of the maximum activity.

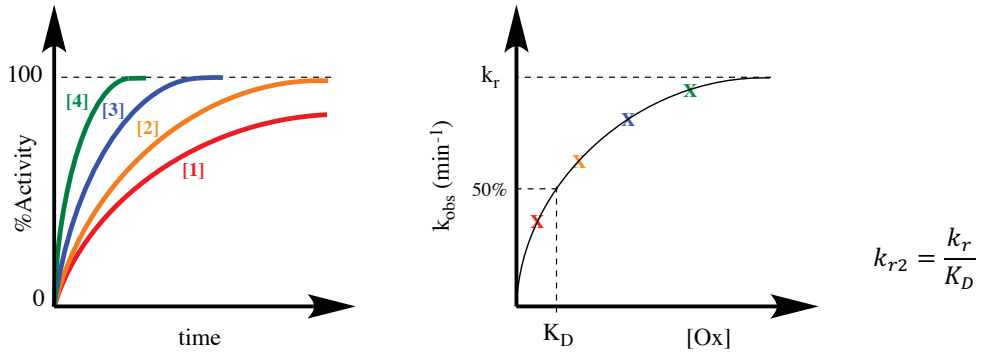

$$\%Activity = 100.(1 - e^{-k_{obs}t})$$

$$k_{obs} = \frac{k_r.[OX]}{K_D + [OX]}$$

(a) (b)

Figure 4.1.1 Plots and determination of reactivation constants.

Some examples of the curves obtained for the reactivation of VX-*h*AChE using hybrid reactivator **2.8** are shown below.

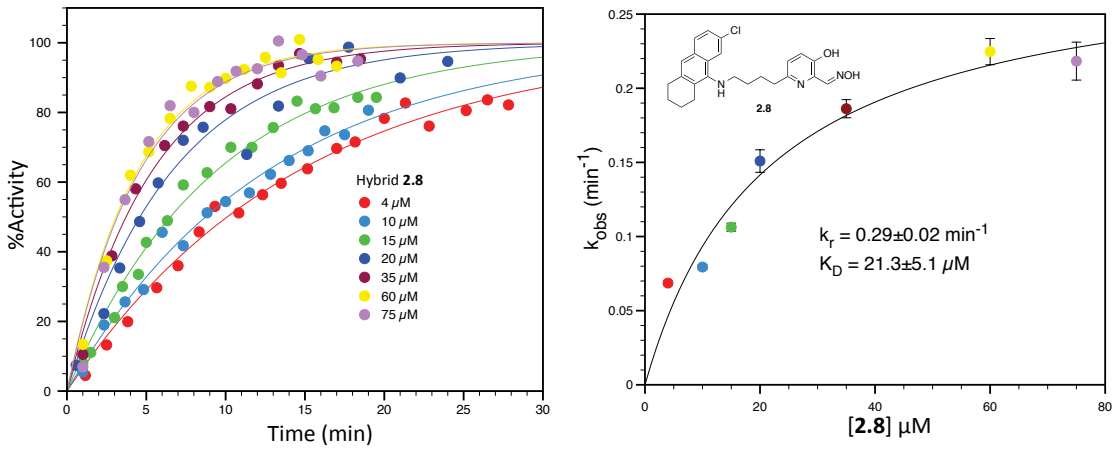

(a) (b)

Figure 4.1.2 Example of reactivation plots to determine the reactivation constant (hybrid reactivator **2.8**) for VX-*h*AChE.

In order to evaluate the *in vitro* potencies of all newly synthesised hybrids (Figure 4.1.4), the results will be compared to the efficacies measured for the standard reactivators and our most potent lead hybrid compound **2.4**.

Notably, the first encouraging result concerned the solubility of the new hybrids. Disappointingly, it has not been possible to evaluate many of the molecules synthesised in the past due to poor solubility properties. As a consequence of the improved solubility characteristics of the new hybrids, all of them have been tested and evaluated for CWA intoxications (VX, Sarin and Tabun) along with pesticides poisoning (ethyl paraoxon). It is important to mention that due to the relocation of IRBA institute in the past 2 years, regulations prevented the manipulation of samples contaminated with CWA. Hence, surrogate nerve agents were used meanwhile.

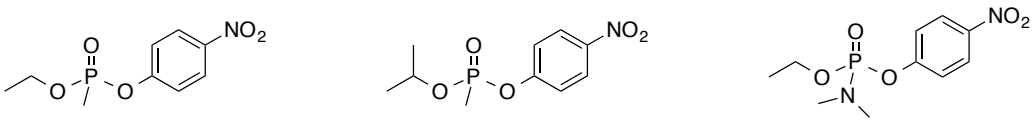

VX surrogate Sarin surrogate Tabun surrogate

Figure 4.1.3 Nerve agent surrogates.

To facilitate the understanding of the results, the *in vitro* evaluation is organised according to the OPNA used for a preliminary discussion before being generally reviewed. All reactivation curves are reported in the experimental section (section A.8).

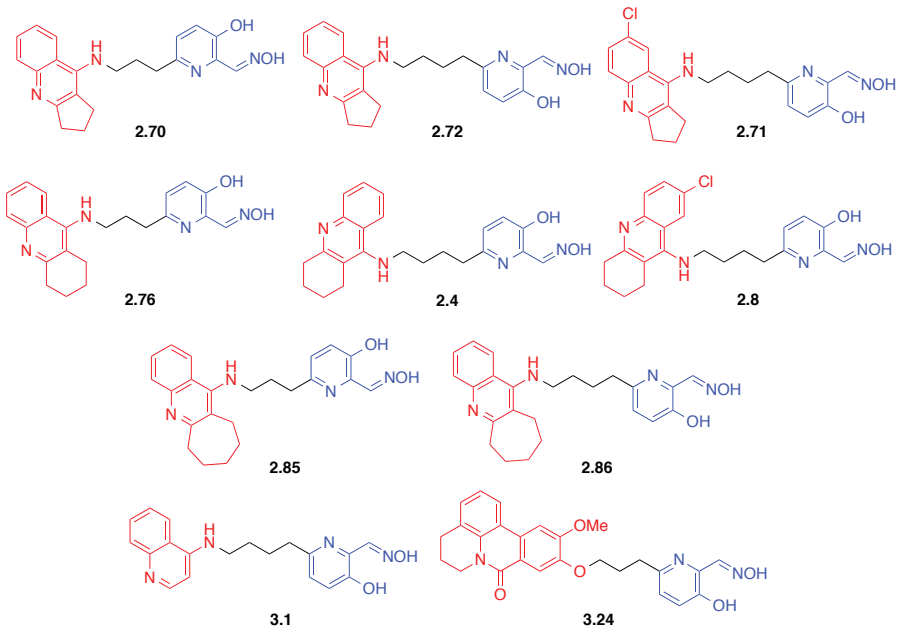

Figure 4.1.4 Structures of hybrid reactivators synthesised and evaluated.

4.1.2 Reactivation of VX-*h*AChE

The results for the *in vitro* reactivation of VX-inhibited *h*AChE are described in Table 4.1.1 and the reactivation efficacies (k_{r2}) are plotted below to facilitate the visualisation of the results.

	VX-*h*AChE			
Reactivator	K_D (μM)	k_r (min^{-1})	k_{r2} (mM^{-1} min^{-1})	%reactivation at 100 μM compared to Hi-6
2-PAM	215 ± 75	0.06 ± 0.01	0.28	-
Trimedoxime	n.d.[a]	n.d.[a]	0.50	-
Obidoxime	54 ± 12	0.60 ± 0.05	11	-
Hi-6	50 ± 26	0.44 ± 15	9	100
2.4[245]	31 ± 6	0.72 ± 0.07	22	
2.70[b]				
2.71[b]				
2.72	7.97 ± 1.34	0.14 ± 0.005	17.1	85
2.76[b]				
2.8	21 ± 5.1	0.29 ± 0.02	13.6	
2.85	21 ± 1.89	0.23 ± 0.006	10.6	4
2.86[b]				
3.1	3.9 ± 0.5	0.14 ± 0.003	33.9	94
3.24[b]				

Table 4.1.1 Reactivation constants for VX-inhibited *h*AChE. ([a]not determined if [OX] << K_D, then there is a linear dependence between k_{obs} and [Ox]: $k_{obs}= (k_r/K_D)[Ox]$. In this case, k_r and K_D cannot be determined, but $k_{r2}= k_r/K_D$ is the slope of the line; [b]underway).

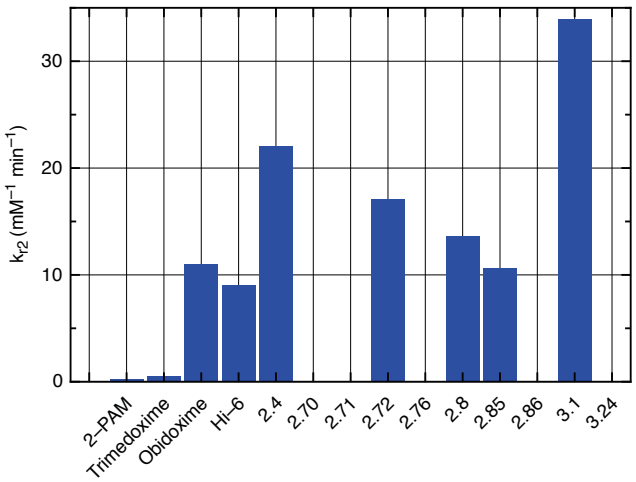

Figure 4.1.5 Corresponding chart for VX reactivation.

Quite remarkably, all hybrids exhibited a potency of reactivation higher than the standard reactivators. The novel hybrids outperformed from 1- to 4-fold Hi-6 and obidoxime currently the most efficient drug for VX poisoning. Besides, they outclassed 2-PAM from 45- to 121-fold. It is important to highlight the fact that if most analogues of hybrid **2.4** almost reach the efficiency of the lead compound, they also exhibited a better binding affinity towards the phosphylated AChE compared to **2.4**, as they displayed a smaller K_D value. This outcome validates one of our first goals of improving the affinity of the lead compound **2.4**. To our delight, hybrid **3.1** was shown to be the most potent drug synthesised as it has an efficacy 1.5-fold better, an affinity 8-fold better and slightly inferior reactivation rate compared to reactivator **2.4**. Last but not least, hybrid **3.1** caused as much reactivation as Hi-6 at 100 μM.

Interestingly, the low percentage of reactivation of compound **2.85** compared to Hi-6 (4%) can be explained by a good inhibitory ability of the reactivator. This trend is also observed with the other OPNAs.

4.1.3 Reactivation of Sarin-*h*AChE

The results for the *in vitro* reactivation of Sarin-inhibited *h*AChE are described in Table 4.1.2.

	Sarin-*h*AChE			
Reactivator	K_D (μM)	k_r (min^{-1})	k_{r2} (mM^{-1} min^{-1})	%reactivation at 100 μM compared to Hi-6
2-PAM	27.6	0.25	9.1	-
Trimedoxime	n.d.[a]	n.d.[a]	n.d.	-
Obidoxime	31.3	0.94	29.9	-
Hi-6	50.1	0.68	13.5	100
2.4	20.4 ± 3	0.38 ± 0.01	16	23
2.70[b]				
2.71[b]				
2.72	49.8 ± 6.6	0.34 ± 0.014	12.6	66
2.76[b]				
2.8	11.5 ± 3	0.14 ± 0.007	11.8	71
2.85	32.6 ± 4	0.25 ± 0.01	7.7	4
2.86[b]				
3.1	29.97 ± 3	0.46 ± 0.016	18.3	70
3.24[b]				

Table 4.1.2 Reactivation constants for Sarin-inhibited *h*AChE. ([a]not determined if [OX] << K_D, then there is a linear dependence between k_{obs} and [Ox]: $k_{obs}= (k_r/K_D)[Ox]$. In this case, k_r and K_D cannot be determined, but $k_{r2}= k_r/K_D$ is the slope of the line; [b]underway).

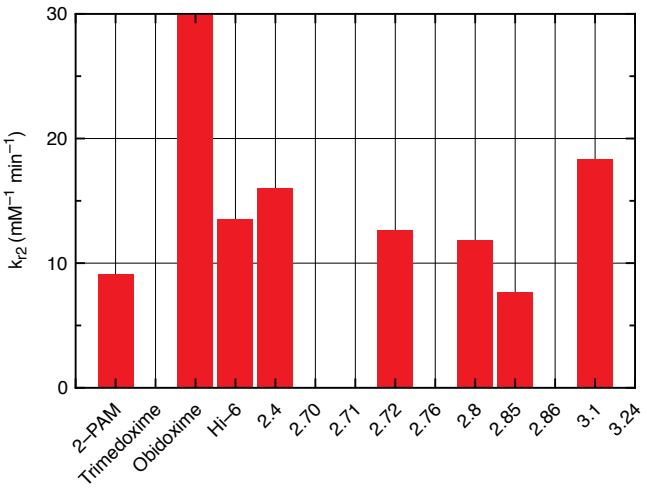

Figure 4.1.6 Corresponding chart for Sarin reactivation.

While the synthesised hybrids exhibited a potency of reactivation higher than 2-PAM and Hi-6, they remained slightly lower than obidoxime. They outclassed 2-PAM from 1- to 2-fold and Hi-6 up to 1.4-fold. Most analogues exhibited similar affinity (K_D) and reacted as fast as our lead compound **2.4**. However, they also displayed higher percentage reactivation compared to hybrid **2.4** at 100 μM, which only reactivated 23% compared to Hi-6. Notably, hybrid **3.1** appeared to be the most potent drug synthesised in term of efficacy (1.2-fold better than **2.4**), affinity (similar to **2.4**), reactivation rate (1.2-fold faster), capable of reactivating almost as much as Hi-6 at 100 μM (70%).

4.1.4 Reactivation of Tabun-*h*AChE

The results for the *in vitro* reactivation of Tabun-inhibited *h*AChE are described in Table 4.1.3.

	Tabun-*h*AChE			
Reactivator	K_D (μM)	k_r (min^{-1})	k_{r2} (mM^{-1} min^{-1})	%reactivation at 100 μM compared to Hi-6
2-PAM	706 ± 76	0.010 ± 0.0005	0.01	-
Trimedoxime	27 ± 4	0.085 ± 0.005	0.6	-
Obidoxime	250 ± 110	0.040 ± 0.006	0.16	-
Hi-6	n.r.[b]	n.r.[b]	n.r.[b]	0
2.4[245]	7.1 ± 1.5	0.021 ± 0.001	3.0	
2.70[c]				
2.71[c]				
2.72	9.4 ± 1.4	0.34 ± 0.014	12.6	96
2.76[c]				
2.8	10.4 ± 2.6	0.136 ± 0.007	11.8	70
2.85	6.0 ± 2.9	0.075 ± 0.006	12.4	3
2.86[c]				
3.1	5.8 ± 1.9	0.36 ± 0.02	62.4	97
3.24[c]				

Table 4.1.3 Reactivation constants for Tabun-inhibited *h*AChE. ([a]not determined if [OX] << K_D, then there is a linear dependence between k_{obs} and [Ox]: $k_{obs}= (k_r/K_D)[Ox]$. In this case, k_r and K_D cannot be determined, but $k_{r2}= k_r/K_D$ is the slope of the line; [b]no reactivation observed until [Ox]= 5mM; [c]underway).

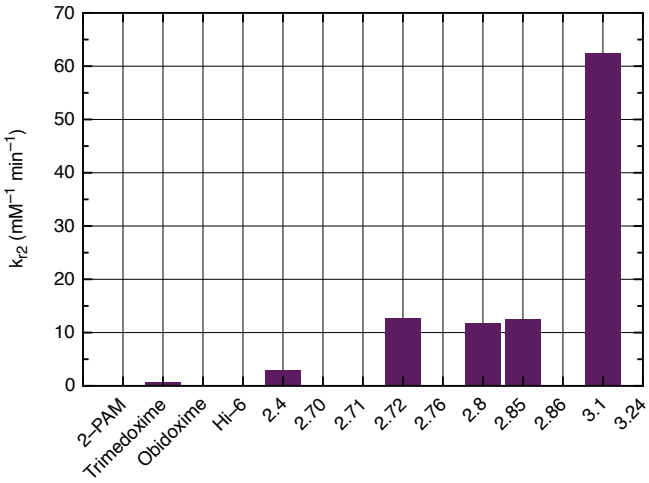

Figure 4.1.7 Corresponding chart for Tabun reactivation.

Most significantly, all hybrid reactivators exhibited a potency of reactivation much higher than all standard reactivators and the lead compound **2.4**. They outperformed trimedoxime, the only known reactivator moderately effective against Tabun poisoning, from 20- to 104-fold. These results are explained by a better affinity towards the active site (K_D much smaller) and a faster reactivation (k_r superior). Exceptionally, hybrid **3.1** stood out once again, exhibiting an efficacy 21-fold better, an affinity 1.2-fold better and reactivation rate 17-fold faster than reactivator **2.4**. Hybrid **3.1** showed also a quantitative reactivation of Tabun-poisoned *h*AChE at 100 μM.

4.1.5 Reactivation of Paraoxon-*h*AChE

The results for the *in vitro* reactivation of ethyl paraoxon-inhibited *h*AChE are described in Table 4.1.4.

	Ethyl paraoxon-*h*AChE			
Reactivator	K_D (μM)	k_r (min^{-1})	k_{r2} (mM^{-1} min^{-1})	%reactivation at 100 μM compared to Hi-6
2-PAM[129]	187.3 ± 19	0.17 ± 0.007	0.91	-
Trimedoxime[149]	62 ± 19	0.97 ± 0.01	16	-
Obidoxime[149]	65 ± 17	1.22 ± 0.01	19	-
Hi-6	210 ± 31	0.63 ± 0.04	3	100
2.4[245]	3.6 ± 0.2	0.111 ± 0.002	31	
2.70[a]				
2.71[a]				
2.72	7.2 ± 0.66	0.07 ± 0.001	9.5	90
2.76[a]				
2.8	5.7 ± 1.7	0.11 ± 0.01	19.2	
2.85	19.5 ± 2.6	0.023 ± 0.0008	1.2	7
2.86[a]				
3.1	9.3 ± 1.38	0.19 ± 0.001	20.4	100
3.24[a]				

Table 4.1.4 Reactivation constants for ethyl paraoxon-inhibited *h*AChE. ([a]underway).

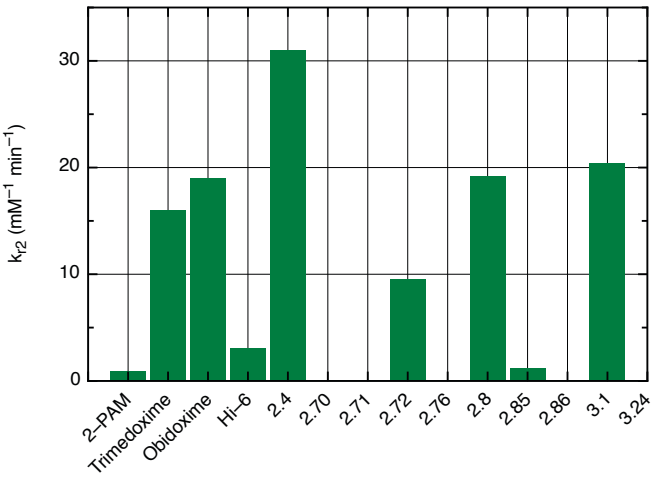

Figure 4.1.8 Corresponding chart for Paraoxon reactivation.

The hybrids also exhibited good potencies for the reactivation of *h*AChE poisoned by pesticides. Some of them (hybrids **2.8** and **3.1**) were more effective than all standard reactivators with enhanced affinity, albeit hybrid **2.4** remained the most effective candidate. However, hybrid **3.1** was shown to be 1.7-fold faster than hybrid **2.4** and quantitatively reactivated the inhibited enzyme at 100 μM.

4.1.6 General outcomes

All reactivation efficacies (k_{r2}) are herein plotted to facilitate the visualisation of the results (Figure 4.1.9).

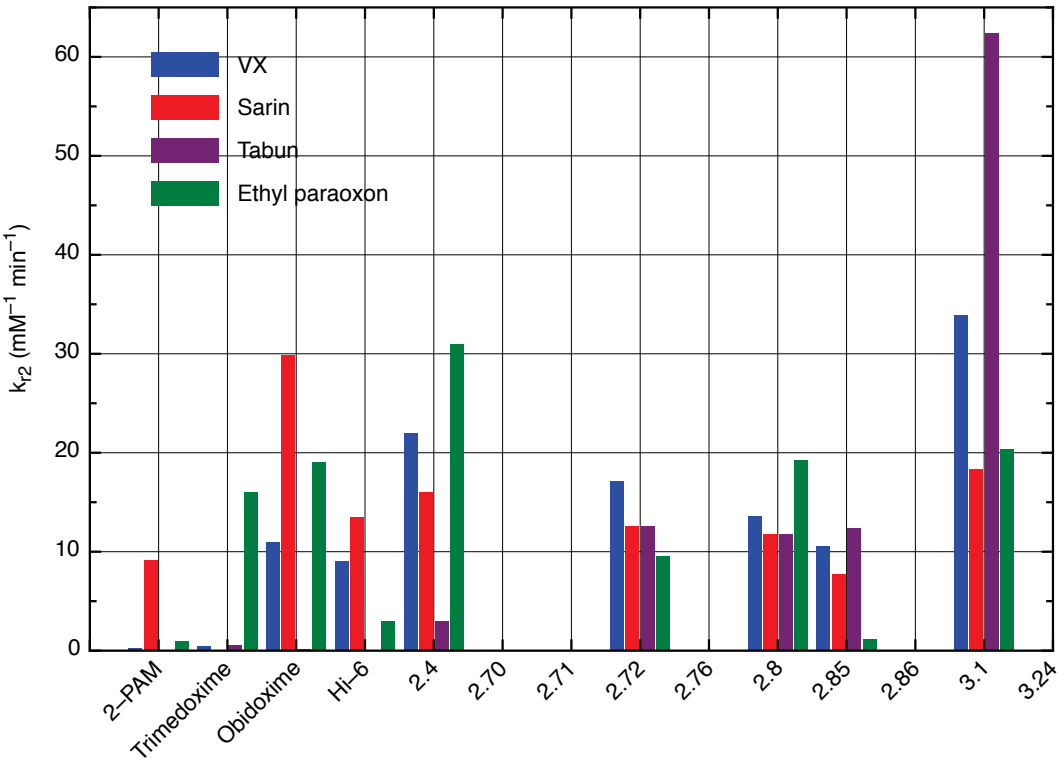

Figure 4.1.9 Reactivation efficacies (k_{r2}) of standard reactivators and synthesised hybrids for VX-, Sarin-, Tabun and ethyl Paraoxon-inhibited *h*AChE.

It is clear that the synthesised drugs are in general more effective *in vitro* than the standard reactivators (2-PAM, trimedoxime, obidoxime and Hi-6) for all OPNA tested. While the lead compound **2.4** exhibited similar potency than its direct analogues (hybrids **2.8**, **2.72** and **2.85**) for VX, Sarin and Paraoxon poisoning. The new hybrids are generally superior against Tabun intoxication (Figure 4.1.9) giving them a broad spectrum capability for reactivating different

types of OPNA poisoned AChE. Besides, it is important to highlight the fact that they displayed a better affinity (K_D smaller) compared to **2.4**, validating one of our first goals of enhancing the affinity of the lead compound **2.4** towards the inhibited enzyme. However, measurement of the IC_{50} for each candidate is required to make sure that the synthesised hybrids are not competitive inhibitors for the native enzyme, as observed for compound **2.4** (*vide supra*, section 2.1.1). Thus, the results are described in Table 4.1.5.

Reactivator	IC_{50} (M)
tacrine **2.6**[322]	$0.20 \pm 0.02\ 10^{-6}$
2.4[245]	$0.25 \pm 0.02\ 10^{-6}$
2.70[a]	
2.71[a]	
2.72	$1.2 \pm 0.1\ 10^{-3}$
2.76[a]	
2.8	$0.48 \pm 0.06\ 10^{-3}$
2.85	$1.15 \pm 0.1\ 10^{-6}$
2.86[a]	
3.1	$0.75 \pm 0.05\ 10^{-3}$
3.24[a]	

Table 4.1.5 Inhibition of native *h*AChE ([a]underway).[6]

Interestingly, towards the native enzyme, hybrid **2.8** displayed a 3-orders-of-magnitude enhancement in inhibitory activity compared to its analogue **2.4** (Table 4.1.5). This inhibition potency decrease is due to the hindrance introduced by the chlorine substituent at C7, and its interaction with the PAS. This topic will be further discussed within the structural investigation (*vide infra*, section 4.3). Interestingly, a 7-membered ring in the PSL moiety in hybrid **2.85** seems to enhance the interactions with the PAS increasing the inhibition potency. With such low value of 1.15 µM, hybrid **2.85** is considered as a competitive inhibitor, confirming the observation made in previous reactivation assays.

[6] All IC_{50} curves are reported in the experimental part (section A.6).

Finally, the most important results lie in hybrid **3.1** that outperformed all other reactivators (standard and lead compounds) for both CWAs and pesticides. Remarkably, it outclassed trimedoxime by 104-fold for Tabun poisoning and the percentage of reactivation at 100 μM was shown to be quantitative or near quantitative compared to Hi-6 (currently on the way to become the drug in use in the auto-injector). Also encouraging is the finding that hybrid **3.1** exhibited a mM inhibitory potency (1.4 ± 0.1 mM) as a poor competitive inhibitor of *h*AChE (Table 4.1.5).

4.2 Pharmacokinetics on mice

After validating the concept of bifunctional hybrid reactivator *in vitro*, we are currently on the basis of the *in vivo* investigation at IRBA.[7]

In order to improve the solubility of the drug and its pharmacology, Dr. Rachid Baati has prepared different salts (acetate and hydrochloride) of the reactivator **2.4**. Preliminary studies on mice have showed the importance of the salt counter ion and are here under briefly described (Table 4.2.1).

oxime	concentration (μmol kg^{-1})	MRT[a] (min)	t_{max}[b] (min)	Reactivation max (%)
2.4	23.3	31 ± 3	5.5 ± 1	5.1 ± 1.1
2.4•AcOH	23.3	23 ± 2	6 ± 0.5	18.7 ± 1.6
2.4•HCl	23.3	20 ± 0.5	3.5	23 ± 2.3
2.4•HCl	100		underway	

Table 4.2.1 Results of reactivation studies on mice after VX intoxication. [a]Mean residence time. [b]Time corresponding when the curve reaches $\%E_{react}$.

The mean residence time (MRT) corresponds to how long the molecule spends in the organism before being eliminated: the lower the value, the lesser the effectiveness of the compound. Low MRT values can be particularly problematic for some OPNAs such as VX that tend to remain in the fat of the organism, diffusing slowly into the circulation. The value of t_{max} corresponds to the time at which the reactivation reaches its maximum: the lower, the better. Hypothetically, with a t_{max} of 1 h, the poisoned person could die before the drug would start to have its full effectiveness. Therefore, the best candidate should display the highest MRT and $\%E_{react}$ alongside a lower t_{max}. The preliminary tests were made at a concentration corresponding to the limit of solubility observed with hybrid **2.4**, only 5% reactivation was observed. Interestingly, this maximum reactivation value increased by 3.6 and 4.5 fold when the acetate salt and the hydrochloride salt of hybrid **2.4** were employed, respectively.

Assays with higher concentrations of hybrid **2.4** hydrochloride are currently underway, along with preliminary assays involving hybrid **3.1** hydrochloride salt.

[7] Acknowledgment: Dr. Guilhem Calas for conducing the preliminary *in vivo* assays.

4.3 Structural biology

Structural biology studies have been conducted to support our *in vitro* results and were carried out at the Institut de Biologie Structurale, (IBS, Grenoble, France) in the laboratories of Dr. Martin Weik. As a very powerful instrument that provides time–average pictures of biological macromolecules, X-ray crystallography helps scientists to improve their understanding of biological functions on a molecular level that usually requires knowledge about both structural and dynamic aspects of, for example, an enzyme. Importantly for AChE, one of natures fastest enzymes,[31,323] X-ray crystallographic structures of AChE from *Torpedo Californica* (*Tc*AChE) complexed with our hybrid reactivators have been obtained with a view to understanding the interactions with both active and peripheral binding sites of the enzyme. Orthorhombic-1 crystals of *Tc*AChE[50] were soaked into the mother liquor solution containing 1 mM reactivator and 5% DMSO, loop-mounted and flash-cooled at 100 K. The diffraction data were collected at the European Synchrotron Radiation Facility (ESRF, Grenoble, France).

Initially, computational docking studies predicted that a substituted tacrine, such as 7-chloro derivative (hybrid **2.8**, Figure 4.3.1, b) would create a steric clash with residues of the PAS at the entrance of the active site gorge, thus decreasing binding compared to the lead tacrine hybrid **2.4**.

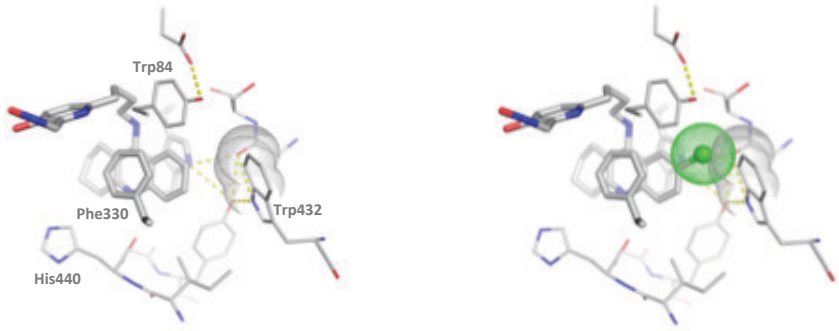

(a) (b)

Figure 4.3.1 Computational calculations predicting steric clash at the PAS due to the presence of a chloro substituent (hybrid **2.8**, b) compared to its unchlorinated analogue (hybrid **2.4**, a).

To our delight, these predictions were confirmed by isolation of crystallographic structures of *Tc*AChE complexed with both new hybrids **2.4** and **2.8** (Figure 4.3.2 and Figure 4.3.5).[8] In complexes with our lead compound **2.4** (Figure 4.3.2), two molecules of reactivator are observed in the gorge. At the catalytic site (bottom of the gorge), **2.4** is oriented "upside-down" pointing the carbon linker to the PAS. The tacrine moiety is sandwiched between the residues Trp84 and Phe330 by making strong π–π interactions (Figure 4.3.3). The presence of a molecule **2.4** in the active site prevents the oxime function of the molecule located at the PAS to enter into the gorge as originally designed for the effective reactivation reaction.

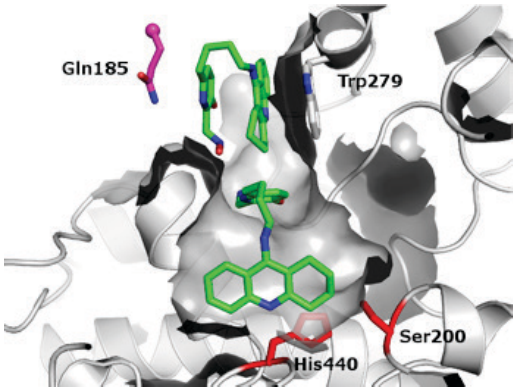

Figure 4.3.2 Binding of two hybrid reactivators **2.4** in the gorge active site of *Tc*AChE. The CAS residues are displayed in red (His440 and Ser200) while the PAS residues are in white (Trp279). Resolution 2.6 Å. 2 mFo-DFc at 1 σ level.

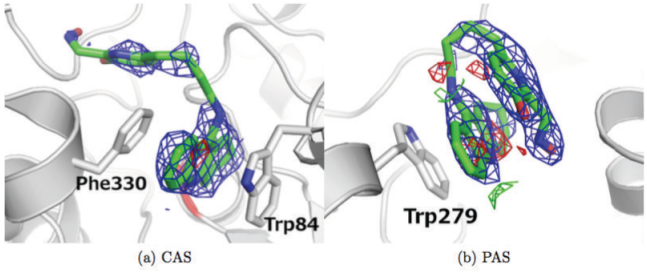

Figure 4.3.3 2 Fo-Fc electron density maps at 1 σ level (blue mesh) and Fo-Fc at +3 and -3 σ level (green and red mesh respectively) for hybrid **2.4** in the gorge of *Tc*AChE. Panels show the ligand at CAS (a, left), with the position of the catalytic serine (in red), and PAS (b, right) of *Tc*AChE.

[8] Acknowledgment: Dr. Gianluca Santoni for obtaining X-ray crystallographic structures of *Tc*AChE complexed with hybrid reactivators **2.4** and **2.8** in the frame of his PhD (University of Grenoble, France).

At the PAS, the tacrine moiety of the second molecule of **2.4** is making strong π–π interactions with Trp279 confirming the strategy for the mode of binding of bifunctional reactivators (Figure 4.3.2 and Figure 4.3.3, b). However, the pyridine aldoxime moiety orientation observed is not suitable for effective reactivation. Instead of pointing down towards the gorge active site, the carbon linker forms a U-turn, stacking the oxime between the tacrine moiety and Trp279 and the hydrogen bonds with Tyr334 and Gly335 (in yellow Figure 4.3.4). Additionally, the presence of residue Gln185 (in magenta Figure 4.3.2, Figure 4.3.4 and Figure 4.3.5) from the symmetry-related enzyme in the crystal contributes to stabilise the oxime in this conformation (side chain lies parallel to the pyridine aldoxime moiety at 3.6 Å, Figure 4.3.4). Specific to orthorhombic-1 crystals packing, this distance problem can be solved using trigonal crystals that are differently organised. Thus the vicinity of the symmetry-related enzyme should not affect the soaking. Unfortunately, this experiment has not yet been fruitful, due to the difficulty in growing trigonal *Tc*AChE crystals.

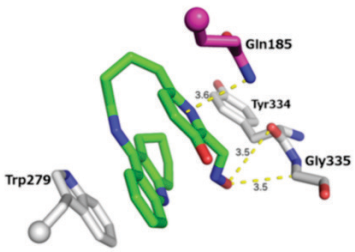

Figure 4.3.4 Binding of Hybrid Reactivator 1 at the PAS region of *Tc*AChE (distance of hydrogen bonds are expressed in Å).

Notably, the tacrine moiety of both molecules is well defined, while the electron density of the linker and the oxime function are slightly less clear (Figure 4.3.3). This observation can be either due to a side reaction (carboxylation), a higher mobility of this part of the molecule, and/or a partial hydrolysis of the oxime function under crystallographic conditions.

In the complex of hybrid **2.8** (Figure 4.3.5), only one molecule of reactivator is displayed in the gorge. The electron density map showed the presence of a tacrine moiety at the PAS, stacking with the residue Trp279 by π–π interactions. The presence of the chlorine in this hybrid clearly defined the orientation of the reactivator by being the strongest peak in terms of electron density. The same rotation of the pyridine aldoxime described above is observed due to the symmetrical artefact partner that helps the stabilisation of this conformation.

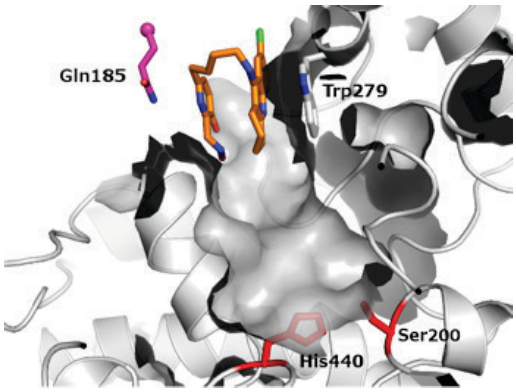

Figure 4.3.5 Binding of hybrid reactivator **2.8** in the gorge active site of *Tc*AChE. The CAS residues are displayed in red (His440 and Ser200) while the PAS residues are in white (Trp279). Resolution 2.9 Å. 2mFo-DFc at 1σ level.

However, no electron density has been found in the CAS, in contrast to the complex with hybrid **2.4**. This observation confirmed the fact that steric hindrance caused by the chlorine atom prevents the hybrid entering the gorge, and it binds only at the peripheral site. This result supports the difference of affinity observed between hybrids **2.4** and **2.8** (K_D and IC_{50}, section 4.1) and thus confirms the action of a chlorine substituent in such position.

4.4 Irritancy assays[9]

In this part, we were interested by the irritation potency expressed by the PSL moieties used in the hybrid syntheses. Lindsay and co-workers have shown that human transient receptor potential ankyrin 1 (TRPA1) is a receptor for irritants on nociceptive neurons involved in pain perception in humans.[324] Hence, a series of four acridine analogues (hereunder, Figure 4.4.1) were investigated at Dstl for testing the activity as agonists of TRPA1.

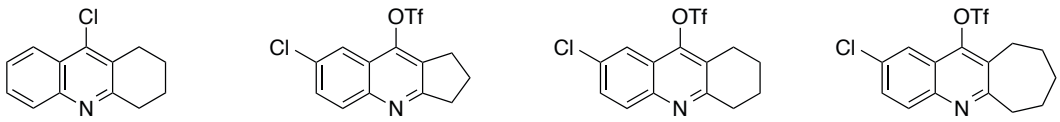

4.1 **2.59** **2.22.3** **2.60**

Figure 4.4.1 Analogues tested for irritancy assays.

[9] Acknowledgment: Christopher D. Lindsay and Christopher Green (Dstl) for obtaining and analysing the biological data supplied for the irritancy assay.

From the graph of the data (Figure 4.4.2), it can be seen that only product **4.1** and *trans*-cinnamaldehyde generated a dose-response curves that reached a plateau at the highest concentrations tested, providing EC_{50} estimates of 118 μM (95%CI 103 - 136 μM) and 391 μM (95%CI 337 - 454 μM) respectively.

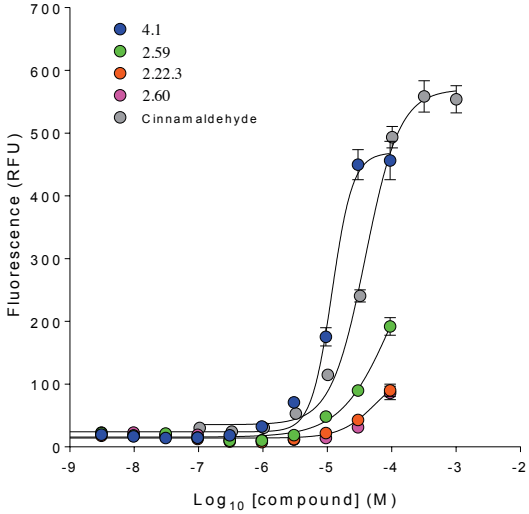

Figure 4.4.2 Concentration response relationships for tested scaffolds and *trans*-cinnamaldehyde.

The limited solubility of the acridine analogues restricted the dose range to 0 - 94.5 μM. Within this range, the dose-response titration curves for **2.59**, **2.22.3** and **2.60** did not reach a plateau, so curve fits (and therefore EC_{50}) could not be obtained. However the acridine analogues were ranked on the basis of the maximum mean % fluorescence intensity relative to *trans*-cinnamaldehyde they induced at 94.5 μM (the highest concentration used). This gave an order of potency for these compounds as follows:

4.1 (79.2% ± 5.6) > **2.59** (31.8% ± 2.5) > **2.22.3** (13.7% ± 1.8) > **2.60** (12.5% ± 1.9)

(mean±sem relative to *trans*-cinnamaldehyde).

Scaffold **4.1** therefore appeared to be the most potent of the acridine analogues tested for TRPA1 agonist activity, and therefore it is the most likely to be an irritant in humans.

4.5 Conclusion

The biological evaluation of the newly synthesised hybrids has yielded exciting results. First of all, the direct analogues of the lead compound **2.4** proved to be more potent than the standard reactivators for various OPNA intoxications. Then, for an effective reactivation, they showed higher binding affinity towards inhibited enzyme and lower affinity towards the native enzyme. These encouraging results are protected in a registered patent (Pyridine derivatives as uncharged reactivators of human acetylcholinesterase and their preparation and use for the treatment of nervous and respiratory failure, *WO2015075082 A1 20150528*).

Notably, this evaluation allowed us to discover a new class of quinoline hybrid reactivators with compound **3.1**, which outperformed all known reactivators (standard and lead compounds) for both CWA and pesticide intoxications. Extraordinarily, it outclassed by far (104-fold) trimedoxime, known to be to date the only reactivator moderately effective for Tabun poisoning. Consequently, thanks to its exceptional abilities, hybrid **3.1** shows promise for the title of the first broad-spectrum reactivator. This discovery has been recently patented by our team (Broad Spectrum Reactivators of OPNA-inhibition of human cholinesterases, *EP15306257*). Additionally, the irritancy potency of the tacrine scaffold reinforce the potential of hybrid **3.1** as better reactivator.

Structural biology studies supported our *in vitro* investigations and confirmed our design hypothesis. For instance, X-ray crystallographic structures have confirmed that our hypothesis concerning an additional substituent introduced into our lead compound to decrease its binding affinity and favour interactions at the peripheral site of the gorge active site exclusively.

Pleasingly, preliminary studies on mice have shown an improvement of reactivation potency working with the hydrochloride salt of the hybrid. Therefore, further studies will be conducted with the hybrid **3.1** hydrochloride.

Unfortunately, the biological evaluation of some hybrids such as **2.70**, **2.71**, **2.76**, **2.86** and **3.24** are currently underway and an update will be given during the viva.

Finally, as medicinal chemistry project, we keep in mind that measurement of log*P* is another important parameter (among Lipinski's rules) that has to be done to determine the druglikeness of such compound and will be investigated in the following weeks.

Chapter 5: General conclusions

The main goals of this research were to design, synthesise and evaluate the potency of novel uncharged bifunctional hybrid reactivators as potential future drugs against organophosphorus nerve agents (chemical warfare agents and pesticides) intoxications. Carried out in on both sides of the Channel, this research was also accomplished in close collaboration with Dr. Florian Nachon's team (IRBA), Dr. Martin Weik's team (IBS) and Prof. Pierre-Yves Renard's team (COBRA, University of Rouen),

After describing the hazards represented by organophosphorus nerve agents and their mechanism of action on humans, a literature review was provided to assess all the potential and actual treatments that have been developed in the past six decades (Chapter 1). Among those, we have highlighted the lack of truly effective treatments along with major drawbacks that hamper the current "tritherapy" with standard reactivators. On the top of the list, the blood brain barrier penetration issue prevents the reactivation of central AChE and despite lots of studies, there is no effective solution reported. Additionally, the effectiveness of any potential treatment for emergency use (e.g. battlefield) is decreased due to the fact that no broad spectrum reactivator has been found that is effective against all types of organophosphorus nerve agent poisoning.

Therefore our strategy focussed on the design and the synthesis of novel hybrids bearing a peripheral site ligand in order to improve the affinity of the reactivator towards the enzyme active site and a lipophilic uncharged reactivating function (3-hydroxypyridine aldoxime) to improve the passage across the blood brain barrier and reactivate the inhibited enzyme located in the central nervous system. The peripheral site ligand aims to improve the affinity of the reactivating function by cation-π or π-π interactions in the enzyme active site. However, this affinity has to be controlled and cannot be too strong in order to avoid creating competitive inhibitors. They must be uncharged to facilitate the blood brain barrier crossing and use the 3-hydroxypyridine aldoxime moiety as reactivating function to avoid the recapture phenomenon. Finally, these novel hybrids require great flexibility in order to penetrate inside the active site and optimally position themselves to efficiently reach the phosphylated serine.

Following the preliminary investigations explored by our group, the first targets consisted of analogues of the lead compound (tacrine moiety as PSL connected to the reactivating function 3-hydroxypyridine aldoxime through a 4 methylene linker) by modifying the structure of the

tacrine moiety or the length of the connecting arm. Through this structure-activity relationship study (Chapter 2), one of the main purposes was to explore the influence of adding a substituent (e.g. chlorine) in a key position, or altering the size of the aliphatic ring, on the enzyme (native and inhibited) affinity.

Revising the previously described synthetic route allowed us to discover precious novel trifluoromethanesulfonate scaffolds that have also the potential to be used to rapidly access functionalised *N*-alkylated tacrines (and analogues) for pharmaceutical research. The overall pathway has also been shortened and seven bifunctional hybrids have been isolated after multi-step syntheses in ~20% overall yields. Their biological evaluation has showed interesting improvements in terms of reactivation potency (Chapter 4), but also in affinity. In general, they were slightly more efficient that the standard reactivators (e.g. 2-PAM, Hi-6, obidoxime and trimedoxime) for VX, Sarin and Paraoxon poisoning. They also showed tremendous enhancement with respect to Tabun intoxications. From a design perspective, hybrid **2.8** showed the influence of a chlorine atom at C7 of the tacrine PSL that attenuated the affinity with the enzyme peripheral site without losing reactivating potency. This result is in accordance with the structural biology evaluation.

Today, attempts on dynamic crystallisation involving theses hybrids are currently underway in collaboration with Dr. Martin Weik's team (IBS, Grenoble) in order to improve our understanding of the mechanism of action on the molecular scale. Furthermore, additional reactivation assays are being carried out with other organophosphorus nerve agents and on the butyrylcholinesterase.

Following the bifunctional hybrid strategy, we have also designed and synthesised hybrid reactivators based on novel PSL scaffolds such as an alkaloid and quinoline. While the oxoassoanine-based hybrid was found to be quite challenging to synthesise, the quinoline-based hybrid **3.1** was rapidly isolated in reasonable overall yield. Outstandingly, the evaluation of hybrid **3.1** showed unprecedented reactivation potency by outclassing all known reactivators (standard and lead compound) for all chemical warfare agents (VX, Sarin and Tabun) and pesticides (Paraoxon) tested. Quite remarkably, it outperformed by 104-fold the standard reactivator trimedoxime for Tabun intoxication and it showed quantitative reactivation compared to Hi-6 in almost in every assay. Finally, hybrid **3.1** exhibited a millimolar inhibiting potency reducing the potential threat of competitive inhibition. Consequently, we have discovered a new lead compound that displayed tremendous reactivation potency and may prove to deserve the title of MVP "*Most Valuable Protector*".

Chapter 6: Résumé de thèse en français

6.1 Introduction

6.1.1 Agents neurotoxiques organophosphorés

Les organophosphorés (OPs) sont devenus des éléments essentiels de l'arsenal chimique militaire moderne pouvant être utilisés à des fins terroristes. Depuis leur découverte par celui qui est aujourd'hui considéré comme le « père des agents neurotoxiques », l'allemand Gerhard Schrader, les OPs tels que le gaz Sarin, le Cyclosarin, le Tabun, le VX et le Soman sont considérés comme des armes de destruction massive (Figure 6.1.1). Les récents évènements tragiques en France perpétrés par des terroristes en Janvier 2015, et d'autres de part le monde (Halabja, 1988 ; Tokyo, 1995 ; Syrie, 2013), démontrent hélas une recrudescence sans précédent d'actes malveillants terroristes contre les populations civiles et militaires, contribuant à élever le risque d'attaques chimiques à un niveau alarmant et ce, malgré l'accord des Nations Unies suite à la Convention Internationale de 1993 sur l'Interdiction des Armes Chimiques. Par ailleurs, les intoxications par les pesticides organophosphorés (Paraoxon, Parathion ou TEPP, Figure 6.1.1) accidentelles restent courantes en milieu agricole et dans les pays en voie de développement.

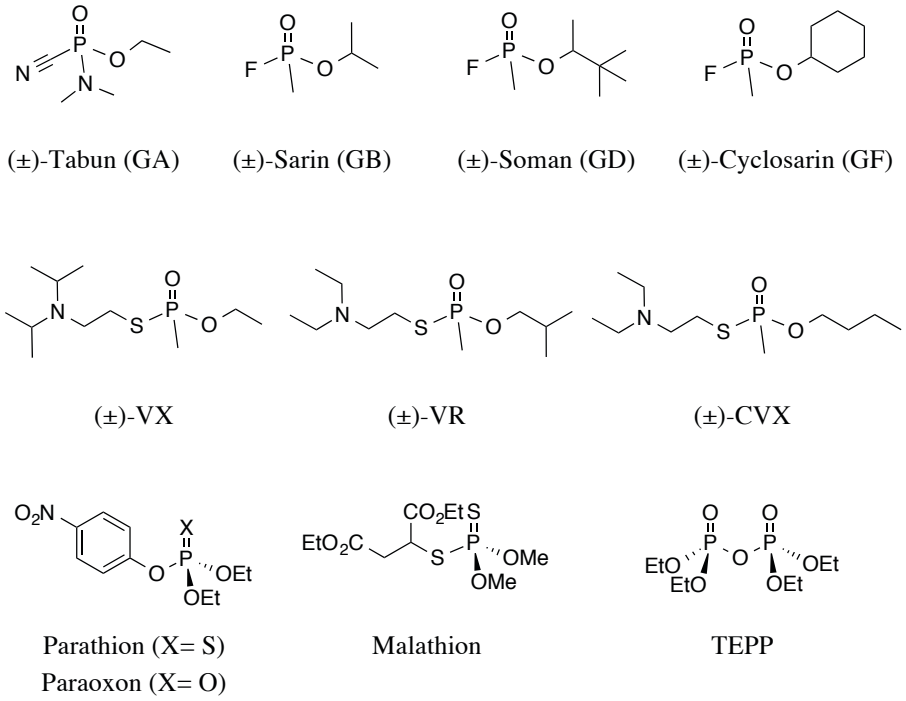

Figure 6.1.1 Principaux gaz de guerre et pesticides organophosphorés.

A l'heure actuelle à travers le monde, on dénombre chaque année pas moins de 3 millions d'intoxications accidentelles liées aux organophosphorés parmi lesquelles 230 000 conduisent à la mort des individus. Toutes les populations sont ainsi concernées : les agriculteurs utilisant quotidiennement des pesticides organophosphorés; les chimistes travaillant dans l'industrie chimique ou pharmaceutique et manipulant des OPs; les populations civiles vivant aux abords des champs traités par les pesticides mais également ceux intoxiqués lors d'attaques (chimiques) terroristes comme en témoigne l'histoire depuis la Guerre Iran/Irak, Halabja en 1988; les attentats du métro japonais de Tokyo en 1995; ou encore les récents affrontements dans la banlieue de Damas en Syrie en Août 2013 avec une attaque d'ampleur au gaz Sarin; et enfin les militaires lors de leurs missions sur les différents théâtres d'opération. Il convient par ailleurs de noter qu'il existe des stocks considérables de gaz de combats disséminés dans le monde entier, que les traités internationaux imposent de détruire dans des conditions de sécurité maximale. En 2010, seulement 60% des réserves mondiales d'armes chimiques sont signalées détruites par le secrétariat technique de l'Organisation internationale pour l'Interdiction des Armes Chimiques (OIAC). Cette destruction à hauts risques expose les manipulateurs à de grande quantité d'OPs, ce qui nécessite d'avoir à disposition des contre-mesures médicales d'urgences adaptées et efficaces en cas d'intoxications accidentelles.

6.1.2 Cible biologique des agents neurotoxiques organophosphorés

La toxicité aiguë de ces OPs résulte de l'inhibition irréversible de l'acetylcholinesterase (AChE), une enzyme impliquée dans les mécanismes de transmission de l'influx nerveux à travers l'organisme: dans les jonctions interneuronales et neuromusculaires. La terminaison nerveuse libère un médiateur chimique, l'acétylcholine, qui permet la transmission du message nerveux d'une cellule à l'autre. Une fois l'information transmise, l'acétylcholine est rapidement métabolisée par l'AChE, ce qui permet au système de revenir à son état de repos. L'inhibition de l'enzyme par des neurotoxiques comme les OPs entraîne une accumulation du médiateur chimique dans l'espace synaptique, qui maintient de ce fait une transmission permanente de l'influx nerveux, laquelle conduit généralement à la tétanie musculaire (respiratoire) et à la mort.

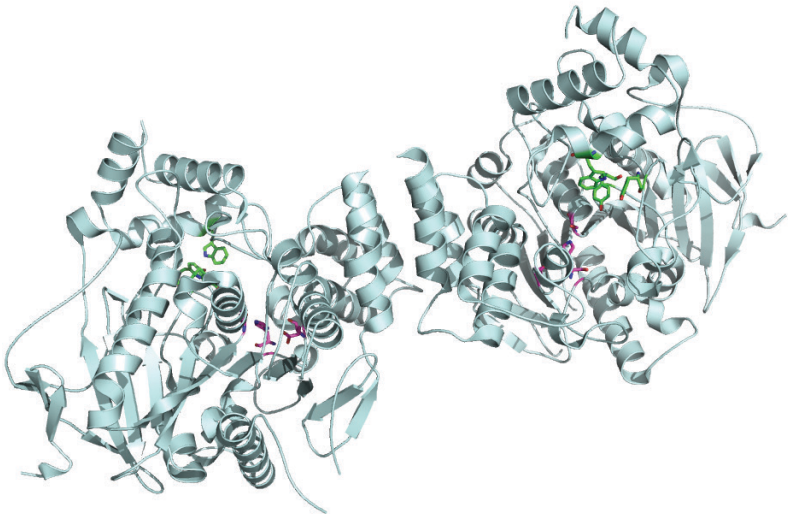

Figure 6.1.2 Structure dimère de l'AChE (cyan, code pdb 4ey4) montrant dans chaque monomère le site actif de l'enzyme : site anionique périphérique (Tyr72, Tyr124 and Trp286 en vert) et le site catalytique (Ser203, Glu334 and His447 en magenta).

6.1.3 Traitements actuels

Les pouvoirs publics ont récemment pris des mesures politiques drastiques pour limiter ce risque et investissent dans le développement de contre-mesures médicales efficaces en vue de remédier à ces empoisonnements et aux potentielles attaques terroristes chimiques à grande échelle, désastreuses pour les populations civiles. Les traitements actuels traitent plutôt l'inhibition périphérique alors que l'inhibition centrale (au niveau du système nerveux central) n'est traitée que de manière symptomatique traduisant l'inefficacité de la trithérapie utilisée. Actuellement en France, le traitement contre les intoxications aigües aux composés organophosphorés (gaz de combat et pesticides) consiste à l'administration d'un cocktail de trois molécules combinées dans l'auto-injecteur Ineurope® bi-compartimenté fabriqué, par la Pharmacie Centrale des Armées. Le méthylsulfate de Pralidoxime (molécule chargée positivement!) réactivant essentiellement l'acétylcholinestérase périphérique, le sulfate d'Atropine (un antispasmodique) et le chlorhydrate d'Avizafone (une prodrogue du Diazépam) agissant comme anticonvulsivant (Figure 6.1.3).

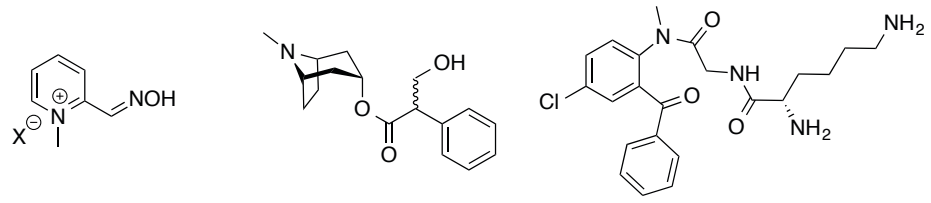

pralidoxime (2-PAM) atropine avizafone

Figure 6.1.3 Cocktail de molécules actuellement utilisé dans le traitement des OPs.

Cependant, seul 10% de la pralidoxime pénètre la BHE pour atteindre l'AChE inhibée au niveau du système nerveux central du fait de sa charge positive constante! La limitation est donc de taille, car il faut utiliser beaucoup de produits en termes de concentration pour avoir un effet bénéfique. D'autres composés réactivateurs tels que l'obidoxime, le HI-6 ou HLö-7 sont également utilisés et se montrent plus performants *in vitro* mais en raison de leurs deux charges (positives) rémanentes, ils rencontrent les mêmes limitations (Figure 6.1.4).

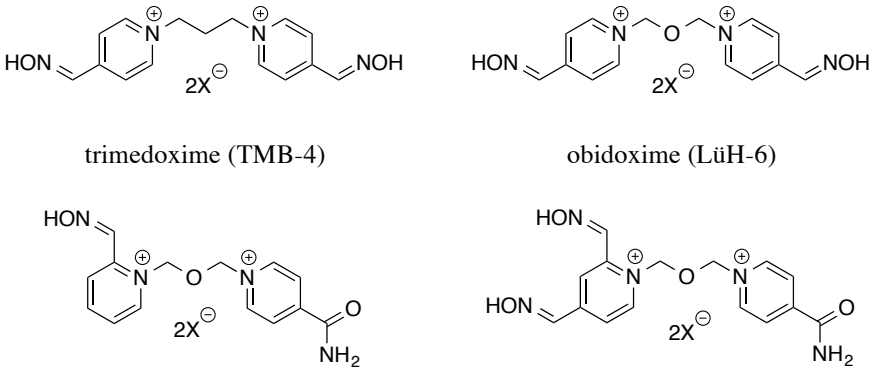

trimedoxime (TMB-4) obidoxime (LüH-6)

asoxime (Hi-6) HLö-7

Figure 6.1.4 Principaux réactivateurs de référence.

Cependant, malgré plus de 60 ans de recherche, il n'existe pas de réactivateur universel: un antidote donné n'est moyennement efficace que pour un gaz de combat donné. Pour remédier à ces problèmes, nous avons développé un nouveau concept de molécules hybrides bifonctionnelles en rupture technologique avec l'état de l'art. Dans leur conception, nos molécules possèdent un ligand du site périphérique (PSL : un motif tétrahydroacridine ou dérivé) de l'AChE et une partie réactivatrice (3-hydroxypyridine aldoxime) liée de façon covalente par un linker de taille optimisée (Figure 6.1.5). La présence du PSL permet de

« vectoriser » de façon intelligente le réactivateur vers le site catalytique de l'enzyme inhibée, afin de déphosphoryler (i.e., réactiver) cinétiquement et chimiquement de façon efficace l'enzyme.

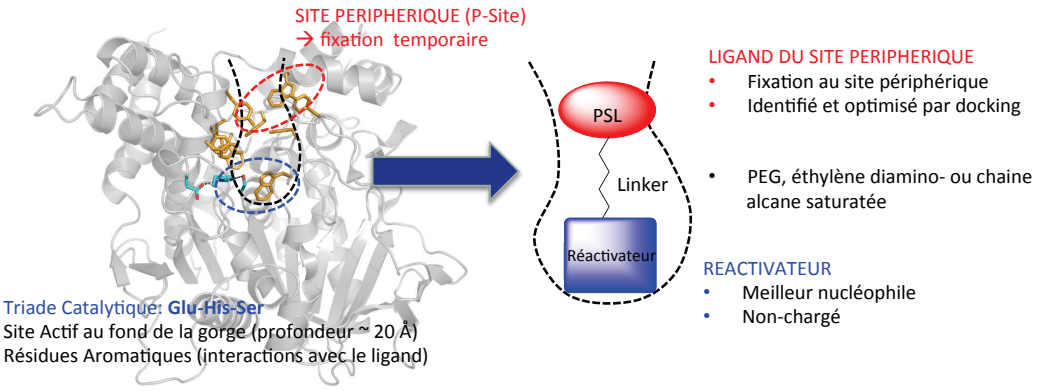

Figure 6.1.5 Concept des réactivateurs hybrids.

Ce projet dual à caractère civil et militaire vise à développer de nouveaux médicaments d'urgences hautement efficaces capables de soigner les personnes intoxiquées par les composés organophosphorés de façon accidentelles ou lors d'attaques chimiques terroristes. Dans ce contexte, le principal objectif de cette thèse est d'élaborer par « design », synthétiser, et évaluer biologiquement de nouvelles molécules hybrides bifonctionnelles non-chargées capables de pénétrer la barrière hématoencéphalique (BHE) et réactiver de manière plus efficace l'enzyme inhibée. Ce projet a été financé dans le cadre des thèses en cotutelle franco-britannique (Convention 2012.60.0040, Arrangement Technique n° 57) entre la DGA (Direction Générale de l'Armement) et la Dstl (Defence Science Technology Laboratory). Les travaux de recherche ont été réalisés en collaboration à l'Université de Strasbourg UMR CNRS 7515 (Institut de Chimie et Procédés pour l'Energie, l'Environnement, et la Santé - ICPEES) au sein de l'équipe du Dr. Rachid Baati et à l'Université de Southampton (School of Chemistry) au sein de l'équipe du Prof. Richard C. D. Brown.

6.2 Résultats

6.2.1 Synthèses de nouveaux réactivateurs hybrides bifonctionnels non-chargées possédant un motif tacrine et/ou analogue.

La synthèse des hybrides bifonctionnels avait été préalablement explorée dans notre groupe et a conduit à la découverte de nouveaux réactivateurs à fort potentiel par comparaison aux réactivateurs de référence. Ainsi la molécule possédant un motif tacrine couplé à une partie réactivatrice 3-hydroxypyridine aldoxime **2.4** s'est révélée être le meilleur composé lors de l'évaluation biologique *in vitro* sur divers neurotoxiques tels que le VX, le Sarin, le Tabun et le Paraoxon.

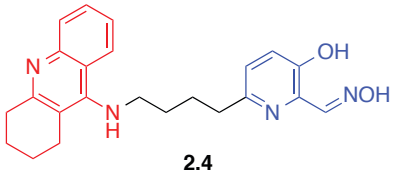

2.4

Figure 6.2.1 Hybride bifonctionnel **2.4**.

Cependant, la mesure de son pouvoir d'inhibition a démontré sa capacité à devenir un inhibiteur compétitif de l'enzyme native (autrement dit après réactivation). Pour palier à ce problème, l'un des premiers objectifs de ces travaux de recherche était d'élaborer et synthétiser des analogues de ce composé dans le but de diminuer son affinité pour le site périphérique du site actif de l'enzyme tout en conservant ou même améliorant ses propriétés réactivatrices.

De ce fait, une famille de sept molécules bifonctionnelles innovantes a tout d'abord été développée et brevetée au sein de notre laboratoire (Figure 6.2.2). Faisant face à la difficulté de reproduire certains résultats de synthèses décrits dans la littérature concernant la *N*-alkylation de tacrine, la voie de synthèse a tout d'abord été modifiée par une approche électrophile du substrat (Scheme 6.2.1).

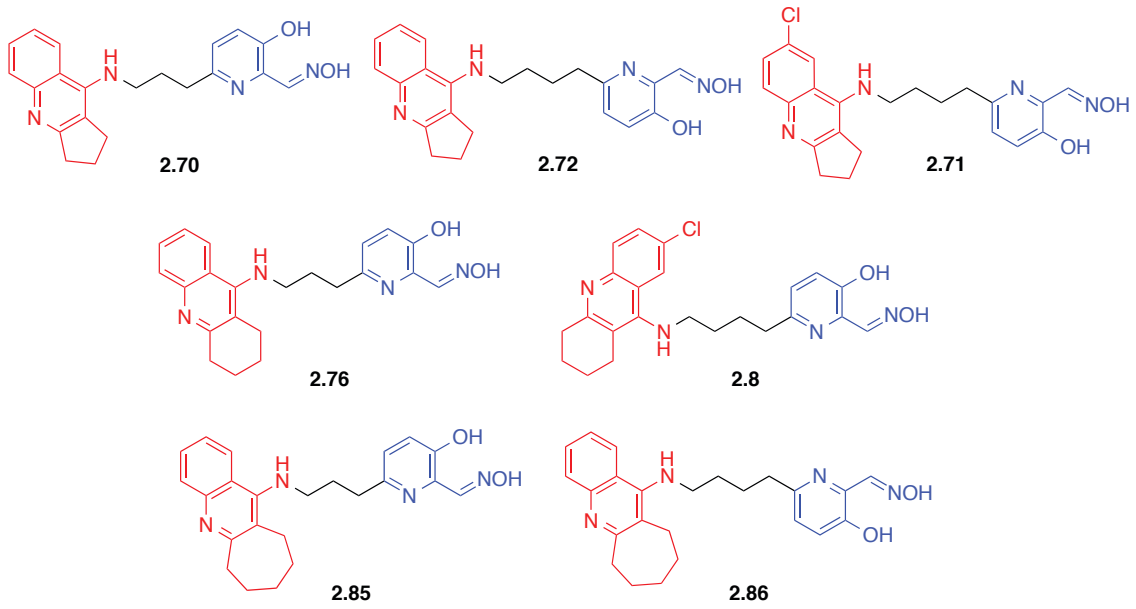

Figure 6.2.2 Famille de nouveaux hybrides réactivateurs synthétisée.

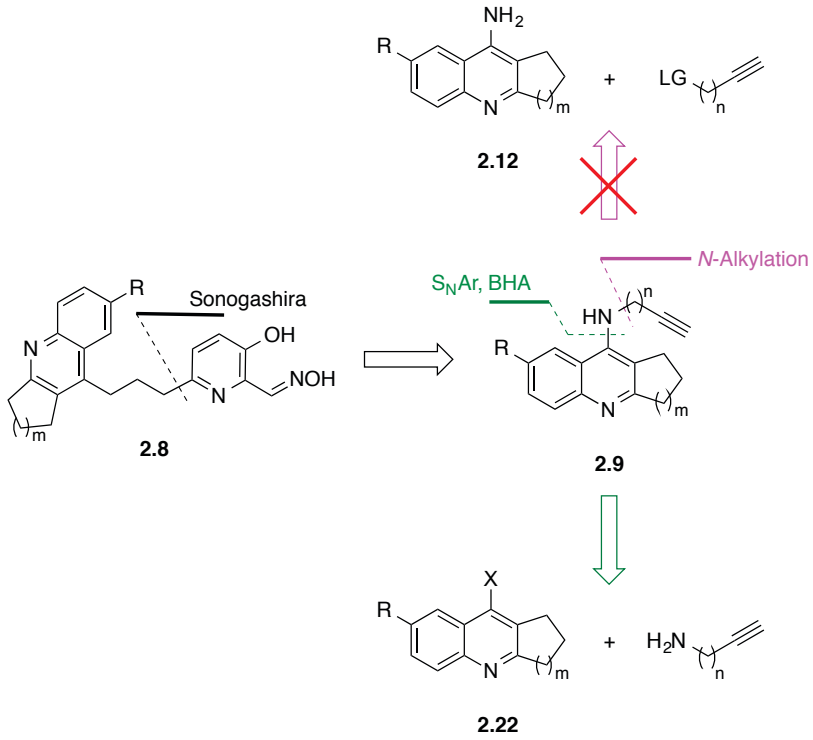

Scheme 6.2.1 Stratégies rétrosynthétiques.

Les dérivés dichlorés **2.55**, **2.22.1** et **2.56** sont tout d'abord obtenus par déshydratation intermoléculaire entre l'acide 5-chloroanthranilique **2.24** (produit de départ commun) et la cétone cyclique correspondante (pentanone, hexanone et heptanone respectivement, Scheme 6.2.2). Ces derniers sont hydrolysés dans des tubes scellés à 200 °C en présence d'acide acétique pour former les cétones conjuguées correspondantes avant d'être finalement engagés dans une réaction de triflation pour former les triflates correspondant en présence d'anhydride triflique avec de très bons rendements.

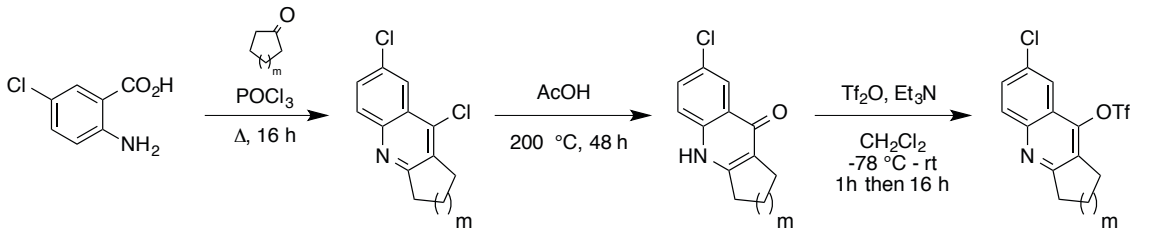

2.24

2.55 m = 1, 82%
2.22.1 m = 2, quant
2.56 m = 3, 80%

2.57 m = 1, quant
2.24 m = 2, quant
2.58 m = 3, 89%

2.59 m = 1, 65%
2.22.3 m = 2, 90%
2.60 m = 3, 90 %

Scheme 6.2.2 Synthèses des triflates **2.59**, **2.22.3** et **2.60**.

Pour des raisons de clarté dans la lecture, les prochaines étapes, conduisant à la formation des hybrides bifunctionnels précédemment présentés (Figure 6.2.2), sont décrites ci-contre avec une molécule générique commune à tous les réactivateurs. Le triflate préalablement formé permet la formation de l'alcyne vrai correspondant en présence de l'amine choisi (propargylamine ou 1-amino-3-butyne) à l'aide d'un couplage de Buchwald-Hartwig pallado-catalysé et assisté par microondes. Ce dernier est ensuite engagé dans un couplage de Sonogashira en présence de la methyl 3-benzyloxy-6-bromopicolinate **2.10** synthétisé en trois étapes avec un bon rendement à partir de l'acide 3-hydropicolinique (Scheme 6.2.3). Ensuite une hydrogénation sous pression atmosphérique en présence du catalyseur de Pearlman permet parallèlement de réduire le nouvel alcyne formé en alcane ainsi que de déprotéger la position phénolique de la pyridine « one pot ». Finalement, l'adduit formé permet l'obtention de l'hybride bifonctionnel désiré par une séquence de trois réactions impliquant (a) la protection de la position phénolique avec un groupement TBS, (b) la réduction de l'ester méthylique en aldéhyde utilisant DIBAL-H et (c) la formation de l'oxime.

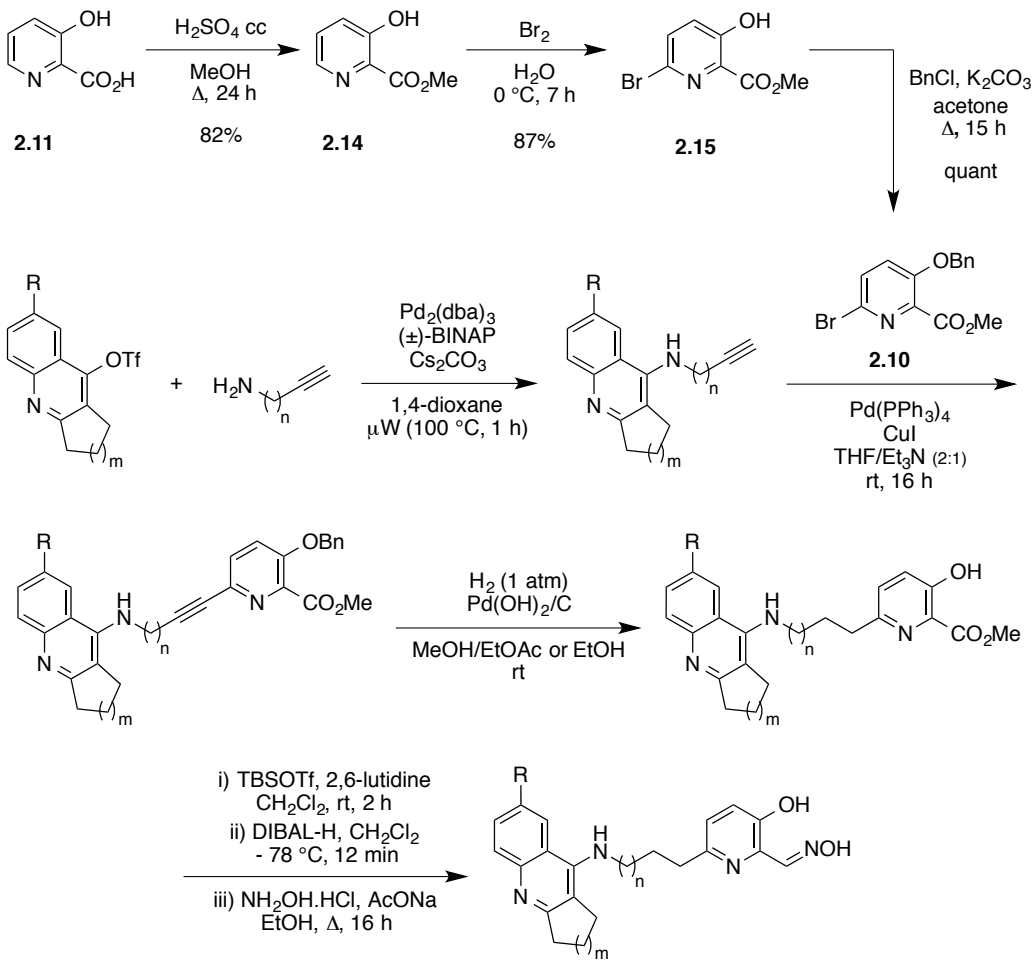

Scheme 6.2.3 Nouvelle voie de synthèse générale des nouveaux hybrides bifonctionnels.

Cette nouvelle approche nous a permis de découvrir de nouveaux triflates qui ont fait l'objet en parallèle d'une étude de réactivité sur la réaction de couplage de Buchwald-Hartwig démontrant un accès simple et rapide à des *N*-tacrines fonctionnalisées pour le domaine pharmaceutique (Scheme 6.2.4 et Scheme 6.2.5).

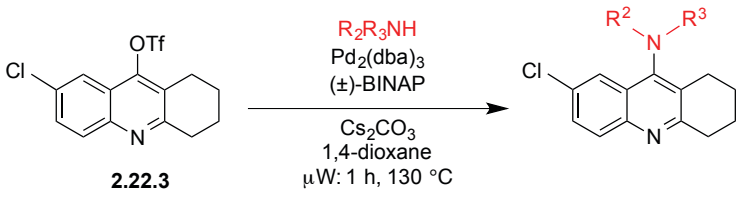

Scheme 6.2.4 Réaction d'amination de Buchwald-Hartwig.

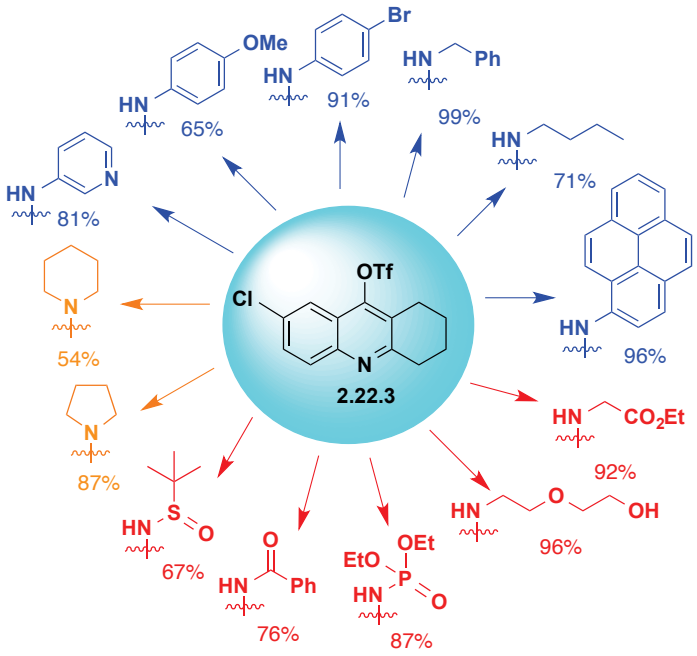

Scheme 6.2.5 Résultats montrant la réactivité variée de la réaction de couplage.

6.2.2 Synthèses de nouveaux réactivateurs hybrides bifonctionnels non-chargées possédant un motif quinoline ou alcaloïde.

Utilisant la nouvelle stratégie de synthèse optimisée, un nouvel hybride **3.1** basé sur un nouveau motif de PSL tel que la quinoléine a été synthétisé après avoir été élaboré par simplification moléculaire. L'hybride **3.1** a été obtenue à partir de la 4-bromoquinoléine en 6 étapes avec un rendement global non-optimisé de 22%. Cette étude est complétée par la synthèse originale d'un nouvel hybride **3.24** possédant un motif alcaloïde oxoassoanine.

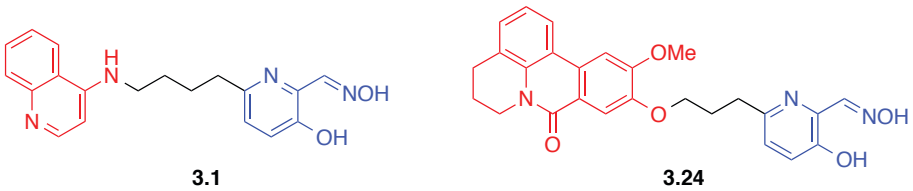

Figure 6.2.3 Deuxième génération de réactivateurs hybrides synthétisée.

6.2.3 Evaluation biologique

La dernière partie de ces travaux de thèses est consacrée à l'évaluation biologique des réactivateurs synthétisés. La majeure partie de ces évaluations a été réalisée dans les laboratoires accrédités du Dr. Florian Nachon de l'Institut de Recherche Biomédicale de l'Armée (IRBA) due à la manipulation des OPs. La détermination des capacités réactivatrice *in vitro* (constantes caractéristiques) des hybrides synthétisés se fait par à l'aide du test d'Ellman et se mesure par spectrophotométrie.

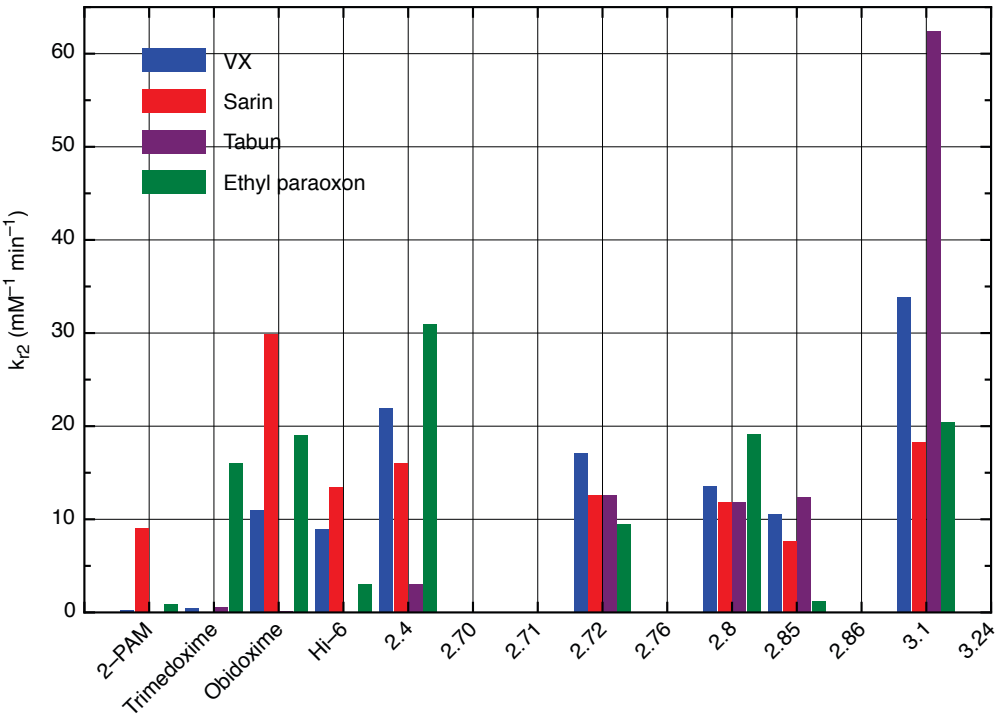

Figure 6.2.4 Constante de réactivation de second ordre (k_{r2}) des réactivateurs de référence et des hybrides synthétisés pour des intoxications au VX-, Sarin- Tabun- et éthyle paraoxon *in vitro*.

Les hybrides évalués révèlent des propriétés de réactivation de l'AChE (in vitro) inégalées et supérieures à tous les antidotes utilisés à l'heure actuelle dans le monde et approuvés par la FDA (tels que 2-PAM, Hi-6, obidoxime, HLö-7, et trimedoxine, Figure 6.2.4). De plus, l'hybride **3.1** possèdent un très large spectre de réactivité puisqu'elle réactive l'AChE inhibée par les gaz de combat (VX, Sarin et Tabun) et les pesticides (Paraoxon). En plus du spectre de réactivité, l'hybride **3.1** a démontré une réactivation quantitative sur quasiment chaque test et la mesure de sa capacité inhibitrice de l'enzyme native permet de l'écarter de la liste des inhibiteurs compétitifs potentiels. Ces résultats nous ont ainsi permis de découvrir la première molécule pouvant prétendre au titre de « premier réactivateur universel ».

L'évaluation biologique s'accompagne de structures RX de nos molécules dans le site active de l'enzyme isolées par l'équipe du Dr. Martin Weik (Institut de Biologie Structurale, Grenoble), conduites en parallèle, et confirmant les résultats obtenus par l'étude *in vitro*.

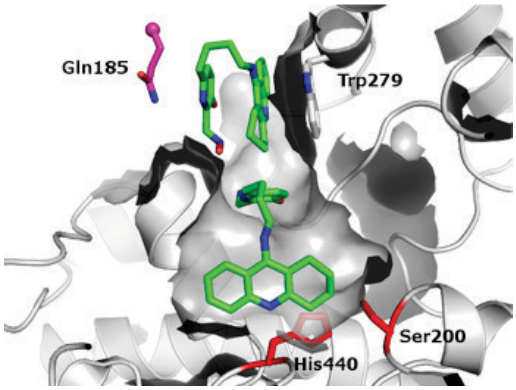

Figure 6.2.5 Structure RX de l'hybride **2.4** dans le site actif de la *Tc*AChE.

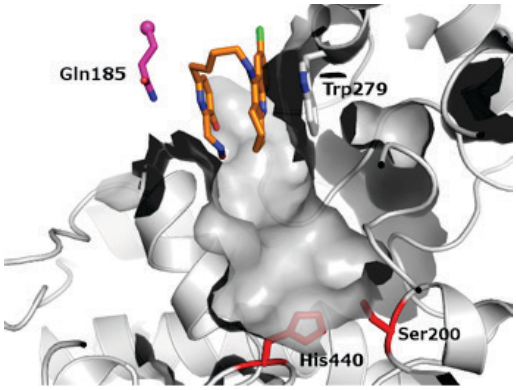

Figure 6.2.6 Structure RX de l'hybride **2.8** dans le site actif de la *Tc*AChE.

Ces structures RX confirment l'effet stérique de l'atome de chlore dans la position désirée afin de diminuer l'affinité de l'hybride pour le site périphérique du site actif de l'enzyme. Dans le cas de l'hybride **2.4**, deux molécules sont identifiées dans le site actif : une au niveau de site catalytique et une au niveau du site périphérique. Cependant, avec un atome de chlore en position 7, seule une molécule de réactivateur **2.8** est observée et elle se situe au niveau du site périphérique. Ainsi, l'atome de chlore permet au réactivateur de ne pas être inhibiteur compétitif en empêchant de rester dans le site actif de l'enzyme. Ce résultat permet également de justifier la diminution du pouvoir inhibiteur observé de l'hybride **2.8** (IC_{50}, 0.48 mM) par rapport à l'hybride **2.4** (IC_{50}, 0.25 µM).

6.3 Conclusion

Après avoir présenté les problèmes que posent les traitements actuels, à travers ces travaux de recherche nous sommes parvenus élaborer, synthétiser et évaluer le potentiel de réactivation de nouveaux hybrides bifonctionnels non chargés contre les empoisonnements aux gaz de guerre et pesticides. Explorant des recherches préliminaires effectuées au sein de notre laboratoire, le premier objectif consistait à développer des analogues structurels d'hybride possédant une tacrine en tant que PSL et une fonction réactivatrice 3-hydroxypyridine 2-aldoxime liées par un bras espaceur de 4 atomes de carbone. A travers cette étude de relation structure-activité, l'un des principaux objectifs étaient d'étudier l'influence sur l'affinité avec l'AChE (native ou inhibée) d'un substituent tel qu'un atome de chlore en position 7 sur le motif tacrine. La révision de la voie de synthèse de ces hybrides bifonctionnels nous a permis de découvrir de nouveaux triflates possédant un fort potentiel pour obtenir rapidement des tacrines *N*-fonctionnalisées pour la recherche pharmaceutique. Sept nouveaux hybrides ont été ainsi obtenus par une voie de synthèse multi-étapes raccourcie par rapport à la littérature et avec un rendement moyen de 20% environ. Leur évaluation biologique a montré une amélioration de la réactivation et de l'affinité des hybrides comparés aux réactivateurs de référence (2-PAM, Hi-6, obidoxime et trimedoxime) pour des intoxications au VX, Sarin et Paraoxon. De plus, ils ont montré une très nette amélioration pour un empoisonnement au Tabun. L'évaluation biologique s'accompagne de structures RX, conduites en parallèle, et confirmant les résultats obtenus par l'étude *in vitro*. Des essais de cristallisation dynamique en collaboration avec l'IBS de Grenoble (Dr. Martin Weik) sont actuellement en cours, en vue de mieux comprendre les mécanismes d'action à l'échelle moléculaire, ainsi que des tests de réactivation de la butyrylcholinesterase (BuChE) et d'autre OPs à l'IRBA (Dr. Florian Nachon).

Combinant cette stratégie d'hybrides bifonctionnels à la stratégie de simplification moléculaire, de nouveaux hybrides possédant un motif de PSL tel que la quinoléine ou le plus original alcaloïde oxoassoanine ont été synthétisés. Si ce dernier s'est révélé posséder une synthèse stimulante, l'hybride possédant un motif quinoléine a été obtenue par une voie de synthèse relativement courte. De plus, l'évaluation biologique de l'hybride **3.1** a révélé un potentiel de réactivation sans précédent surpassant tous les réactivateurs que ce soit pour les gaz de combat et les pesticides. Egalement, cet hybride possède un pouvoir inhibiteur de l'AChE relativement faible (de l'ordre du mM) réduisant son potentiel d'action d'inhibiteur compétitif. A travers cette étude, nous avons ainsi découvert un nouveau composé possédant un potentiel de réactivation incroyable et pouvant prétendre au titre de premier réactivateur universel de l'AChE et de MVP « *Most Valuable Protector* ».

Experimental

A.1 General Methods

Chemicals were purchased from Sigma-Aldrich, Fisher Scientific, Alfa Aesar, Fluorochem or Apollo Scientific. All air/moisture sensitive reactions were carried out under an inert atmosphere, in oven-dried or flame-dried glassware. The solvents toluene, THF and Et_2O (from Na/benzophenone), MeCN, MeOH (from $Mg(OMe)_2$) and CH_2Cl_2 (from CaH_2) were distilled before use, and where appropriate, other reagents and solvents were purified using standard techniques.[325] TLC was performed on aluminium-precoated plates coated with silica gel 60 containing F_{254} indicator; visualised under UV light (254 nm) and/or by staining with anisaldehyde, ceric ammonium molybdate, iodine, phosphomolybdic acid, potassium permanganate or vanillin. Flash column chromatography was performed using high purity silica gel, Geduran®, pore size 60 Å, 230-400 mesh particle size, purchased from Sigma-Aldrich or Merck. Fourier-transform infrared (FT-IR) spectra are reported in wavenumbers (cm^{-1}) and were collected as solids or neat liquids on a Nicolet 380 fitted with a Smart Orbit Goldengate attachment using OMNIC software package. ^{1}H NMR, ^{13}C NMR, ^{19}F NMR and ^{31}P NMR spectra were recorded in $CDCl_3$, DMSO-*d6*, Methanol-*d4* solutions (purchased from Cambridge Isotope Laboratories, Inc.) at 298 K using Bruker DPX400, AVII400, AVIIHD400 (400, 101, 376 and 162 MHz respectively) and at 353 K using Bruker AVII400 (400 and 101 MHz respectively) or Bruker AVIIHD500 (500 and 126 MHz respectively) spectrometers. Chemical shifts values (δ) are reported in ppm relative to residual chloroform (δ 7.26 ppm for ^{1}H, δ 77.16 ppm for ^{13}C), dimethyl sulfoxide (δ 2.50 ppm for ^{1}H, δ 39.52 ppm for ^{13}C) and methanol (δ 3.31 ppm for ^{1}H, δ 49.00 ppm ^{13}C). All spectra were reprocessed using ACD/Labs software (version: 12.1 to 15.1) or NMRnotebook (version 2.70). Coupling constants (*J*) were recorded in Hz. The following abbreviations for the multiplicity of the peaks are s (singlet), d (doublet), t (triplet), q (quartet), quin (quintet), sxt (sextet), sep (septet), br (broad), and m (multiplet). Melting points were obtained using a STUART® Scientific SMP3 apparatus and are uncorrected. Electrospray low resolution mass spectra were recorded on a Waters ZMD quadrupole spectrometer or Waters (Manchester, UK) TQD triple quadrupole analyser. High resolution mass spectra were obtained using Bruker APEX III FT-ICR mass spectrometer or MaXis (Bruker Daltonics, Bremen, Germany) mass spectrometer equipped with a Time of Flight analyser. HRMS were recorded using positive ion electrospray ionization (ESI^+). Microwave synthesis was performed in a sealed tube using a CEM® Discover or a Biotage® Initiator microwave synthesis apparatus.

A.2 General Procedures

A.2.1 Procedure A: Lewis-acid mediated intermolecular cyclodehydration.

A cycloketone (1.1 equiv) was added to a dried flask containing 5-chloroanthranilic acid (**2.23**, 1.0 equiv). After cooling the mixture to 0 °C, the phosphorus oxyhalide POX_3 (8.8 equiv) was added. The reaction mixture was heated under reflux for 16 h. Upon completion, the reaction mixture was poured carefully onto iced-water. The solution was then brought to alkalinity (pH ~ 9) using a saturated aqueous K_2CO_3 solution. The desired product was extracted with $CHCl_3$, washed with water and brine. The combined organic solution was dried over anhydrous Na_2SO_4, filtered and concentrated under reduced pressure. The crude black oil was purified by column chromatography to afford the product.

A.2.2 Procedure B: Trifluoromethanesulfonate formation.

To a suspension of 1,2,3,4-tetrahydroacridin-9-(10*H*)-one derivative (1.0 equiv) in dry Et_3N (1.1 equiv) in dry CH_2Cl_2 (0.1 M), triflic anhydride (1.1 equiv) was added dropwise at –78 °C. The reaction mixture was stirred for 1 h at –78 °C. Then the cooling bath was removed and the reaction mixture was allowed to slowly warm to rt, and stirring was continued for 16 h. Upon completion, the solvent was removed under reduced pressure and the resulting dark yellow oil was purified by column chromatography to afford the desired triflate.

A.2.3 Procedure C: Palladium-catalysed amination under microwave irradiation.

A microwave tube containing a magnetic stirrer bar was charged with the desired aryl triflate or halide (1.0 equiv), $Pd_2(dba)_3$ (0.04 equiv), (±)-BINAP (0.08 equiv) and Cs_2CO_3 (2.5 equiv). The vessel was sealed with a septum and purged with Ar, before degassed 1,4-dioxane (0.3 M in aryl triflate/halide) and the desired aminoalkyne (1.3 equiv) were introduced through the septum. The resulting mixture was heated for 1 h at 100 °C under microwave irradiation. After cooling, the reaction mixture was concentrated and purified by column chromatography to afford the desired terminal alkyne.

A.2.4 Procedure D: "*One-pot*" alkyne reduction and *O*-debenzylation.

To a degassed solution of the alkyne (1.0 equiv) obtained by procedure D in dry MeOH, EtOH or EtOAc (0.01 M in alkyne), $Pd(OH)_2/C$ (20% wt. with 50% moisture, 0.2 equiv) was added. After evaporating and flushing with H_2 (Caution! Hydrogen gas is highly flammable and forms explosive mixtures with air, manipulations should be conducted in a well-ventilated fume hood. Keep away from ignition source/heat/sparks/open flames/hot surfaces) five times, the reaction mixture was stirred for 7 h at rt under H_2 (1 atm.). Upon completion, the catalyst was removed by filtration through celite, the solvent was removed under reduced pressure and the residue was either purified or subjected to the subsequent step.

A.2.5 Procedure E: TBS protection of the phenolic function.

To a 0.1 M solution of the reduced product (1.0 equiv) obtained by procedure E in dry CH_2Cl_2, 2,6-lutidine (3.0 equiv), and TBSOTf (3.0 equiv) were successively added at rt. The reaction mixture was stirred under Ar for 1.5 h at rt. Upon completion, the reaction mixture was quenched with saturated aqueous $CuSO_4$ solution. After separation, the aqueous phase was extracted with CH_2Cl_2 and the combined organic solution was dried over anhydrous Na_2SO_4, filtered and concentrated under reduced pressure. After drying *in vacuo*, the residue was subjected to the subsequent step.

A.2.6 Procedure F: DIBAL-H Reduction of methyl ester to aldehyde.

To a 0.1 M solution of the crude product (1.0 equiv) of procedure F in dry CH_2Cl_2 at –78 °C, a solution of DIBAL-H (1.0 M in CH_2Cl_2, 3.0 equiv) was added dropwise. The reaction mixture was stirred at –78 °C for between 12 min and 120 min. Upon completion, the reaction mixture was quenched at –78 °C with MeOH, and the cooling bath was removed. When the mixture warmed to rt, it was washed with a solution of NaOH (1.0 M aqueous). The aqueous phase was then extracted with CH_2Cl_2 and the combined organic solution was dried over anhydrous Na_2SO_4, filtered and concentrated under reduced pressure. After drying *in vacuo*, the residue was purified by column chromatography to afford the desired aldehyde.

A.2.7 Procedure G: Oximation (Oxime formation).

A 0.3 M solution of the aldehyde obtained by procedure G (1.0 equiv), hydroxylamine hydrochloride (1.5 equiv) and CH_3CO_2Na (1.5 equiv) in dry EtOH was stirred for 15 h at reflux. Upon completion, the reaction mixture was concentrated under reduced pressure and purified by column chromatography to afford the desired hybrid reactivator.

A.3 Characterisation Data

Methyl 3-hydroxypicolinate (**2.14**)

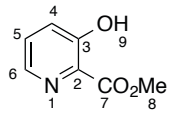

$C_7H_7NO_3$

MW: 153.14 g.mol^{-1}

To a suspension of 3-hydroxypicolinic acid **2.11** (5.000 g, 35.94 mmol, 1.0 equiv) in MeOH (70.0 mL), concentrated H_2SO_4 (5.75 mL, 107.82 mmol, 3.0 equiv) was added dropwise. The reaction mixture was stirred for 24 h under reflux. Upon completion, the reaction mixture was brought to alkalinity (pH ~ 9) with a saturated aqueous solution of K_2CO_3. The mixture was extracted three times with EtOAc (200 mL). The combined organic solution was dried over anhydrous Na_2SO_4, filtered and concentrated under reduced pressure to afford **2.14** as a white solid (4.530 g, 29.47 mmol, 82%). Spectroscopic data were consistent with those reported in literature.[238]

TLC Rf 0.39 (petroleum ether/EtOAc 3:7).

^{1}H NMR (400 MHz, $CDCl_3$) δ (ppm) 10.64 (s, 1H, **9**), 8.30 (dd, *J* = 4.9, 2.2 Hz, 1H, **4**), 7.44 (dd, *J* = 8.8, 4.9 Hz, 1H, **5**), 7.40 (dd, *J* = 8.8, 2.2 Hz, 1H, **6**), 4.07 ppm (s, 3H, **8**).

LRMS (ESI$^+$) *m/z* 154.0 $[M+H]^+$.

HRMS (ESI$^+$) *m/z* calcd for $C_7H_8NO_3$ $[M+H]^+$, 154.0499, found 154.0501 Da.

(ESI$^+$) *m/z* calcd for $C_7H_7NNaO_3$ $[M+Na]^+$, 176.0318, found 176.0318 Da.

Methyl 6-bromo-3-hydroxypicolinate (**2.15**)

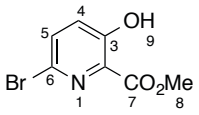

$C_7H_6BrNO_3$

MW: 232.03 g.mol^{-1}

To a suspension of **2.14** (2.000 g, 13.06 mmol, 1.0 equiv) in water (80.0 mL), Br_2 (672 µL, 13.06 mmol, 1.0 equiv) was added dropwise and portionwise (8 x 84 µL over 4 h) at 0 °C. The reaction mixture was stirred for 3 h at 0 °C, then for 2 h at rt. Upon completion, the solution was extracted twice with CH_2Cl_2 (150 mL). The combined organic solution was washed with a saturated aqueous solution of $Na_2S_2O_3$ (50 mL), brine, dried over anhydrous Na_2SO_4, filtered and concentrated under reduced pressure. The residue was purified by column chromatography (petroleum ether/EtOAc 85:15) to afford **2.15** as a white powder (2.641 g, 11.36 mmol, 87%). Spectroscopic data were consistent with those reported in literature.[262]

TLC Rf 0.60 (petroleum ether/EtOAc 8:2).

^{1}H NMR (400 MHz, $CDCl_3$) δ (ppm) 10.71 (s, 1H, **9**), 7.58 (d, *J* = 8.8 Hz, 1H, **5**), 7.31 (d, *J* = 8.8 Hz, 1H, **4**), 4.07 ppm (s, 3H, **8**).

LRMS (ESI$^+$) *m/z* 231.9 [M^{79}Br+H]$^+$, 233.9 [M^{81}Br+H]$^+$.

HRMS (ESI$^+$) *m/z* calcd for $C_7H_7{}^{79}BrNO_3$ [M+H]$^+$, 231.9604, found 231.9606 Da.

(ESI$^+$) *m/z* calcd for $C_7H_6{}^{79}BrNNaO_3$ [M+Na]$^+$, 253.9423, found 253.9425 Da.

Methyl 3-benzyloxy-6-bromopicolinate (**2.10**)

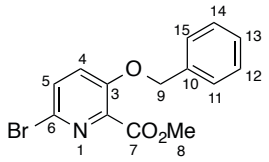

$C_{14}H_{12}BrNO_3$

MW: 322.16 g.mol^{-1}

To a suspension of **2.15** (2.000 g, 8.62 mmol, 1.0 equiv) and anhydrous K_2CO_3 (5.360 g, 38.78 mmol, 4.5 equiv) in acetone (120 mL), benzyl bromide (3.07 mL, 25.86 mmol, 3.0 equiv) was slowly added. The reaction mixture was stirred for 16 h at reflux. Upon completion, the resulting mixture was filtered and concentrated under reduced pressure. The residue was purified by column chromatography (petroleum ether/EtOAc 9:1) afforded **2.10** as a white powder (2.730 g, 8.62 mmol, quant.). Spectroscopic data were consistent with those reported in literature.[262]

TLC Rf 0.28 (petroleum ether/EtOAc 8:2).

^{1}H NMR (400 MHz, $CDCl_3$) δ (ppm) 7.51 (d, *J* = 8.7 Hz, 1H, **5**), 7.46-7.34 (m, 5H, **11**, **12**, **13**, **14** & **15**), 7.25 (d, *J* = 8.7 Hz, 1H, **4**), 5.22 (s, 2H, **9**), 3.98 ppm (s, 3H, **8**).

LRMS (ESI$^+$) *m/z* 322.0 [M^{79}Br+H]$^+$, 324.0 [M^{81}Br+H]$^+$,
(ESI$^+$) *m/z* 343.9 [M^{79}Br+Na]$^+$, 346.0 [M^{81}Br+Na]$^+$,
(ESI$^+$) *m/z* 664.9 [2M^{79}Br+Na]$^+$, 667.0 [2M^{81}Br+Na]$^+$,

HRMS (ESI$^+$) *m/z* calcd for $C_{14}H_{12}{}^{79}BrNNaO_3$ [M+Na]$^+$, 343.9893, found 343.9890 Da.

7-Chloro-1,2,3,4-tetrahydroacridin-9-amine (**2.12**)

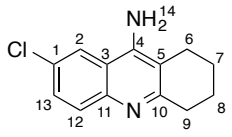

$C_{13}H_{13}ClN_2$

MW: 232.71 g.mol^{-1}

To a solution of commercially available 2-amino-5-chlorobenzonitrile (2.000 g, 13.10 mmol, 1.0 equiv) in toluene (39 mL), cyclohexanone (1.49 mL, 14.40 mmol, 1.1 equiv) was added. The reaction mixture was stirred for 15 min at rt. BF_3•OEt_3 (1.78 mL, 1.1 equiv) was added dropwise via syringe, and the reaction mixture was heated for 24 h under reflux. Upon completion, the reaction mixture was cooled to rt, toluene was decanted and the remaining solid were treated with an aqueous solution of NaOH (2.0 M, 40 mL) and heated for 24 h at reflux. Upon completion, the reaction mixture was cooled to rt and extracted with $CHCl_3$ (200 mL). The combined organic solution was washed with brine, dried over anhydrous Na_2SO_4, filtered and concentrated under reduced pressure to afford **2.12** as an off-white solid (1.22 g, 5.240 mmol, 40%).

TLC Rf 0.23 (petroleum ether/EtOAc 95:5).

IR (neat) ν_{max} 3466 (s), 3321 (m), 3139 (m), 2939 (m), 2855 (m), 1651 (s), 1572 (s), 1562 (s), 1489 (s), 1446 (m), 1408 (m), 1373 (s), 1294 (w), 1278 (w), 1265 (w), 1166 (m), 1120 (w), 1081 (w) cm^{-1}.

^{1}H NMR (400 MHz, $CDCl_3$) δ (ppm) 7.82 (d, *J* = 9.0 Hz, 1H, **12**), 7.66 (d, *J* = 2.2 Hz, 1H, **2**), 7.49 (dd, *J* = 2.2, 9.0 Hz, 1H, **13**), 4.58 (br s, 2H, **14**), 3.01 (t, *J* = 6.1 Hz, 2H, **9**), 2.61 (t, *J* = 6.2 Hz, 2H, **6**), 1.98-1.90 (m, 4H, **7** & **8**).

^{13}C NMR (101 MHz, $CDCl_3$) δ (ppm) 159.16 (**10**), 145.67 (**4**), 145.14 (**11**), 130.76 (**13**), 129.60 (**1**), 129.35 (**12**), 119.09 (**2**), 117.98 (**3**), 111.42 (**5**), 34.24 (**9**), 23.94 (**6**), 22.92 (**8**), 22.83 (**7**).

LRMS (ESI$^+$) *m/z* 233.1 [M^{35}Cl+H]$^+$, 235.0 [M^{37}Cl+H]$^+$.

HRMS (ESI$^+$) *m/z* calcd for $C_{13}H_{14}{}^{35}ClN_2$ [M+H]$^+$, 233.0840, found 233.0835 Da.

But-3-yn-1-yl 4-methylbenzenesulfonate (**2.17**)

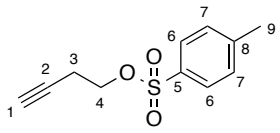

$C_{11}H_{12}O_3S$

MW: 224.27 g.mol^{-1}

To a solution of 3-butyn-1-ol **2.16** (1.500 g, 21.401 mmol, 1.0 equiv) and pyridine (3.46 mL, 42.802 mmol, 2.0 equiv) in CH_2Cl_2 (25 mL), was added 4-methyl-benzenesulfonyl chloride (6.120 g, 32.102 mmol, 1.5 equiv) at 0 °C. Upon addition, the reaction mixture was warmed to rt, and stirred for 16 h at rt. Upon, completion, the reaction mixture was treated with H_2O (25 mL) and extracted with CH_2Cl_2 (25 mL). The combined organic solution was washed with an aqueous HCl (1.0 M) solution, saturated aqueous $NaHCO_3$ solution, H_2O, and brine. The organic solution was dried over $MgSO_4$, filtered and concentrated under reduced pressure. The residue was purified by column chromatography (silica gel, petroleum ether/EtOAc 9:1) to afford **2.17** (4.795 g, 21.400, quant) as colourless oil. Spectroscopic data were consistent with those reported in literature.[326]

TLC Rf 0.46 (petroleum ether/EtOAc 9:1).

^{1}H NMR (400 MHz, $CDCl_3$) δ (ppm) 7.80 (d, *J* = 8.0 Hz, 2H, **6**), 7.35 (d, *J* = 8.0 Hz, 1H, **7**), 4.10 (t, *J* = 7.2 Hz, 2H, **4**), 2.55 (td, *J* = 7.2, 2.8 Hz, 2H, **3**), 2.45 (s, 3H, **9**), 1.97 (t, *J* = 2.8 Hz, 1H, **1**).

7,9-Dichloro-1,2,3,4-tetrahydroacridine (**2.22.1**)

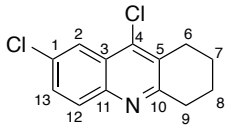

$C_{13}H_{11}Cl_2N$

MW: 252.14 g.mol^{-1}

2.22.1 was obtained according to general procedure A using 2-amino-5-chlorobenzoic acid **2.23** (5.000 g, 29.14 mmol, 1.0 equiv), cyclohexanone (3.30 mL, 32.05 mmol, 1.1 equiv) and $POCl_3$ (23.90 mL, 8.8 equiv). The crude product was purified by column chromatography (silica gel, petroleum ether/EtOAc 9:1) to afford **2.22.1** as an off-white powder (6.700 g, 26.52 mmol, 91%).

TLC Rf 0.20 (petroleum ether/EtOAc 9:1).

IR (neat) ν_{max} 2941 (m), 2863 (w), 1579 (m), 1473 (s), 1423 (w), 1392 (w), 1362 (w), 1340 (w), 1309 (s), 1286 (w), 1245 (w), 1211 (m), 1166 (w), 1146 (w), 1080 cm^{-1}.

^{1}H NMR (400 MHz, $CDCl_3$) δ (ppm) 8.15 (d, *J* = 2.4 Hz, 1H, **2**), 7.92 (d, *J* = 8.8 Hz, 1H, **12**), 7.60 (dd, *J* = 8.8, 2.4 Hz, 1H, **13**), 3.11 (t, *J* = 5.6 Hz, 2H, **9**), 3.02 (t, *J* = 6.8 Hz, 2H, **6**), 1.94–1.91 (m, 4H, **7** & **8**).

^{13}C NMR (101 MHz, $CDCl_3$) δ (ppm) 160.05 (**10**), 140.55 (**11**), 134.85 (**5**), 132.67 (**1**), 130.41 (**13**), 130.07 (**12**), 129.56 (**4**), 126.28 (**3**), 122.89 (**2**), 34.25 (**9**), 27.73 (**6**), 22.70 (**8**), 22.66 (**7**).

LRMS (ESI$^+$) *m/z* 252.0 [M^{35}Cl+H]$^+$, 254.0 [M^{37}Cl+H]$^+$.

HRMS (ESI$^+$) *m/z* calcd for $C_{13}H_{12}{}^{35}Cl_2N$ [M+H]$^+$, 252.0341, found 252.0336 Da.

9-Bromo-7-chloro-1,2,3,4-tetrahydroacridine (**2.22.2**)

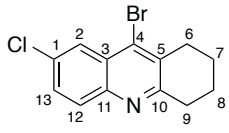

$C_{13}H_{11}BrClN$

MW: 296.59 g.mol^{-1}

2.22.2 was obtained according to general procedure A using 2-amino-5-chlorobenzoic acid (1.000 g, 5.830 mmol, 1.0 equiv), cyclohexanone (662 μL, 32.05 mmol, 1.1 equiv) and $POBr_3$ (14.70 g, 51.24 mmol, 8.8 equiv). The crude product was purified by column chromatography (silica gel, petroleum ether/EtOAc 9:1) to afford **2.22.2** as yellow solid (0.400 g, 1.341 mmol, 23%).

TLC Rf 0.28 (petroleum ether/EtOAc 9:1).

IR (neat) ν_{max} 2935 (m), 2861 (w), 1608 (w), 1577 (m), 1543 (m), 1470 (s), 1424 (m), 1388 (m), 1359 (m), 1308 (s), 1282 (w), 1241 (w), 1209 (m), 1165 (w), 1142 (w), 1078 (m) cm^{-1}.

^{1}H NMR (400 MHz, $CDCl_3$) δ (ppm) 8.10 (d, *J* = 2.3 Hz, 1H, **2**), 7.86 (d, *J* = 8.9 Hz, 1H, **12**), 7.54 (dd, *J* = 8.9, 2.3 Hz, 1H, **13**), 3.10-3.07 (m, 2H, **9**), 2.97-2.94 (m, 2H, **6**), 1.92 (m, 4H, **7** & **8**).

^{13}C NMR (101 MHz, $CDCl_3$) δ (ppm) 159.95 (**10**), 145.08 (**11**), 134.82 (**5**), 132.79 (**1**), 132.40 (**4**), 130.45 (**13**), 130.24 (**12**), 127.78 (**3**), 125.47 (**2**), 34.32 (**9**), 31.01 (**6**), 23.01 (**8**), 22.69 (**7**).

LRMS (ESI$^+$) *m/z* 296.0 [M^{79}Br^{35}Cl+H]$^+$, 298.0 [M^{81}Br^{35}Cl+H]$^+$.

HRMS (ESI$^+$) *m/z* calcd for $C_{13}H_{12}{}^{79}Br^{35}ClN$ [M+H]$^+$, 295.9839, found 295.9836 Da.

7-Chloro-1,2,3,4-tetrahydroacridin-9-(10*H*)-one (**2.24**)

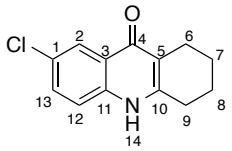

$C_{13}H_{12}ClNO$

MW: 233.70 g.mol^{-1}

2.22.1 (2.000 g, 7.930 mmol, 1.0 equiv) was dissolved in glacial AcOH (20 mL) and heated in a sealed tube for 16 h at 200 °C. Upon completion, the crude material was poured carefully onto iced-water. The mixture was filtered, washed with cold water and co-evaporated with toluene. Finally, the residue was dried under reduced pressure to afford **2.24** as an off-white powder (1.850 g, 7.920 mmol, quant). Spectroscopic data were consistent with those reported in literature.[327]

TLC Rf 0.06 (petroleum ether/EtOAc 4:1).

^{1}H NMR (400 MHz, DMSO-*d6*) δ (ppm) 11.63 (br s, 1H, **14**), 7.99 (d, *J* = 2.4 Hz, 1H, **2**), 7.61 (dd, *J* = 8.8, 2.4 Hz, 1H, **13**), 7.52 (d, *J* = 8.8 Hz, 1H, **12**), 2.71 (t, *J* = 6.0 Hz, 2H, **9**), 2.44 (t, *J* = 6.0 Hz, 2H, **6**), 1.77–1.69 (m, 4H, **7** & **8**).

LRMS (ESI$^+$) *m/z* 234.0 [M^{35}Cl+H]$^+$, 236.0 [M^{37}Cl+H]$^+$.

7-Chloro-1,2,3,4-tetrahydroacridin-9-yl trifluoromethanesulfonate (**2.22.3**)

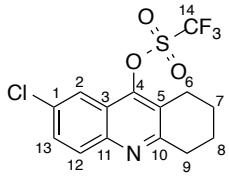

$C_{14}H_{11}ClF_3NO_3S$

MW: 365.75 g.mol^{-1}

2.22.3 was obtained according to general procedure B using **2.24** (1.760 g, 7.530 mmol, 1.0 equiv), Et_3N (1.15 mL, 8.280 mmol, 1.1 equiv) and Tf_2O (1.39 mL, 8.280 mmol, 1.1 equiv) and CH_2Cl_2 (88 mL). The crude product was purified by column chromatography (silica gel, petroleum ether/EtOAc 4:1) to afford **2.22.3** as a white powder (2.396 g, 6.551 mmol, 87%).

TLC Rf 0.40 (petroleum ether/EtOAc 4:1).

MP 86–87 °C (hexane).

IR (neat) ν_{max} 2945 (m), 2870 (w), 1601 (m), 1551 (w), 1477 (m), 1412 (s), 1344 (m), 1323 (m), 1213 (s), 1134 (s), 1082 (m), 1018 (s) cm^{-1}.

^{1}H NMR (400 MHz, $CDCl_3$) δ (ppm) 7.96 (d, *J* = 9.0 Hz, 1H, **12**), 7.93 (d, *J* = 2.3 Hz, 1H, **2**), 7.64 (dd, *J* = 9.0, 2.3 Hz, 1H, **13**), 3.16 (t, *J* = 6.6 Hz, 2H, **9**), 3.04 (t, *J* = 6.5 Hz, 2H, **6**), 2.04-1.89 (m, 4H, **7** & **8**).

^{13}C NMR (101 MHz, $CDCl_3$) δ (ppm) 161.57 (**10**), 148.82 (**4**), 146.46 (**11**), 133.57 (**1**), 131.13 (**13**), 130.48 (**12**), 125.33 (**3**), 121.60 (**5**), 119.93 (**2**), 118.79 (q, *J* = 316.4 Hz, **14**), 33.79 (**9**), 24.32 (**6**), 22.42 (**8**), 21.93 (**7**).

^{19}F NMR (376 MHz, $CDCl_3$) δ (ppm) –72.64.

LRMS (ESI$^+$) *m/z* 366.0 [M^{35}Cl+H]$^+$, 368.0 [M^{37}Cl+H]$^+$.

HRMS (ESI$^+$) *m/z* calcd for $C_{14}H_{12}{}^{35}ClF_3NO_3S$ [M+H]$^+$, 366.0182, found 366.0183 Da.

7-Chloro-9-iodo-1,2,3,4-tetrahydroacridine (**2.22.5**)

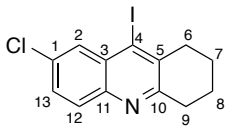

$C_{13}H_{11}ClIN$

MW: 343.59 g.mol^{-1}

To the solution of **2.22.5** (0.100 g, 0.430 mmol, 1.1 equiv), CuI (0.082 g, 0.430 mmol, 1.1 equiv), and I_2 (0.109 g, 0.430 mmol, 1.1 equiv) in CH_2I_2 (1.15 mL), isoamylnitrite (173 µL, 1.290 mmol, 3.0 equiv) was added at 85 °C. The reaction mixture was stirred for 2 h at 85 °C. After cooling to rt, a saturated aqueous solution of $Na_2S_2O_3$ (10 mL) was added and the reaction mixture was brought to alkalinity (pH ~ 9) using a saturated aqueous K_2CO_3 solution. The desired product was extracted with CH_2Cl_2, dried over Na_2SO_4, filtered and concentrated under reduced pressure. The crude iodide was purified by column chromatography (petroleum ether/EtOAc 98:2 to 95:5) to afford **2.22.5** as yellow solid (0.063 g, 0.185 mmol, 43%).

TLC Rf 0.30 (petroleum ether/EtOAc 95:5).

IR (neat) ν_{max} 2926 (m), 2860 (w), 1568 (m), 1540 (m), 1468 (s), 1418 (m), 1384 (m), 1304 (m), 1207 (m), 1166 (m), 1139 (m), 1080 (m) cm^{-1}.

^{1}H NMR (400 MHz, $CDCl_3$) δ (ppm) 8.03 (d, *J* = 2.3 Hz, 1H, **2**), 7.85 (d, *J* = 8.9 Hz, 1H, **12**), 7.53 (dd, *J* = 8.9, 2.3 Hz, 1H, **13**), 3.10-3.06 (m, 2H, **9**), 2.93-2.89 (m, 2H, **6**), 1.93-1.90 (m, 4H, **7** & **8**).

^{13}C NMR (101 MHz, $CDCl_3$) δ (ppm) 159.47 (**10**), 144.61 (**11**), 136.86 (**5**), 133.17 (**1**), 130.83 (**3**), 130.67 (**13**), 130.49 (**12**), 130.27 (**2**), 118.91 (**4**), 37.48 (**6**), 34.27 (**9**), 23.81 (**8**), 21.77 (**7**).

LRMS (ESI$^+$) *m/z* 344.0 [M^{35}Cl^{127}I+H]$^+$.

HRMS (ESI$^+$) *m/z* calcd for $C_{13}H_{12}{}^{35}Cl^{127}IN$ [M+H]$^+$, 343.9698, found 343.9690 Da.

N-(But-3-yn-1-yl)-7-chloro-1,2,3,4-tetrahydroacridin-9-amine (**2.9**)

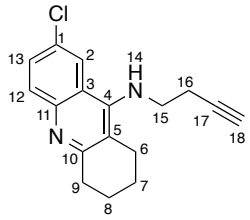

$C_{17}H_{17}ClN_2$

MW: 284.79 g.mol^{-1}

Terminal alkyne **2.9** was obtained according to general procedure C using **2.22.3** (0.150 g, 0.410 mmol, 1.0 equiv), $Pd_2(dba)_3$ (0.015 g, 0.016 mmol, 0.04 equiv), (±)-BINAP (0.022 g, 0.032 mmol, 0.08 equiv), Cs_2CO_3 (0.334 g, 1.025 mmol, 2.5 equiv), 1,4-dioxane (3.0 mL) and commercially available 1-amino-3-butyne (44 μL, 0.533 mmol, 1.3 equiv). The crude alkyne was purified by column chromatography (silica gel, Et_2O/MeOH 98:2) to afford **2.9** as yellow wax (0.099 g, 0.349 mmol, 85%).

TLC Rf 0.30 (Et_2O/MeOH 98:2).

IR (neat) ν_{max} 3303 (m), 3081 (w), 2946 (w), 2871 (w), 2156 (w), 1668 (s), 1583 (s), 1516 (m), 1417 (w), 1351 (m), 1200 (s), 1176 (s), 1128 (s) cm^{-1}.

^{1}H NMR (400 MHz, $CDCl_3$) δ (ppm) 7.96 (d, *J* = 2.2 Hz, 1H, **2**), 7.84 (d, *J* = 8.9 Hz, 1H, **12**), 7.49 (dd, *J* = 2.2, 8.9 Hz, 1H, **13**), 4.23 (t, *J* = 5.8 Hz, 1H, **14**), 3.58 (q, *J* = 6.2 Hz, 2H, **15**), 3.05 (t, *J* = 6.0 Hz, 2H, **9**), 2.80 (t, *J* = 6.4 Hz, 2H, **6**), 2.46 (td, *J* = 6.1, 2.6 Hz, 2H, **16**), 2.15 (t, *J* = 2.6 Hz, 1H, **18**), 1.98-1.87 (m, 4H, **7** & **8**).

^{13}C NMR (101 MHz, $CDCl_3$) δ (ppm) 159.40 (**10**), 149.21 (**4**), 146.11 (**11**), 130.80 (**13**), 129.80 (**12**), 129.28 (**1**), 121.98 (**2**), 121.80 (**3**), 119.00 (**5**), 81.67 (**17**), 71.16 (**18**), 47.58 (**15**), 34.27 (**9**), 24.88 (**6**), 23.06 (**8**), 22.88 (**7**), 21.04 (**16**).

LRMS (ESI$^+$) *m/z* 285.1 [M^{35}Cl+H]$^+$, 287.1 [M^{37}Cl+H]$^+$.

HRMS (ESI$^+$) *m/z* calcd for $C_{17}H_{18}{}^{35}ClN_2$ [M+H]$^+$, 285.1153, found 285.1159 Da.

N-Benzyl-7-chloro-1,2,3,4-tetrahydroacridin-9-amine (**2.27**)

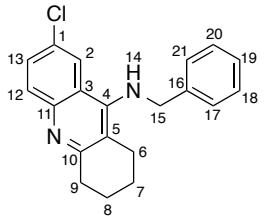

$C_{20}H_{19}ClN_2$

MW: 322.84 g.mol^{-1}

Amine **2.27** was obtained according to general procedure C using **2.22.3** (0.050 g, 0.137 mmol, 1.0 equiv), $Pd_2(dba)_3$ (0.008 g, 0.008 mmol, 0.06 equiv), (±)-BINAP (0.011 g, 0.016 mmol, 0.12 equiv), Cs_2CO_3 (0.112 g, 0.343 mmol, 2.5 equiv), 1,4-dioxane (1.7 mL) and benzylamine (22 µL, 0.206 mmol, 1.5 equiv). The crude amine was purified by column chromatography (silica gel, petroleum ether/EtOAc 1:1) to afford **2.27** as yellow wax (0.044 g, 0.137 mmol, quant).

TLC Rf 0.23 (petroleum ether/EtOAc 1:1).

IR (neat) ν_{max} 3065 (w), 3028 (w), 2930 (s), 2859 (s), 1580 (s), 1554 (s), 1484 (s), 1452 (m), 1427 (m), 1346 (m), 1118 (m), 1078 (m) cm^{-1}.

^{1}H NMR (400 MHz, $CDCl_3$) δ (ppm) 7.97 (d, *J* = 2.3 Hz, 1H, **2**), 7.87 (d, *J* = 9.0 Hz, 1H, **12**), 7.50 (dd, *J* = 9.0, 2.3 Hz, 1H, **13**), 7.39-7.28 (m, 5H, **17**, **18**, **19**, **20** & **21**), 4.58 (s, 2H, **15**), 4.11 (br s, 1H, **14**), 3.04 (t, *J* = 6.4 Hz, 2H, **9**), 2.59 (t, *J* = 6.3 Hz, 2H, **6**), 1.92-1.81 (m, 4H, **7** & **8**).

^{13}C NMR (101 MHz, $CDCl_3$) δ (ppm) 159.18 (**10**), 149.83 (**4**), 146.04 (**11**), 139.56 (**16**), 130.62 (**13**), 129.73 (**1**), 129.36 (**12**), 129.08 (2C, **18** & **20**), 128.04 (**19**), 127.81 (2C, **17** & **21**), 122.18 (**2**), 121.28 (**3**), 117.99 (**5**), 53.84 (**15**), 34.12 (**9**), 24.83 (**6**), 22.98 (**8**), 22.77 (**7**).

LRMS (ESI$^+$) *m/z* 323.1 [M^{35}Cl+H]$^+$, 325.1 [M^{37}Cl+H]$^+$.

HRMS (ESI$^+$) *m/z* calcd for $C_{20}H_{20}{}^{35}ClN_2$ [M+H]$^+$, 323.1310, found 323.1313 Da.

N-Benzyl-1,2,3,4-tetrahydroacridin-9-amine (**2.27b**)

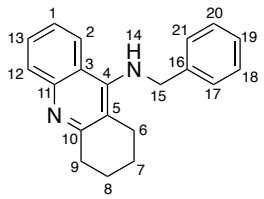

$C_{20}H_{20}N_2$

MW: 288.39 g.mol^{-1}

Amine **2.27b** was obtained according to general procedure C using **2.62** (0.050 g, 0.151 mmol, 1.0 equiv), $Pd_2(dba)_3$ (0.008 g, 0.009 mmol, 0.06 equiv), (±)-BINAP (0.012 g, 0.018 mmol, 0.12 equiv), Cs_2CO_3 (0.123 g, 0.378 mmol, 2.5 equiv), 1,4-dioxane (1.7 mL) and benzylamine (25 µL, 0.227 mmol, 1.5 equiv). The crude amine was purified by column chromatography (silica gel, petroleum ether/EtOAc/MeOH 1:1:0.2) to afford **2.27b** as yellow oil (0.042 g, 0.145 mmol, 96%).

TLC Rf 0.15 (petroleum ether/EtOAc/MeOH 1:1:0.2).

IR (neat) ν_{max} 3321 (w), 3060 (w), 2932 (s), 2859 (m), 1581 (s), 1561 (s), 1495 (s), 1452 (w), 1418 (w), 1349 (w), 1123 (w), 1028 (m) cm^{-1}.

^{1}H NMR (400 MHz, $CDCl_3$) δ (ppm) 7.98 (d, *J* = 8.0 Hz, 1H, **12**), 7.93 (d, *J* = 8.8 Hz, 1H, **2**), 7.57 (t, *J* = 8.0 Hz, 1H, **13**), 7.39-7.30 (m, 6H, **1**, **17**, **18**, **19**, **20** & **21**), 4.61 (s, 2H, **15**), 4.15 (br s, 1H, **14**), 3.07 (t, *J* = 6.3 Hz, 2H, **9**), 2.64 (t, *J* = 6.3 Hz, 2H, **6**), 1.94-1.82 (m, 4H, **7** & **8**).

^{13}C NMR (101 MHz, $CDCl_3$) δ (ppm) 159.93 (**10**), 150.51 (**4**), 147.77 (**11**), 139.92 (**16**), 129.09 (**13**), 129.00 (2C, **18** & **20**), 128.47 (**12**), 127.86 (**19**), 127.76 (2C, **17** & **21**), 124.09 (**1**), 122.88 (**2**), 120.59 (**3**), 117.12 (**5**), 53.78 (**15**), 34.29 (**9**), 24.94 (**6**), 23.14 (**8**), 22.93 (**7**).

LRMS (ESI$^+$) *m/z* 289.0 $[M+H]^+$.

HRMS (ESI$^+$) *m/z* calcd for $C_{20}H_{21}N_2$ $[M+H]^+$, 289.1699, found 289.1696 Da.

N-Butyl-7-chloro-1,2,3,4-tetrahydroacridin-9-amine (**2.28**)

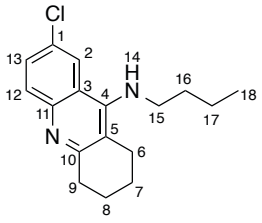

$C_{17}H_{21}ClN_2$

MW: 288.82 g.mol^{-1}

Amine **2.28** was obtained according to general procedure C using **2.22.3** (0.050 g, 0.137 mmol, 1.0 equiv), $Pd_2(dba)_3$ (0.008 g, 0.008 mmol, 0.06 equiv), (±)-BINAP (0.011 g, 0.016 mmol, 0.12 equiv), Cs_2CO_3 (0.112 g, 0.343 mmol, 2.5 equiv), 1,4-dioxane (1.7 mL) and *n*-butylamine (20 µL, 0.206 mmol, 1.5 equiv). The crude amine was purified by column chromatography (silica gel, petroleum ether/EtOAc 1:1) to afford **2.28** as yellow oil (0.028 g, 0.097 mmol, 71%).

TLC Rf 0.24 (petroleum ether/EtOAc 1:1).

IR (neat) ν_{max} 3339 (w), 2927 (s), 2860 (s), 1578 (s), 1556 (s), 1487 (s), 1431 (m), 1359 (m), 1263 (w), 1115 (m), 1081 (m) cm^{-1}.

^{1}H NMR (400 MHz, $CDCl_3$) δ (ppm) 7.93 (d, *J* = 2.3 Hz, 1H, **2**), 7.82 (d, *J* = 9.0 Hz, 1H, **12**), 7.47 (dd, *J* = 2.3, 9.0 Hz, 1H, **13**), 3.87 (br s, 1H, **14**), 3.46 (t, *J* = 7.1 Hz, 2H, **15**), 3.05-3.01 (m, 2H, **9**), 2.70-2.66 (m, 2H, **6**), 1.93- 1.89 (m, 4H, **7**+**8**), 1.65 (quin, *J* = 7.3 Hz, 2H, **16**), 1.43 (sxt, *J* = 7.4 Hz, 2H, **17**), 0.96 (t, *J* = 7.3 Hz, 3H, **18**).

^{13}C NMR (101 MHz, $CDCl_3$) δ (ppm) 158.96 (**10**), 150.21 (**4**), 146.11 (**11**), 130.59 (**13**), 129.22 (**1**), 129.15 (**12**), 122.25 (**2**), 121.09 (**3**), 116.84 (**5**), 49.39 (**15**), 34.17 (**9**), 34.02 (**6**), 24.84 (**16**), 23.10 (**8**), 22.84 (**7**), 20.24 (**17**), 13.99 (**18**).

LRMS (ESI$^+$) *m/z* 289.1 [M^{35}Cl+H]$^+$, 291.1 [M^{37}Cl+H]$^+$.

HRMS (ESI$^+$) *m/z* calcd for $C_{17}H_{22}{}^{35}ClN_2$ [M+H]$^+$, 289.1466, found 289.1462 Da.

N-(Pyren-2-yl)-7-chloro-1,2,3,4-tetrahydroacridin-9-amine (**2.29**)

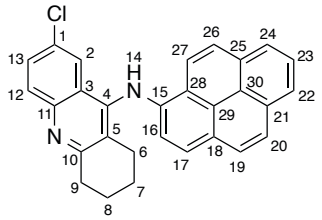

$C_{29}H_{21}ClN_2$

MW: 432.95 g.mol^{-1}

Amine **2.29** was obtained according to general procedure C using **2.22.3** (0.050 g, 0.137 mmol, 1.0 equiv), $Pd_2(dba)_3$ (0.008 g, 0.008 mmol, 0.06 equiv), (±)-BINAP (0.011 g, 0.016 mmol, 0.12 equiv), Cs_2CO_3 (0.112 g, 0.343 mmol, 2.5 equiv), 1,4-dioxane (1.7 mL) and 1-aminopyrene (0.045 g, 0.206 mmol, 1.5 equiv). The crude amine was purified by column chromatography (silica gel, petroleum ether/EtOAc 4:1) to afford **2.29** as green solid (0.057 g, 0.132 mmol, 96%).

TLC Rf 0.14 (petroleum ether/EtOAc 4:1).

IR (neat) ν_{max} 3361 (m), 3037 (w), 2920 (m), 2853 (m), 1601 (m), 1551 (s), 1512 (s), 1482 (s), 1466 (m), 1370 (s), 1333 (m), 1272 (m), 1089 (w) cm^{-1}.

^{1}H NMR (500 MHz, DMSO-*d6*) δ (ppm) 8.86 (br s, 1H, **14**), 8.68 (d, *J* = 9.0 Hz, 1H, **12**), 8.22-8.18 (m, 3H), 8.09 (d, *J* = 2.3 Hz, 1H, **2**), 8.04-7.99 (m, 3H), 7.96-7.94 (m, 2H), 7.66 (dd, *J* = 9.0, 2.3 Hz, 1H, **13**), 6.96 (d, *J* = 8.6 Hz, 1H), 3.08-3.04 (m, 2H, **9**), 2.72-2.67 (m, 1H, **6a**), 2.35-2.31 (m, 1H, **6b**), 1.91-1.59 (m, 4H, **7** & **8**).

^{13}C NMR (126 MHz, DMSO-*d6*) δ (ppm) 160.51 (**10**), 145.60 (**11**), 143.54 (**15**), 139.59 (**4**), 131.54, 131.21, 130.71, 129.40, 129.11, 127.44, 126.41, 126.06, 125.91, 125.33, 124.86, 124.77, 124.48, 124.45 (2C), 124.30, 123.94, 122.40, 122.35, 119.56, 115.16, 33.46 (**9**), 25.59 (**6**), 22.31 (**8**), 21.99 (**7**).

LRMS (ESI$^+$) *m/z* 433.1 [M^{35}Cl+H]$^+$, 435.1 [M^{37}Cl+H]$^+$.

HRMS (ESI$^+$) *m/z* calcd for $C_{29}H_{22}{}^{35}ClN_2$ [M+H]$^+$, 433.1466, found 433.1475 Da.

N-Phenyl-7-chloro-1,2,3,4-tetrahydroacridin-9-amine (**2.30**)

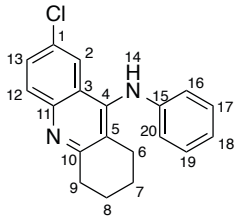

$C_{19}H_{17}ClN_2$

MW: 308.81 g.mol^{-1}

Amine **2.30** was obtained according to general procedure C using **2.22.3** (0.050 g, 0.137 mmol, 1.0 equiv), $Pd_2(dba)_3$ (0.008 g, 0.008 mmol, 0.06 equiv), (±)-BINAP (0.011 g, 0.016 mmol, 0.12 equiv), Cs_2CO_3 (0.112 g, 0.343 mmol, 2.5 equiv), 1,4-dioxane (1.7 mL) and aniline (19 µL, 0.206 mmol, 1.5 equiv). The crude amine was purified by column chromatography (silica gel, petroleum ether/EtOAc 7:3) to afford **2.30** as yellow solid (0.034 g, 0.110 mmol, 80%).

TLC Rf 0.39 (petroleum ether/EtOAc 1:1).

IR (neat) ν_{max} 3247 (w), 3041 (w), 2948 (w), 2869 (w), 1669 (s), 1579 (s), 1558 (m), 1496 (s), 1435 (m), 1404 (s), 1374 (m), 1199 (s), 1131 (s) cm^{-1}.

^{1}H NMR (400 MHz, $CDCl_3$) δ (ppm) 7.92 (d, *J* = 9.0 Hz, 1H, **12**), 7.76 (d, *J* = 2.3 Hz, 1H, **2**), 7.52 (dd, *J* = 9.0, 2.3 Hz, 1H, **13**), 7.24-7.19 (m, 2H, **17** & **19**), 6.92 (t, *J* = 7.4 Hz, 1H, **18**), 6.67 (d, *J* = 8.1 Hz, 2H, **16** & **20**), 5.83 (br s, 1H, **14**), 3.13 (t, *J* = 6.5 Hz, 2H, **9**), 2.72 (t, *J* = 6.4 Hz, 2H, **6**), 2.00-1.80 (m, 4H, **7** & **8**).

^{13}C NMR (101 MHz, $CDCl_3$) δ (ppm) 160.50 (**10**), 145.89 (**11**), 144.30 (**15**), 142.55 (**4**), 130.99 (**1**), 130.60 (**13**), 129.70 (**12**), 129.52 (2C, **17** & **19**), 124.82 (**3**), 124.24 (**5**), 122.25 (**18**), 121.05 (**2**), 116.56 (2C, **16** & **20**), 34.15 (**9**), 25.61 (**6**), 22.87 (**8**), 22.70 (**7**).

LRMS (ESI$^+$) *m/z* 309.1 [M^{35}Cl+H]$^+$, 311.1 [M^{37}Cl+H]$^+$.

HRMS (ESI$^+$) *m/z* calcd for $C_{19}H_{18}{}^{35}ClN_2$ [M+H]$^+$, 309.1153, found 309.1151 Da.

N-(4-Bromophenyl)-7-chloro-1,2,3,4-tetrahydroacridin-9-amine (**2.31**)

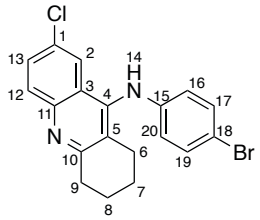

$C_{19}H_{16}BrClN_2$

MW: 387.70 g.mol^{-1}

Amine **2.31** was obtained according to general procedure C using **2.22.3** (0.050 g, 0.137 mmol, 1.0 equiv), $Pd_2(dba)_3$ (0.008 g, 0.008 mmol, 0.06 equiv), (±)-BINAP (0.011 g, 0.016 mmol, 0.12 equiv), Cs_2CO_3 (0.112 g, 0.343 mmol, 2.5 equiv), 1,4-dioxane (1.7 mL) and 4-bromoaniline (0.024 g, 0.137 mmol, 1.0 equiv). The crude amine was purified by column chromatography (silica gel, petroleum ether/EtOAc 75:25) to afford **2.31** as yellow solid (0.048 g, 0.125 mmol, 91%).

TLC Rf 0.29 (petroleum ether/EtOAc 75:25).

IR (neat) ν_{max} 3244 (w), 2927 (m), 2855 (w), 1670 (s), 1578 (s), 1506 (m), 1487 (s), 1404 (s), 1200 (s), 1132 (m) cm^{-1}.

^{1}H NMR (400 MHz, $CDCl_3$) δ (ppm) 8.48 (br s, 1H, **14**), 8.12 (d, *J* = 9.2 Hz, 1H, **12**), 7.89 (d, *J* = 2.0 Hz, 1H, **2**), 7.52-7.49 (m, 3H, **13**, **17** & **19**), 6.92 (d, *J* = 8.6 Hz, 2H, **20** & **16**), 3.26 (t, *J* = 6.2 Hz, 2H, **9**), 3.39 (t, *J* = 6.3 Hz, 2H, **6**), 1.93-1.81 (m, 4H, **7** & **8**).

^{13}C NMR (101 MHz, $CDCl_3$) δ (ppm) 155.33 (**10**), 150.93 (**11**), 139.53 (**15**), 136.38 (**4**), 133.24 (**13**), 132.67 (**17**), 132.60 (**19**), 129.18 (**1**), 128.37 (**12**), 125.44 (**3**), 123.84 (**16**), 122.16 (**2**), 119.92 (**20**), 118.82 (**5**), 117.80 (**18**), 28.67 (**9**), 26.30 (**6**), 21.72 (**8**), 20.60 (**7**).

LRMS (ESI$^+$) *m/z* 387.0 $[M^{79}Br^{35}Cl+H]^+$, 389.0 $[M^{81}Br^{35}Cl+H]^+$.

HRMS (ESI$^+$) *m/z* calcd for $C_{19}H_{17}{}^{79}Br^{35}ClN_2$ $[M+H]^+$, 387.0257, found 387.0258 Da.

N-(4-Methoxyphenyl)-7-chloro-1,2,3,4-tetrahydroacridin-9-amine (**2.32**)

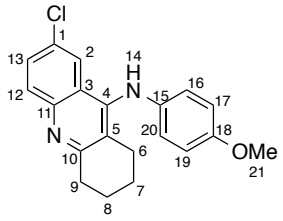

$C_{20}H_{19}ClN_2O$

MW: 338.83 g.mol^{-1}

Amine **2.32** was obtained according to general procedure C using **2.22.3** (0.050 g, 0.137 mmol, 1.0 equiv), $Pd_2(dba)_3$ (0.008 g, 0.008 mmol, 0.06 equiv), (±)-BINAP (0.011 g, 0.016 mmol, 0.12 equiv), Cs_2CO_3 (0.112 g, 0.343 mmol, 2.5 equiv), 1,4-dioxane (1.7 mL) and *p*-Anisidine (0.025 g, 0.206 mmol, 1.5 equiv). The crude amine was purified by column chromatography (silica gel, petroleum ether/EtOAc 75:25) to afford **2.32** as yellow solid (0.030 g, 0.089 mmol, 65%).

TLC Rf 0.18 (petroleum ether/EtOAc 75:25).

IR (neat) ν_{max} 3271 (w), 2947 (w), 2840 (w), 1779 (w), 1668 (s), 1581 (s), 1559 (m), 1507 (s), 1436 (m), 1404 (m), 1245 (s), 1198 (s), 1170 (s), 1134 (s), 1031 (w) cm^{-1}.

^{1}H NMR (400 MHz, $CDCl_3$) δ (ppm) 8.46 (br s, 1H, **14**), 7.95 (d, *J* = 8.9 Hz, 1H, **12**), 7.69 (d, *J* = 2.1 Hz, 1H, **2**), 7.49 (dd, *J* = 8.9 Hz, 2.1, 1H, **13**), 7.05 (d, *J* = 9.0 Hz, 2H, **16** & **20**), 6.88 (d, *J* = 8.8, 2H, **17** & **19**), 3.82 (s, 3H, **21**), 3.11 (t, *J* = 5.9 Hz, 2H, **9**), 2.48 (t, *J* = 5.9 Hz, 2H, **6**), 1.88-1.81 (m, 4H, **7** & **8**).

^{13}C NMR (101 MHz, $CDCl_3$) δ (ppm) 159.09 (**10**), 153.65 (**18**), 152.26 (**11**), 136.99 (**4**), 133.57 (**13**), 132.25 (**15**), 131.74 (**1**), 126.03 (2C, **16** & **20**), 123.93 (**2**), 122.19 (**12**), 117.42 (**3**), 115.30 (2C, **17** & **19**), 114.59 (**5**), 55.81 (**21**), 28.50 (**9**), 24.37 (**6**), 21.73 (**8**), 20.63 (**7**).

LRMS (ESI$^+$) *m/z* 339.1 [M^{35}Cl+H]$^+$, 341.1 [M^{37}Cl+H]$^+$.

HRMS (ESI$^+$) *m/z* calcd for $C_{20}H_{20}{}^{35}ClN_2O$ [M+H]$^+$, 339.1259, found 339.1260 Da.

7-Chloro-9-(pyrrolidin-1-yl)-1,2,3,4-tetrahydroacridine (**2.33**)

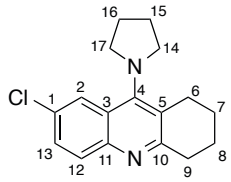

$C_{17}H_{19}ClN_2$

MW: 286.80 g.mol^{-1}

Amine **2.33** was obtained according to general procedure C using **2.22.3** (0.050 g, 0.137 mmol, 1.0 equiv), $Pd_2(dba)_3$ (0.008 g, 0.008 mmol, 0.06 equiv), (±)-BINAP (0.011 g, 0.016 mmol, 0.12 equiv), Cs_2CO_3 (0.112 g, 0.343 mmol, 2.5 equiv), 1,4-dioxane (1.7 mL) and pyrrolidine (57 μL, 0.206 mmol, 1.5 equiv). The crude amine was purified by column chromatography (silica gel, petroleum ether/EtOAc 9:1) to afford **2.33** as yellow wax (0.034 g, 0.119 mmol, 87%).

TLC Rf 0.20 (petroleum ether/EtOAc 9:1).

IR (neat) ν_{max} 2929 (s), 2858 (s), 1567 (s), 1477 (s), 1450 (m), 1427 (m), 1380 (s), 1150 (w), 1101 (w) cm^{-1}.

^{1}H NMR (400 MHz, $CDCl_3$) δ (ppm) 7.89-7.87 (m, 2H, **2** & **12**), 7.48 (dd, *J* = 9.0, 2.3 Hz, 1H, **13**), 3.38 (t, *J* = 6.5 Hz, 4H, **14** & **17**), 3.09 (t, *J* = 6.6 Hz, 2H, **9**), 2.81 (t, *J* = 6.3 Hz, 2H, **6**), 2.15-2.08 (m, 4H, **15** & **16**), 1.98-1.91 (m, 2H, **7**), 1.87-1.81 (m, 2H, **8**).

^{13}C NMR (101 MHz, $CDCl_3$) δ (ppm) 160.77 (**10**), 150.30 (**4**), 146.29 (**11**), 130.67 (**13**), 130.59 (**1**), 129.95 (**3**), 129.08 (**12**), 127.36 (**5**), 123.02 (**2**), 51.28 (2C, **14**+**17**), 34.05 (**9**), 26.62 (2C, **15** & **16**), 26.57 (**6**), 22.99 (2C, **7** & **8**).

LRMS (ESI$^+$) *m/z* 287.1 [M^{35}Cl+H]$^+$, 289.1 [M^{37}Cl+H]$^+$.

HRMS (ESI$^+$) *m/z* calcd for $C_{17}H_{20}{}^{35}ClN_2$ [M+H]$^+$, 287.1310, found 287.1310 Da.

7-Chloro-9-(piperidin-1-yl)-1,2,3,4-tetrahydroacridine (**2.34**)

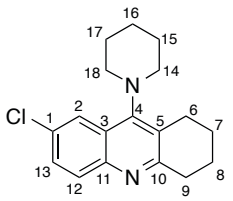

$C_{18}H_{21}ClN_2$

MW: 300.83 g.mol^{-1}

Amine **2.34** was obtained according to general procedure C using **2.22.3** (0.050 g, 0.137 mmol, 1.0 equiv), $Pd_2(dba)_3$ (0.008 g, 0.008 mmol, 0.06 equiv), (±)-BINAP (0.011 g, 0.016 mmol, 0.12 equiv), Cs_2CO_3 (0.112 g, 0.343 mmol, 2.5 equiv), 1,4-dioxane (1.7 mL) and piperidine (16 μL, 0.164 mmol, 1.2 equiv). The crude amine was purified by column chromatography (silica gel, petroleum ether/EtOAc 9:1) to afford **2.34** as colorless oil (0.022 g, 0.074 mmol, 54%).

TLC Rf 0.32 (petroleum ether/EtOAc 9:1).

IR (neat) ν_{max} 2929 (s), 2858 (s), 1667 (m), 1476 (s), 1450 (m), 1427 (m), 1380 (m), 1150 (w), 1099 (m) cm^{-1}.

^{1}H NMR (400 MHz, $CDCl_3$) δ (ppm) 8.09 (d, *J* = 2.4 Hz, 1H, **2**), 7.86 (d, *J* = 8.9 Hz, 1H, **12**), 7.49 (dd, *J* = 2.4, 8.9 Hz, 1H, **13**), 3.23 (t, *J* = 5.0 Hz, 4H, **14** & **18**), 3.09 (t, *J* = 6.7 Hz, 2H, **9**), 2.90 (t, *J* = 6.4 Hz, 2H, **6**), 1.96-1.89 (m, 2H, **16**), 1.88-1.74 (m, 8H, **7**, **8**, **15** & **17**).

^{13}C NMR (101 MHz, $CDCl_3$) δ (ppm) 160.80 (**10**), 153.62 (**4**), 146.26 (**11**), 130.61 (**1**), 130.40 (**13**), 129.15 (**12**), 128.23 (**3**), 127.00 (**5**), 123.29 (**2**), 52.08 (2C, **14** & **18**), 34.16 (**9**), 27.11 (2C, **15** & **17**), 27.07 (**6**), 24.70 (**16**), 23.11 (**8**), 22.91 (**7**).

LRMS (ESI$^+$) *m/z* 301.1 [M^{35}Cl+H]$^+$, 303.1 [M^{37}Cl+H]$^+$.

HRMS (ESI$^+$) *m/z* calcd for $C_{18}H_{22}{}^{35}ClN_2$ [M+H]$^+$, 301.1466, found 301.1472 Da.

N-Allyl-7-chloro-1,2,3,4-tetrahydroacridin-9-amine (**2.35**)

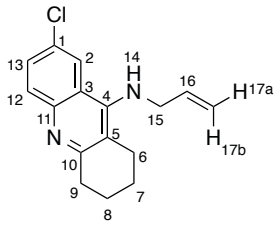

$C_{16}H_{17}ClN_2$

MW: 272.78 g.mol^{-1}

Amine **2.35** was obtained according to general procedure C using **2.22.3** (0.050 g, 0.137 mmol, 1.0 equiv), $Pd_2(dba)_3$ (0.008 g, 0.008 mmol, 0.06 equiv), (±)-BINAP (0.011 g, 0.016 mmol, 0.12 equiv), Cs_2CO_3 (0.112 g, 0.343 mmol, 2.5 equiv), 1,4-dioxane (1.7 mL) and allylamine (16 μL, 0.206 mmol, 1.5 equiv). The crude amine was purified by column chromatography (silica gel, petroleum ether/EtOAc 1:1) to afford **2.35** as white powder (0.024 g, 0.088 mmol, 64%).

TLC Rf 0.16 (petroleum ether/EtOAc 1:1).

IR (neat) ν_{max} 3290 (m), 3089 (w), 2945 (m), 2871 (w), 1669 (s), 1584 (s), 1518 (m), 1417 (w), 1349 (w), 1325 (w), 1200 (s), 1176 (s), 1131 (s) cm^{-1}.

^{1}H NMR (400 MHz, $CDCl_3$) δ (ppm) 7.91 (d, *J* = 2.3 Hz, 1H, **2**), 7.85 (d, *J* = 8.9 Hz, 1H, **12**), 7.48 (dd, *J* = 8.9, 2.3 Hz, 1H, **13**), 6.05-5.95 (m, 1H, **16**), 5.38 (dd, *J* = 17.0, 1.5 Hz, 1H, **17b**), 5.24 (dd, *J* = 10.3, 1.3 Hz, 1H, **17a**), 4.05 (d, *J* = 5.4 Hz, 2H, **15**), 3.97 (br s, 1H, **14**), 3.06-3.03 (m, 2H, **9**), 2.74-2.70 (m, 2H, **6**), 1.95-1.89 (m, 4H, **7** & **8**).

^{13}C NMR (101 MHz, $CDCl_3$) δ (ppm) 159.03 (**10**), 149.89 (**4**), 145.92 (**11**), 135.62 (**16**), 130.53 (**13**), 129.66 (**1**), 129.36 (**12**), 122.11 (**2**), 121.22 (**3**), 117.71 (**5**), 117.36 (**17**), 51.90 (**15**), 34.09 (**9**), 24.86 (**6**), 23.04 (**7**), 22.80 (**8**).

LRMS (ESI$^+$) *m/z* 273.1 [M^{35}Cl+H]$^+$, 275.1 [M^{37}Cl+H]$^+$.

HRMS (ESI$^+$) *m/z* calcd for $C_{16}H_{18}{}^{35}ClN_2$ [M+H]$^+$, 273.1153, found 273.1146 Da.

7-Chloro-*N*-(prop-2-yn-1-yl)-1,2,3,4-tetrahydroacridin-9-amine (**2.36**)

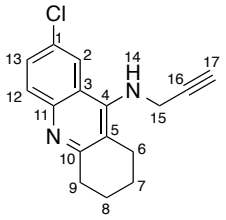

$C_{16}H_{15}ClN_2$

MW: 270.76 g.mol^{-1}

Amine **2.36** was obtained according to general procedure C using **2.22.3** (0.100 g, 0.274 mmol, 1.0 equiv), $Pd_2(dba)_3$ (0.010 g, 0.011 mmol, 0.04 equiv), (±)-BINAP (0.015 g, 0.022 mmol, 0.08 equiv), Cs_2CO_3 (0.223 g, 0.685 mmol, 2.5 equiv), 1,4-dioxane (3.0 mL) and commercially available propargylamine (23 μL, 0.356 mmol, 1.3 equiv). The crude amine was purified by column chromatography (silica gel, Et_2O) to afford **2.36** as a white solid (0.067 g, 0.247 mmol, 90%).

TLC Rf 0.37 (Et_2O).

MP 135–137 °C (hexane).

IR (neat) ν_{max} 3304 (m), 2943 (m), 2865 (m), 2154 (w), 1669 (s), 1583 (s), 1567 (s), 1517 (m), 1417 (w), 1338 (m), 1199 (s), 1178 (s), 1130 (s) cm^{-1}.

^{1}H NMR (400 MHz, $CDCl_3$) δ (ppm) 7.90 (d, *J* = 2.0 Hz, 1H, **2**), 7.86 (d, *J* = 8.9 Hz, 1H, **12**), 7.51 (dd, *J* = 2.0, 8.9 Hz, 1H, **13**), 4.21-4.11 (m, 2H, **15**), 4.07 (br s, 1H, **14**), 3.07 (t, *J* = 7.1 Hz, 2H, **9**), 2.85 (t, *J* = 5.3 Hz, 2H, **6**), 2.28 (s, 1H, **17**), 2.00-1.85 (m, 4H, **7** & **8**).

^{13}C NMR (101 MHz, $CDCl_3$) δ (ppm) 159.60 (**10**), 148.63 (**4**), 130.89 (**13**), 130.36 (**1**), 129.44 (**12**), 121.99 (**3**), 121.69 (**2**), 120.31 (**5**), 81.10 (**17**), 72.92 (**16**), 38.67 (**15**), 34.25 (**9**), 24.89 (**6**), 22.99 (**8**), 22.82 (**7**).

LRMS (ESI$^+$) *m/z* 271.1 [M^{35}Cl+H]$^+$, 273.1 [M^{37}Cl+H]$^+$.

HRMS (ESI$^+$) *m/z* calcd for $C_{16}H_{16}{}^{35}ClN_2$ [M+H]$^+$, 271.0992, found 271.0996 Da.

N-(Pyridin-3-yl)-7-chloro-1,2,3,4-tetrahydroacridin-9-amine (**2.37**)

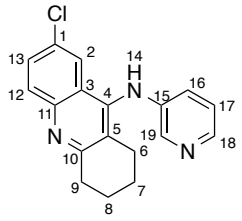

$C_{18}H_{16}ClN_3$

MW: 309.80 g.mol^{-1}

Amine **2.37** was obtained according to general procedure C using **2.22.3** (0.050 g, 0.137 mmol, 1.0 equiv), $Pd_2(dba)_3$ (0.008 g, 0.008 mmol, 0.06 equiv), (±)-BINAP (0.011 g, 0.016 mmol, 0.12 equiv), Cs_2CO_3 (0.112 g, 0.343 mmol, 2.5 equiv), 1,4-dioxane (1.7 mL) and 3-aminopyridine (0.019 g, 0.206 mmol, 1.5 equiv). The crude amine was purified by column chromatography (silica gel, petroleum ether/EtOAc 6:4) to afford **2.37** as yellow solid (0.034 g, 0.111 mmol, 81%).

TLC Rf 0.30 (petroleum ether/EtOAc 6:4).

IR (neat) ν_{max} 3229 (m), 3088 (w), 2935 (m), 2863 (m), 1586 (s), 1557 (m), 1480 (s), 1374 (m), 1286 (w), 1093 (w) cm^{-1}.

^{1}H NMR (400 MHz, $CDCl_3$) δ (ppm) 8.18-8.15 (m, 2H, **18** & **19**), 7.93 (d, *J* = 9.0 Hz, 1H, **12**), 7.73 (d, *J* = 2.3 Hz, 1H, **2**), 7.54 (dd, *J* = 2.3, 9.0 Hz, 1H, **13**), 7.12-7.08 (m, 1H, **16**), 6.81-6.78 (m, 1H, **17**), 6.02 (br s, 1H, **14**), 3.13 (t, *J* = 6.5 Hz, 2H, **9**), 2.71 (t, *J* = 6.4 Hz, 2H, **6**), 1.99-1.92 (m, 2H, **8**), 1.87-1.81 (m, 2H, **7**).

^{13}C NMR (101 MHz, $CDCl_3$) δ (ppm) 160.72 (**10**), 145.93 (**4**), 141.90 (**18**), 141.19 (**11**), 140.90 (**15**), 138.64 (**19**), 131.56 (**1**), 130.84 (**13**), 129.96 (**12**), 125.84 (**5**), 124.30 (**3**), 123.92 (**2**), 121.99 (**16**), 121.81 (**17**), 34.13 (**9**), 25.75 (**6**), 22.80 (**8**), 22.60 (**7**).

LRMS (ESI$^+$) *m/z* 310.1 [M^{35}Cl+H]$^+$, 312.1 [M^{37}Cl+H]$^+$.

HRMS (ESI$^+$) *m/z* calcd for $C_{18}H_{17}{}^{35}ClN_3$ [M+H]$^+$, 310.1105, found 310.1101 Da.

N-(7-Chloro-1,2,3,4-tetrahydroacridin-9-yl)-2-methylpropane-2-sulfinamide (**2.38**)

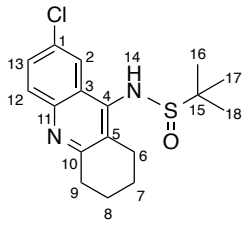

$C_{17}H_{21}ClN_2OS$

MW: 336.88 g.mol^{-1}

Amine **2.38** was obtained according to general procedure C using **2.22.3** (0.050 g, 0.137 mmol, 1.0 equiv), $Pd_2(dba)_3$ (0.008 g, 0.008 mmol, 0.06 equiv), (±)-BINAP (0.011 g, 0.016 mmol, 0.12 equiv), Cs_2CO_3 (0.112 g, 0.343 mmol, 2.5 equiv), 1,4-dioxane (1.7 mL) and 2-methyl-2-propane sulfonamide (0.025 g, 0.206 mmol, 1.5 equiv). The crude amine was purified by column chromatography (silica gel, petroleum ether/EtOAc/MeOH 75:25:0.02) to afford **2.38** as yellow solid (0.031 g, 0.092 mmol, 67%).

TLC Rf 0.10 (petroleum ether/EtOAc/MeOH 75:25:0.02).

IR (neat) ν_{max} 3353 (w), 3242 (w), 2932 (m), 2864 (w), 1650 (s), 1573 (s), 1491 (s), 1445 (w), 1375 (w), 1031 (s) cm^{-1}.

^{1}H NMR (400 MHz, $CDCl_3$) δ (ppm) 7.83 (d, *J* = 9.0 Hz, 1H, **12**), 7.68 (d, *J* = 2.2 Hz, 1H, **2**), 7.49 (dd, *J* = 2.2, 9.0 Hz, 1H, **13**), 4.68 (br s, 1H, **14**), 3.01 (t, *J* = 5.9 Hz, 2H, **9**), 2.61 (t, *J* = 6.1 Hz, 2H, **6**), 1.99-1.90 (m, 4H, **7** & **8**), 1.23 (s, 9H, **16**, **17** & **18**).

^{13}C NMR (101 MHz, $CDCl_3$) δ (ppm) 158.64 (**10**), 146.36 (**4**), 144.46 (**11**), 130.01 (**1**), 129.60 (**13**), 129.53 (**12**), 119.41 (**2**), 117.81 (**3**), 111.20 (**5**), 55.53 (**15**), 33.74 (**9**), 23.81 (**6**), 22.74 (**7**), 22.71 (**8**), 22.26 (3C, **16**, **17** & **18**).

LRMS (ESI$^+$) *m/z* 337.1 [M^{35}Cl+H]$^+$, 339.1 [M^{37}Cl+H]$^+$.

HRMS (ESI$^+$) *m/z* calcd for $C_{17}H_{22}{}^{35}ClN_2OS$ [M+H]$^+$, 337.1136, found 337.1136 Da.

N-(7-Chloro-1,2,3,4-tetrahydroacridin-9-yl)benzamide (**2.39**)

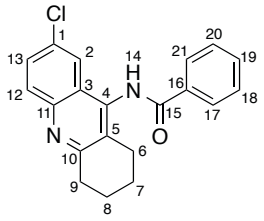

$C_{20}H_{17}ClN_2O$

MW: 336.82 g.mol^{-1}

Amine **2.39** was obtained according to general procedure C using **2.22.3** (0.050 g, 0.137 mmol, 1.0 equiv), $Pd_2(dba)_3$ (0.008 g, 0.008 mmol, 0.06 equiv), (±)-BINAP (0.011 g, 0.016 mmol, 0.12 equiv), Cs_2CO_3 (0.112 g, 0.343 mmol, 2.5 equiv), 1,4-dioxane (1.7 mL) and benzamide (0.025 g, 0.206 mmol, 1.5 equiv). The crude amine was purified by column chromatography (silica gel, petroleum ether/EtOAc/MeOH 6:4:0.02) to afford **2.39** as white solid (0.035 g, 0.104 mmol, 76%).

TLC Rf 0.38 (petroleum ether/EtOAc/MeOH 6:7:0.02).

IR (neat) ν_{max} 3248 (m), 2934 (s), 2862 (m), 1649 (s), 1591 (m), 1511 (s), 1482 (s), 1282 (m), 1082 (w) cm^{-1}.

^{1}H NMR (400 MHz, $CDCl_3$) δ (ppm) 8.01 (d, *J* = 7.6 Hz, 2H, **17** & **21**), 7.94 (m, 2H, **14**, **13**), 7.75 (d, *J* = 2.4 Hz, 1H, **2**), 7.67-7.61 (m, 1H, **13**), 7.58-7.52 (m, 3H, **18**, **19** & **20**), 3.14 (t, *J* = 6.6 Hz, 2H, **9**), 2.87 (t, *J* = 6.5 Hz, 2H, **6**), 2.01-1.95 (m, 2H, **7**), 1.90-1.83 (m, 2H, **8**).

^{13}C NMR (101 MHz, $CDCl_3$) δ (ppm) 165.94 (**15**), 160.47 (**10**), 145.40 (**11**), 137.77 (**4**), 133.44 (**16**), 132.72 (**19**), 132.11 (**1**), 130.62 (**13**), 129.95 (**12**), 129.13 (2C, **18** & **20**), 128.98 (**5**), 127.69 (2C, **17** & **21**), 124.97 (**3**), 121.31 (**2**), 34.07 (**9**), 25.79 (**6**), 22.73 (**8**), 22.43 (**7**).

LRMS (ESI$^+$) *m/z* 337.1 [M^{35}Cl+H]$^+$, 339.1 [M^{37}Cl+H]$^+$.

HRMS (ESI$^+$) *m/z* calcd for $C_{20}H_{18}{}^{35}ClN_2O$ [M+H]$^+$, 337.1102, found 337.1101 Da.

Diethyl (7-Chloro-1,2,3,4-tetrahydroacridin-9-yl)phosphoramide (**2.40**)

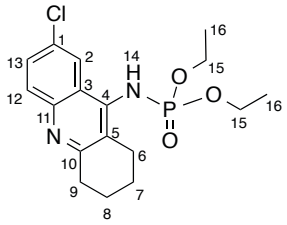

$C_{17}H_{22}ClN_2O_3P$

MW: 368.80 g.mol^{-1}

Amine **2.40** was obtained according to general procedure C using **2.22.3** (0.050 g, 0.137 mmol, 1.0 equiv), $Pd_2(dba)_3$ (0.008 g, 0.008 mmol, 0.06 equiv), (±)-BINAP (0.011 g, 0.016 mmol, 0.12 equiv), Cs_2CO_3 (0.112 g, 0.343 mmol, 2.5 equiv), 1,4-dioxane (1.7 mL) and diethyl phosphoramidate (0.032 g, 0.206 mmol, 1.5 equiv). The crude amine was purified by column chromatography (silica gel, petroleum ether/EtOAc/MeOH 1:1:0.02) to afford **2.40** as an off-white solid (0.044 g, 0.119 mmol, 87%).

TLC Rf 0.31 (petroleum ether/EtOAc/MeOH 1:1:0.02).

IR (neat) ν_{max} 3083 (w), 2931 (m), 2861 (m), 1584 (m), 1549 (s), 1501 (s), 1482 (s), 1361 (m), 1235 (s), 1203 (m), 1165 (m), 1097 (w), 1034 (s) cm^{-1}.

^{1}H NMR (400 MHz, $CDCl_3$) δ (ppm) 8.24 (d, *J* = 2.1 Hz, 1H, **2**), 7.87 (d, *J* = 8.9 Hz, 1H, **12**), 7.54-7.51 (m, 1H, **13**), 4.87 (br s, 1H, **14**), 4.20-4.10 (m, 4H, **15**), 3.11-3.00 (m, 4H, **6** & **9**), 1.98-1.86 (m, 4H, **7** & **8**), 1.36-1.27 (m, 6H, **16**).

^{13}C NMR (101 MHz, $CDCl_3$) δ (ppm) 160.36 (**10**), 145.56 (**4**), 131.40 (**11**), 130.28 (**1**), 129.74 (2C, **12** & **13**), 127.32 (**3**), 125.42 (**5**), 122.58 (**2**), 63.82 (**15**), 63.76 (**15**), 34.13 (**6**), 25.69 (**9**), 22.71 (2C, **7** & **8**), 16.34 (**16**), 16.27 (**16**).

^{31}P NMR (162 MHz, $CDCl_3$) δ (ppm) 2.95.

LRMS (ESI$^+$) *m/z* 369.1 [M^{35}Cl+H]$^+$, 371.1 [M^{37}Cl+H]$^+$.

HRMS (ESI$^+$) *m/z* calcd for $C_{17}H_{23}{}^{35}ClN_2O_3P$ [M+H]$^+$, 369.1129, found 369.1133 Da.

2-(2-((7-Chloro-1,2,3,4-tetrahydroacridin-9-yl)amino)ethoxy)ethan-1-ol (**2.41**)

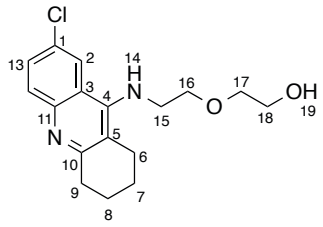

$C_{17}H_{21}ClN_2O_2$

MW: 320.82 g.mol^{-1}

Amine **2.41** was obtained according to general procedure C using **2.22.3** (0.050 g, 0.137 mmol, 1.0 equiv), $Pd_2(dba)_3$ (0.008 g, 0.008 mmol, 0.06 equiv), (±)-BINAP (0.011 g, 0.016 mmol, 0.12 equiv), Cs_2CO_3 (0.112 g, 0.343 mmol, 2.5 equiv), 1,4-dioxane (1.7 mL) and 2-(2-aminoethoxy)ethan-1-ol (21 μL, 0.206 mmol, 1.5 equiv). The crude amine was purified by column chromatography (silica gel, EtOAc/MeOH 97:3) to afford **2.41** as an off-white solid (0.042 g, 0.132 mmol, 96%).

TLC Rf 0.16 (EtOAc/MeOH 97:3).

IR (neat) ν_{max} 3346 (s), 2931 (s), 2861 (s), 1645 (m), 1580 (s), 1558 (s), 1487 (s), 1436 (m), 1341 (w), 1258 (s), 1117 (s), 1071 (s), 1030 (s) cm^{-1}.

^{1}H NMR (400 MHz, $CDCl_3$) δ (ppm) 7.97 (d, *J* = 2.2 Hz, 1H, **2**), 7.84 (d, *J* = 8.9 Hz, 1H, **12**), 7.48 (dd, *J* = 2.2, 8.9 Hz, 1H, **13**), 5.48 (br s, 1H, **14**), 4.63 (br s, 1H, **19**), 3.83-3.81 (m, 2H, **17**), 3.63-3.60 (m, 6H, **15**, **16** & **18**), 3.05- 3.02 (m, 2H, **9**), 2.76-2.73 (m, 2H, **6**), 1.93-1.88 (m, 4H, **7** & **8**).

^{13}C NMR (101 MHz, $CDCl_3$) δ (ppm) 158.07 (**10**), 150.68 (**4**), 129.97 (2C, **12** & **13**), 129.24 (**1**), 122.22 (**2**), 120.91 (**3**), 117.72 (**5**), 72.41 (**17**), 70.31 (**16**), 61.97 (**18**), 48.65 (**15**), 33.18 (**9**), 24.58 (**6**), 22.84 (**7**), 22.52 (**8**).

LRMS (ESI$^+$) *m/z* 321.1 [M^{35}Cl+H]$^+$, 323.1 [M^{37}Cl+H]$^+$.

HRMS (ESI$^+$) *m/z* calcd for $C_{17}H_{22}{}^{35}ClN_2O_2$ [M+H]$^+$, 321.1364, found 321.1361 Da.

Ethyl (7-chloro-1,2,3,4-tetrahydroacridin-9-yl)glycinate (**2.42**)

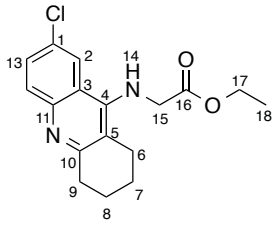

$C_{17}H_{19}ClN_2O_2$

MW: 318.80 g.mol^{-1}

Amine **2.42** was obtained according to general procedure C using **2.22.3** (0.050 g, 0.137 mmol, 1.0 equiv), $Pd_2(dba)_3$ (0.008 g, 0.008 mmol, 0.06 equiv), (±)-BINAP (0.011 g, 0.016 mmol, 0.12 equiv), Cs_2CO_3 (0.112 g, 0.343 mmol, 2.5 equiv), 1,4-dioxane (1.7 mL), glycine ethyl ester hydrochloride (0.029 g, 0.206 mmol, 1.5 equiv) and Et_3N (29 μL, 0.206 mmol, 1.5 equiv). The crude amine was purified by column chromatography (silica gel, petroleum ether/EtOAc/MeOH 6:4:0.02) to afford **2.42** as pale yellow oil (0.040 g, 0.126 mmol, 92%).

TLC Rf 0.29 (petroleum ether/EtOAc/MeOH 6:4:0.02).

IR (neat) ν_{max} 3385 (m), 2935 (m), 2862 (w), 1736 (s), 1582 (s), 1557 (m), 1487 (s), 1435 (w), 1373 (s), 1339 (w), 1210 (s), 1161 (m), 1023 (w) cm^{-1}.

^{1}H NMR (400 MHz, $CDCl_3$) δ (ppm) 7.87 (d, *J* = 2.3 Hz, 1H, **2**), 7.83 (d, *J* = 8.9 Hz, 1H, **12**), 7.47 (dd, *J* = 8.9, 2.3 Hz, 1H, **13**), 4.86 (t, *J* = 5.0 Hz, 1H, **14**), 4.24 (q, *J* = 7.2 Hz, 2H, **17**), 4.19 (d, *J* = 4.9 Hz, 2H, **15**), 3.04-3.01 (m, 2H, **9**), 2.86-2.83 (m, 2H, **6**), 1.92-1.88 (m, 4H, **7** & **8**), 1.28 (t, *J* = 7.2 Hz, 3H, **18**).

^{13}C NMR (101 MHz, $CDCl_3$) δ (ppm) 171.58 (**16**), 159.22 (**10**), 149.42 (**4**), 145.91 (**11**), 130.66 (**13**), 129.65 (**1**), 129.26 (**12**), 121.81 (**2**), 120.82 (**3**), 117.77 (**5**), 62.01 (**17**), 50.34 (**15**), 34.11 (**9**), 24.63 (**6**), 22.95 (**8**), 22.76 (**7**), 14.26 (**18**).

LRMS (ESI$^+$) *m/z* 319.1 [M^{35}Cl+H]$^+$, 321.1 [M^{37}Cl+H]$^+$.

HRMS (ESI$^+$) *m/z* calcd for $C_{17}H_{20}{}^{35}ClN_2O_2$ [M+H]$^+$, 319.1208, found 319.1210 Da.

7-Chloro-9-(phenylethynyl)-1,2,3,4-tetrahydroacridine (**2.43**)

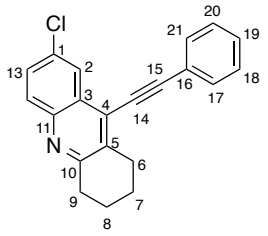

$C_{21}H_{16}ClN$

MW: 317.82 g.mol^{-1}

To a mixture of **2.22.3** (0.100 g, 0.273 mmol, 1.0 equiv), $Pd[PPh_3]_4$ (0.031 g, 0.027 mmol, 0.1 equiv) and CuI (0.010 g, 0.055 mmol, 0.2 equiv), was added Et_3N (1.4 mL) and phenylacetylene (36 μL, 0.328 mmol, 1.2 equiv). The reaction mixture stirred for 12 h at 85 °C. After completion, the reaction mixture was cooled to rt. A saturated aqueous solution of K_2CO_3 (5.0 mL) was added and the mixture was extracted with CH_2Cl_2 (3 x 5 mL), dried over anhydrous Na_2SO_4, filtered and concentrated under reduced pressure. The crude was purified by column chromatography (silica gel, petroleum ether/EtOAc 9:1) to afford **2.43** as a brown solid (0.085 mg, 0.268 mmol, 98%).

TLC Rf 0.27 (petroleum ether/EtOAc 9:1).

IR (neat) ν_{max} 3058 (w), 2934 (m), 2862 (m), 2204 (s), 1598 (m), 1566 (s), 1477 (s), 1358 (m), 1204 (w), 1078 (m) cm^{-1}.

^{1}H NMR (400 MHz, $CDCl_3$) δ (ppm) 8.21 (d, *J* = 2.3 Hz, 1H, **2**), 7.90 (d, *J* = 8.9 Hz, 1H, **12**), 7.68-7.65 (m, 2H, **17** & **21**), 7.56 (dd, *J* = 8.9, 2.3 Hz, 1H, **13**), 7.44-7.41 (m, 3H, **18**, **19** & **20**), 3.16 (t, *J* = 6.2 Hz, 2H, **9**), 3.11 (t, *J* = 6.2 Hz, 2H, **6**), 2.01-1.91 (m, 4H, **7** & **8**).

^{13}C NMR (101 MHz, $CDCl_3$) δ (ppm) 159.29 (**10**), 144.50 (**11**), 133.82 (**4**), 132.10 (**1**), 131.98 (2C, **18** & **20**), 130.46 (**13**), 129.84 (**12**), 129.47 (**19**), 128.71 (2C, **17** & **21**), 127.39 (**5**), 127.29 (**3**), 124.46 (**2**), 122.46 (**16**), 103.99 (**15**), 83.58 (**14**), 34.08 (**9**), 28.64 (**6**), 22.94 (**8**), 22.75 (**7**).

LRMS (ESI$^+$) *m/z* 318.1 [M^{35}Cl+H]$^+$, 320.1 [M^{37}Cl+H]$^+$.

HRMS (ESI$^+$) *m/z* calcd for $C_{21}H_{17}{}^{35}ClN$ [M+H]$^+$, 318.1044, found 318.1043 Da.

7-Chloro-9-phenyl-1,2,3,4-tetrahydroacridine (**2.44a**) and 7,9-diphenyl-1,2,3,4-tetrahydroacridine (**2.44b**)

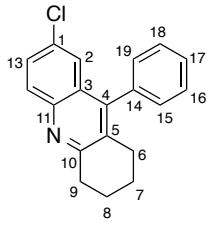

$C_{19}H_{16}ClN$

MW: 293.79 g.mol^{-1}

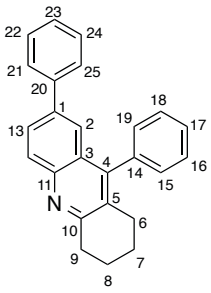

$C_{25}H_{21}N$

MW: 335.45 g.mol^{-1}

To a mixture of **2.22.3** (0.100 g, 0.273 mmol, 1.0 equiv), phenylboronic acid (0.040 g, 0.328 mmol, 1.2 equiv), $Pd[PPh_3]_4$ (0.009 g, 0.008 mmol, 0.1 equiv) and K_2CO_3 (0.075 g, 0.546 mmol, 2.0 equiv), was added THF/H_2O (v/v, 1:1, 1.2 mL). The reaction mixture stirred for 12 h at 85 °C. After completion, the reaction mixture was cooled to rt. A saturated aqueous solution of K_2CO_3 (5 mL) was added and the mixture was extracted with CH_2Cl_2 (3 x 5 mL), dried over anhydrous Na_2SO_4, filtered and concentrated under reduced pressure. The resulting dark orange oil was purified by column chromatography (silica gel, petroleum ether/EtOAc 9:1) to afford **2.44a** as white solid (0.056 mg, 0.194 mmol, 71%) and **2.44b** as brown oil (0.026 g, 0.076 mmol, 28%).

- 7-Chloro-9-phenyl-1,2,3,4-tetrahydroacridine (**2.44a**):

TLC Rf 0.31 (petroleum ether/EtOAc 9:1).

IR (neat) ν_{max} 3058 (w), 2935 (m), 2861 (m), 1605 (m), 1571 (m), 1479 (s), 1442 (w), 1353 (m), 1165 (m), 1075 (m) cm^{-1}.

^{1}H NMR (400 MHz, $CDCl_3$) δ (ppm) 7.94 (d, *J* = 9.0 Hz, 1H, **12**), 7.56-7.45 (m, 4H, **15**, **16**, **18** & **19**), 7.28 (d, *J* =2.3 Hz, 1H, **2**), 7.23-7.19 (m, 2H, **13**, **17**), 3.17 (t, *J* = 6.6 Hz, 2H, **9**), 2.59 (t, *J* = 6.6 Hz, 2H, **6**), 1.99-1.91 (m, 2H, **8**), 1.81-1.72 (m, 2H, **7**).

^{13}C NMR (101 MHz, $CDCl_3$) δ (ppm) 159.64 (**10**), 145.90 (**11**), 144.81 (**4**), 136.52 (**14**), 131.30 (**5**), 130.18 (**13**), 129.60 (**1**), 129.39 (**17**), 129.15 (2C, **16** & **18**), 128.96 (2C, **15** & **19**), 128.20 (**12**), 127.54 (**3**), 124.69 (**2**), 34.33 (**9**), 28.24 (**6**), 23.03 (**7**), 22.93 (**8**).

LRMS (ESI$^+$) *m/z* 294.1 [M^{35}Cl+H]$^+$, 296.1 [M^{37}Cl+H]$^+$.

HRMS (ESI$^+$) *m/z* calcd for $C_{19}H_{17}{}^{35}ClN$ [M+H]$^+$, 294.1044, found 294.1038 Da.

- 7,9-diphenyl-1,2,3,4-tetrahydroacridine (**2.44b**):

TLC Rf 0.22 (petroleum ether/EtOAc 9:1).

IR (neat) ν_{max} 3057 (m), 2934 (m), 2860 (m), 1601 (w), 1570 (m), 1483 (s), 1452 (m), 1357 (m), 1165 (w), 1074 (w) cm^{-1}.

^{1}H NMR (400 MHz, $CDCl_3$) δ (ppm) 8.02 (d, *J* = 8.8 Hz, 1H, **12**), 7.79 (dd, *J* =2.2, 8.8 Hz, 1H, **13**), 7.47-7.37 (m, 6H, **15**, **19**, **21**, **22**, **24** & **25**), 7.33-7.12 (m, 5H, **2**, **16**, **17**, **18** & **23**), 3.14 (t, *J* = 6.6 Hz, 2H, **9**), 2.53 (t, *J* = 6.5 Hz, 2H, **6**), 1.93-1.87 (m, 2H, **7**), 1.75-1.69 (m, 2H, **8**).

^{13}C NMR (101 MHz, $CDCl_3$) δ (ppm) 159.24 (**10**), 146.95 (**11**), 145.77 (**4**), 140.99 (**14**), 138.23 (**20**), 137.12 (**1**), 129.25 (2C, **16** & **18**), 128.97 (**5**), 128.89 (3C, **13**, **15** & **19**), 128.83 (2C, **22** & **24**), 128.28 (**17**), 127.97 (**23**), 127.49 (2C, **21** & **25**), 127.43 (**12**), 126.95 (**3**), 123.73 (**2**), 34.32 (**9**), 28.25 (**6**), 23.16 (**7**), 23.03 (**8**).

LRMS (ESI^+) *m/z* 336.1 $[M+H]^+$.

HRMS (ESI^+) *m/z* calcd for $C_{25}H_{22}N$ $[M+H]^+$, 336.1772, found 336.1771 Da.

7-Chloro-1,2,3,4-tetrahydroacridin-9-carbonitrile (**2.45a**) and 5,6,7,8-tetrahydroacridin-2,9-dicarbonitrile (**2.45b**)

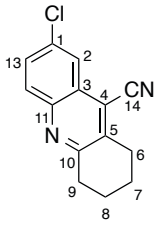

$C_{14}H_{11}ClN_2$

MW: 242.71 g.mol^{-1}

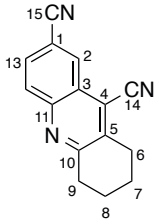

$C_{15}H_{11}N$

MW: 233.27 g.mol^{-1}

A microwave tube containing a magnetic stirrer bar was charged with **2.22.3** (0.050 g, 0.137 mmol, 1.0 equiv), $Pd[PPh_3]_4$ (0.016 g, 0.014 mmol, 0.1 equiv), zinc cyanide (0.023 g, 0.192 mmol, 1.4 equiv) and degased DMF (650 µL). The vessel was sealed with a septum and purged with Ar. The reaction mixture was stirred and heated for 15 min at 160 °C using a microwave apparatus. After cooling, the reaction mixture was poured onto water (10 mL), extracted with CH_2Cl_2 (3 x 10 mL), dried over anhydrous Na_2SO_4, filtered and concentrated under reduced pressure. The residue was purified by column chromatography (silica gel, petroleum ether/EtOAc 95:5) to afford **2.45a** as white solid (0.025 mg, 0.103 mmol, 75%) and **2.45b** as an off-white solid (0.008 g, 0.034 mmol, 25%).

- 7-Chloro-1,2,3,4-tetrahydroacridin-9-carbonitrile (**2.45a**):

TLC Rf 0.58 (petroleum ether/EtOAc 7:3).

IR (neat) ν_{max} 2960 (s), 2867 (m), 1578 (m), 1479 (s), 1423 (m), 1344 (m), 1211 (m), 1149 (m), 1078 (m) cm^{-1}.

^{1}H NMR (400 MHz, $CDCl_3$) δ (ppm) 8.05 (d, *J* = 2.4 Hz, 1H, **2**), 7.97 (d, *J* = 9.0 Hz, 1H, **12**), 7.66 (dd, *J* = 2.2, 9.0 Hz, 1H, **13**), 3.20 (t, *J* = 6.3 Hz, 2H, **9**), 3.14 (t, *J* = 6.4 Hz, 2H, **6**), 2.05-1.95 (m, 4H, **7** & **8**).

^{13}C NMR (101 MHz, $CDCl_3$) δ (ppm) 159.72 (**10**), 144.57 (**11**), 136.86 (**5**), 134.36 (**1**), 131.21 (**13**), 130.92 (**12**), 125.80 (**3**), 123.37 (**2**), 116.73 (**14**), 114.55 (**4**), 33.74 (**9**), 28.81 (**6**), 22.61 (**8**), 22.16 (**7**).

LRMS (ESI$^+$) *m/z* 243.0 $[M^{35}Cl+H]^+$, 245.0 $[M^{37}Cl+H]^+$.

HRMS (ESI$^+$) *m/z* calcd for $C_{14}H_{12}{}^{35}ClN_2$ $[M+H]^+$, 243.0683, found 243.0679 Da.

- 5,6,7,8-Tetrahydroacridin-2,9-dicarbonitrile (**2.45b**):

TLC Rf 0.35 (petroleum ether/EtOAc 7:3).

IR (neat) ν_{max} 2949 (s), 2872 (s), 2227 (s), 1578 (s), 1489 (s), 1419 (m), 1397 (s), 1344 (m), 1220 (s) cm^{-1}.

^{1}H NMR (400 MHz, $CDCl_3$) δ (ppm) 8.46 (d, *J* = 1.9 Hz, 1H, **2**), 8.13 (d, *J* = 8.8 Hz, 1H, **12**), 7.88 (dd, *J* = 8.8, 1.9 Hz, 1H, **13**), 3.25 (t, *J* = 6.1 Hz, 2H, **9**), 3.20 (t, *J* = 6.4 Hz, 2H, **6**), 2.08-1.98 (m, 4H, **7** & **8**).

^{13}C NMR (101 MHz, $CDCl_3$) δ (ppm) 163.22 (**10**), 146.90 (**11**), 138.10 (**5**), 131.01 (**13**), 130.87 (**12**), 130.52 (**2**), 124.52 (**3**), 118.14 (**15**), 117.93 (**4**), 113.98 (**14**), 111.89 (**1**), 34.09 (**9**), 28.91 (**6**), 22.41 (**8**), 22.00 (**7**).

LRMS (ESI$^+$) *m/z* 234.1 $[M+H]^+$.

HRMS (ESI$^+$) *m/z* calcd for $C_{15}H_{11}N_3$ $[M+H]^+$, 234.1026, found 234.1026 Da.

7-Chloro-9-(phenylthio)-1,2,3,4-tetrahydroacridine (**2.46**)

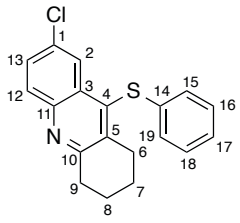

$C_{19}H_{16}ClNS$

MW: 325.85 g.mol^{-1}

Thioether **2.46** was obtained according to general procedure C using **2.22.3** (0.050 g, 0.137 mmol, 1.0 equiv), $Pd_2(dba)_3$ (0.008 g, 0.008 mmol, 0.06 equiv), (±)-BINAP (0.011 g, 0.016 mmol, 0.12 equiv), Cs_2CO_3 (0.112 g, 0.343 mmol, 2.5 equiv), 1,4-dioxane (1.7 mL) and thiophenol (21 μL, 0.206 mmol, 1.5 equiv). The crude material was purified by column chromatography (silica gel, petroleum ether/EtOAc 9:1) to afford **2.46** as bright yellow oil (0.037 g, 0.114 mmol, 83%).

TLC Rf 0.23 (petroleum ether/EtOAc 9:1).

IR (neat) ν_{max} 3060 (w), 2939 (s), 2861 (s), 1604 (m), 1581 (m), 1561 (m), 1472 (s), 1439 (m), 1336 (w), 1304 (m), 1204 (m), 1077 (s) cm^{-1}.

^{1}H NMR (400 MHz, $CDCl_3$) δ (ppm) 8.42 (d, *J* = 2.3 Hz, 1H, **2**), 7.95 (d, *J* = 8.9 Hz, 1H, **12**), 7.58 (dd, *J* = 8.9, 2.3 Hz, 1H, **13**), 7.21-7.16 (m, 3H, **15**, **17** & **19**), 6.99-6.97 (m, 2H, **16** & **18**), 3.15 (t, *J* = 6.5 Hz, 2H, **9**), 3.02 (t, *J* = 6.5 Hz, 2H, **6**), 1.96-1.81 (m, 4H, **7** & **8**).

^{13}C NMR (101 MHz, $CDCl_3$) δ (ppm) 160.08 (**10**), 145.25 (**11**), 138.06 (**4**), 137.41 (**14**), 135.62 (**1**), 132.72 (**3**), 130.65 (**13**), 130.06 (**5** & **17**), 129.42 (2C, **15** & **19**), 127.45 (2C, **16** & **18**), 126.11 (**12**), 124.92 (**2**), 34.40 (**9**), 29.02 (**6**), 22.93 (**8**), 22.72 (**7**).

LRMS (ESI$^+$) *m/z* 326.0 [M^{35}Cl+H]$^+$, 328.0 [M^{37}Cl+H]$^+$.

HRMS (ESI$^+$) *m/z* calcd for $C_{19}H_{17}{}^{35}ClNS$ [M+H]$^+$, 326.0765, found 326.0770 Da.

9-(Benzyloxy)-7-chloro-1,2,3,4-tetrahydroacridine (**2.47**)

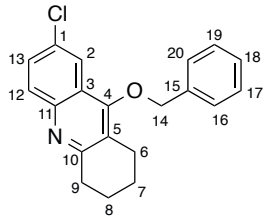

$C_{20}H_{18}ClNO$

MW: 323.82 g.mol^{-1}

Ether **2.47** was obtained according to general procedure C using **2.22.3** (0.050 g, 0.137 mmol, 1.0 equiv), $Pd_2(dba)_3$ (0.008 g, 0.008 mmol, 0.06 equiv), (±)-BINAP (0.011 g, 0.016 mmol, 0.12 equiv), Cs_2CO_3 (0.112 g, 0.343 mmol, 2.5 equiv), 1,4-dioxane (1.7 mL) and benzyl alcohol (21 μL, 0.206 mmol, 1.5 equiv). The crude material was purified by column chromatography (silica gel, petroleum ether/EtOAc 9:1) to afford **2.47** as pale white wax (0.027 g, 0.082 mmol, 60%) with traces of benzyl alcohol in 1:1 ratio.

TLC Rf 0.20 (petroleum ether/EtOAc 9:1).

IR (neat) ν_{max} 3260 (w), 3032 (w), 2929 (s), 2861 (s), 1588 (s), 1556 (m), 1481 (s), 1454 (s), 1344 (s), 1330 (s), 1211 (w), 1095 (s), 1062 (m) cm^{-1}.

^{1}H NMR (400 MHz, $CDCl_3$) δ (ppm) 7.94 (d, *J* = 2.3 Hz, 1H, **2**), 7.91 (d, *J* = 9.2 Hz, 1H, **12**), 7.55-7.27 (m, 6H, **13**, **16**, **17**, **18**, **19** & **20**), 5.06 (s, 2H, **14**), 3.10 (t, *J* = 6.6 Hz, 2H, **9**), 2.91 (t, *J* = 6.7 Hz, 2H, **6**), 1.98-1.92 (m, 2H, **7**), 1.86-1.80 (m, 2H, **8**).

^{13}C NMR (101 MHz, $CDCl_3$) δ (ppm) 161.47 (**10**), 158.86 (**4**), 146.42 (**11**), 136.54 (**15**), 131.36 (**1**), 130.28 (**13**), 129.93 (**12**), 128.86 (2C, **16** & **20**), 128.72 (**18**), 128.68 (2C, **17** & **19**), 123.96 (**5**), 123.42 (**3**), 120.90 (**2**), 75.81 (**14**), 33.82 (**9**), 23.88 (**6**), 22.95 (**8**), 22.42 (**7**).

LRMS (ESI$^+$) *m/z* 324.1 [M^{35}Cl+H]$^+$, 326.1 [M^{37}Cl+H]$^+$.

HRMS (ESI$^+$) *m/z* calcd for $C_{20}H_{19}{}^{35}ClNO$ [M+H]$^+$, 324.1150, found 324.1154 Da.

Methyl 3-(benzyloxy)-6-(4-((7-chloro-1,2,3,4-tetrahydroacridin-9-yl)amino)but-1-yn-1-yl)picolinate (**2.49**)

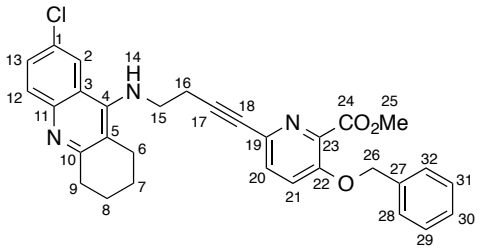

$C_{31}H_{28}ClN_3O_3$

MW: 526.03 g.mol^{-1}

To a degassed solution of methyl 3-benzyloxy-6-bromopicolinate (0.348 g, 1.081 mmol, 1.1 equiv) in THF/Et_3N (7 mL/ 5 mL), $Pd[PPh_3]_4$ (0.114 g, 0.098 mmol, 0.1 equiv) and CuI (0.037 g, 0.197 mmol, 0.2 equiv) were added. After bubbling the reaction mixture with Ar for 5 min at rt, a degassed solution (also bubbled with Ar) of terminal alkyne **2.9** obtained by procedure C (0.280 g, 0.983 mmol, 1.0 equiv) in THF (3 mL) was added dropwise and the reaction mixture was stirred for 16 h at rt. After completion, the reaction mixture was concentrated under reduced pressure and the residue was purified by column chromatography (silica gel, EtOAc) to afford the desired acetylene **2.49** as yellow wax (0.425 g, 0.806 mmol, 82%).

TLC Rf 0.23 (EtOAc).

IR (neat) ν_{max} 3368 (w), 3062 (w), 2932 (m), 2862 (m), 2171 (w), 1733 (s), 1580 (m), 1557 (m), 1486 (m), 1450 (s), 1435 (s), 1382 (w), 1349 (w), 1290 (m), 1271 (s), 1209 (s), 1098 (s) cm^{-1}.

^{1}H NMR (400 MHz, $CDCl_3$) δ (ppm) 7.96 (d, *J* = 2.2 Hz, 1H, **2**), 7.84 (d, *J* = 8.9 Hz, 1H, **12**), 7.48 (dd, *J* = 8.9, 2.2 Hz, 1H, **13**), 7.45-7.27 (m, 7H, **20**, **21**, **28**, **29**, **30**, **31** & **32**), 5.22 (s, 2H, **26**), 4.28 (br s, 1H, **14**), 3.97 (s, 3H, **25**), 3.68 (q, *J* = 6.2 Hz, 2H, **15**), 3.03 (t, *J* = 5.9 Hz, 2H, **9**), 2.82 (t, *J* = 5.8 Hz, 2H, **6**), 2.68 (t, *J* = 6.2 Hz, 2H, **16**), 1.93-1.82 (m, 4H, **7** & **8**).

^{13}C NMR (101 MHz, $CDCl_3$) δ (ppm) 164.86 (**24**), 159.25 (**10**), 153.33 (**22**), 149.31 (**4**), 145.80 (**11**), 140.43 (**23**), 135.51 (**19**), 134.65 (**27**), 130.57 (**13**), 130.10 (**20**), 129.81 (**1**), 129.31 (**12**), 128.89 (**29** & **31**), 128.42 (**30**), 127.04 (**28** & **32**), 121.88 (**2**), 121.86 (**21**), 121.62 (**3**), 118.84 (**5**), 86.68 (**17**), 81.80 (**18**), 70.98 (**26**), 52.87 (**25**), 47.36 (**15**), 34.15 (**9**), 25.03 (**6**), 22.96 (**7**), 22.73 (**8**), 22.01 (**16**).

LRMS (ESI$^+$) *m/z* 526.2 [M^{35}Cl+H]$^+$, 528.2 [M^{37}Cl+H]$^+$.

HRMS (ESI$^+$) *m/z* calcd for $C_{31}H_{28}{}^{35}ClN_3O_3$ [M+H]$^+$, 526.1897, found 526.1895 Da.

Methyl 6-(4-((7-chloro-1,2,3,4-tetrahydroacridin-9-yl)amino)butyl)-3-hydroxypicolinate (**2.50**)

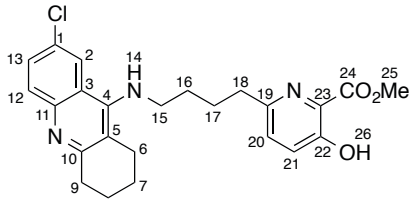

$C_{24}H_{26}ClN_3O_3$

MW: 439.94 g.mol^{-1}

2.50 was obtained according to general procedures D using **2.49** (0.097 g, 0.184 mmol, 1.0 equiv), $Pd(OH)_2/C$ (20% wt. with 50% moisture, 0.050 g, 0.037 mmol, 0.2 equiv) and EtOAc (2.6 mL). The crude product was purified by column chromatography (silica gel, CH_2Cl_2/MeOH 9:1) to afford **2.50** as pale yellow wax (0.065 g, 0.147 mmol, 80%).

TLC Rf 0.40 (CH_2Cl_2/MeOH 9:1).

IR (neat) ν_{max} 3390 (w), 2926 (s), 2855 (m), 1674 (s), 1579 (s), 1467 (s), 1445 (s), 1354 (w), 1296 (m), 1212 (s), 1101 (m) cm^{-1}.

^{1}H NMR (400 MHz, $CDCl_3$) δ (ppm) 10.60 (br s, 1H, **26**), 7.92 (d, *J* = 2.2 Hz, 1H, **2**), 7.86 (d, *J* = 9.0 Hz, 1H, **12**), 7.48 (dd, *J* = 2.2, 9.0 Hz, 1H, **13**), 7.30 (d, *J* = 8.8, 1H, **21**), 7.25 (d, *J* = 8.8, 1H, **20**), 4.02 (s, 3H, **25**), 3.50 (t, *J* = 7.0 Hz, 2H, **15**), 3.04 (m, 2H, **9**), 2.83 (t, *J* = 7.5 Hz, 2H, **18**), 2.66 (m, 2H, **6**), 2.16 (s, 1H, **14**), 1.92-1.87 (m, 4H, **7** & **8**), 1.86-1.79 (m, 2H, **17**), 1.78-1.68 (m, 2H, **16**).

^{13}C NMR (101 MHz, $CDCl_3$) δ (ppm) 170.17 (**24**), 158.54 (**10**), 157.43 (**19**), 153.28 (**22**), 150.26 (**4**), 145.11 (**11**), 130.17 (**23**), 129.41 (**12**), 129.28 (**20**), 129.04 (**13**), 128.81 (**1**), 126.93 (**21**), 122.15 (**2**), 120.84 (**3**), 116.75 (**5**), 53.31 (**25**), 49.30 (**15**), 37.16 (**18**), 33.82 (**9**), 31.29 (**16**), 27.25 (**17**), 24.87 (**6**), 22.99 (**7**), 22.68 (**8**).

LRMS (ESI$^+$) *m/z* 440.2 [M^{35}Cl+H]$^+$, 442.2 [M^{37}Cl+H]$^+$.

HRMS (ESI$^+$) *m/z* calcd for $C_{24}H_{26}{}^{35}ClN_3O_3$ [M+H]$^+$, 440.1740, found 440.1736 Da.

tert-Butyl prop-2-yn-1-ylcarbamate (**2.53.1**)

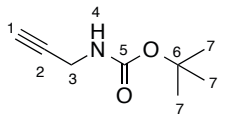

$C_8H_{13}NO_2$

MW: 155.20 $g.mol^{-1}$

To a solution of propargylamine (0.250 g, 4.539 mmol, 1.0 equiv) in CH_2Cl_2 (9mL), was added di-*tert*-butyl dicarbonate (1.04 mL, 4.539 mmol, 1.0 equiv) at 0 °C. The reaction mixture was stirred for 1 h at 0 °C. Upon completion, the solvent was removed under reduced pressure to afford **2.53.1** as colourless oil (0.669 g, 4.312 mmol, 95%). Spectroscopic data were consistent with those reported in literature.[328]

TLC Rf 0.38 (petroleum ether/EtOAc 9:1).

^{1}H NMR (400 MHz, $CDCl_3$) δ (ppm) 4.69 (br s, 1H, **4**), 3.92 (s, 2H, **3**), 2.21 (t, J = 2.5 Hz, 1H, **1**), 1.45 (s, 9H, **7**).

^{13}C NMR (101 MHz, $CDCl_3$) δ (ppm) 155.38 (**5**), 84.78 (**6**), 80.22 (**2**), 71.38 (**1**), 30.56 (**3**), 28.49 (3C, **7**).

LRMS (ESI^+) m/z 156.0 $[M+H]^+$.

tert-Butyl but-3-yn-1-ylcarbamate (**2.53.2**)

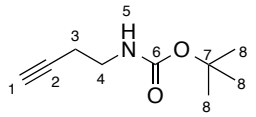

$C_9H_{15}NO_2$

MW: 169.22 g.mol^{-1}

To a solution of 1-amino-3-butyne (0.250 g, 3.617 mmol, 1.0 equiv) in CH_2Cl_2 (7 mL), was added di-*tert*-butyl dicarbonate (831 μL, 3.617 mmol, 1.0 equiv) at 0 °C. The reaction mixture was stirred for 1 h at 0 °C. Upon completion, the solvent was removed under reduced pressure to afford **2.53.2** as colourless oil (0.539 g, 3.472 mmol, 96%). Spectroscopic data were consistent with those reported in literature.[328]

TLC Rf 0.42 (petroleum ether/EtOAc 9:1).

IR (neat) ν_{max} 3304 (s), 2979 (m), 2934 (w), 2396 (w), 2150 (w), 1775 (w), 1697 (s), 1518 (s), 1393 (m), 1367 (m), 1251 (s), 1172 (w), 1074 (w) cm^{-1}.

^{1}H NMR (400 MHz, $CDCl_3$) δ (ppm) 4.84 (br s, 1H, **5**), 3.28 (dd, *J* = 11.6, 5.8 Hz, 2H, **3**), 2.38 (t, *J* = 6.2 Hz, 2H, **4**), 1.99 (s, 1H, **1**), 1.45 (s, 9H, **8**).

^{13}C NMR (101 MHz, $CDCl_3$) δ (ppm) 155.85 (**6**), 81.81 (**7**), 79.65 (**2**), 69.97 (**1**), 39.41 (**4**), 28.54 (3C, **7**), 20.14 (**3**).

LRMS (ESI$^+$) *m/z* 192.0 $[M+Na]^+$.

HRMS (ESI$^+$) *m/z* calcd for $C_9H_{15}NNaO_2$ $[M+Na]^+$, 192.0993, found 192.0995 Da.

tert-Butyl pent-4-yn-1-ylcarbamate (**2.53.3**)

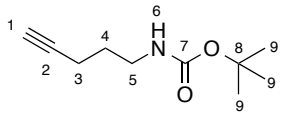

$C_{10}H_{17}NO_2$

MW: 183.25 g.mol^{-1}

To a solution of 1-amino-3-butyne (0.250 g, 3.007 mmol, 1.0 equiv) in CH_2Cl_2 (6 mL), was added di-*tert*-butyl dicarbonate (650 µL, 3.007 mmol, 1.0 equiv) at 0 °C. The reaction mixture was stirred for 1 h at 0 °C. Upon completion, the solvent was removed under reduced pressure to afford **2.53.3** as colourless oil (0.534 g, 2.917 mmol, 97%). Spectroscopic data were consistent with those reported in literature.[328]

TLC Rf 0.46 (petroleum ether/EtOAc 9:1).

IR (neat) ν_{max} 3303 (s), 2977 (m), 2933 (w), 2401 (w), 2150 (w), 1697 (s), 1518 (s), 1394 (m), 1366 (m), 1252 (s), 1171 (s) cm^{-1}.

^{1}H NMR (400 MHz, $CDCl_3$) δ (ppm) 4.64 (br s, 1H, **6**), 3.23 (q, *J* = 6.8 Hz, 2H, **5**), 2.24 (td, *J* = 6.8, 2.5 Hz, 2H, **3**), 1.96 (t, *J* = 2.5 Hz, 1H, **1**), 1.71 (quin, *J* = 6.8 Hz, 2H, **4**), 1.44 (s, 9H, **9**).

^{13}C NMR (101 MHz, $CDCl_3$) δ (ppm) 156.08 (**7**), 85.33 (**2**), 83.60 (**8**), 69.10 (**1**), 39.73 (**5**), 28.79 (**4**), 28.56 (3C, **9**), 16.03 (**3**).

LRMS (ESI$^+$) *m/z* 206.1 [M+Na]$^+$.

HRMS (ESI$^+$) *m/z* calcd for $C_{10}H_{17}NNaO_2$ [M+Na]$^+$, 206.1151, found 206.1153 Da.

Methyl 3-(benzyloxy)-6-(3-((*tert*-butoxycarbonyl)amino)prop-1-yn-1-yl)picolinate (**2.52.1**)

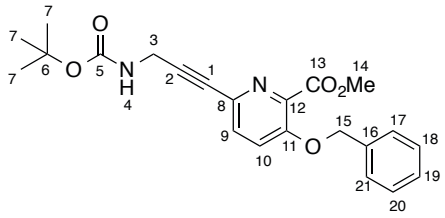

$C_{22}H_{24}N_2O_5$

MW: 396.44 g.mol^{-1}

Following the procedure described for the Sonogashira coupling to form compound **2.49**, acetylene **2.52.1** was obtained using terminal alkyne **2.53.1** (0.050 g, 0.322 mmol, 1.0 equiv), methyl 3-benzyloxy-6-bromopicolinate (0.114 g, 0.354 mmol, 1.1 equiv), $Pd[PPh_3]_4$ (0.036 g, 0.032 mmol, 0.1 equiv), CuI (0.012 g, 0.064 mmol, 0.2 equiv), THF (4 mL) and Et_3N (2 mL). The crude material was purified by column chromatography (silica gel, petroleum ether/EtOAc 7:3) to afford **2.52.1** as colourless oil (0.111 g, 0.279 mmol, 84%).

TLC Rf 0.23 (petroleum ether/EtOAc 7:3).

IR (neat) ν_{max} 3350 (s), 2976 (m), 2929 (m), 2150 (w), 1705 (s), 1566 (w), 1498 (s), 1450 (s), 1435 (s), 1365 (m), 1267 (s), 1209 (s), 1163 (s), 1097 (s) cm^{-1}.

^{1}H NMR (400 MHz, $CDCl_3$) δ (ppm) 7.44-7.27 (m, 7H, **9**, **10**, **17**, **18**, **19**, **20** & **21**), 5.20 (s, 2H, **15**), 4.88 (br s, 1H, **4**), 4.14 (d, *J* = 4.4 Hz, 2H, **3**), 3.96 (s, 3H, **14**), 1.46 (s, 9H, **7**).

^{13}C NMR (101 MHz, $CDCl_3$) δ (ppm) 164.71 (**13**), 155.31 (**5**), 153.42 (**11**), 140.25 (**8**), 135.43 (**12**), 134.34 (**16**), 130.25 (**9**), 128.80 (2C, **18** & **20**), 128.33 (**19**), 126.95 (2C, **17** & **21**), 121.74 (**10**), 85.33 (**2**), 81.48 (**1**), 80.09 (**6**), 70.88 (**15**), 52.78 (**14**), 31.07 (**3**), 28.41 (3C, **7**).

LRMS (ESI$^+$) *m/z* 397.1 $[M+H]^+$.

HRMS (ESI$^+$) *m/z* calcd for $C_{22}H_{25}N_2O_5$ $[M+H]^+$, 397.1758, found 397.1765 Da. (ESI$^+$) *m/z* calcd for $C_{22}H_{24}N_2NaO_5$ $[M+Na]^+$, 419.1577, found 419.1586 Da.

Methyl 3-(benzyloxy)-6-(4-((*tert*-butoxycarbonyl)amino)but-1-yn-1-yl)picolinate (**2.52.2**)

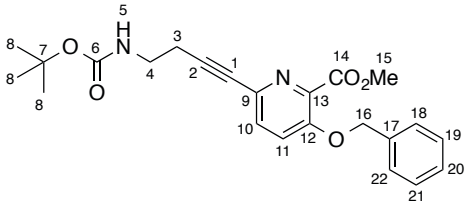

$C_{23}H_{26}N_2O_5$

MW: 410.47 g.mol^{-1}

Following the procedure described for the Sonogashira coupling to form compound **2.49**, acetylene **2.52.2** was obtained using terminal alkyne **2.53.2** (0.058 g, 0.342 mmol, 1.0 equiv), methyl 3-benzyloxy-6-bromopicolinate (0.121 g, 0.377 mmol, 1.1 equiv), Pd[PPh_3]$_4$ (0.039 g, 0.034 mmol, 0.1 equiv), CuI (0.013 g, 0.068 mmol, 0.2 equiv), THF (4 mL) and Et_3N (2 mL). The crude material was purified by column chromatography (silica gel, petroleum ether/EtOAc 65:25) to afford **2.52.2** as colourless oil (0.128 g, 0.311 mmol, 91%).

TLC Rf 0.27 (petroleum ether/EtOAc 3:2).

IR (neat) ν_{max} 3360 (m), 2978 (m), 2233 (m), 1703 (s), 1500 (m), 1450 (s), 1390 (m), 1365 (m), 1267 (s), 1207 (s), 1165 (s), 1097 (s) cm^{-1}.

^{1}H NMR (400 MHz, $CDCl_3$) δ (ppm) 7.44-7.28 (m, 7H, **10**, **11**, **18**, **19**, **20**, **21** & **22**), 5.20 (s, 2H, **16**), 4.88 (br s, 1H, **5**), 3.96 (s, 3H, **15**), 3.36 (q, *J* = 6.4 Hz, 2H, **4**), 2.60 (t, *J* = 6.5 Hz, 2H, **3**), 1.45 (s, 9H, **8**).

^{13}C NMR (101 MHz, $CDCl_3$) δ (ppm) 164.77 (**14**), 155.75 (**6**), 153.09 (**12**), 140.08 (**9**), 135.47 (**13**), 135.01 (**17**), 130.20 (**10**), 128.74 (2C, **19** & **21**), 128.25 (**20**), 126.92 (2C, **18** & **22**), 121.80 (**11**), 87.41 (**2**), 80.47 (**1**), 79.44 (**7**), 70.83 (**16**), 52.71 (**15**), 39.18 (**4**), 28.40 (3C, **8**), 20.97 (**3**).

LRMS (ESI$^+$) *m/z* 411.1 [M+H]$^+$.

HRMS (ESI$^+$) *m/z* calcd for $C_{23}H_{27}N_2O_5$ [M+H]$^+$, 411.1915, found 411.1922 Da. (ESI$^+$) *m/z* calcd for $C_{22}H_{26}N_2NaO_5$ [M+Na]$^+$, 433.1734, found 433.1743 Da.

Methyl 3-(benzyloxy)-6-(5-((*tert*-butoxycarbonyl)amino)pent-1-yn-1-yl)picolinate (**2.52.3**)

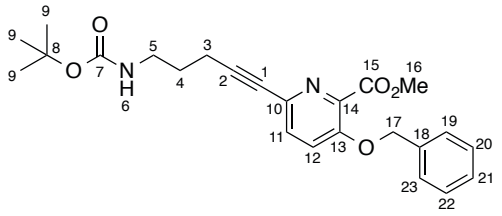

$C_{24}H_{28}N_2O_5$

MW: 424.50 g.mol^{-1}

Following the procedure described for the Sonogashira coupling to form compound **2.49**, acetylene **2.52.3** was obtained using terminal alkyne **2.53.3** (0.062 g, 0.338 mmol, 1.0 equiv), methyl 3-benzyloxy-6-bromopicolinate (0.120 g, 0.372 mmol, 1.1 equiv), Pd[PPh_3]$_4$ (0.039 g, 0.034 mmol, 0.1 equiv), CuI (0.013 g, 0.068 mmol, 0.2 equiv), THF (4 mL) and Et_3N (2 mL). The crude material was purified by column chromatography (silica gel, petroleum ether/EtOAc 65:25) to afford **2.52.3** as colourless oil (0.139 g, 0.328 mmol, 97%).

TLC Rf 0.27 (petroleum ether/EtOAc 3:2).

IR (neat) ν_{max} 3367 (w), 2976 (w), 2231 (w), 1693 (s), 1512 (m), 1450 (s), 1434 (s), 1390 (m), 1365 (m), 1265 (s), 1207 (s), 1164 (s), 1097 (s) cm^{-1}.

^{1}H NMR (400 MHz, $CDCl_3$) δ (ppm) 7.45-7.27 (m, 7H, **11**, **12**, **19**, **20**, **21**, **22** & **23**), 5.20 (s, 2H, **17**), 4.80 (br s, 1H, **6**), 3.96 (s, 3H, **16**), 3.26 (q, *J* = 6.2 Hz, 2H, **5**), 2.46 (t, *J* = 7.1 Hz, 2H, **3**), 1.80 (quin, *J* = 7.0 Hz, 2H, **4**), 1.45 (s, 9H, **9**).

^{13}C NMR (101 MHz, $CDCl_3$) δ (ppm) 164.83 (**15**), 156.01 (**7**), 152.98 (**13**), 140.06 (**10**), 135.53 (**14**), 135.29 (**18**), 130.05 (**11**), 128.74 (2C, **20** & **22**), 128.24 (**21**), 126.93 (2C, **19** & **23**), 121.82 (**12**), 89.26 (**2**), 79.87 (**1**), 79.20 (**8**), 70.84 (**17**), 52.68 (**16**), 39.78 (**5**), 28.43 (4C, **4** & **9**), 16.86 (**3**).

LRMS (ESI$^+$) *m/z* 425.2 [M+H]$^+$.

HRMS (ESI$^+$) *m/z* calcd for $C_{24}H_{29}N_2O_5$ [M+H]$^+$, 425.2071, found 425.2070 Da. (ESI$^+$) *m/z* calcd for $C_{24}H_{28}N_2NaO_5$ [M+Na]$^+$, 447.1890, found 447.1890 Da.

6-(4-((7-Chloro-1,2,3,4-tetrahydroacridin-9-yl)amino)butyl)-3-hydroxypicolinaldehyde oxime (**2.8**)

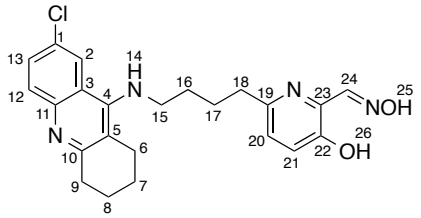

$C_{23}H_{25}ClN_4O_2$

MW: 424.93 g.mol^{-1}

Oxime **2.8** was obtained according to general procedures E, F and G using for procedure E, **2.50** (0.050 g, 0.113 mmol, 1.0 equiv), imidazole (0.031 g, 0.455 mmol, 4.0 equiv), TBSCl (0.038 g, 0.251 mmol, 2.2 equiv) in dry DMF (1.0 mL). The presence of the desired silylether was supported by TLC and LRMS (ESI$^+$, *m/z* 554.2 [M+H]$^+$). After drying *in vacuo*, the crude product was subjected to procedure F using DIBAL-H (226 µL of a 1.0 M solution in CH_2Cl_2, 0.226 mmol, 2.0 equiv) in CH_2Cl_2 (2.0 mL). After drying *in vacuo*, the crude material was deprotected using TBAF (226 µL of a 1.0 M solution in THF, 0.226 mmol, 1.1 equiv) in THF (2.0 mL). The presence of the desired aldehyde was supported by TLC and LRMS (ESI$^+$, *m/z* 410.0 [M+H]$^+$). After drying *in vacuo*, the crude product was subjected to procedure G hydroxylamine hydrochloride (0.005 g, 0.073 mmol, 1.5 equiv) and CH_3CO_2Na (0.006 g, 0.073 mmol, 1.5 equiv) in EtOH (1.0 mL). The residue was purified by column chromatography (silica gel, CH_2Cl_2/MeOH 9:1) to afford **2.8** as yellow solid (0.010 g, 0.024 mmol, 19% over 4 steps).

TLC Rf 0.23 (CH_2Cl_2/MeOH 9:1).

IR (neat) ν_{max} 3324 (s), 2928 (s), 2857 (m), 1635 (m), 1574 (s), 1520 (m), 1466 (s), 1361 (w), 1331 (w), 1273 (s), 1167 (w), 1028 (m) cm^{-1}.

^{1}H NMR (500 MHz, $CDCl_3$) δ (ppm) 10.16 (br s, 2H, **26** & **25**), 8.25 (s, 1H, **24**), 7.87-7.85 (m, 2H, **2** & **12**), 7.48 (dd, *J* = 9.0, 2.0 Hz, 1H, **13**), 7.06 (d, *J* = 8.52 Hz, 1H, **20**), 6.92 (d, *J* = 8.37 Hz, 1H, **21**), 4.08 (br s, 1H, **14**), 3.52 (t, *J* = 6.7 Hz, 2H, **15**), 3.06 (m, 2H, **9**), 2.75 (t, *J* = 7.1 Hz, 2H, **18**), 2.61 (m, 2H, **6**), 1.94-1.88 (m, 4H, **7** & **8**), 1.87-1.83 (m, 2H, **17**), 1.76-1.72 (m, 2H, **16**).

^{13}C NMR (126 MHz, $CDCl_3$) δ (ppm) 158.04 (**24**), 153.12 (**19**), 152.59 (**10**), 152.45 (**22**), 150.56 (**23**), 144.86 (**11**), 135.55 (**24**), 129.71 (**21**), 129.29 (**20**), 129.22 (**1**), 124.34 (**13**), 123.73 (**21**), 122.28 (**2**), 120.13 (**3**), 115.75 (**5**), 48.81 (**15**), 36.73 (**18**), 33.05 (**9**), 30.99 (**16**), 26.56 (**17**), 24.69 (**6**), 22.85 (**7**), 22.47 (**8**).

LRMS (ESI$^+$) *m/z* 425.2 [M^{35}Cl+H]$^+$, 427.2 [M^{37}Cl+H]$^+$.

HRMS (ESI$^+$) *m/z* calcd for $C_{23}H_{25}{}^{35}ClN_4O_2$ [M+H]$^+$, 425.1744, found 425.1746 Da.

7,9-Dichloro-2,3-dihydro-1*H*-cyclopenta[*b*]quinoline (**2.55**)

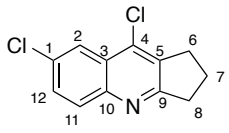

$C_{12}H_9Cl_2N$

MW: 238.11 g.mol^{-1}

2.55 was obtained according to general procedure A using 2-amino-5-chlorobenzoic acid **2.24** (5.000 g, 29.14 mmol, 1.0 equiv), cyclopentanone (2.84 mL, 32.05 mmol, 1.1 equiv) and $POCl_3$ (23.90 mL, 8.8 equiv). The crude product was purified by column chromatography (silica gel, petroleum ether/EtOAc 4:1) to afford **2.55** as an off-white powder (5.689 g, 23.89 mmol, 82%).

TLC Rf 0.26 (petroleum ether/EtOAc 4:1).

IR (neat) ν_{max} 2962 (m), 2887 (w), 1620 (m), 1603 (m), 1552 (m), 1483 (s), 1438 (m), 1424 (m), 1372 (s), 1327 (m), 1289 (m), 1235 (m), 1161 (w), 1076 (s) cm^{-1}.

^{1}H NMR (400 MHz, $CDCl_3$) δ (ppm) 8.13 (d, *J* = 2.3 Hz, 1H, **2**), 7.94 (d, *J* = 8.9 Hz, 1H, **11**), 7.60 (dd, *J* = 8.9, 2.3 Hz, 1H, **12**), 3.22 (t, *J* = 7.7 Hz, **8**), 3.17 (t, *J* = 7.5 Hz, **6**), 2.25 (quin, *J* = 7.6 Hz, 2H, **7**).

^{13}C NMR (101 MHz, $CDCl_3$) δ (ppm) 168.15 (**9**), 147.12 (**10**), 136.58 (**4**), 135.18 (**5**), 132.60 (**1**), 130.65 (**12**), 130.16 (**11**), 126.27 (**3**), 122.83 (**2**), 35.64 (**8**), 30.62 (**6**), 22.77 (**7**).

LRMS (ESI$^+$) *m/z* 238.0 [M^{35}Cl+H]$^+$, 240.0 [M^{37}Cl+H]$^+$.

HRMS (ESI$^+$) *m/z* calcd for $C_{12}H_9{}^{35}Cl_2N$ [M+H]$^+$, 238.0190, found 238.0196 Da.

2,11-Dichloro-7,8,9,10-tetrahydro-6*H*-cyclohepta[*b*]quinoline (**2.56**)

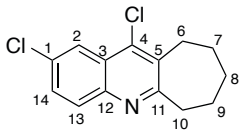

$C_{14}H_{13}Cl_2N$

MW: 266.17 g.mol^{-1}

2.56 was obtained according to general procedure A using 2-amino-5-chlorobenzoic acid **2.24** (5.000 g, 29.14 mmol, 1.0 equiv), cycloheptanone (2.78 mL, 32.05 mmol, 1.1 equiv) and $POCl_3$ (23.90 mL, 8.8 equiv). The crude product was purified by column chromatography (silica gel, petroleum ether/EtOAc 9:1) to afford **2.56** as an off-white powder (6.205 g, 21.23 mmol, 80%).

TLC Rf 0.31 (petroleum ether/EtOAc 9:1).

IR (neat) ν_{max} 2924 (s), 2853 (s), 1584 (s), 1551 (m), 1475 (s), 1455 (m), 1440 (m), 1335 (m), 1317 (m), 1255 (w), 1186 (m), 1080 (m) cm^{-1}.

^{1}H NMR (400 MHz, $CDCl_3$) δ (ppm) 8.13 (d, *J* = 2.3 Hz, 1H, **2**), 7.89 (d, *J* = 8.9 Hz, 1H, **13**), 7.57 (dd, *J* = 8.9, 2.3 Hz, 1H, **14**), 3.22-3.17 (m, 4H, **6** & **10**), 1.92-1.86 (m, 2H, **9**), 1.81-1.71 (m, 4H, **7** & **8**).

^{13}C NMR (101 MHz, $CDCl_3$) δ (ppm) 167.27 (**11**), 144.95 (**12**), 138.68 (**4**), 134.99 (**5**), 132.76 (**1**), 130.65 (**14**), 130.10 (**13**), 126.36 (**3**), 123.69 (**2**), 40.33 (**10**), 31.89 (**8**), 30.57 (**6**), 27.50 (**9**), 26.91 (**7**).

LRMS (ESI$^+$) *m/z* 266.0 [M^{35}Cl+H]$^+$, 268.0 [M^{37}Cl+H]$^+$.

HRMS (ESI$^+$) *m/z* calcd for $C_{14}H_{13}{}^{35}Cl_2N$ [M+H]$^+$, 266.0503, found 266.0497 Da.

7-Chloro-1,2,3,4-tetrahydro-9*H*-cyclopenta[*b*]quinolin-9-one (**2.57**)

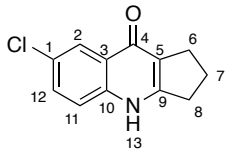

$C_{12}H_{10}ClNO$

MW: 219.67 g.mol^{-1}

2.55 (5.000 g, 21.00 mmol, 1.0 equiv) was dissolved in glacial AcOH (50 mL) and heated in a sealed tube for 16 h at 200 °C. Upon completion, the crude material was poured carefully onto iced-water. The mixture was filtered, washed with cold water and co-evaporated with toluene. Finally, the residue was dried under reduced pressure to afford **2.57** as an off-white powder (4.613 g, 21.00 mmol, quant).

TLC Rf 0.05 (petroleum ether/EtOAc 7:3).

IR (neat) ν_{max} 3082 (w), 2917 (m), 2853 (w), 1628 (m), 1568 (s), 1495 (s), 1463 (s), 1428 (m), 1412 (m), 1357 (m), 1297 (w), 1279 (w), 1168 (m), 1068 (w) cm^{-1}.

^{1}H NMR (400 MHz, DMSO-*d6*) δ (ppm) 12.54 (s, 1H, **13**), 8.06 (m, 1H, **2**), 7.63 (m, 2H, **11** & **12**), 3.03 (t, *J* = 7.7 Hz, 2H, **8**), 2.74 (t, *J* = 7.06 Hz, 2H, **6**), 2.06 (quin, *J* = 6.8 Hz, 2H, **7**).

^{13}C NMR (101 MHz, DMSO-*d6*) δ (ppm) 155.96 (**9**), 138.58 (**10**), 131.14 (**12**), 127.63 (**1**), 125.35 (**3**), 123.61 (**2**), 120.51 (**11**), 120.02 (**5**), 31.85 (**8**), 27.58 (**6**), 21.49 (**7**).

LRMS (ESI^{+}) *m/z* 220.0 [M^{35}Cl+H]$^{+}$, 222.0 [M^{37}Cl+H]$^{+}$.

HRMS (ESI^{+}) *m/z* calcd for $C_{12}H_{11}{}^{35}ClNO$ [M+H]$^{+}$, 220.0528, found 220.0525 Da.

2-Chloro-5,6,7,8,9,10-hexahydro-11*H*-cyclohepta[*b*]quinolin-11-one (**2.58**)

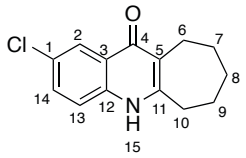

$C_{14}H_{14}ClNO$

MW: 247.72 g.mol^{-1}

2.56 (5.440 g, 20.44 mmol, 1.0 equiv) was dissolved in glacial AcOH (50 mL) and heated in a sealed tube for 16 h at 200 °C. Upon completion, the crude material was poured carefully onto iced-water. The mixture was filtered, washed with cold water and co-evaporated with toluene. Finally, the residue was dried under reduced pressure to afford **2.58** as an off-white powder (4.557 g, 18.39 mmol, 90%).

TLC Rf 0.07 (petroleum ether/EtOAc 4:1).

IR (neat) ν_{max} 3057 (w), 2916 (s), 2848 (s), 1634 (m), 1584 (m), 1549 (s), 1494 (s), 1472 (s), 1435 (m), 1404 (m), 1362 (m), 1213 (m), 1173 (m), 1074 (w) cm^{-1}.

^{1}H NMR (400 MHz, DMSO-*d6*) δ (ppm) 11.57 (br s, 1H, **15**), 7.99 (d, *J* = 2.5 Hz, 1H, **2**), 7.61 (dd, *J* = 8.9, 2.5 Hz, 1H, **14**), 7.52 (d, *J* = 8.9 Hz, 1H, **13**), 2.84-2.82 (m, 2H, **10**), 2.78-2.75 (m, 2H, **6**), 1.82-1.77 (m, 2H, **8**), 1.69-1.65 (m, 2H, **7**), 1.48-1.43 (m, 2H, **9**).

^{13}C NMR (101 MHz, DMSO-*d6*) δ (ppm) 173.61 (**4**), 153.47 (**11**), 137.31 (**12**), 130.97 (**14**), 127.10 (**1**), 124.42 (**13**), 124.23 (**2**), 121.07 (**5**), 120.23 (**13**), 33.56 (**10**), 31.77 (**8**), 27.03 (**7**), 25.64 (**9**), 23.04 (**6**).

LRMS (ESI^{+}) *m/z* 248.1 [M^{35}Cl+H]$^{+}$, 250.1 [M^{37}Cl+H]$^{+}$.

HRMS (ESI^{+}) *m/z* calcd for $C_{14}H_{15}{}^{35}ClNO$ [M+H]$^{+}$, 248.0847, found 248.0843 Da.

7-Chloro-2,3-dihydro-1*H*-cyclopenta[*b*]quinolin-9-yl trifluoromethanesulfonate (**2.59**)

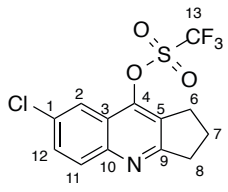

$C_{13}H_9ClF_3NO_3S$

MW: 351.72 g.mol^{-1}

Triflate **2.59** was obtained according to general procedure B using **2.57** (4.613 g, 21.00 mmol, 1.0 equiv), Et_3N (3.22 mL, 23.10 mmol, 1.1 equiv) and Tf_2O (3.89 mL, 23.10 mmol, 1.1 equiv) and CH_2Cl_2 (230 mL). The crude product was purified by column chromatography (silica gel, petroleum ether/EtOAc 4:1) to afford **2.59** as an off-white powder (4.801 g, 13.65 mmol, 65%).

TLC Rf 0.35 (petroleum ether/EtOAc 4:1).

MP 90–92 °C (hexane).

IR (neat) ν_{max} 2967 (m), 2869 (w), 1645 (m), 1611 (m), 1556 (w), 1487 (m), 1417 (s), 1376 (m), 1331 (m), 1300 (m), 1240 (s), 1213 (s), 1138 (s), 1101 (m), 1078 (m), 1008 (s), 1002 (s) cm^{-1}.

^{1}H NMR (400 MHz, $CDCl_3$) δ (ppm) 8.01 (d, *J* = 9.0 Hz, 1H, **11**), 7.92 (d, *J* = 2.3 Hz, 1H, **2**), 7.66 (dd, *J* = 9.0, 2.3 Hz, 1H, **12**), 3.25 (q, *J* = 7.8 Hz, 4H, **6** & **8**), 2.28 (quin, *J* = 7.6 Hz, 2H, **7**).

^{13}C NMR (101 MHz, $CDCl_3$) δ (ppm) 170.69 (**9**), 148.39 (**4**), 146.82 (**10**), 133.51 (**5**), 130.99 (**12**), 130.60 (**11**), 128.54 (**1**), 121.64 (**3**), 119.81 (**2**), 118.72 (q, *J* = 323.4 Hz, **13**), 35.36 (**8**), 29.16 (**6**), 23.52 (**7**).

^{19}F NMR (376 MHz, $CDCl_3$) δ (ppm) –73.11.

LRMS (ESI$^+$) *m/z* 352.0 [M^{35}Cl+H]$^+$, 354.0 [M^{37}Cl+H]$^+$.

HRMS (ESI$^+$) *m/z* calcd for $C_{13}H_9{}^{35}ClF_3NO_3S$ [M+H]$^+$, 352.0022, found 352.0021 Da.

2-Chloro-7,8,9,10-tetrahydro-6*H*-cyclohepta[*b*]quinolin-11-yl trifluoromethanesulfonate (**2.60**)

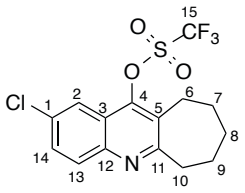

$C_{15}H_{13}ClF_3NO_3S$

MW: 379.78 g.mol^{-1}

Triflate **2.60** was obtained according to general procedure B using **2.58** (4.410 g, 17.80 mmol, 1.0 equiv), Et_3N (2.68 mL, 19.58 mmol, 1.1 equiv) and Tf_2O (3.25 mL, 19.58 mmol, 1.1 equiv) and CH_2Cl_2 (196 mL). The crude product was purified by column chromatography (silica gel, petroleum ether/EtOAc 9:1) to afford **2.60** as a pale pink powder (6.084 g, 16.02 mmol, 90%).

TLC Rf 0.28 (petroleum ether/EtOAc 9:1).

MP 88–89 °C (hexane).

IR (neat) ν_{max} 2929 (m), 2857 (m), 1601 (m), 1554 (w), 1479 (m), 1410 (s), 1345 (w), 1323 (w), 1240 (s), 1209 (s), 1134 (s), 1109 (w), 1081 (m), 1005 (s) cm^{-1}.

^{1}H NMR (400 MHz, $CDCl_3$) δ (ppm) 7.95 (d, *J* = 9.0 Hz, 1H, **13**), 7.90 (d, *J* = 2.3 Hz, 1H, **2**), 7.63 (dd, *J* = 9.0, 2.3 Hz, 1H, **14**), 3.26-3.23 (m, 2H, **10**), 3.04-3.01 (m, 2H, **6**), 1.93-1.87 (m, 2H, **9**), 1.84-1.76 (m, 4H, **7** & **8**).

^{13}C NMR (101 MHz, $CDCl_3$) δ (ppm) 166.87 (**11**), 147.48 (**4**), 146.00 (**12**), 133.61 (**1**), 130.92 (**14**), 130.64 (**13**), 130.19 (**5**), 121.75 (**3**), 120.26 (**2**), 118.78 (q, *J* = 324.0 Hz, **15**), 40.44 (**10**), 31.83 (**8**), 27.63 (**6**), 27.47 (**7**), 26.71 (**9**).

^{19}F NMR (376 MHz, $CDCl_3$) δ (ppm) –72.58.

LRMS (ESI$^+$) *m/z* 380.0 [M^{35}Cl+H]$^+$, 382.0 [M^{37}Cl+H]$^+$.

HRMS (ESI$^+$) *m/z* calcd for $C_{15}H_{13}{}^{35}ClF_3NO_3S$ [M+H]$^+$, 380.0335, found 380.0332 Da.

1,2,3,4-Tetrahydroacridin-9-yl trifluoromethanesulfonate (**2.62**)

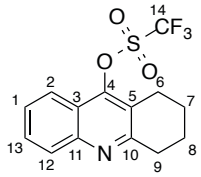

$C_{14}H_{12}F_3NO_3S$

MW: 331.31 g.mol^{-1}

Triflate **2.62** was obtained according to general procedure B using 1,2,3,4-tetrahydro-9-acridanone **2.61** (2.000 g, 10.04 mmol, 1.0 equiv), Et_3N (1.53 mL, 11.04 mmol, 1.1 equiv) and Tf_2O (1.86 mL, 11.04 mmol, 1.1 equiv) and CH_2Cl_2 (100 mL). The crude product was purified by column chromatography (silica gel, petroleum ether/EtOAc 4:1) to afford **2.62** as a white powder (2.830 g, 8.530 mmol, 85%).

TLC Rf 0.80 (petroleum ether/EtOAc 1:1).

MP 55–56 °C (hexane).

IR (neat) ν_{max} 2946 (m), 2875 (w), 1626 (m), 1603 (m), 1556 (w), 1487 (m), 1405 (s), 1326 (m), 1201 (s), 1128 (s), 1003 (s) cm^{-1}.

^{1}H NMR (400 MHz, $CDCl_3$) δ (ppm) 8.04 (d, *J* = 8.6 Hz, 1H, **2**), 7.99 (d, *J* = 8.4 Hz, 1H, **12**), 7.72 (t, *J* = 8.0 Hz, 1H, **1**), 7.59 (t, *J* = 7.7 Hz, 1H, **13**), 3.18 (t, *J* = 6.6 Hz, 2H, **9**), 3.05 (t, *J* = 6.4 Hz, 2H, **6**), 2.04-1.88 (m, 4H, **7** & **8**).

^{13}C NMR (101 MHz, $CDCl_3$) δ (ppm) 161.12 (**10**), 149.99 (**4**), 148.10 (**11**), 130.09 (**13**), 128.77 (**12**), 127.42 (**1**), 124.14 (**3**), 120.87 (**5**), 120.82 (**2**), 118.78 (q, *J* = 319.9 Hz, **14**), 33.83 (**9**), 24.24 (**6**), 22.53 (**8**), 22.04 (**7**).

^{19}F NMR (376 MHz, $CDCl_3$) δ (ppm) –72.87.

LRMS (ESI$^+$) *m/z* 332.1 $[M+H]^+$.

HRMS (ESI$^+$) *m/z* calcd for $C_{14}H_{13}F_3NO_3S$ $[M+H]^+$, 332.0563, found 332.0563 Da.

7-Chloro-*N*-(prop-2-yn-1-yl)-2,3-dihydro-1*H*-cyclopenta[*b*]quinolin-9-amine (**2.63**)

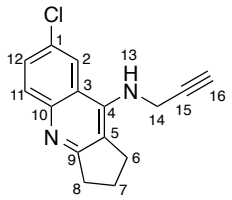

$C_{15}H_{13}ClN_2$

MW: 256.73 g.mol^{-1}

Terminal alkyne **2.63** was obtained according to general procedure C using **2.59** (0.100 g, 0.284 mmol, 1.0 equiv), $Pd_2(dba)_3$ (0.010 g, 0.011 mmol, 0.04 equiv), (±)-BINAP (0.015 g, 0.023 mmol, 0.08 equiv), Cs_2CO_3 (0.231 g, 0.710 mmol, 2.5 equiv), 1,4-dioxane (3.0 mL) and commercially available propargylamine (23 μL, 0.369 mmol, 1.3 equiv). The crude alkyne was purified by column chromatography (silica gel, Et_2O) to afford **2.63** as yellow solid (0.066 g, 0.256 mmol, 90%).

TLC Rf 0.31 (Et_2O).

MP 144–146 °C (hexane).

IR (neat) ν_{max} 3294 (s), 2958 (m), 2867 (w), 1597 (m), 1562 (s), 1524 (s), 1493 (m), 1435 (m), 1404 (s), 1338 (m), 1165 (m), 1130 (m), 1092 (m) cm^{-1}.

^{1}H NMR (400 MHz, $CDCl_3$) δ (ppm) 7.86 (d, *J* = 8.9 Hz, 1H, **11**), 7.73 (d, *J* = 2.2 Hz, 1H, **2**), 7.51 (dd, *J* = 8.9, 2.2 Hz, 1H, **12**), 4.65 (br s, 1H, **13**), 4.31 (dd, *J* = 6.6, 2.5 Hz, 2H, **14**), 3.26 (t, *J* = 7.3 Hz, 2H, **8**), 3.07 (t, *J* = 7.8 Hz, 2H, **6**), 2.32 (t, *J* = 2.5 Hz, 1H, **16**), 2.18 (quin, *J* = 7.5 Hz, 2H, **7**).

^{13}C NMR (101 MHz, $CDCl_3$) δ (ppm) 169.39 (**9**), 147.05 (**4**), 144.55 (**10**), 131.02 (**12**), 130.24 (**1**), 129.16 (**11**), 120.36 (**5**), 119.50 (**2**), 117.32 (**3**), 80.97 (**15**), 73.00 (**16**), 35.84 (**14**), 35.09 (**8**), 30.31 (**6**), 23.43 (**7**).

LRMS (ESI$^+$) *m/z* 256.9 [M^{35}Cl+H]$^+$, 258.9 [M^{37}Cl+H]$^+$.

HRMS (ESI$^+$) *m/z* calcd for $C_{15}H_{14}{}^{35}ClN_2$ [M+H]$^+$, 257.0840, found 257.0843 Da.

7-Chloro-*N*-(prop-2-yn-1-yl)-2,3-dihydro-1*H*-cyclopenta[*b*]quinolin-9-amine (**2.64**)

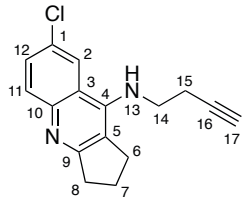

$C_{16}H_{15}ClN_2$

MW: 270.76 g.mol^{-1}

Terminal alkyne **2.64** was obtained according to general procedure C using **2.59** (0.150 g, 0.426 mmol, 1.0 equiv), $Pd_2(dba)_3$ (0.016 g, 0.017 mmol, 0.04 equiv), (±)-BINAP (0.023 g, 0.034 mmol, 0.08 equiv), Cs_2CO_3 (0.347 g, 1.065 mmol, 2.5 equiv), 1,4-dioxane (3.0 mL) and commercially available 1-amino-3-butyne (45 μL, 0.554 mmol, 1.3 equiv). The crude was purified by column chromatography (silica gel, Et_2O) to afford **2.64** as a white solid (0.098 g, 0.362 mmol, 85%).

TLC Rf 0.19 (Et_2O).

MP 125–127 °C (hexane).

IR (neat) ν_{max} 3309 (s), 2955 (w), 2845 (w), 2125 (w), 1689 (w), 1562 (s), 1535 (s), 1489 (m), 1461 (w), 1416 (m), 1403 (m), 1354 (m), 1168 (w), 1130 (m), 1095 (m) cm^{-1}.

^{1}H NMR (400 MHz, $CDCl_3$) δ (ppm) 7.84 (d, *J* = 8.8 Hz, 1H, **11**), 7.78 (d, *J* = 2.2Hz, 1H, **2**), 7.49 (dd, *J* = 8.8, 2.2 Hz, 1H, **12**), 4.80 (br s, 1H, **13**), 3.72 (q, *J* = 6.4 Hz, 2H, **14**), 3.16 (t, *J* = 7.3 Hz, 2H, **8**), 3.05 (t, *J* = 7.8 Hz, 2H, **6**), 2.52 (td, *J* = 6.4, 2.6 Hz, 2H, **15**), 2.23-2.07 (m, 3H, **7** & **17**).

^{13}C NMR (101 MHz, $CDCl_3$) δ (ppm) 169.22 (**9**), 147.08 (**4**), 145.20 (**10**), 130.90 (**12**), 129.95 (**1**), 129.10 (**11**), 120.35 (**5**), 119.68 (**2**), 116.48 (**3**), 81.62 (**16**), 71.34 (**17**), 44.22 (**14**), 35.08 (**8**), 30.71 (**6**), 23.36 (**7**), 20.88 (**15**).

LRMS (ESI$^+$) *m/z* 271.0 [M^{35}Cl+H]$^+$, 273.0 [M^{37}Cl+H]$^+$.

HRMS (ESI$^+$) *m/z* calcd for $C_{16}H_{16}{}^{35}ClN_2$ [M+H]$^+$, 271.0997, found 271.0999 Da.

Methyl 3-(benzyloxy)-6-(3-((7-chloro-2,3-dihydro-1*H*-cyclopenta[*b*]quinolin-9-yl)amino)prop-1-yn-1yl)picolinate (**2.65**)

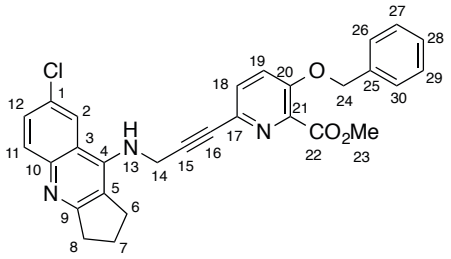

$C_{29}H_{24}ClN_3O_3$

MW: 497.98 g.mol^{-1}

Following the procedure described for the Sonogashira coupling to form compound **2.49**, acetylene **2.65** was obtained using terminal alkyne **2.63** (0.120 g, 0.467 mmol, 1.0 equiv), methyl 3-benzyloxy-6-bromopicolinate **2.10** (0.166 g, 0.514 mmol, 1.1 equiv), Pd[PPh_3]$_4$ (0.054 g, 0.047 mmol, 0.1 equiv), CuI (0.018 g, 0.094 mmol, 0.2 equiv), THF (6 mL) and Et_3N (3 mL). The crude material was purified by column chromatography (silica gel, EtOAc) to afford **2.65** as yellow solid (0.209 g, 0.420 mmol, 90%).

TLC Rf 0.29 (EtOAc).

MP 178–180 °C (hexane).

IR (neat) ν_{max} 3331 (m), 2951 (m), 2865 (m), 2229 (w), 1731 (s), 1596 (s), 1534 (m), 1450 (s), 1434 (s), 1403 (m), 1293 (s), 1269 (s), 1212 (s), 1099 (s) cm^{-1}.

^{1}H NMR (400 MHz, $CDCl_3$) δ (ppm) 7.86 (d, *J* = 8.9 Hz, 1H, **11**), 7.77 (d, *J* = 2.2 Hz, 1H, **2**), 7.51 (dd, *J* = 8.9, 2.2 Hz, 1H, **12**), 7.44-7.30 (m, 6H, **18**, **26**, **27**, **28**, **29** & **30**), 7.29-7.27 (s, 1H, **19**), 5.20 (s, 2H, **24**), 4.69 (t, *J* = 6.2 Hz, 1H, **13**), 4.52 (d, *J* = 6.5 Hz, 2H, **14**), 3.96 (s, 3H, **23**), 3.29 (t, *J* = 7.3 Hz, 2H, **8**), 3.07 (t, *J* = 7.8 Hz, 2H, **6**), 2.17 (quin, *J* = 7.5 Hz, 2H, **7**).

^{13}C NMR (101 MHz, $CDCl_3$) δ (ppm) 169.33 (**22**), 164.72 (**9**), 153.61 (**20**), 146.98 (**4**), 144.66 (**10**), 140.49 (**21**), 135.40 (**17**), 134.06 (**25**), 130.88 (**18**), 130.37 (**12**), 130.19 (**1**), 129.14 (**11**), 128.91 (2C, **27** & **29**), 128.45 (**28**), 127.01 (2C, **26** & **30**), 121.76 (**2**), 120.34 (**5**), 119.70 (**19**), 117.22 (**3**), 85.84 (**15**), 83.07 (**16**), 70.97 (**24**), 52.91 (**23**), 36.52 (**14**), 35.06 (**8**), 30.43 (**6**), 23.44 (**7**).

LRMS (ESI$^+$) *m/z* 498.0 [M^{35}Cl+H]$^+$, 500.0 [M^{37}Cl+H]$^+$.

HRMS (ESI$^+$) *m/z* calcd for $C_{29}H_{25}{}^{35}ClN_3O_3$ [M+H]$^+$, 498.1579, found 498.1590 Da.

Methyl 3-(benzyloxy)-6-(4-((7-chloro-2,3-dihydro-1*H*-cyclopenta[*b*]quinolin-9-yl)amino)but-1-yn-1-yl)picolinate (**2.66**)

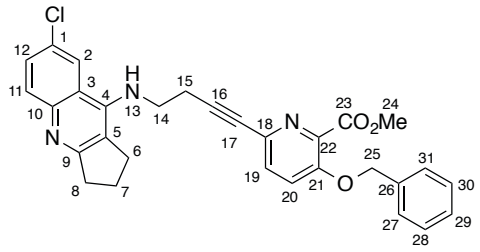

$C_{30}H_{26}ClN_3O_3$

MW: 512.01 g.mol^{-1}

Following the procedure described for the Sonogashira coupling to form compound **2.49**, acetylene **2.66** was obtained using terminal alkyne **2.64** (0.164 g, 0.606 mmol, 1.0 equiv), methyl 3-benzyloxy-6-bromopicolinate **2.10** (0.215 g, 0.666 mmol, 1.1 equiv), Pd[PPh_3]$_4$ (0.070 g, 0.061 mmol, 0.1 equiv), CuI (0.023 g, 0.121 mmol, 0.2 equiv), THF (8 mL) and Et_3N (4 mL). The crude material was purified by column chromatography (silica gel, EtOAc/MeOH 10:0 to 9:1) to afford **2.66** as yellow wax (0.233 g, 0.455 mmol, 75%).

TLC Rf 0.29 (EtOAc).

MP 178–180 °C (hexane).

IR (neat) ν_{max} 3333 (w), 2951 (m), 2865 (m), 2118 (w), 1731 (s), 1596 (m), 1561 (s), 1536 (m), 1489 (m), 1450 (s), 1435 (s), 1417 (m), 1405 (m), 1352 (m), 1271 (s), 1209 (s), 1098 (s) cm^{-1}.

^{1}H NMR (400 MHz, $CDCl_3$) δ (ppm) 7.85 (d, *J* = 8.9 Hz, 1H, **11**), 7.79 (d, *J* = 2.0 Hz, 1H, **2**), 7.73-7.60 (m, 1H, **12**), 7.49-7.28 (m, 7H, **19**, **20**, **27**, **28**, **29**, **30** & **31**), 5.21 (s, 2H, **25**), 4.92 (br s, 1H, **13**), 3.96 (s, 3H, **24**), 3.80 (q, *J* = 6.2 Hz, 2H, **14**), 3.17 (t, *J* = 7.3 Hz, 2H, **8**), 3.05 (t, *J* = 7.8 Hz, 2H, **6**), 2.72 (t, *J* = 6.4 Hz, 2H, **15**), 2.16 (quin, *J* = 7.5 Hz, 2H, **7**).

^{13}C NMR (101 MHz, $CDCl_3$) δ (ppm) 169.21 (**23**), 164.81 (**9**), 153.37 (**21**), 147.02 (**4**), 145.14 (**10**), 140.32 (**22**), 135.48 (**18**), 134.58 (**26**), 130.82 (**1**), 130.22 (**19**), 128.98 (**12**), 128.85 (2C, **28** & **30**), 128.66 (**29**), 128.53 (**11**), 128.37 (**2**), 127.00 (2C, **27** & **31**), 121.87 (**20**), 120.36 (**5**), 119.68 (**3**), 86.32 (**16**), 81.87 (**17**), 70.93 (**25**), 52.83 (**24**), 43.88 (**14**), 35.01 (**8**), 30.77 (**6**), 23.29 (**7**), 21.80 (**14**).

LRMS (ESI$^+$) *m/z* 512.1 [M^{35}Cl+H]$^+$, 514.1 [M^{37}Cl+H]$^+$.

HRMS (ESI$^+$) *m/z* calcd for $C_{30}H_{27}{}^{35}ClN_3O_3$ [M+H]$^+$, 512.1735, found 512.1733 Da.

Methyl 6-(4-((7-chloro-2,3-dihydro-1*H*-cyclopenta[*b*]quinolin-9-yl)amino)butyl)-3-hydroxypicolinate (**2.68**) and methyl 6-(4-((2,3-dihydro-1*H*-cyclopenta[*b*]quinolin-9-yl)amino)butyl)-3-hydroxypicolinate (**2.69**)

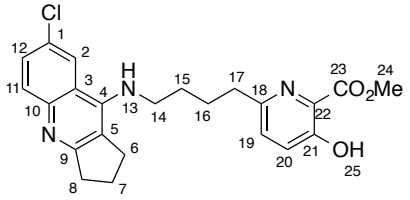

$C_{23}H_{24}ClN_3O_3$

MW: 425.91 g.mol^{-1}

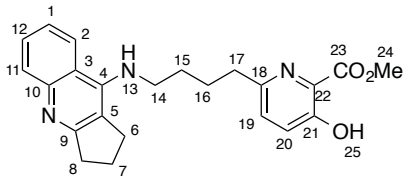

$C_{23}H_{25}N_3O_3$

MW: 391.47 g.mol^{-1}

2.68 and **2.69** were obtained according to general procedures D using **2.66** (0.215 g, 0.420 mmol, 1.0 equiv), $Pd(OH)_2/C$ (20% wt. with 50% moisture, 0.120 g, 0.084 mmol, 0.2 equiv) and EtOH (42 mL). The residue was purified by column chromatography (silica gel, CH_2Cl_2/MeOH 9:1) to afford **2.68** as yellow wax (0.020 g, 0.047 mmol, 11%) and **2.69** as yellow wax (0.126 g, 0.322 mmol, 77%).

- Methyl 6-(4-((7-chloro-2,3-dihydro-1*H*-cyclopenta[*b*]quinolin-9-yl)amino)butyl)-3-hydroxypicolinate (**2.68**):

TLC Rf 0.38 (CH_2Cl_2/MeOH 9:1).

IR (neat) ν_{max} 3227 (m), 2950 (m), 2858 (m), 1673 (s), 1587 (m), 1561 (s), 1533 (m), 1465 (s), 1443 (s), 1417 (s), 1368 (s), 1299 (s), 1206 (s), 1100 (s) cm^{-1}.

^{1}H NMR (400 MHz, $CDCl_3$) δ (ppm) 10.55 (br s, 1H, **25**), 7.89-7.77 (m, 2H, **2** & **12**), 7.44 (d, *J* = 8.9 Hz, 1H, **11**), 7.33-7.22 (m, 2H, **19** & **20**), 5.19 (br s, 1H, **13**), 3.96 (s, 3H, **24**), 3.63 (q, *J* = 6.0 Hz, 2H, **14**), 3.16 (t, *J* = 7.2 Hz, 2H, **8**), 3.03 (t, *J* = 7.7 Hz, 2H, **17**), 2.85 (t, *J* = 7.4 Hz, 2H, **6**), 2.10 (quin, *J* = 7.4 Hz, 2H, **7**), 1.92-1.63 (m, 4H, **15** & **16**).

^{13}C NMR (101 MHz, $CDCl_3$) δ (ppm) 170.07 (**23**), 168.28 (**9**), 157.40 (**18**), 153.30 (**21**), 146.41 (**4**), 145.71 (**10**), 129.72 (**12**), 129.69 (**22**), 129.41 (**19**), 129.23 (**11**), 128.93 (**1**), 127.00 (**20**), 119.95 (**2**), 119.64 (**3**), 114.52 (**5**), 53.19 (**24**), 45.57 (**14**), 36.82 (**16**), 34.61 (**8**), 31.08 (**15**), 30.27 (**6**), 27.11 (**17**), 23.23 (**7**).

LRMS (ESI$^+$) *m/z* 426.0 [M^{35}Cl+H]$^+$, 428.0 [M^{37}Cl+H]$^+$.

HRMS (ESI$^+$) *m/z* calcd for $C_{23}H_{25}{}^{35}ClN_3O_3$ [M+H]$^+$, 426.1579, found 426.1588 Da.

- Methyl 6-(4-((2,3-dihydro-1*H*-cyclopenta[*b*]quinolin-9-yl)amino)butyl)-3-hydroxypicolinate (**2.69**)

TLC Rf 0.21 (CH_2Cl_2/MeOH 9:1).

IR (neat) ν_{max} 3236 (m), 2951 (m), 2857 (m), 1674 (m), 1585 (s), 1561 (s), 1466 (s), 1446 (m), 1427 (m), 1210 (s), 1101 (m) cm^{-1}.

^{1}H NMR (400 MHz, $CDCl_3$) δ (ppm) 10.58 (br s, 1H, **25**), 8.20 (d, *J* = 7.8 Hz, 1H, **2**), 8.07 (d, *J* = 8.4 Hz, 1H, **11**), 7.60 (t, *J* = 7.6 Hz, 1H, **12**), 7.37 (t, *J* = 7.8 Hz, 1H, **1**), 7.33 (m, 2H, **19** & **20**), 3.92 (s, 3H, **24**), 3.83 (q, *J* = 5.7 Hz, 2H, **14**), 3.27 (t, *J* = 7.8 Hz, 2H, **8**), 3.20 (t, *J* = 7.3 Hz, 2H, **17**), 2.90 (t, J = 7.1 Hz, 2H, **6**), 2.17 (quin, *J* = 7.5 Hz, 2H, **7**), 1.95-1.79 (m, 4H, **15** & **16**).

^{13}C NMR (101 MHz, $CDCl_3$) δ (ppm) 169.96 (**23**), 162.85 (**9**), 157.28 (**18**), 153.30 (**21**), 150.91 (**4**), 140.97 (**10**), 130.66 (**12**), 129.40 (**19**), 128.76 (**11**), 126.87 (**20**), 125.18 (**1**), 122.69 (2C, **2** & **22**), 117.82 (**3**), 112.02 (**5**), 53.16 (**24**), 44.71 (**14**), 36.93 (**17**), 32.48 (**8**), 31.31 (**6**), 30.84 (**15**), 26.92 (**16**), 29.92 (**7**).

LRMS (ESI$^+$) *m/z* 392.0 [M+H]$^+$.

HRMS (ESI$^+$) *m/z* calcd for $C_{23}H_{26}N_3O_3$ [M+H]$^+$, 392.1969, found 392.1971 Da.

6-(3-((2,3-Dihydro-1*H*-cyclopenta[*b*]quinolin-9-yl)amino)propyl)-3-hydroxypicolin-aldehyde oxime (**2.70**)

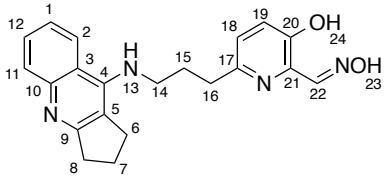

$C_{21}H_{22}N_4O_2$

MW: 362.43 g.mol^{-1}

Oxime **2.70** was obtained according to general procedures D, E, F and G using for procedure D **2.65** (0.117 g, 0.235 mmol, 1.0 equiv), $Pd(OH)_2/C$ (20% wt. with 50% moisture, 0.066 g, 0.047 mmol, 0.2 equiv) and EtOH (23.5 mL). The presence of the desired phenolic alkane was supported by TLC and LRMS (ESI$^+$, *m/z* 377.9 $[M+H]^+$). After drying *in vacuo*, the crude product was subjected to procedure E using 2,6-lutidine (82 μL, 0.705 mmol, 3.0 equiv), TBSOTf (162 μL, 0.705 mmol, 3.0 equiv) in CH_2Cl_2 (4.0 mL). The presence of the desired silylether was supported by TLC and LRMS (ESI$^+$, *m/z* 492.1 $[M+H]^+$). After drying *in vacuo*, the crude material was subjected to procedure F using DIBAL-H (705 μL of a 1.0 M solution in CH_2Cl_2, 0.705 mmol, 3.0 equiv) in CH_2Cl_2 (4.0 mL). The presence of the desired aldehyde was supported by TLC and LRMS (ESI$^+$, *m/z* 347.9 $[M+H]^+$). After drying *in vacuo*, the crude product was subjected to procedure G using hydroxylamine hydrochloride (0.025 g, 0.353 mmol, 1.5 equiv) and CH_3CO_2Na (0.029 g, 0.353 mmol, 1.5 equiv) in EtOH (8.0 mL). The crude oxime was purified by column chromatography (silica gel, CH_2Cl_2/MeOH 85:15) to afford **2.70** as yellow foam (0.049 g, 0.134 mmol, 57% over 4 steps).

TLC Rf 0.30 (CH_2Cl_2/MeOH 8:2).

IR (neat) ν_{max} 2925 (m), 2856 (m), 1635 (w), 1586 (s), 1570 (m), 1465 (m), 1424 (m), 1369 (m), 1271 (m), 1028 (m), 921 (w) cm^{-1}.

^{1}H NMR (400 MHz, CD_3OD) δ (ppm) 8.20-8.13 (m, 2H, **2** & **22**), 7.76 (ddd, *J* = 8.4, 7.5, 2.0 Hz, 1H, **12**), 7.69 (dd, *J* = 8.2, 0.9 Hz, 1H, **11**), 7.53 (ddd, *J* = 8.6, 7.8, 1.3 Hz, 1H, **1**), 7.18 (ABq, $\Delta\delta_{AB}$ = 0.04,[10] *J* = 8.0 Hz, 2H, **18** & **19**), 3.81 (t, *J* = 7.1 Hz, 2H, **14**), 3.20 (t, *J* = 7.5 Hz, 2H, **8**), 3.11 (t, *J* = 7.9 Hz, 2H, **6**), 2.87 (t, *J* = 7.1 Hz, 2H, **16**), 2.28-2.08 (m, 4H, **7** & **15**).

^{13}C NMR (101 MHz, CD_3OD) δ (ppm) 163.14 (**9**), 153.82 (**17**), 153.72 (**20**), 153.32 (**4**), 152.52 (**22**), 140.37 (**10**), 136.47 (**21**), 133.08 (**12**), 127.00 (**1**), 126.02 (**19**), 125.57

[10] Non-first order AB system (Cf. results and discussion, section 2.4.2)

(**18**), 123.52 (**2**), 121.63 (**11**), 118.66 (**3**), 113.54 (**5**), 45.23 (**14**), 34.79 (**16**), 32.86 (**6**), 32.46 (**8**), 31.90 (**15**), 23.70 (**7**).

LRMS (ESI$^+$) *m/z* 363.3 $[M+H]^+$.

HRMS (ESI$^+$) *m/z* calcd for $C_{21}H_{23}N_4O_2$ $[M+H]^+$, 363.1816, found 363.1821 Da.

6-(4-((7-Chloro-2,3-dihydro-1*H*-cyclopenta[*b*]quinolin-9-yl)amino)butyl)-3-hydroxy-picolinaldehyde oxime (**2.71**)

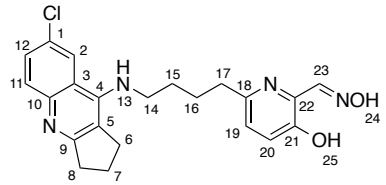

$C_{22}H_{23}ClN_4O_2$

MW: 410.90 g.mol^{-1}

Oxime **2.71** was obtained according to general procedures E, F and G using for procedure E **2.68** (0.020 g, 0.047 mmol, 1.0 equiv), 2,6-lutidine (16 µL, 0.141 mmol, 3.0 equiv), TBSOTf (32 µL, 0.141 mmol, 3.0 equiv) in CH_2Cl_2 (2.0 mL). The presence of the desired silylether was supported by TLC and LRMS (ESI$^+$, *m/z* 540.1 [M+H]$^+$). After drying *in vacuo*, the crude was subjected to procedure F using DIBAL-H (141 µL of a 1.0 M solution in CH_2Cl_2, 0.141 mmol, 3.0 equiv) in CH_2Cl_2 (2.0 mL). The presence of the desired aldehyde was supported by TLC and LRMS (ESI$^+$, *m/z* 396.0 [M+H]$^+$). After drying *in vacuo*, the crude was directly subjected to the subsequent procedure G using hydroxylamine hydrochloride (0.005 g, 0.071 mmol, 1.5 equiv) and CH_3CO_2Na (0.006 g, 0.071 mmol, 1.5 equiv) in EtOH (3.0 mL). The crude oxime was purified by column chromatography (silica gel, CH_2Cl_2/MeOH 9:1) to afford **2.71** as a white solid (0.015 g, 0.037 mmol, 79% over 3 steps).

TLC Rf 0.45 (CH_2Cl_2/MeOH 8:2).

MP 162–164 °C (MeOH/hexane 1:2).

IR (neat) ν_{max} 3062 (w), 2926 (s), 2856 (s), 1652 (w), 1567 (s), 1540 (m), 1486 (m), 1465 (s), 1420 (m), 1270 (m), 1027 (m) 947 (w) cm^{-1}.

^{1}H NMR (400 MHz, CD_3OD) δ (ppm) 8.21 (d, *J* = 2.2 Hz, 1H, **2**), 8.18 (s, 1H, **23**), 7.69 (d, *J* = 8.3 Hz, 1H, **11**), 7.60 (dd, *J* = 8.3, 2.2 Hz, 1H, **12**), 7.15 (ABq, ΔδAB = 1.27, *J* = 8.6 Hz, 2H, **19** & **20**), 3.64 (t, *J* = 7.0 Hz, 2H, **14**), 3.19 (t, *J* = 7.2 Hz, 2H, **8**), 2.99 (t, *J* = 7.8 Hz, 2H, **6**), 2.76 (t, *J* = 7.2 Hz, 2H, **17**), 2.14 (quin, *J* = 7.6 Hz, 2H, **7**), 1.89-1.75 (m, 2H, **16**), 1.75-1.69 (m, 2H, **15**).

^{13}C NMR (101 MHz, CD_3OD) δ (ppm) 164.38 (**9**), 154.12 (**18**), 153.72 (**21**), 152.65 (**23**), 152.30 (**4**), 139.87 (**10**), 136.31 (**22**), 133.01 (**12**), 132.56 (**1**), 125.89 (**11**), 125.48 (**19**), 124.29 (**2**), 122.96 (**20**), 119.91 (**3**), 114.29 (**5**), 45.48 (**14**), 37.12 (**17**), 33.12 (**8**), 32.42 (**6**), 31.25 (**15**), 27.59 (**16**), 23.73 (**7**).

LRMS (ESI$^+$) *m/z* 411.0 [M^{35}Cl+H]$^+$, 413.0 [M^{37}Cl+H]$^+$.

HRMS (ESI$^+$) *m/z* calcd for $C_{22}H_{24}{}^{35}ClN_4O_2$ [M+H]$^+$, 411.1582, found 411.1583 Da.

6-(4-((2,3-Dihydro-1*H*-cyclopenta[*b*]quinolin-9-yl)amino)butyl)-3-hydroxypicolin-aldehyde oxime (**2.72**)

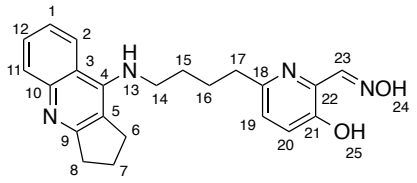

$C_{22}H_{24}N_4O_2$

MW: 376.46 g.mol^{-1}

Oxime **2.72** was obtained according to general procedures E, F and G using for procedure E **2.69** (0.120 g, 0.307 mmol, 1.0 equiv), 2,6-lutidine (107 µL, 0.920 mmol, 3.0 equiv), TBSOTf (211 µL, 0.920 mmol, 3.0 equiv) in CH_2Cl_2 (4.0 mL). The presence of the desired silylether was supported by TLC and LRMS (ESI$^+$, *m/z* 506.2 $[M+H]^+$). After drying *in vacuo*, the crude was subjected to procedure F using DIBAL-H (920 µL of a 1.0 M solution in CH_2Cl_2, 0.920 mmol, 3.0 equiv) in CH_2Cl_2 (4.0 mL). The presence of the desired aldehyde was supported by TLC and LRMS (ESI$^+$, *m/z* 362.0 $[M+H]^+$). After drying *in vacuo*, the crude was directly subjected to the subsequent procedure G using hydroxylamine hydrochloride (0.032 g, 0.461 mmol, 1.5 equiv) and CH_3CO_2Na (0.038 g, 0.461 mmol, 1.5 equiv) in EtOH (10.0 mL). The crude oxime was purified by column chromatography (silica gel, CH_2Cl_2/MeOH 85:15) to afford **2.72** as a white solid (0.077 g, 0.206 mmol, 67% over 3 steps).

TLC Rf 0.34 (CH_2Cl_2/MeOH 8:2).

MP 202–204 °C ($CHCl_3$).

IR (neat) ν_{max} 3263 (m), 2929 (m), 2858 (w), 1632 (m), 1582 (s), 1526 (m), 1463 (s), 1422 (m), 1371 (m), 1273 (m), 1166 (m), 1017 (s), 923 (w) cm^{-1}.

^{1}H NMR (400 MHz, CD_3OD) δ (ppm) 8.25 (d, *J* = 8.3 Hz, 1H, **2**), 8.15 (s, 1H, **23**), 7.81 (ddd, *J* = 8.6, 7.6, 1.2 Hz, 1H, **12**), 7.76-7.68 (m, 1H, **11**), 7.59 (ddd, *J* = 8.5, 7.2, 1.2 Hz, 1H, **1**), 7.16 (ABq, $\Delta\delta_{AB}$ = 0.28,[11] *J* = 8.6 Hz, 2H, **19** & **20**), 3.77 (t, *J* = 7.0 Hz, 2H, **14**), 3.27 (t, *J* = 6.8 Hz, 2H, **8**), 3.13 (t, *J* = 8.0 Hz, 2H, **6**), 2.78 (t, *J* = 7.1 Hz, 2H, **17**), 2.23 (quin, *J* = 7.6 Hz, 2H, **7**), 1.96-1.67 (m, 4H, **15** & **16**).

^{13}C NMR (101 MHz, CD_3OD) δ (ppm) 162.93 (**9**), 154.13 (**18**), 153.77 (**21**), 153.18 (**4**), 152.70 (**23**), 140.05 (**10**), 136.34 (**22**), 133.34 (**12**), 127.21 (**1**), 125.93 (**20**), 125.53 (**19**), 123.58 (**2**), 121.42 (**11**), 118.72 (**3**), 113.66 (**5**), 45.49 (**14**), 37.12 (**17**), 32.76 (**6**), 32.46 (**8**), 31.35 (**15**), 27.57 (**16**), 23.74 (**7**).

[11] Non-first order AB system (Cf. results and discussion, section 2.4.2)

LRMS (ESI$^+$) *m/z* 377.0 $[M+H]^+$.

HRMS (ESI$^+$) *m/z* calcd for $C_{22}H_{25}N_4O_2$ $[M+H]^+$, 377.1972, found 377.1971 Da.

N-(Prop-2-yn-1-yl)-1,2,3,4-tetrahydroacridin-9-amine (**2.73**)

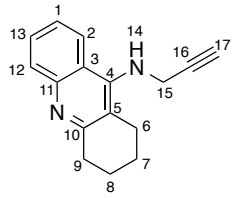

$C_{16}H_{16}N_2$

MW: 236.32 g.mol^{-1}

Terminal alkyne **2.73** was obtained according to general procedure C using **2.62** (0.100 g, 0.302 mmol, 1.0 equiv), $Pd_2(dba)_3$ (0.011 g, 0.012 mmol, 0.04 equiv), (±)-BINAP (0.016 g, 0.025 mmol, 0.08 equiv), Cs_2CO_3 (0.246 g, 0.755 mmol, 2.5 equiv), 1,4-dioxane (3.0 mL) and commercially available propargylamine (25 μL, 0.392 mmol, 1.3 equiv). The crude material was purified by column chromatography (silica gel, Et_2O/MeOH 9:1) to afford **2.73** as yellow solid (0.064 g, 0.272 mmol, 90%).

TLC Rf 0.30 (Et_2O/MeOH 9:1).

MP 120–122 °C (hexane).

IR (neat) ν_{max} 3291 (s), 3063 (w), 2931 (s), 2862 (m), 2233 (w), 1615 (w), 1582 (s), 1562 (s), 1497 (s), 1434 (w), 1407 (m), 1375 (w), 1330 (m), 1111 (m) cm^{-1}.

^{1}H NMR (400 MHz, $CDCl_3$) δ (ppm) 7.93 (t, *J* = 7.8 Hz, 2H, **2** & **12**), 7.58 (t, *J* = 7.3 Hz, 1H, **13**), 7.41 (t, *J* = 7.7 Hz, 1H, **1**), 4.17 (br s, 3H, **14** & **15**), 3.10 (t, *J* = 5.9 Hz, 2H, **9**), 2.85 (t, *J* = 5.8 Hz, 2H, **6**), 2.28 (s, 1H, **17**), 1.98-1.87 (m, 4H, **7** & **8**).

^{13}C NMR (101 MHz, $CDCl_3$) δ (ppm) 159.10 (**10**), 149.44 (**4**), 147.51 (**11**), 129.11 (**13**), 128.63 (**12**), 124.65 (**1**), 122.48 (**2**), 121.09 (**3**), 119.06 (**5**), 81.35 (**16**), 72.70 (**17**), 38.64 (**15**), 34.23 (**9**), 24.92 (**6**), 23.12 (**8**), 22.91 (**7**).

LRMS (ESI$^+$) *m/z* 237.0 $[M+H]^+$.

HRMS (ESI$^+$) *m/z* calcd for $C_{16}H_{17}N_2$ $[M+H]^+$, 237.1386, found 237.1383 Da.

Methyl 3-(benzyloxy)-6-(3-((1,2,3,4-tetrahydroacridin-9-yl)amino)prop-1-yn-1-yl)picolinate (**2.74**)

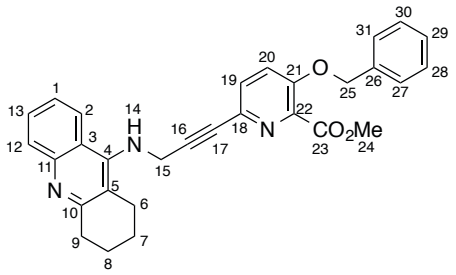

$C_{30}H_{27}N_3O_3$

MW: 477.56 g.mol^{-1}

Following the procedure described for the Sonogashira coupling to form compound **2.49**, acetylene **2.74** was obtained using terminal alkyne **2.73** (0.150 g, 0.635 mmol, 1.0 equiv), methyl 3-benzyloxy-6-bromopicolinate **2.10** (0.225 g, 0.698 mmol, 1.1 equiv), $Pd[PPh_3]_4$ (0.073 g, 0.064 mmol, 0.1 equiv), CuI (0.024 g, 0.128 mmol, 0.2 equiv), THF (6 mL) and Et_3N (3 mL). The crude product was purified by column chromatography (silica gel, EtOAc/MeOH 98:2 to 9:1) to afford **2.74** as yellow wax (0.285 g, 0.597 mmol, 94%).

TLC Rf 0.23 (EtOAc/MeOH 9:1).

IR (neat) ν_{max} 3367 (w), 2935 (m), 2870 (m), 2233 (w), 1732 (s), 1562 (m), 1496 (m), 1450 (m), 1434 (m), 1380 (w), 1293 (m), 1268 (m), 1207 (s), 1095 (s) cm^{-1}.

^{1}H NMR (400 MHz, $CDCl_3$) δ (ppm) 7.94 (t, *J* = 7.2 Hz, 2H, **2** & **12**), 7.55 (t, *J* = 7.2 Hz, 1H, **13**), 7.42-7.27 (m, 6H, **1**, **27**, **28**, **29**, **30** & **31**), 7.23-7.17 (m, 2H, **19** & **20**), 5.14 (s, 2H, **25**), 4.33 (d, *J* = 5.3 Hz, 2H, **15**), 4.25-4.22 (m, 1H, **14**), 3.92 (s, 3H, **24**), 3.06 (m, 2H, **9**), 2.83 (m, 2H, **6**), 1.87 (m, 4H, **7** & **8**).

^{13}C NMR (101 MHz, $CDCl_3$) δ (ppm) 164.70 (**23**), 159.05 (**10**), 153.36 (**21**), 149.31 (**4**), 147.42 (**11**), 140.37 (**22**), 135.35 (**18**), 134.12 (**26**), 130.12 (**19**), 128.94 (**13**), 128.78 (2C, **28** & **30**), 128.51 (**12**), 128.32 (**29**), 126.92 (2C, **27** & **31**), 124.56 (**1**), 122.52 (**2**), 121.64 (**20**), 121.31 (**3**), 119.31 (**5**), 86.32 (**16**), 82.93 (**17**), 70.85 (**25**), 52.75 (**24**), 39.23 (**15**), 34.16 (**9**), 24.89 (**6**), 22.97 (**8**), 22.79 (**7**).

LRMS (ESI$^+$) *m/z* 478.0 $[M+H]^+$.

HRMS (ESI$^+$) *m/z* calcd for $C_{30}H_{28}N_3O_3$ $[M+H]^+$, 478.2125, found 478.2127 Da.

Methyl 3-(benzyloxy)-6-(3-((7-chloro-1,2,3,4-tetrahydroacridin-9-yl)amino)prop-1-yn-1-yl)picolinate (**2.74b**)

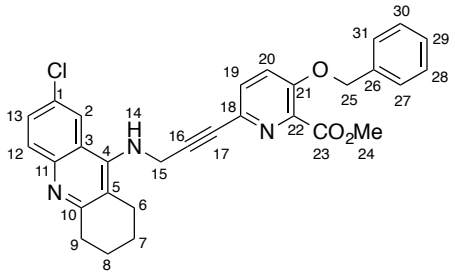

$C_{30}H_{26}ClN_3O_3$

MW: 512.01 g.mol^{-1}

Following the procedure described for the Sonogashira coupling to form compound **2.49**, acetylene **2.74b** was obtained using terminal alkyne **2.36** (0.080 g, 0.295 mmol, 1.0 equiv), methyl 3-benzyloxy-6-bromopicolinate (0.105 g, 0.325 mmol, 1.1 equiv), $Pd[PPh_3]_4$ (0.034 g, 0.030 mmol, 0.1 equiv), CuI (0.011 g, 0.059 mmol, 0.2 equiv), THF (5 mL) and Et_3N (2.5 mL). The crude product was purified by column chromatography (silica gel, EtOAc) to afford **2.74b** as yellow wax (0.107 g, 0.209 mmol, 71%).

TLC Rf 0.28 (EtOAc).

IR (neat) ν_{max} 3352 (m), 3064 (w), 2936 (s), 2861 (m), 2171 (w), 1732 (s), 1581 (m), 1560 (m), 1486 (m), 1451 (s), 1436 (s), 1382 (m), 1330 (m), 1293 (s), 1269 (s), 1211 (s), 1099 (s) cm^{-1}.

^{1}H NMR (400 MHz, $CDCl_3$) δ (ppm) 7.97 (d, *J* = 2.0 Hz, 1H, **2**), 7.89 (d, *J* = 8.9 Hz, 1H, **12**), 7.67 (dd, *J* = 8.9, 2.0 Hz, 1H, **13**), 7.55-7.28 (m, 7H, **19**, **20**, **27**, **28**, **29**, **30** & **31**), 5.20 (s, 2H, **25**), 4.34 (d, *J* = 6.5 Hz, 2H, **15**), 4.20-4.13 (m, 1H, **14**), 3.96 (s, 3H, **24**), 3.07 (t, *J* = 5.8 Hz, 2H, **9**), 2.87 (t, *J* = 5.3 Hz, 2H, **6**), 1.96-1.86 (m, 4H, **7** & **8**).

^{13}C NMR (101 MHz, $CDCl_3$) δ (ppm) 164.78 (**24**), 159.65 (**10**), 153.58 (**21**), 140.60 (**22**), 135.46 (**4**), 134.14 (**11**), 132.31 (**18**), 132.20 (**26**), 130.79 (**1**), 130.44 (**19**), 130.24 (**13**), 129.51 (**12**), 128.94 (2C, **28** & **32**), 128.71 (**3**), 128.59 (**5**), 128.49 (**29**), 127.05 (2C, **27** & **31**), 121.82 (**2**), 121.77 (**20**), 86.05 (**16**), 83.32 (**17**), 71.04 (**25**), 52.90 (**24**), 39.42 (**15**), 34.27 (**9**), 24.98 (**6**), 22.95 (**8**), 22.79 (**7**).

LRMS (ESI$^+$) *m/z* 512.0 [M^{35}Cl+H]$^+$, 514.0 [M^{37}Cl+H]$^+$.

HRMS (ESI$^+$) *m/z* calcd for $C_{30}H_{27}{}^{35}ClN_3O_3$ [M+H]$^+$, 512.1735, found 512.1739 Da.

Methyl 3-hydroxy-6-(3-((1,2,3,4-tetrahydroacridin-9-yl)amino)propyl)picolinate (**2.75**)

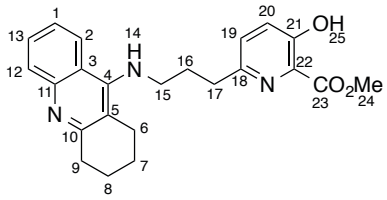

$C_{23}H_{25}N_3O_3$

MW: 391.47 g.mol^{-1}

2.75 was obtained according to general procedures D using **2.74** (0.100 g, 0.209 mmol, 1.0 equiv), $Pd(OH)_2/C$ (20% wt. with 50% moisture, 0.088 g, 0.060 mmol, 0.3 equiv) and MeOH (2.1 mL). The crude product was purified by column chromatography (silica gel, CH_2Cl_2/MeOH 9:1) to afford **2.75** as a white solid (0.079 g, 0.203 mmol, 97%).

TLC Rf 0.40 (CH_2Cl_2/MeOH 9:1).

MP 108–110 °C (hexane).

IR (neat) ν_{max} 3243 (m), 3044 (w), 2923 (m), 2845 (m), 1728 (w), 1672 (s), 1635 (m), 1575 (s), 1523 (m), 1466 (s), 1445 (s), 1363 (m), 1329 (m), 1307 (m), 1211 (s), 1102 (m) cm^{-1}.

^{1}H NMR (400 MHz, $CDCl_3$) δ (ppm) 10.54 (br s, 1H, **25**), 8.48 (t, *J* = 6.2 Hz, 1H, **12**), 8.24 (d, *J* = 8.7 Hz, 1H, **2**), 7.64 (t, *J* = 7.5 Hz, 1H, **13**), 7.43-7.28 (m, 3H, **1**, **19** & **20**), 6.82 (br s, 1H, **14**), 4.03-3.92 (m, 5H, **15** & **24**), 3.28 (m, 2H, **9**), 2.92 (t, *J* = 7.0 Hz, 2H, **17**), 2.77-2.55 (m, 2H, **6**), 2.22 (quin, *J* = 6.5 Hz, 2H, **16**), 1.95-1.76 (m, 4H, **7** & **8**).

^{13}C NMR (101 MHz, $CDCl_3$) δ (ppm) 169.80 (**23**), 157.57 (**18**), 155.46 (**10**), 151.97 (**21**), 139.93 (**4**), 139.28 (**11**), 132.07 (**13**), 129.75 (**19**), 128.94 (**22**), 127.40 (**12**), 125.20 (**20**), 123.93 (**1**), 121.49 (**2**), 116.49 (**3**), 111.35 (**5**), 53.26 (**24**), 46.78 (**16**), 33.80 (**17**), 30.21 (**9**), 28.91 (**16**), 24.46 (**6**), 22.25 (**7**), 20.90 (**8**).

LRMS (ESI$^+$) *m/z* 391.9 $[M+H]^+$.

HRMS (ESI$^+$) *m/z* calcd for $C_{23}H_{26}N_3O_3$ $[M+H]^+$, 392.1969, found 392.1969 Da.

3-Hydroxy-6-(3-((1,2,3,4-tetrahydroacridin-9-yl)amino)propyl)picolinaldehyde oxime (**2.76**)

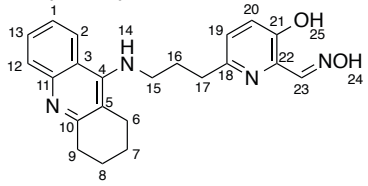

$C_{22}H_{24}N_4O_2$

MW: 376.46 g.mol^{-1}

Oxime **2.76** was obtained according to general procedures E, F and G using for procedure E, **2.75** (0.014 g, 0.037 mmol, 1.0 equiv), imidazole (0.010 g, 0.148 mmol, 4.0 equiv), TBSCl (0.012 g, 0.081 mmol, 2.2 equiv) in dry DMF (1.1 mL). The presence of the desired silylether was supported by TLC and LRMS (ESI$^+$, *m/z* 506.1 $[M+H]^+$). After drying *in vacuo*, the crude was subjected to procedure F using DIBAL-H (52 μL of a 1.0 M solution in CH_2Cl_2, 0.052 mmol, 2.0 equiv) in CH_2Cl_2 (1.0 mL). The presence of the desired silylether aldehyde was supported by analysis by TLC and LRMS (ESI$^+$, *m/z* 476.2 $[M+H]^+$). After drying *in vacuo*, the crude product was deprotected using TBAF (14 μL of a 1.0 M solution in THF, 0.014 mmol, 1.1 equiv) in THF (1.0 mL). The presence of the desired aldehyde was supported by TLC and LRMS (ESI$^+$, *m/z* 362.0 $[M+H]^+$). After drying *in vacuo*, the crude material was subjected to procedure G using hydroxylamine hydrochloride (0.002 g, 0.018 mmol, 1.5 equiv) and CH_3CO_2Na (0.002 g, 0.018 mmol, 1.5 equiv) in EtOH (1.0 mL). The crude oxime was purified by column chromatography (silica gel, CH_2Cl_2/MeOH 9:1) to afford **2.76** as yellow solid (0.004 g, 0.011 mmol, 27% over 4 steps).

TLC Rf 0.21 (CH_2Cl_2/MeOH 9:1).

IR (neat) ν_{max} 3355 (s), 2927 (s), 2855 (s), 1635 (s), 1574 (s), 1521 (m), 1465 (s), 1416 (w), 1360 (m), 1330 (m), 1272 (s), 1168 (m), 1019 (m) cm^{-1}.

^{1}H NMR (400 MHz, CD_3OD) δ (ppm) 8.28 (d, *J* = 8.4 Hz, 1H, **12**), 7.97 (s, 1H, **23**), 7.84-7.80 (m, 1H, **1**), 7.72 (d, *J* = 8.3 Hz, 1H, **2**), 7.51 (t, *J* = 7.7 Hz, 3H, **13**), 7.19 (d, *J* = 8.5 Hz, 1H, **20**), 7.11 (d, *J* = 8.5 Hz, 1H, **19**), 4.03 (t, *J* = 6.6 Hz, 2H, **15**), 3.01-2.93 (m, 2H, **9**), 2.85 (t, *J* = 6.9 Hz, 2H, **17**), 2.55-2.53 (m, 2H, **6**), 2.25 (quin, *J* = 6.7 Hz, 2H, **16**), 1.98 (br s, 1H, **14**), 1.96-1.87 (m, 4H, **7** & **8**).

^{13}C NMR (101 MHz, CD_3OD) δ (ppm) 157.98 (**10**), 153.75 (**18**), 153.11 (**21**), 152.65 (**23**), 151.41 (**4**), 139.72 (**11**), 136.41 (**18**), 134.01 (**13**), 126.49 (**19**), 126.17 (**20**), 125.97 (**12**), 125.47 (**1**), 120.02 (**2**), 116.98 (**3**), 112.74 (**5**), 48.38 (**15**), 34.97 (**17**), 30.68 (**9**), 29.20 (**6**), 24.84 (**16**), 22.88 (**7**), 21.75 (**8**).

LRMS (ESI$^+$) *m/z* 377.1 $[M+H]^+$.

HRMS (ESI$^+$) *m/z* calcd for $C_{22}H_{25}N_4O_2$ $[M+H]^+$, 377.1972, found 377.1970 Da.

2-Chloro-*N*-(prop-2-yn-1-yl)-7,8,9,10-tetrahydro-6*H*-cyclohepta[*b*]quinolin-11-amine (**2.77**)

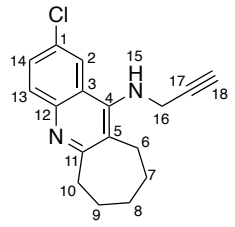

$C_{17}H_{17}ClN_2$

MW: 284.79 g.mol^{-1}

Terminal alkyne **2.77** was obtained according to general procedure C using **2.60** (0.100 g, 0.264 mmol, 1.0 equiv), $Pd_2(dba)_3$ (0.010 g, 0.011 mmol, 0.04 equiv), (±)-BINAP (0.015 g, 0.023 mmol, 0.08 equiv), Cs_2CO_3 (0.216 g, 0.660 mmol, 2.5 equiv), 1,4-dioxane (3.0 mL) and commercially available propargylamine (19 μL, 0.343 mmol, 1.3 equiv). The crude alkyne was purified by column chromatography (silica gel, Et_2O/hexane 1:1) to afford **2.77** as a yellow foam (0.063 g, 0.222 mmol, 84%).

TLC Rf 0.27 (Et_2O/hexane 1:1).

IR (neat) ν_{max} 3297 (m), 2920 (s), 2850 (m), 2207 (w), 1585 (s), 1562 (m), 1485 (s), 1438 (m), 1380 (m), 1331 (m), 1149 (m), 1080 (s) cm^{-1}.

^{1}H NMR (400 MHz, $CDCl_3$) δ (ppm) 7.90 (d, *J* = 2.2 Hz, 1H, **2**), 7.88 (d, *J* = 8.9 Hz, 1H, **13**), 7.52 (dd, *J* = 8.9, 2.2 Hz, 1H, **14**), 4.08-3.92 (m, 3H, **15** & **16**), 3.19-3.16 (m, 2H, **10**), 2.98-2.95 (m, 2H, **6**), 2.26 (t, *J* = 2.2 Hz, 1H, **18**), 1.92-1.86 (m, 2H, **9**), 1.82-1.72 (m, 4H, **7** & **8**).

^{13}C NMR (101 MHz, $CDCl_3$) δ (ppm) 165.85 (**11**), 147.16 (**4**), 145.48 (**12**), 131.13 (**1**), 131.04 (**14**), 129.28 (**13**), 127.60 (**3**), 123.63 (**5**), 121.67 (**2**), 80.16 (**17**), 73.03 (**18**), 40.34 (**16**), 39.53 (**10**), 32.02 (**8**), 28.52 (**6**), 27.75 (**9**), 26.93 (**7**).

LRMS (ESI$^+$) *m/z* 284.9 [M^{35}Cl+H]$^+$, 286.9 [M^{37}Cl+H]$^+$.

HRMS (ESI$^+$) *m/z* calcd for $C_{17}H_{18}{}^{35}ClN_2$ [M+H]$^+$, 285.1153, found 285.1160 Da.

N-(But-3-yn-1-yl)-2-chloro-7,8,9,10-tetrahydro-6*H*-cyclohepta[*b*]quinolin-11-amine (**2.78**)

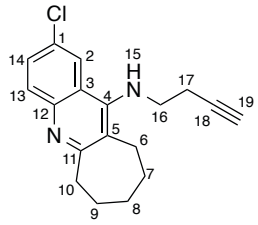

$C_{18}H_{19}ClN_2$

MW: 298.81 g.mol^{-1}

Terminal alkyne **2.78** was obtained according to general procedure C using **2.60** (0.100 g, 0.264 mmol, 1.0 equiv), $Pd_2(dba)_3$ (0.010 g, 0.011 mmol, 0.04 equiv), (±)-BINAP (0.015 g, 0.023 mmol, 0.08 equiv), Cs_2CO_3 (0.216 g, 0.660 mmol, 2.5 equiv), 1,4-dioxane (3.0 mL) and commercially available 1-amino-3-butyne (28 μL, 0.343 mmol, 1.3 equiv). The crude was purified by column chromatography (silica gel, Et_2O/hexane 1:1) to afford **2.78** as an off-white solid (0.073 g, 0.245 mmol, 93%).

TLC Rf 0.26 (Et_2O/hexane 1:1).

MP 97–98 °C (hexane).

IR (neat) ν_{max} 3300 (m), 2920 (s), 2850 (m), 2118 (w), 1585 (s), 1560 (s), 1485 (s), 1384 (m), 1346 (m), 1199 (w), 1150 (m), 1121 (m), 1082 (m) cm^{-1}.

^{1}H NMR (400 MHz, $CDCl_3$) δ (ppm) 7.99 (d, *J* = 2.2 Hz, 1H, **2**), 7.87 (d, *J* = 9.1Hz, 1H, **13**), 7.51 (dd, *J* = 9.1, 2.2 Hz, 1H, **14**), 4.14 (br s, 1H, **15**), 3.40 (q, *J* = 6.1 Hz, 2H, **16**), 3.24-3.09 (m, 2H, **10**), 3.05-2.87 (m, 2H, **6**), 2.45 (dt, *J* = 2.7, 6.1 Hz, 2H, **17**), 2.18 (t, *J* = 2.6 Hz, 1H, **19**), 1.94-1.83 (m, 2H, **9**), 1.83-1.94 (m, 4H, **7** & **8**).

^{13}C NMR (101 MHz, $CDCl_3$) δ (ppm) 165.82 (**11**), 147.87 (**4**), 145.46 (**12**), 130.96 (**14**), 130.79 (**1**), 129.12 (**13**), 126.67 (**3**), 123.62 (**5**), 121.67 (**2**), 81.86 (**18**), 71.09 (**19**), 48.67 (**16**), 40.27 (**10**), 32.03 (**8**), 28.37 (**6**), 27.63 (**9**), 26.92 (**7**), 20.68 (**17**).

LRMS (ESI$^+$) *m/z* 299.1 [M^{35}Cl+H]$^+$, 301.1 [M^{37}Cl+H]$^+$.

HRMS (ESI$^+$) *m/z* calcd for $C_{18}H_{20}{}^{35}ClN_2$ [M+H]$^+$, 299.1310, found 299.1307 Da.

Methyl 3-(benzyloxy)-6-(3-((2-chloro-7,8,9,10-tetrahydro-6*H*-cyclohepta[*b*]quinolin-11-yl)amino)prop-1-yn-1-yl)picolinate (**2.79**)

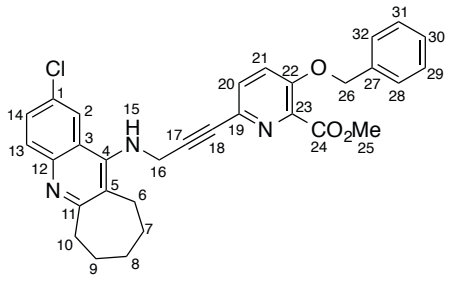

$C_{31}H_{28}ClN_3O_3$

MW: 526.03 g.mol^{-1}

Following the procedure described for the Sonogashira coupling to form compound **2.49**, acetylene **2.79** was obtained using terminal alkyne **2.77** (0.118 g, 0.310 mmol, 1.0 equiv), methyl 3-benzyloxy-6-bromopicolinate **2.10** (0.110 g, 0.341 mmol, 1.1 equiv), $Pd[PPh_3]_4$ (0.036 g, 0.031 mmol, 0.1 equiv), CuI (0.012 g, 0.062 mmol, 0.2 equiv), THF (6.0 mL) and Et_3N (3.0 mL). The crude acetylene was purified by column chromatography (silica gel, EtOAc/hexane 1:1) to afford **2.79** as yellow wax (0.145 g, 0.270 mmol, 87%).

TLC Rf 0.21 (EtOAc/hexane 1:1).

IR (neat) ν_{max} 3371 (w), 2920 (m), 2850 (m), 2233 (w), 1732 (s), 1585 (m), 1562 (m), 1485 (m), 1450 (s), 1435 (s), 1380 (w), 1292 (s), 1265 (s), 1208 (s), 1145 (m), 1095 (s) cm^{-1}.

^{1}H NMR (400 MHz, $CDCl_3$) δ (ppm) 7.99 (d, *J* = 2.1 Hz, 1H, **2**), 7.91 (d, *J* = 8.8 Hz, 1H, **13**), 7.53 (dd, *J* = 8.8, 2.1 Hz, 1H, **14**), 7.45-7.26 (m, 7H, **20**, **21**, **28**, **29**, **30**, **31** & **32**), 5.20 (s, 2H, **26**), 4.21 (d, *J* = 6.7, 2H, **16**), 3.96 (s, 3H, **25**), 3.20-3.17 (m, 2H, **10**), 3.02-2.99 (m, 2H, **6**), 1.88-1.86 (m, 2H, **9**), 1.80-1.74 (m, 4H, **7** & **8**).

^{13}C NMR (101 MHz, $CDCl_3$) δ (ppm) 165.89 (**24**), 164.71 (**11**), 153.46 (**22**), 147.19 (**4**), 145.41 (**12**), 140.38 (**23**), 135.41 (**19**), 134.13 (**27**), 131.12 (**1**), 130.99 (**20**), 130.13 (**14**), 129.24 (**13**), 128.85 (2C, **29** & **31**), 128.38 (**30**), 128.02 (**3**), 126.98 (2C, **28** & **32**), 123.87 (**5**), 121.74 (**2**), 121.68 (**21**), 86.21 (**18**), 83.40 (**17**), 70.92 (**26**), 52.83 (**25**), 40.30 (2C, **10** & **16**), 31.96 (**8**), 28.34 (**6**), 27.72 (**9**), 26.87 (**7**).

LRMS (ESI$^+$) *m/z* 526.0 $[M^{35}Cl+H]^+$, 528.0 $[M^{37}Cl+H]^+$.

HRMS (ESI$^+$) *m/z* calcd for $C_{31}H_{29}{}^{35}ClN_3O_3$ $[M+H]^+$, 529.1892, found 529.1893 Da.

Methyl 3-(benzyloxy)-6-(4-((2-chloro-7,8,9,10-tetrahydro-6*H*-cyclohepta[*b*] quinolin-11-yl)amino)but-1-yn-1-yl)picolinate (**2.80**)

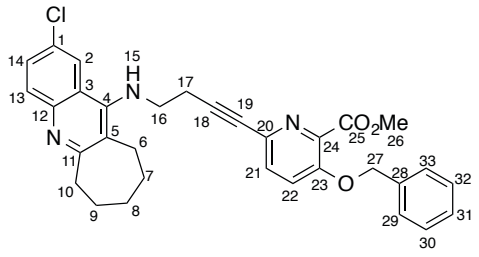

$C_{32}H_{30}ClN_3O_3$

MW: 540.06 g.mol^{-1}

Following the procedure described for the Sonogashira coupling to form compound **2.49**, acetylene **2.80** was obtained using terminal alkyne **2.78** (0.270 g, 0.904 mmol, 1.0 equiv), methyl 3-benzyloxy-6-bromopicolinate **2.10** (0.320 g, 0.994 mmol, 1.1 equiv), $Pd[PPh_3]_4$ (0.104 g, 0.090 mmol, 0.1 equiv), CuI (0.034 g, 0.181 mmol, 0.2 equiv), THF (10.0 mL) and Et_3N (5.0 mL). The crude acetylene was purified by column chromatography (silica gel, EtOAc/hexane 7:3) to afford **2.80** as yellow wax (0.465 g, 0.859 mmol, 95%).

TLC Rf 0.33 (EtOAc/hexane 7:3).

IR (neat) ν_{max} 3375 (w), 2922 (m), 2851 (m), 2229 (w), 1734 (s), 1585 (m), 1560 (m), 1487 (m), 1450 (s), 1435 (m), 1383 (m), 1292 (s), 1269 (s), 1209 (s), 1097 (s) cm^{-1}.

^{1}H NMR (400 MHz, $CDCl_3$) δ (ppm) 7.98 (d, *J* =2.1 Hz, 1H, **2**), 7.86 (d, *J* = 8.8 Hz, 1H, **13**), 7.49 (dd, *J* = 8.8, 2.1 Hz, 1H, **14**), 7.46-7.27 (m, 7H, **21**, **22**, **29**, **30**, **31**, **32** & **33**), 5.21 (s, 2H, **27**), 4.18 (br s, 1H, **15**), 3.96 (s, 3H, **26**), 3.56-3.42 (m, 2H, **16**), 3.24-3.06 (m, 2H, **10**), 3.03-2.90 (m, 2H, **6**), 2.66 (t, *J* = 6.1 Hz, 2H, **17**), 1.92-1.82 (m, 2H, **9**), 1.82-1.66 (m, 4H, **7** & **8**).

^{13}C NMR (101 MHz, $CDCl_3$) δ (ppm) 165.89 (**25**), 164.86 (**11**), 153.30 (**23**), 147.89 (**4**), 145.39 (**12**), 140.46 (**24**), 135.52 (**20**), 134.73 (**28**), 130.94 (**21**), 130.78 (**1**), 130.14 (**14**), 129.12 (**13**), 128.85 (2C, **30** & **32**), 128.37 (**31**), 127.01 (2C, **29** & **33**), 126.53 (**3**), 123.57 (**5**), 121.82 (**2**), 121.55 (**22**), 87.09 (**18**), 81.75 (**19**), 70.96 (**27**), 52.80 (**26**), 48.50 (**16**), 40.28 (**10**), 32.02 (**8**), 28.30 (**6**), 27.78 (**9**), 26.89 (**7**), 21.67 (**17**).

LRMS (ESI$^+$) *m/z* 540.1 $[M^{35}Cl+H]^+$, 542.1 $[M^{37}Cl+H]^+$.

HRMS (ESI$^+$) *m/z* calcd for $C_{32}H_{31}{}^{35}ClN_3O_3$ $[M+H]^+$, 540.2048, found 540.2049 Da.

Methyl 3-hydroxy-6-(3-((7,8,9,10-tetrahydro-6H-cyclohepta[b]quinolin-11-yl)amino)propyl) picolinate (**2.81**)

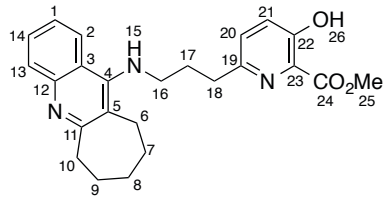

$C_{24}H_{27}N_3O_3$

MW: 405.50 g.mol^{-1}

2.81 was obtained according to general procedures D using **2.79** (0.100 g, 0.190 mmol, 1.0 equiv), $Pd(OH)_2/C$ (20% wt. with 50% moisture, 0.080 g, 0.057 mmol, 0.3 equiv) and EtOH (10 mL). The crude product was purified by column chromatography (silica gel, CH_2Cl_2/MeOH 9:1) to afford **2.81** as a white wax (0.069 g, 0.171 mmol, 90%).

TLC Rf 0.32 (CH_2Cl_2/MeOH 9:1).

IR (neat) ν_{max} 3297 (m), 2926 (m), 2854 (m), 1674 (s), 1634 (w), 1585 (s), 1566 (s), 1467 (s), 1445 (s), 1362 (m), 1302 (m), 1212 (s), 1101 (m) cm^{-1}.

^{1}H NMR (400 MHz, $CDCl_3$) δ (ppm) 10.46 (br s, 1H, **26**), 8.32 (d, *J* = 8.3 Hz, 1H, **2**), 8.22 (d, *J* = 8.6 Hz, 1H, **13**), 7.58 (t, *J* = 7.7 Hz, 1H, **14**), 7.38 (t, *J* = 7.7 Hz, 1H, **1**), 7.32-7.22 (m, 2H, **20** & **21**), 6.46 (br s, 1H, **15**), 3.95 (s, 3H, **25**), 3.62 (t, *J* = 6.7 Hz, 2H, **16**), 3.38-3.25 (m, 2H, **10**), 2.94-2.80 (m, 4H, **6** & **18**), 2.17 (quin, *J* = 7.0 Hz, 2H, **17**), 1.90- 1.74 (m, 4H, **7** & **9**), 1.70-1.57 (m, 2H, **8**).

^{13}C NMR (101 MHz, $CDCl_3$) δ (ppm) 169.87 (**24**), 161.26 (**11**), 157.44 (**19**), 153.82 (**4**), 152.35 (**22**), 140.48 (**12**), 130.76 (**23**), 129.60 (**14**), 128.88 (**20**), 127.19 (**13**), 125.69 (**1**), 123.66 (**21**), 122.91 (**2**), 119.33 (**3**), 118.92 (**5**), 53.22 (**25**), 48.12 (**16**), 35.71 (**18**), 34.17 (**10**), 31.53 (**8**), 30.48 (**6**), 27.61 (**9**), 27.42 (**17**), 26.24 (**7**).

LRMS (ESI$^+$) *m/z* 406.2 $[M+H]^+$.

HRMS (ESI$^+$) *m/z* calcd for $C_{24}H_{28}N_3O_3$ $[M+H]^+$, 406.2125, found 406.2127 Da.

Methyl 3-hydroxy-6-(4-((7,8,9,10-tetrahydro-6*H*-cyclohepta[*b*]quinolin-11-yl)amino)butyl)picolinate (**2.82**)

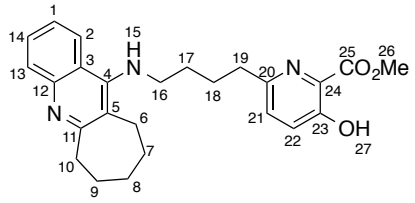

$C_{25}H_{29}N_3O_3$

MW: 419.53 g.mol^{-1}

2.82 was obtained according to general procedures D using **2.80** (0.060 g, 0.111 mmol, 1.0 equiv), $Pd(OH)_2/C$ (20% wt. with 50% moisture, 0.047 g, 0.033 mmol, 0.3 equiv) and EtOH (10 mL). The crude product was purified by column chromatography (silica gel, CH_2Cl_2/MeOH 9:1) to afford **2.82** as an off-white wax (0.042 g, 0.100 mmol, 90%).

TLC Rf 0.26 (CH_2Cl_2/MeOH 9:1).

IR (neat) ν_{max} 3336 (w), 2920 (s), 2852 (s), 1672 (s), 1585 (s), 1564 (s), 1498 (m), 1466 (s), 1442 (s), 1370 (m), 1298 (m), 1205 (s), 1099 (s) cm^{-1}.

^{1}H NMR (400 MHz, $CDCl_3$) δ (ppm) 10.60 (br s, 1H, **27**), 8.02 (d, *J* = 7.6 Hz, 1H, **2**), 7.89 (d, *J* = 8.3 Hz, 1H, **13**), 7.58 (dt, *J* = 7.6, 1.1 Hz, 1H, **14**), 7.40 (ddd, *J* = 8.4, 7.0, 1.2 Hz, 1H, **1**), 7.34-7.19 (m, 2H, **21** & **22**), 4.01 (s, 3H, **26**), 3.34 (t, *J* = 6.8 Hz, 2H, **16**), 3.27-3.13 (m, 2H, **10**), 2.96-2.86 (m, 2H, **6**), 2.82 (t, *J* = 7.6 Hz, 2H, **19**), 2.04-1.59 (m, 10H, **7**, **8**, **9**, **17** & **18**).

^{13}C NMR (101 MHz, $CDCl_3$) δ (ppm) 170.15 (**25**), 164.84 (**11**), 157.36 (**20**), 153.38 (**23**), 150.31 (**4**), 145.92 (**12**), 129.25 (**14**), 128.99 (**21**), 128.69 (**22**), 128.45 (**24**), 126.84 (**13**), 124.95 (**1**), 123.49 (**3**), 122.07 (**2**), 121.79 (**5**), 53.23 (**26**), 50.40 (**16**), 39.52 (**19**), 37.18 (**10**), 32.01 (**8**), 31.01 (**6**), 28.27 (**9**), 27.72 (**17**), 27.32 (**7**), 26.87 (**18**).

LRMS (ESI$^+$) *m/z* 420.0 $[M+H]^+$.

HRMS (ESI$^+$) *m/z* calcd for $C_{25}H_{30}N_3O_3$ $[M+H]^+$, 420.2282, found 420.2282 Da.

3-Hydroxy-6-(3-((7,8,9,10-tetrahydro-6*H*-cyclohepta[*b*]quinolin-11-yl)amino)propyl)-picolinaldehyde (**2.83**)

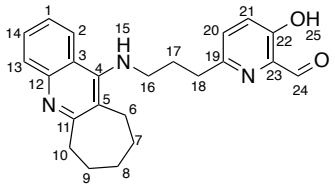

$C_{23}H_{25}N_3O_2$

MW: 375.47 g.mol^{-1}

Aldehyde **2.83** was obtained according to general procedures E and F using for procedure E, **2.81** (0.015 g, 0.037 mmol, 1.0 equiv), imidazole (0.010 g, 0.148 mmol, 4.0 equiv), TBSCl (0.012 g, 0.081 mmol, 2.2 equiv) in dry DMF (1.1 mL). The presence of the desired silylether was supported by TLC and LRMS (ESI$^+$, *m/z* 520.1 [M+H]$^+$). After drying *in vacuo*, the crude product was subjected to procedure F using DIBAL-H (62 μL of a 1.0 M solution in CH_2Cl_2, 0.062 mmol, 2.0 equiv) in CH_2Cl_2 (1.0 mL). The presence of the desired silylether aldehyde was supported by TLC and LRMS (ESI$^+$, *m/z* 490.1 [M+H]$^+$). After drying *in vacuo*, the crude material was deprotected using TBAF (30 μL of a 1.0 M solution in THF, 0.030 mmol, 1.1 equiv) in THF (1.0 mL). The crude aldehyde was purified by column chromatography (silica gel, CH_2Cl_2/MeOH 95:5 to 9:1) to afford **2.83** as a bright yellow wax (0.010 g, 0.027 mmol, 71% over 3 steps).

TLC Rf 0.30 (CH_2Cl_2/MeOH 9:1).

IR (neat) ν_{max} 3279 (w), 2922 (m), 2855 (m), 1660 (s), 1585 (s), 1566 (m), 1497 (w), 1464 (s), 1427 (s), 1348 (m), 1287 (m), 1154 (m) cm^{-1}.

^{1}H NMR (400 MHz, $CDCl_3$) δ (ppm) 10.01 (s, 1H, **24**), 8.16 (d, *J* = 8.2 Hz, 1H, **13**), 7.98 (d, *J* = 8.4 Hz, 1H, **2**), 7.60 (t, *J* = 7.6 Hz, 1H, **14**), 7.42 (d, *J* = 7.8 Hz, 1H, **1**), 7.29 (m, 2H, **20** & **21**), 3.51 (t, *J* = 6.7 Hz, 2H, **16**), 3.33-3.19 (m, 2H, **10**), 2.97-2.83 (m, 4H, **6** & **18**), 2.17 (quin, *J* = 7.1 Hz, 2H, **17**), 1.91-1.75 (m, 4H, **7** & **9**), 1.72-1.62 (m, 2H, **8**).

^{13}C NMR (101 MHz, $CDCl_3$) δ (ppm) 198.49 (**24**), 157.32 (**19**), 153.48 (**22**), 135.86 (**14**), 130.06 (**20**), 126.93 (**21**), 125.45 (**1**), 122.28 (**2** & **13**), 49.19 (**16**), 34.31 (**18**), 31.83 (**10**), 30.70 (**8**), 29.84 (**6**), 27.90 (**9**), 27.69 (**17**), 26.61 (**7**). Short run was made due to the stability of aldehyde, thus some quaternary carbons were not visible (**3**, **4**, **5**, **11**, **23** and **12**)

LRMS (ESI$^+$) *m/z* 375.9 [M+H]$^+$.

HRMS (ESI$^+$) *m/z* calcd for $C_{23}H_{26}N_3O_2$ [M+H]$^+$, 376.2021, found 376.2020 Da.

3-Hydroxy-6-(4-((7,8,9,10-tetrahydro-6*H*-cyclohepta[*b*]quinolin-11-yl)amino)butyl)-picolinaldehyde (**2.84**)

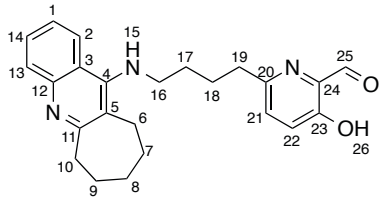

$C_{24}H_{27}N_3O_2$

MW: 389.50 g.mol^{-1}

Aldehyde **2.84** was obtained according to general procedures E and F using for procedure E, **2.82** (0.060 g, 0.143 mmol, 1.0 equiv), 2,6-lutidine (50 μL, 0.429 mmol, 3.0 equiv), TBSOTf (99 μL, 0.429 mmol, 3.0 equiv) in CH_2Cl_2 (1.5 mL). The presence of the desired silylether was supported by TLC and LRMS (ESI$^+$, *m/z* 534.2 $[M+H]^+$). After drying *in vacuo*, the crude product was subjected to procedure F using DIBAL-H (429 μL of a 1.0 M solution in CH_2Cl_2, 0.429 mmol, 3.0 equiv) in CH_2Cl_2 (1.5 mL). The crude aldehyde was purified by column chromatography (silica gel, CH_2Cl_2/MeOH 95:5 to 9:1) to afford **2.84** as a bright yellow wax (0.028 g, 0.072 mmol, 50% over 2 steps).

TLC Rf 0.27 (CH_2Cl_2/MeOH 9:1).

IR (neat) ν_{max} 3313 (w), 2922 (s), 2852 (s), 1660 (s), 1585 (s), 1568 (m), 1463 (s), 1284 (m), 1260 (m), 1153 (m), 1090 (m), 1018 (w) cm^{-1}.

^{1}H NMR (400 MHz, $CDCl_3$) δ (ppm) 9.99 (s, 1H, **25**), 8.13 (d, *J* = 8.3 Hz, 1H, **2**), 8.05-7.90 (m, 1H, **13**), 7.58 (t, *J* = 7.0 Hz, 1H, **14**), 7.41 (t, *J* = 7.7 Hz, 1H, **1**), 7.33-7.19 (m, 2H, **21** & **22**), 3.49 (t, *J* = 6.5 Hz, 2H, **16**), 3.33-3.14 (m, 2H, **10**), 2.92-2.85 (m, 2H, **6**), 2.81 (t, *J* = 7.1 Hz, 2H, **19**), 1.90-1.75 (m, 7H, **7a**, **9**, **17** & **18**), 1.75-1.53 (m, 3H, **7b** & **8**).

^{13}C NMR (101 MHz, $CDCl_3$) δ (ppm) 198.68 (**25**), 163.09 (**11**), 157.19 (**20**), 154.21 (**23**), 151.88 (**4**), 143.34 (**12**), 135.88 (**24**), 129.89 (**21**), 129.77 (**14**), 126.65 (**22**), 125.37 (**13**), 122.47 (**1**), 122.42 (**2**), 121.40 (**3**), 120.55 (**5**), 49.91 (**16**), 36.84 (**19**), 31.81 (**10**), 30.93 (**8**), 29.81 (**6**), 27.91 (**9**), 27.62 (**17**), 26.88 (**18**), 26.59 (**7**).

LRMS (ESI$^+$) *m/z* 390.1 $[M+H]^+$.

HRMS (ESI$^+$) *m/z* calcd for $C_{24}H_{28}N_3O_2$ $[M+H]^+$, 390.2176, found 390.2182 Da.

3-Hydroxy-6-(3-((7,8,9,10-tetrahydro-6*H*-cyclohepta[*b*]quinolin-11-yl)amino)propyl)-picolin aldehyde oxime (**2.85**)

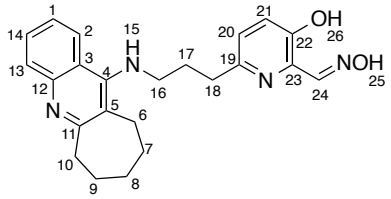

$C_{23}H_{26}N_4O_2$

MW: 390.49 g.mol^{-1}

Oxime **2.85** was obtained according to general procedures G using **2.83** (0.010 g, 0.027 mmol, 1.0 equiv), hydroxylamine hydrochloride (0.003 g, 0.041 mmol, 1.5 equiv) and CH_3CO_2Na (0.004 g, 0.041 mmol, 1.5 equiv) in EtOH (1.0 mL). The crude oxime was purified by column chromatography (silica gel, CH_2Cl_2/MeOH 9:1) to afford **2.85** as a bright yellow wax (0.009 g, 0.023 mmol, 87%).

TLC Rf 0.26 (CH_2Cl_2/MeOH 9:1).

IR (neat) ν_{max} 3275 (w), 2924 (s), 2854 (s), 1635 (m), 1585 (s), 1522 (m), 1466 (s), 1427 (m), 1272 (m), 1167 (w), 1022 (w) cm^{-1}.

^{1}H NMR (400 MHz, CD_3OD) δ (ppm) 8.23 (d, *J* = 8.6 Hz, 1H, **13**), 8.05 (s, 1H, **24**), 7.84-7.74 (m, 2H, **2** & **14**), 7.56 (m, 1H, **1**), 7.18 (d, *J* = 8.4 Hz, 1H, **21**), 7.06 (d, *J* = 8.4 Hz, 1H, **20**), 3.76 (t, *J* = 6.7 Hz, 2H, **16**), 3.21-3.05 (m, 2H, **10**), 2.96-2.86 (m, 2H, **6**), 2.82 (t, *J* = 7.0 Hz, 2H, **18**), 2.26-2.15 (m, 2H, **17**), 1.98-1.87 (m, 3H, **15** & **7**), 1.83-1.81 (m, 2H, **7**), 1.69-1.57 (m, 2H, **8**).

^{13}C NMR (101 MHz, CD_3OD) δ (ppm) 160.60 (**11**), 157.47 (**19**), 153.96 (**22**), 153.20 (**4**), 152.86 (**24**), 139.60 (**12**), 136.62 (**23**), 133.46 (**14**), 127.21 (**13**), 126.09 (**1**), 125.56 (**20**), 125.12 (**21**), 121.45 (**2**), 119.40 (**3**), 118.54 (**5**), 35.85 (**16**), 34.89 (**10**), 32.41 (**8**), 31.34 (**18**), 31.05 (**17**), 28.20 (**6**), 28.06 (**9**), 27.10 (**7**).

LRMS (ESI$^+$) *m/z* 391.2 [M+H]$^+$.

HRMS (ESI$^+$) *m/z* calcd for $C_{23}H_{27}N_4O_2$ [M+H]$^+$, 391.2129, found 391.2136 Da.

3-Hydroxy-6-(4-((7,8,9,10-tetrahydro-6*H*-cyclohepta[*b*]quinolin-11-yl)amino)butyl)-picolinaldehyde oxime (**2.86**)

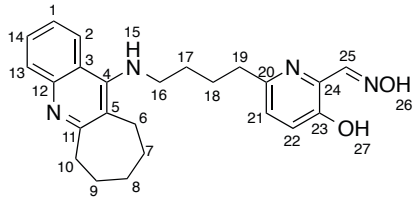

$C_{24}H_{28}N_4O_2$

MW: 404.51 g.mol^{-1}

Oxime **2.86** was obtained according to general procedures G using **2.84** (0.020 g, 0.051 mmol, 1.0 equiv), hydroxylamine hydrochloride (0.005 g, 0.077 mmol, 1.5 equiv) and CH_3CO_2Na (0.006 g, 0.077 mmol, 1.5 equiv) in EtOH (1.0 mL). The crude oxime was purified by column chromatography (silica gel, CH_2Cl_2/MeOH 9:1) to afford **2.86** as a bright yellow wax (0.015 g, 0.037 mmol, 73%).

TLC Rf 0.19 (CH_2Cl_2/MeOH 9:1).

IR (neat) ν_{max} 3269 (m), 2924 (s), 2854 (s), 1633 (m), 1583 (s), 1518 (m), 1462 (s), 1427 (s), 1354 (m), 1269 (s), 1198 (m), 1165 (m), 1119 (m), 1022 (m) cm^{-1}.

^{1}H NMR (400 MHz, CD_3OD) δ (ppm) 8.25 (d, *J* = 8.6 Hz, 1H, **2**), 8.13 (s, 1H, **25**), 7.82-7.76 (m, 2H, **13** & **14**), 7.59-7.54 (m, 1H, **1**), 7.18 (d, *J* = 8.4 Hz, 1H, **22**), 7.06 (d, *J* = 8.4 Hz, 1H, **21**), 3.73 (t, *J* = 6.5 Hz, 2H, **16**), 3.18-3.10 (m, 2H, **10**), 2.95-2.93 (m, 2H, **6**), 2.72 (t, *J* = 6.7 Hz, 2H, **19**), 1.99-1.88 (m, 3H, **17** & **18a**), 1.85-1.66 (m, 7H, **7**, **8**, **9** & **18b**).

^{13}C NMR (101 MHz, CD_3OD) δ (ppm) 160.51 (**11**), 156.95 (**20**), 154.10 (**23**), 153.72 (**4**), 152.75 (**25**), 139.92 (**12**), 136.29 (**24**), 133.17 (**14**), 126.98 (**22**), 125.89 (**13**), 125.36 (**21**), 125.19 (**1**), 121.66 (**2**), 119.38 (**3**), 119.00 (**5**), 49.85 (**16**), 37.12 (**19**), 35.82 (**10**), 32.30 (**8**), 30.92 (**6**), 28.05 (**17**), 27.86 (**9**), 27.62 (**7**), 27.00 (**18**).

LRMS (ESI$^+$) *m/z* 405.1 [M+H]$^+$.

HRMS (ESI$^+$) *m/z* calcd for $C_{24}H_{29}N_4O_2$ [M+H]$^+$, 405.2285, found 405.2278 Da.

Quinolin-4-yl trifluoromethanesulfonate (**3.4**)

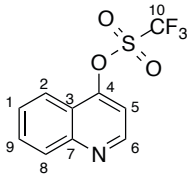

$C_{10}H_6F_3NO_3S$

MW: 277.22 g.mol^{-1}

Triflate **3.4** was obtained according to general procedure B using 4-quinolinol **3.3** (0.500 g, 3.444 mmol, 1.0 equiv), Et_3N (528 μL, 3.789 mmol, 1.1 equiv) and Tf_2O (637 μL, 3.789 mmol, 1.1 equiv) and CH_2Cl_2 (35 mL). The crude triflate was purified by column chromatography (silica gel, EtOAc/hexane 3:2 to 9:1) to afford **3.4** as a white solid (0.286 g, 1.033 mmol, 30%).

TLC Rf 0.71 (EtOAc/hexane 4:1).

MP 77–78 °C (hexane).

IR (neat) ν_{max} 1603 (w), 1560 (w), 1500 (m), 1429 (s), 1392 (m), 1251 (m), 1215 (s), 1138 (s), 1072 (m), 1028 (m), 1009 (m) cm^{-1}.

^{1}H NMR (400 MHz, $CDCl_3$) δ (ppm) 8.99 (d, *J* = 5.0 Hz, 1H, **6**), 8.21 (d, *J* = 8.6 Hz, 1H, **2**), 8.09 (d, *J* = 8.3 Hz, 1H, **8**), 7.86 (t, *J* = 7.8 Hz, 1H, **9**), 7.72 (t, *J* = 7.7 Hz, 1H, **1**), 7.43 (d, *J* = 5.0 Hz, 1H, **5**).

^{13}C NMR (101 MHz, $CDCl_3$) δ (ppm) 152.97 (**4**), 150.74 (**6**), 150.63 (**7**), 131.25(**9**), 129.98 (**8**), 128.61 (**1**), 121.40 (**3**), 120.79 (**2**), 118.93 (q, *J* = 359.0 Hz, **10**), 111.98 (**9**).

^{19}F NMR (376 MHz, $CDCl_3$) δ (ppm) –73.26.

LRMS (ESI$^+$) *m/z* 278.0 $[M+H]^+$.

HRMS (ESI$^+$) *m/z* calcd for $C_{10}H_7F_3NO_3S$ $[M+H]^+$, 278.0093, found 278.0089 Da.

Methyl 3-(benzyloxy)-6-(4-(quinolin-4-ylamino)but-1-yn-1-yl)picolinate (**3.7**)

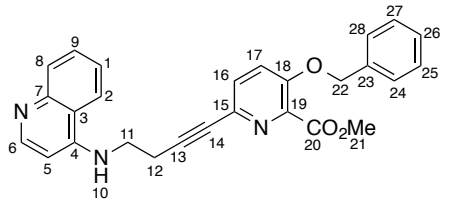

$C_{27}H_{23}N_3O_3$

MW: 437.50 g.mol^{-1}

Acetylene **3.7** was obtained according to general procedure C and Sonogashira coupling using for procedure C, 4-bromoquinoline **3.6** (0.143 g, 0.690 mmol, 1.0 equiv), $Pd_2(dba)_3$ (0.025 g, 0.028 mmol, 0.04 equiv), (±)-BINAP (0.037 g, 0.055 mmol, 0.08 equiv), Cs_2CO_3 (0.562 g, 1.725 mmol, 2.5 equiv), 1,4-dioxane (2.5 mL) and 1-amino-3-butyne (73 μL, 0.897 mmol, 1.3 equiv). After filtration through a small plug of silica, the crude was directly subjected to the subsequent procedure described for the Sonogashira coupling to form compound **2.49**, using methyl 3-benzyloxy-6-bromopicolinate **2.10** (0.244 g, 0.759 mmol, 1.1 equiv), $Pd[PPh_3]_4$ (0.079 g, 0.069 mmol, 0.1 equiv), CuI (0.026 g, 0.138 mmol, 0.2 equiv), THF (10 mL) and Et_3N (5 mL). The crude was purified by column chromatography (silica gel, CH_2Cl_2/MeOH 9:1) to afford **3.7** as an off-white foam (0.181 g, 0.414 mmol, 60% over 2 steps).

TLC Rf 0.30 (CH_2Cl_2/MeOH 8:2).

IR (neat) ν_{max} 3234 (m), 3034 (m), 2950 (m), 2881 (m), 2231 (w), 1733 (s), 1583 (s), 1451 (s), 1383 (m), 1341 (m), 1273 (s), 1211 (s), 1099 (s) cm^{-1}.

^{1}H NMR (400 MHz, $CDCl_3$) δ (ppm) 8.38 (d, *J* = 6.1 Hz, 1H, **6**), 8.33 (d, *J* = 8.3 Hz, 1H, **8**), 8.07 (d, *J* = 8.6 Hz, 1H, **2**), 7.66 (br s, 1H, **10**), 7.64 (t, *J* = 7.7 Hz, 1H, **9**), 7.49-7.26 (m, 8H, **1**, **16**, **17**, **24**, **25**, **26**, **27** & **28**), 6.54 (d, *J* = 6.4 Hz, 1H, **5**), 5.18 (s, 2H, **22**), 3.94 (s, 3H, **21**), 3.72 (q, *J* = 6.0 Hz, 2H, **11**), 2.89 (t, *J* = 6.9 Hz, 2H, **12**).

^{13}C NMR (101 MHz, $CDCl_3$) δ (ppm) 164.98 (**20**), 153.46 (**6**), 153.12 (**18**), 145.67 (**7**), 142.91 (**4**), 140.26 (**19**), 135.50 (**15**), 134.66 (**23**), 131.52 (**9**), 130.27 (**16**), 128.89 (2C, **25** & **27**), 128.45 (**26**), 127.06 (2C, **24** & **28**), 126.14 (**8**), 124.93 (**1**), 121.99 (**17**), 121.95 (**2**), 118.13 (**3**), 98.26 (**5**), 86.31 (**16**), 81.50 (**14**), 71.01 (**22**), 52.90 (**21**), 41.93 (**11**), 19.76 (**12**).

LRMS (ESI$^+$) *m/z* 438.0 [M+H]$^+$.

HRMS (ESI$^+$) *m/z* calcd for $C_{27}H_{24}N_3O_3$ [M+H]$^+$, 438.1812, found 438.1804 Da.

3-Hydroxy-6-(4-(quinolin-4-ylamino)butyl)picolinaldehyde (**3.8**)

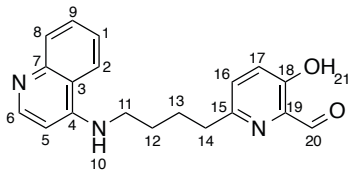

$C_{19}H_{19}N_3O_2$

MW: 321.38 g.mol^{-1}

Aldehyde **3.8** was obtained according to general procedures D, E and F using for procedure D, **3.7** (0.358 g, 0.820 mmol, 1.0 equiv), $Pd(OH)_2/C$ (20% wt. with 50% moisture, 0.230 g, 0.164 mmol, 0.2 equiv) and MeOH (60 mL). The presence of the desired phenolic alkane was supported by TLC and LRMS (ESI$^+$, *m/z* 351.9 $[M+H]^+$). After drying *in vacuo*, the crude product was subjected to procedure E using 2,6-lutidine (286 μL, 2.459 mmol, 3.0 equiv), TBSOTf (564 μL, 2.459 mmol, 3.0 equiv) in CH_2Cl_2 (8.2 mL). The presence of the desired silylether was supported by TLC and LRMS (ESI$^+$, *m/z* 466.1 $[M+H]^+$). After drying *in vacuo*, the crude material was subjected to procedure F using DIBAL-H (2.46 mL of a 1.0 M solution in CH_2Cl_2, 2.456 mmol, 3.0 equiv) in CH_2Cl_2 (8.2 mL). The crude product was purified by column chromatography (silica gel, CH_2Cl_2/MeOH 8:2) to afford **3.8** as a bright yellow wax (0.182 g, 0.566 mmol, 69% over 3 steps).

TLC Rf 0.14 (CH_2Cl_2/MeOH 8:2).

IR (neat) ν_{max} 3275 (b), 2924 (m), 2853 (m), 1668 (m), 1584 (s), 1457 (s), 1340 (m), 1223 (m), 1139 (m) cm^{-1}.

^{1}H NMR (400 MHz, $CDCl_3$) δ (ppm) 10.66 (br s, 1H, **21**), 10.04 (s, 1H, **20**), 8.56 (d, *J* = 4.9 Hz, 1H, **6**), 7.98 (d, *J* = 8.6 Hz, 1H, **8**), 7.74 (d, *J* = 8.1 Hz, 1H, **2**), 7.63 (t, *J* = 7.6 Hz, 1H, **9**), 7.42 (t, *J* = 7.5 Hz, 1H, **1**), 7.34-7.29 (m, 2H, **16** & **17**), 6.43 (d, *J* = 5.1 Hz, 1H, **5**), 5.07 (br s, 1H, **10**), 3.39 (q, *J* = 6.6 Hz, 2H, **11**), 2.90 (t, *J* = 7.5 Hz, 2H, **14**), 2.05-1.79 (m, 4H, **12** & **13**).

^{13}C NMR (101 MHz, $CDCl_3$) δ (ppm) 198.75 (**20**), 154.27 (**18**), 151.27 (**6**), 149.69 (**4**), 130.31 (**9**), 129.95 (**8**), 129.14 (**1**), 126.76 (**16**), 124.76 (**2**), 119.28 (**17**), 98.98 (**5**), 43.31 (**11**), 36.88 (**14**), 28.40 (**12**), 27.28 (**13**). Short run was made due to the stability of aldehyde, thus some quaternary carbons were not visible (**3**, **7**, **15** and **19**).

LRMS (ESI$^+$) *m/z* 322.0 $[M+H]^+$.

HRMS (ESI$^+$) *m/z* calcd for $C_{19}H_{20}N_3O_2$ $[M+H]^+$, 322.1550, found 322.1544 Da.

3-Hydroxy-6-(4-(quinolin-4-ylamino)butyl)picolinaldehyde oxime acetate (**3.1**)

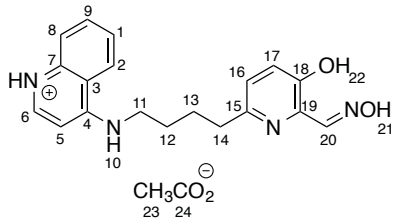

$C_{19}H_{20}N_4O_2$, MW: 336.40 g.mol^{-1}

$C_{19}H_{20}N_4O_2.C_2H_4O_2$, MW: 396.45 g.mol^{-1}

Oxime **3.1** was obtained according to general procedures G using **3.8** (0.102 g, 0.319 mmol, 1.0 equiv), hydroxylamine hydrochloride (0.033 g, 0.479 mmol, 1.5 equiv) and CH_3CO_2Na (0.039 g, 0.479 mmol, 1.5 equiv) in EtOH (10 mL). The crude oxime was purified by column chromatography (silica gel, CH_2Cl_2/MeOH 9:1) to afford **3.1** as a white solid (0.058 g, 0.172 mmol, 54%).

TLC Rf 0.13 (CH_2Cl_2/MeOH 8:2).

MP 197–198 °C (MeOH/hexane 2:3).

IR (neat) ν_{max} 3420 (w), 2928 (w), 2860 (w), 2570 (w, b), 1586 (s), 1538 (s), 1460 (m), 1347 (m), 1262 (s), 1037 (s) cm^{-1}.

^{1}H NMR (500 MHz, CD_3OD) δ (ppm) 8.33 (d, *J* = 6.5 Hz, 1H, **6**), 8.25 (dt, *J* = 8.5, 1.0 Hz, 1H, **8**), 8.23 (s, 1H, **20**), 7.83-7.79 (m, 2H, **2** & **9**), 7.63-7.56 (m, 1H, **1**), 7.25 (d, *J* = 8.5 Hz, 1H, **17**), 7.16 (d, *J* = 8.5 Hz, 1H, **16**), 6.69 (d, *J* = 6.6 Hz, 1H, **5**), 3.54 (t, *J* = 6.8 Hz, 2H, **11**), 2.81 (t, *J* = 7.2 Hz, 2H, **14**), 1.92 (s, 3H, **23**), 1.90-1.77 (m, 4H, **12** & **13**).

^{13}C NMR (126 MHz, CD_3OD) δ (ppm) 155.80 (**4**), 154.21 (**15**), 153.85 (**18**), 152.71 (**20**), 146.03 (**6**), 142.88 (**7**), 136.38 (**19**), 133.21 (**9**), 127.18 (**1**), 126.05 (**17**), 125.45 (**16**), 123.98 (**2**), 123.14 (**8**), 119.09 (**3**), 99.17 (**5**), 44.18 (**11**), 37.27 (**14**), 28.47 (**12**), 28.41 (**13**), 23.38 (**23**).

LRMS (ESI$^+$) *m/z* 337.1 [M+H]$^+$.

HRMS (ESI$^+$) *m/z* calcd for $C_{19}H_{21}N_4O_2$ [M+H]$^+$, 337.1659, found 337.1657 Da.

3-Hydroxy-6-(4-(quinolin-4-ylamino)butyl)picolinaldehyde oxime bis-acetate (**3.1b**)

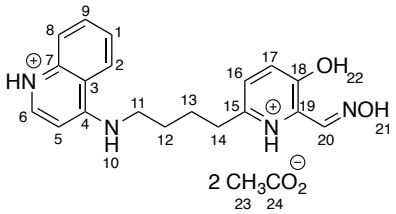

$C_{19}H_{20}N_4O_2$, MW: 336.40 g.mol^{-1}

$C_{19}H_{20}N_4O_2.C_4H_8O_4$, MW: 456.50 g.mol^{-1}

Oxime **3.1** (0.002 g, 0.006 mmol, 1.0 equiv) was dissolve in glacial AcOH (2.0 mL) for 10 min at rt. The solution was lyophilised to lead to the bis-acetate salt **3.1b**.

^{1}H NMR (500 MHz, CD_3OD) δ (ppm) 8.33 (d, *J* = 6.6 Hz, 1H, **6**), 8.29 (m, 1H, **8**), 8.21 (s, 1H, **20**), 7.89-7.85 (m, 1H, **9**), 7.83-7.81 (m, 1H, **2**), 7.64 (ddd, *J* = 8.4, 6.9, 1.4 Hz, 1H, **1**), 7.25 (d, *J* = 8.3 Hz, 1H, **17**), 7.16 (d, *J* = 8.3 Hz, 1H, **16**), 6.74 (d, *J* = 6.7 Hz, 1H, **5**), 3.57 (t, *J* = 6.8 Hz, 2H, **11**), 2.81 (t, *J* = 7.2 Hz, 2H, **14**), 1.93 (s, 6H, **23**), 1.90-1.81 (m, 4H, **12** & **13**).

^{13}C NMR (126 MHz, CD_3OD) δ (ppm) 156.56 (**4**), 154.15 (**15**), 153.84 (**18**), 152.68 (**20**), 144.77 (**6**), 136.39 (**19**), 133.88 (**9**), 127.58 (**1**), 126.05 (**17**), 125.46 (**16**), 123.37 (**2**), 122.80 (**8**), 118.80 (**3**), 99.17 (**5**), 44.30 (**11**), 37.23 (**14**), 28.39 (**12**), 28.34 (**13**), 23.02 (**23**).

N-(But-3-yn-1-yl)pyridin-4-amine (**3.12**)

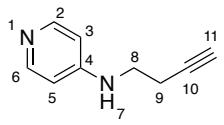

$C_9H_{10}N_2$

MW: 146.19 g.mol^{-1}

To a white suspension of the commercially available 4-bromopyridine hydrochloride (100 mg, 0.514 mmol, 1.0 equiv) in 1-pentanol (3 mL) was added dry Et_3N (143 μL, 1.028 mmol, 2.0 equiv). After few minutes, the white suspension turned to a colourless solution 1-amino-3-butyne (46 μL, 0.565 mmol, 1.1 equiv) was added at rt and the reaction mixture was stirred for 20 h at reflux. After completion, the reaction mixture was dissolved in CH_2Cl_2 (10 mL), washed with a saturated aqueous $NaHCO_3$ solution (10 mL), dried over anhydrous Na_2SO_4, filtered and concentrated under reduced pressure. The pale yellow solution was purified by column chromatography (neutral Al_2O_3, EtOAc/MeOH 98:2 to 9:1) to afford **3.12** as an impure yellow oil (30 mg, 0.206 mmol, 40%).

TLC Rf 0.15 (neutral Al_2O_3, EtOAc/MeOH 95:5).

^{1}H NMR (400 MHz, $CDCl_3$) δ (ppm) 8.18 (d, *J* = 5.4 Hz, 2H, **2** & **6**), 6.44 (d, *J* = 6.1 Hz, 2H, **3** & **5**), 4.67 (br s, 1H, **7**), 3.33 (q, *J* = 6.5 Hz, 2H, **8**), 2.49 (td, *J* = 6.6, 2.6 Hz, 2H, **9**), 2.04 (t, *J* = 2.6 Hz, 1H, **11**).

Methyl 3-(benzyloxy)-6-(4-(pyridin-4-ylamino)but-1-yn-1-yl)picolinate (**3.13**)

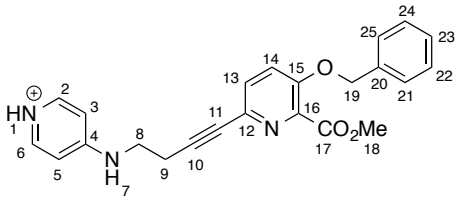

$C_{23}H_{22}N_3O_3$

MW: 388.45 g.mol^{-1}

Following the procedure described for the Sonogashira coupling to form compound **2.49**, acetylene **3.13** was obtained using terminal alkyne **3.12** (0.055 g, 0.376 mmol, 1.0 equiv), methyl 3-benzyloxy-6-bromopicolinate **2.10** (0.133 g, 0.414 mmol, 1.1 equiv), $Pd[PPh_3]_4$ (0.043 g, 0.038 mmol, 0.1 equiv), CuI (0.014 g, 0.075 mmol, 0.2 equiv), THF (4 mL) and Et_3N (2 mL). The crude acetylene was purified by column chromatography (neutral Al_2O_3, CH_2Cl_2/MeOH 98:2) to afford **3.13** as pale yellow wax (0.121 g, 0.312 mmol, 83%).

TLC Rf 0.19 (neutral Al_2O_3, CH_2Cl_2/MeOH 98:2).

IR (neat) ν_{max} 3234 (w), 3031 (w), 2950 (w), 2233 (w), 1732 (s), 1602 (s), 1523 (m), 1450 (m), 1293 (m), 1271 (m), 1212 (s), 1099 (m) cm^{-1}.

^{1}H NMR (400 MHz, $CDCl_3$) δ (ppm) 8.09 (br s, 2H, **2** & **6**), 7.44-7.28 (m, 7H, **13**, **14**, **21**, **22**, **23**, **24** & **25**), 6.48 (br s, 2H, **3** & **5**), 5.21 (s, 2H, **19**), 4.59 (br s, 1H, **7**), 3.96 (s, 3H, **18**), 3.43 (q, *J* = 6.5 Hz, 2H, **8**), 2.73 (t, *J* = 6.6 Hz, 2H, **9**), 2.25 (br s, 1H, **1**).

^{13}C NMR (101 MHz, $CDCl_3$) δ (ppm) 164.86 (**17**), 153.35 (2C, **4** & **15**), 150.17 (2C, **2** & **6**), 140.42 (**16**), 135.54 (**20**), 134.89 (**12**), 130.22 (**13**), 128.91 (2C, **22** & **24**), 128.45 (**23**), 127.05 (2C, **21** & **25**), 121.92 (**14**), 107.84 (2C, **3** & **5**), 86.63 (**10**), 81.25 (**11**), 71.04 (**19**), 52.88 (**18**), 41.14 (**8**), 20.12 (**9**).

LRMS (ESI$^+$) *m/z* 388.3 $[M+H]^+$.

HRMS (ESI$^+$) *m/z* calcd for $C_{23}H_{22}N_3O_3$ $[M+H]^+$, 388.1656, found 388.1661 Da.

3-Hydroxy-6-(4-(pyridin-4-ylamino)butyl)picolinaldehyde oxime (**3.2**)

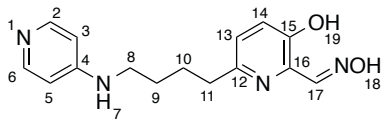

$C_{15}H_{18}N_4O_2$

MW: 286.34 g.mol^{-1}

Oxime **3.2** was obtained according to general procedures D, E, F and G using for procedure D, **3.13** (0.100 g, 0.258 mmol, 1.0 equiv), $Pd(OH)_2/C$ (20% wt. with 50% moisture, 0.036 g, 0.052 mmol, 0.2 equiv) and MeOH (10.0 mL). The presence of the desired phenolic alkane was supported by TLC and LRMS (ESI^+, *m/z* 302.3 $[M+H]^+$). After drying *in vacuo*, the crude was directly subjected to the subsequent procedure E using 2,6-lutidine (77 μL, 0.657 mmol, 3.0 equiv), TBSOTf (151 μL, 0.657 mmol, 3.0 equiv) in CH_2Cl_2 (11.0 mL). The presence of the desired silylether was supported by TLC and LRMS (ESI^+, *m/z* 416.3 $[M+H]^+$). After drying *in vacuo*, the crude was directly subjected to the subsequent procedure F using DIBAL-H (657 μL of a 1.0 M solution in CH_2Cl_2, 0.657 mmol, 3.0 equiv) in CH_2Cl_2 (8.5 mL). The presence of the desired aldehyde was supported by TLC and LRMS (ESI^+, *m/z* 272.1 $[M+H]^+$). After drying *in vacuo*, the crude was directly subjected to the subsequent procedure G using hydroxylamine hydrochloride (0.023 g, 0.329 mmol, 1.5 equiv) and CH_3CO_2Na (0.027 g, 0.329 mmol, 1.5 equiv) in EtOH (1.0 mL). Unfortunately, **3.2** has not been isolated.

3-Isopropoxy-4-methoxybenzaldehyde (**3.32**)

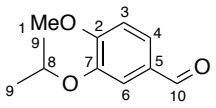

$C_{11}H_{14}O_3$

MW: 194.23 g.mol^{-1}

To a yellow suspension of the commercially available isovanillin (10.00 g, 65.90 mmol, 1.0 equiv) and anhydrous K_2CO_3 (18.20 g, 132.00 mmol, 2.0 equiv) in anhydrous DMF (50 mL), isopropyl bromide (47.5 mL, 506.00 mmol, 7.7 equiv) was added. The yellow reaction mixture gradually turned to pale yellow upon stirring at rt, and the reaction was completed within 48 h. The pale reaction mixture was poured into deionised water (150 mL), extracted with Et_2O (5 x 150 mL) and washed with a 5% aqueous NaOH solution (100 mL). The combined pale yellow organic solution was dried over anhydrous Na_2SO_4, filtered and concentrated *in vacuo*. The yellow oil crude product was purified by column chromatography (silica gel, petroleum ether/EtOAc 3:2) to afford **3.32** as an off-white crystalline solid (11.46 g, 59.00 mmol, 90%). Spectroscopic data were consistent with those reported in literature.[329]

TLC Rf 0.30 (petroleum ether/EtOAc 3:2).

MP 38–40 °C (hexane).

IR (neat) ν_{max} 3073 (w), 2973 (m), 2928 (w), 2842 (w), 1677 (s), 1579 (s), 1504 (s), 1130 (s), 1103 (s) cm^{-1}.

^{1}H NMR (400 MHz, $CDCl_3$) δ (ppm) 9.83 (s, 1H, **10**), 7.44 (dd, *J* = 8.0, 2.0 Hz, 1H, **4**), 7.41 (d, *J* = 2.0 Hz, 1H, **6**), 6.97 (d, *J* = 8.0 Hz, 1H, **3**), 4.63 (sept, *J* = 6.1 Hz, 1H, **8**), 3.93 (s, 3H, **1**), 1.39 (d, *J* = 6.1 Hz, 6H, **9**).

^{13}C NMR (101 MHz, $CDCl_3$) δ (ppm) 190.86 (**10**), 155.61 (**2**), 147.83 (**7**), 130.01 (**5**), 126.39 (**4**), 112.69 (**6**), 110.88 (**3**), 71.28 (**8**), 56.09 (**1**), 21.85 (2C, **9**).

LRMS (ESI$^+$) *m/z* 194.9 [M+H]$^+$.

2-Iodo-5-isopropoxy-4-methoxybenzaldehyde (**3.33**)

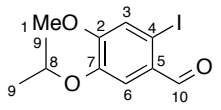

$C_{11}H_{13}IO_3$

MW: 320.12 g.mol^{-1}

To a stirred solution of **3.32** (1.900 g, 9.782 mmol, 1.0 equiv) in dried CH_2Cl_2 (66 mL), dried silver trifluoroacetate (2.485 g, 11.25 mmol, 1.1 equiv) was added. Iodine (2.855 g, 11.25 mmol, 1.1 equiv) was dissolved in dried CH_2Cl_2 (159 mL) and the purplish iodine solution was added dropwise at rt to the suspension over a period of 1 h. Upon addition, the reaction mixture gradually turned to yellow then reddish cloudy. The suspension was heated for 16 h at reflux. Upon completion, the reddish reaction mixture was filtered under suction with celite. The filtrate was washed with a saturated aqueous $Na_2S_2O_3$ solution (2 x 150 mL) and brine (2 x 150 mL), dried over anhydrous Na_2SO_4, filtered and concentrated under reduced pressure. The dark yellow crude iodide was purified by column chromatography (silica gel, hexane/EtOAc 9:1) to afford **3.33** as yellow solid (3.069 g, 9.583 mmol, 98%). Spectroscopic data were consistent with those reported in literature.[311]

TLC Rf 0.40 (hexane/EtOAc 9:1).

MP 74–76 °C (hexane).

IR (neat) ν_{max} 3073 (w), 2970 (m), 2929 (w), 2841 (m), 1676 (s), 1577 (s), 1503 (s), 1132 (s), 1108 (s) cm^{-1}.

^{1}H NMR (400 MHz, $CDCl_3$) δ (ppm) 9.86 (s, 1H, **10**), 7.42 (s, 1H, **6**), 7.31 (s, 1H, **3**), 4.63 (sept, *J* = 6.1 Hz, 1H, **8**), 3.93 (s, 3H, **1**), 1.38 (d, J = 6.1 Hz, 6H, **9**).

^{13}C NMR (101 MHz, $CDCl_3$) δ (ppm) 194.85 (**10**), 155.58 (**2**), 148.02 (**7**), 128.25 (**5**), 122.23 (**3**), 114.19 (**6**), 92.31 (**4**), 71.39 (**8**), 56.40 (**1**), 21.76 (2C, **9**).

LRMS (ESI$^+$) *m/z* 320.7 [M^{127}I+H]$^+$.

2-Iodo-5-isopropoxy-4-methoxybenzoic acid (**3.34**)

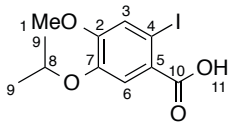

$C_{11}H_{13}IO_4$

MW: 336.12 g.mol^{-1}

To a stirred suspension of **3.33** (2.380 g, 7.434 mmol, 1.0 equiv), NaH_2PO_4 (0.446 g, 3.717 mmol, 0.5 equiv), and H_2O_2 (1.69 mL, of a 30% wt. solution in H_2O, 14.87 mmol, 2.0 equiv) in CH_3CN/H_2O (v/v, 20:1, 91 mL), was added a solution of $NaClO_2$ (1.210 g, 13.38 mmol, 1.8 equiv) in deionised H_2O (7 mL). The pale yellow reaction mixture was stirred for 6 h at 10 °C. The reaction mixture was quenched with a saturated aqueous $Na_2S_2O_3$ solution (30 mL) and washed water (60 mL). The crude was extracted with EtOAc (3 x 150 mL) and the combined organic solution was basified with an aqueous NaOH solution (1.0 M) to alkalinity (pH ~ 9). The extracted aqueous solution was re-acidified with an aqueous HCl solution (2.0 N) to pH 3, and the product was finally re-extracted with CH_2Cl_2 (3 x 75 mL), washed with brine (150 mL), dried over anhydrous Na_2SO_4, filtered and concentrated *in vacuo* to afford **3.34** as white solid (2.373 g, 7.062 mmol, 95%).

TLC Rf 0.21 (hexane/EtOAc 1:1).

MP 167–168 °C (hexane).

IR (neat) ν_{max} 3100-2400 (b), 3079 (w), 2977 (m), 2907 (m), 1692 (s), 1581 (s), 1506 (s), 1139 (s), 1107 (s) cm^{-1}.

^{1}H NMR (400 MHz, $CDCl_3$) δ (ppm) 7.66 (s, 1H, **3**), 7.44 (s, 1H, **6**), 4.59 (sept, J = 6.1 Hz, 1H, **8**), 3.91 (s, 3H, **1**), 1.39 (d, J = 6.1 Hz, 6H, **9**).

^{13}C NMR (101 MHz, $CDCl_3$) δ (ppm) 170.71 (**10**), 154.07 (**2**), 147.07 (**7**), 124.86 (**3**), 124.33 (**5**), 118.59 (**6**), 85.73 (**4**), 71.84 (**8**), 56.44 (**1**), 22.01 (2C, **9**).

LRMS (ESI$^+$) *m/z* 336.8 [M^{127}I+H]$^+$.

HRMS (ESI$^+$) *m/z* calcd for $C_{11}H_{13}{}^{127}INaO_4$ [M+Na]$^+$, 358.9751, found 358.9753 Da.

(3,4-Dihydroquinolin-1(2*H*)-yl)(2-iodo-5-isopropoxy-4-methoxyphenyl)methanone (**3.35**)

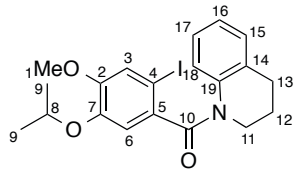

$C_{20}H_{22}INO_3$

MW: 451.30 g.mol^{-1}

To a stirred solution of **3.34** (3.150 g, 9.371 mmol, 1.0 equiv) in dried CH_2Cl_2 (150 mL), oxalyl chloride (0.952 ml, 11.25 mmol, 1.2 equiv) and few drops of anhydrous DMF were added slowly. The reaction was stirred for 30 min at rt. Upon completion, the reaction mixture was concentrated to dryness under reduced pressure. Then, the white residue was re-dissolved in dried CH_2Cl_2 (80 mL), followed by addition of dry Et_3N (1.44 mL, 10.31 mmol, 1.1 equiv) and tetrahydroquinoline (1.29 mL, 10.31 mmol, 1.1 equiv). The reaction mixture was stirred for 4 h at rt and turned from yellow to orange-red. Upon completion, the reaction mixture was concentrated to dryness under reduced pressure. The residue was diluted with CH_2Cl_2 (150 mL), extracted with an aqueous HCl (1.0 M) solution (2 x 100 mL), washed with brine (150 ml), dried over Na_2SO_4, filtered and concentrated under reduced pressure. The brown foamy crude was purified by column chromatography (silica gel, hexane/EtOAc 7:3) to afford **3.35** as an off-white foam (3.606 g, 7.990 mmol, 85%).

TLC Rf 0.47 (hexane/EtOAc 1:1).

MP 62–65 °C (hexane).

IR (neat) ν_{max} 3071 (w), 2973 (m), 2933 (m), 2838 (m), 1638 (s), 1582 (s), 1491 (s), 1147 (s), 1107 (s) cm^{-1}.

^{1}H NMR (500 MHz, DMSO-*d6*, 353 K) δ (ppm) 7.29 (s, 1H, **6**), 7.17 (m, 2H, **17** & **18**), 7.02-6.96 (m, 2H, **15** & **16**), 6.83 (s, 1H, **3**), 4.44 (sept, *J* = 6.1 Hz, 1H, **8**), 3.79 (s, 3H, **1**), 3.67 (t, *J* = 6.1 Hz, 2H, **11**), 2.84 (t, *J* = 6.1 Hz, 2H, **13**), 2.00 (quin, *J* = 6.1 Hz, 2H, **12**), 1.18 (d, *J* = 6.1 Hz, 6H, **9**).

^{13}C NMR (126 MHz, DMSO-*d6*, 353 K) δ (ppm) 168.16 (**10**), 150.74 (**2**), 146.70 (**7**), 137.82 (**5**), 134.84 (**19**), 131.05 (**14**), 128.03 (**15**), 124.89 (**17**), 123.96 (**16**), 123.69 (**3**), 122.29 (**18**), 116.02 (**6**), 82.27 (**4**), 70.89 (**8**), 55.83 (**1**), 44.26 (**11**), 25.96 (**13**), 22.82 (**12**), 21.22 (2C, **9**).

LRMS (ESI$^+$) *m/z* 451.8 [M^{127}I+H]$^+$, 903.0 [2M^{127}I+H]$^+$, 924.9 [2M^{127}I+Na]$^+$.

HRMS (ESI$^+$) *m/z* calcd for $C_{20}H_{23}{}^{127}INO_3$ [M+H]$^+$, 452.0717, found 452.0706 Da.
(ESI$^+$) *m/z* calcd for $C_{20}H_{22}{}^{127}INNaO_3$ [M+Na]$^+$, 474.0537, found 474.0525 Da.

10-Isopropoxy-11-methoxy-5,6-dihydropyrido[3,2,1-*de*]phenanthridin-8(4*H*)-one (**3.36**)

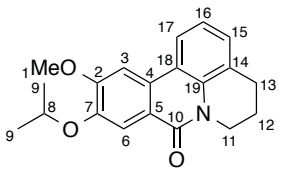

$C_{20}H_{21}NO_3$

MW: 323.39 g.mol^{-1}

18 microwave tubes containing a magnetic stirrer bar each were charged with $PdOAc_2$ (18 x 0.010 g, 0.797 mmol, 0.1 equiv), tri(o-tolyl)phosphine (18 x 0.027 g, 1.595 mmol, 0.2 equiv) and anhydrous K_2CO_3 (18 x 122 mg, 15.95 mmol, 2 equiv). Then a solution of **3.35** (18 x 0.200 g, 7.974 mmol, 1.0 equiv) in anhydrous DMF (18 x 4 mL) was added and each tubes were heated in the microwave reactor for 1 h at 100 °C. The black reaction mixtures obtained were combined and diluted with $CHCl_3$, followed by filtration under suction over celite. The filtrate was extracted with deionised water and $CHCl_3$. The combined organic solution was washed with brine, dried over anhydrous Na_2SO_4, filtered and concentrated to dryness under reduced pressure. The dark orange crude was purified by column chromatography (silica gel, hexane/EtOAc 7:3 to 1:1) followed by trituration with hexane. The pale orange solid was then filtered and washed with ice-cold Et_2O under suction to afford **3.36** as a white crystalline solid (2.243 g, 6.937 mmol, 87%). The product obtained was further recrystallised in CH_2Cl_2 for X-ray crystallography.

TLC Rf 0.26 (hexane/EtOAc 1:1).

MP 201–203 °C (Et_2O).

IR (neat) ν_{max} 3093 (w), 2971 (m), 2923 (m), 2839 (m), 1629 (s), 1588 (s), 1493 (s), 1141 (s), 1110 (s) cm^{-1}.

^{1}H NMR (400 MHz, $CDCl_3$) δ (ppm) 7.98 (dd, *J* = 7.8, 0.7 Hz, 1H, **17**), 7.95 (s, 1H, **3**), 7.59 (s, 1H, **6**), 7.24 (dd, *J* = 7.6, 0.7 Hz, 1H, **15**), 7.18 (dd, *J* = 7.8, 7.6 Hz, 1H, **16**), 4.82 (sept, *J* = 6.1 Hz, 1H, **8**), 4.33-4.30 (m, 2H, **11**), 4.06 (s, 3H, **1**), 3.00 (t, *J* = 6.1 Hz, 2H, **13**), 2.13 (quin, *J* = 6.1 Hz, 2H, **12**), 1.47 (d, *J* = 6.1 Hz, 6H, **9**).

^{13}C NMR (101 MHz, $CDCl_3$) δ (ppm) 160.65 (**10**), 154.04 (**2**), 148.10 (**7**), 133.97 (**19**), 128.35 (**16**), 127.99 (**5**), 125.53 (**14**), 121.61 (**15**), 120.56 (**17**), 119.36 (**18**), 119.01 (**7**), 111.23 (**3**), 103.04 (**6**), 71.03 (**8**), 56.07 (**1**), 42.67 (**11**), 28.24 (**13**), 21.86 (2C, **9**), 20.80 (**12**).

LRMS (ESI$^+$) *m/z* 324.0 [M+H]$^+$, 647.1 [2M+H]$^+$, 669.0 [2M+Na]$^+$, 992.5 [3M+Na]$^+$.

HRMS (ESI$^+$) *m/z* calcd for $C_{20}H_{22}NO_3$ $[M+H]^+$, 324.1594, found 324.1598 Da.
(ESI$^+$) *m/z* calcd for $C_{20}H_{21}NNaO_3$ $[M+Na]^+$, 346.1414, found 346.1417 Da.

X-ray crystal structure.

UNIVERSITY OF Southampton

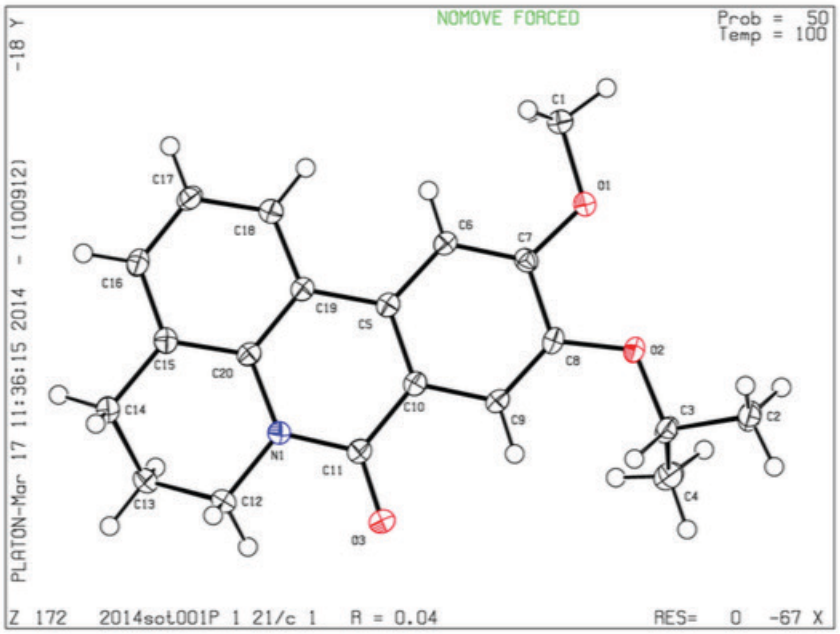

Crystal Data for $C_{20}H_{21}NO_3$ (M =323.39): monoclinic, space group $P2_1/c$ (no. 14), a = 13.168(3) Å, b = 8.042(2) Å, c = 15.372(4) Å, β = 100.476(4)°, V = 1600.7(7) Å^3, Z = 4, T = 100(2) K, μ(MoKα) = 0.090 mm^{-1}, *Dcalc* = 1.342 g/mm^3, 17324 reflections measured (5.39 ≤ 2Θ ≤ 55.07), 3660 unique (R_{int} = 0.0302, R_{sigma} = 0.0216) which were used in all calculations. The final R_1 was 0.0405 (I > 2σ(I)) and wR_2 was 0.1050 (all data).

Table 1 Crystal data and structure refinement for 2014sot0019.

Identification code	2014sot0019
Empirical formula	$C_{20}H_{21}NO_3$
Formula weight	323.39
Temperature/K	100(2)
Crystal system	monoclinic
Space group	$P2_1/c$
a/Å	13.168(3)
b/Å	8.042(2)
c/Å	15.372(4)
α/°	90
β/°	100.476(4)
γ/°	90
Volume/Å^3	1600.7(7)
Z	4
ϱ_{calc}mg/mm^3	1.342
m/mm^{-1}	0.090
F(000)	688.0
Crystal size/mm^3	0.25 × 0.1 × 0.06
Radiation	MoKα (λ = 0.71075)
2Θ range for data collection	5.39 to 55.07°
Index ranges	-17 ≤ h ≤ 13, -10 ≤ k ≤ 10, -18 ≤ l ≤ 19
Reflections collected	17324
Independent reflections	3660 [R_{int} = 0.0302, R_{sigma} = 0.0216]
Data/restraints/parameters	3660/0/220
Goodness-of-fit on F^2	1.050
Final R indexes [I>=2σ (I)]	R_1 = 0.0405, wR_2 = 0.1025
Final R indexes [all data]	R_1 = 0.0430, wR_2 = 0.1050
Largest diff. peak/hole / e Å^{-3}	0.34/-0.21

Table 2 Fractional Atomic Coordinates (×10^4) and Equivalent Isotropic Displacement Parameters (Å^2×10^3) for 2014sot0019. U_{eq} is defined as 1/3 of of the trace of the orthogonalised U_{IJ} tensor.

Atom	*x*	*y*	*z*	U(eq)
O1	1080.2(6)	377.5(10)	4572.5(5)	19.81(18)
O2	355.5(6)	1715(1)	3058.5(5)	18.92(18)
O3	3413.9(6)	4654.3(11)	2109.8(5)	23.9(2)
N1	4769.3(7)	4178.5(11)	3229.6(6)	15.83(19)
C20	5186.1(8)	3578.5(13)	4079.0(7)	15.1(2)
C11	3742.4(8)	4037.3(13)	2843.7(7)	16.8(2)
C10	3082.8(8)	3092.1(13)	3338.8(7)	15.2(2)
C15	6228.3(8)	3904.4(13)	4456.2(7)	16.9(2)
C5	3478.3(8)	2382.1(13)	4159.2(7)	15.1(2)
C18	4988.4(8)	2073.2(14)	5401.8(7)	18.2(2)
C7	1775.5(8)	1251.3(13)	4202.5(7)	16.2(2)

C6	2803.1(8)	1443.7(13)	4583.4(7)	15.9(2)
C8	1379.6(8)	1983.7(13)	3365.3(7)	16.1(2)
C9	2036.3(8)	2887.7(13)	2945.9(7)	16.0(2)
C19	4555.5(8)	2655.3(13)	4554.1(7)	15.2(2)
C12	5430.8(8)	5096.3(14)	2718.4(7)	18.9(2)
C1	1430.7(9)	-295.9(15)	5441.6(7)	22.0(2)
C17	6002.4(8)	2408.1(15)	5772.9(7)	19.6(2)
C14	6920.2(8)	4828.9(15)	3941.5(7)	19.9(2)
C16	6612.7(8)	3318.7(14)	5299.1(7)	18.7(2)
C2	-1257.4(8)	2604.6(15)	2279.3(8)	23.0(2)
C13	6543.9(8)	4519.5(14)	2962.2(7)	19.5(2)
C4	69.8(9)	1469.0(16)	1440.5(8)	25.2(3)
C3	-123.9(8)	2488.4(14)	2227.8(7)	19.2(2)

Table 3 Anisotropic Displacement Parameters ($Å^2×10^3$) for 2014sot0019. The Anisotropic displacement factor exponent takes the form: $-2\pi^2[h^2a^{*2}U_{11}+2hka^*b^*U_{12}+\ldots]$.

Atom	U_{11}	U_{22}	U_{33}	U_{23}	U_{13}	U_{12}
O1	15.0(4)	26.1(4)	17.9(4)	3.5(3)	2.0(3)	-3.7(3)
O2	13.4(4)	22.2(4)	19.5(4)	2.3(3)	-1.3(3)	-2.2(3)
O3	19.8(4)	31.3(5)	19.4(4)	8.1(3)	0.1(3)	-1.9(3)
N1	15.3(4)	17.5(4)	14.7(4)	0.4(3)	2.5(3)	-1.3(3)
C20	16.5(5)	14.9(5)	13.6(5)	-2.1(4)	2.1(4)	1.2(4)
C11	17.1(5)	16.6(5)	16.2(5)	-0.4(4)	1.8(4)	0.4(4)
C10	15.6(5)	14.3(5)	15.5(5)	-1.7(4)	1.9(4)	0.4(4)
C15	15.8(5)	17.5(5)	17.7(5)	-2.5(4)	3.5(4)	-0.2(4)
C5	15.6(5)	14.4(5)	15.0(5)	-2.3(4)	2.1(4)	1.0(4)
C18	17.0(5)	20.7(5)	17.0(5)	1.3(4)	3.2(4)	-0.3(4)
C7	17.0(5)	15.8(5)	16.1(5)	-1.3(4)	4.2(4)	-1.9(4)
C6	15.8(5)	16.9(5)	14.3(5)	-0.1(4)	1.2(4)	0.3(4)
C8	13.2(5)	16.3(5)	17.5(5)	-2.7(4)	-0.5(4)	0.6(4)
C9	15.8(5)	16.4(5)	14.8(5)	0.6(4)	0.0(4)	1.6(4)
C19	15.3(5)	15.3(5)	14.7(5)	-1.1(4)	2.2(4)	1.1(4)
C12	18.1(5)	21.6(5)	17.5(5)	3.4(4)	4.9(4)	-2.3(4)
C1	18.6(5)	30.3(6)	17.0(5)	4.4(4)	2.5(4)	-0.9(4)
C17	17.7(5)	25.6(6)	14.5(5)	0.9(4)	0.3(4)	2.0(4)
C14	16.0(5)	24.1(5)	19.3(5)	0.0(4)	2.7(4)	-2.7(4)
C16	14.2(5)	22.7(5)	18.4(5)	-2.9(4)	0.6(4)	0.1(4)
C2	15.8(5)	24.2(6)	26.9(6)	1.9(5)	-1.9(4)	-1.1(4)
C13	17.2(5)	23.0(5)	19.2(5)	1.4(4)	5.8(4)	-1.7(4)
C4	26.5(6)	25.3(6)	21.9(6)	1.3(5)	-0.4(5)	0.2(5)
C3	16.2(5)	18.2(5)	21.0(5)	2.3(4)	-2.6(4)	0.1(4)

Table 4 Bond Lengths for 2014sot0019.

Atom	Atom	Length/Å	Atom	Atom	Length/Å
O1	C7	1.3582(13)	C15	C16	1.3852(15)
O1	C1	1.4377(13)	C5	C6	1.4127(15)
O2	C8	1.3626(13)	C5	C19	1.4545(15)
O2	C3	1.4570(13)	C18	C19	1.4043(15)
O3	C11	1.2364(13)	C18	C17	1.3798(15)
N1	C20	1.4064(13)	C7	C6	1.3820(14)
N1	C11	1.3790(13)	C7	C8	1.4250(15)
N1	C12	1.4732(13)	C8	C9	1.3764(15)
C20	C15	1.4138(14)	C12	C13	1.5179(15)
C20	C19	1.4123(15)	C17	C16	1.3876(16)
C11	C10	1.4668(15)	C14	C13	1.5174(15)
C10	C5	1.3960(15)	C2	C3	1.5118(15)
C10	C9	1.4100(14)	C4	C3	1.5212(17)
C15	C14	1.5069(15)			

Table 5 Bond Angles for 2014sot0019.

Atom	Atom	Atom	Angle/°	Atom	Atom	Atom	Angle/°
C7	O1	C1	117.20(8)	C17	C18	C19	121.17(10)
C8	O2	C3	118.65(8)	O1	C7	C6	124.27(10)
C20	N1	C12	119.88(9)	O1	C7	C8	115.36(9)
C11	N1	C20	123.90(9)	C6	C7	C8	120.37(10)
C11	N1	C12	116.14(9)	C7	C6	C5	120.94(10)
N1	C20	C15	120.20(9)	O2	C8	C7	115.06(9)
N1	C20	C19	119.57(9)	O2	C8	C9	126.03(10)
C19	C20	C15	120.24(9)	C9	C8	C7	118.91(9)
O3	C11	N1	120.83(10)	C8	C9	C10	120.61(10)
O3	C11	C10	122.65(10)	C20	C19	C5	118.95(9)
N1	C11	C10	116.50(9)	C18	C19	C20	118.52(10)
C5	C10	C11	121.46(9)	C18	C19	C5	122.51(10)
C5	C10	C9	120.95(10)	N1	C12	C13	110.69(9)
C9	C10	C11	117.58(9)	C18	C17	C16	119.69(10)
C20	C15	C14	120.71(9)	C15	C14	C13	108.68(9)
C16	C15	C20	118.88(10)	C15	C16	C17	121.50(10)
C16	C15	C14	120.39(9)	C14	C13	C12	108.75(9)
C10	C5	C6	118.21(9)	O2	C3	C2	104.77(9)
C10	C5	C19	119.37(9)	O2	C3	C4	111.02(9)
C6	C5	C19	122.40(10)	C2	C3	C4	112.64(9)

Table 6 Torsion Angles for 2014sot0019.

A	B	C	D	Angle/°	A	B	C	D	Angle/°
O1	C7	C6	C5	-179.59(10)	C15	C14	C13	C12	58.30(12)
O1	C7	C8	O2	0.58(14)	C5	C10	C9	C8	0.15(16)
O1	C7	C8	C9	-179.89(9)	C18	C17	C16	C15	-0.05(17)
O2	C8	C9	C10	179.24(10)	C7	C8	C9	C10	-0.24(16)
O3	C11	C10	C5	178.78(10)	C6	C5	C19	C20	178.66(9)
O3	C11	C10	C9	0.38(16)	C6	C5	C19	C18	-3.07(16)
N1	C20	C15	C14	-2.76(15)	C6	C7	C8	O2	-179.75(9)
N1	C20	C15	C16	179.04(9)	C6	C7	C8	C9	-0.21(16)
N1	C20	C19	C5	-1.49(15)	C8	O2	C3	C2	-155.84(9)
N1	C20	C19	C18	-179.83(9)	C8	O2	C3	C4	82.31(12)
N1	C11	C10	C5	0.27(15)	C8	C7	C6	C5	0.76(16)
N1	C11	C10	C9	-178.14(9)	C9	C10	C5	C6	0.38(15)
N1	C12	C13	C14	-60.03(12)	C9	C10	C5	C19	-178.44(9)
C20	N1	C11	O3	176.83(10)	C19	C20	C15	C14	177.55(9)
C20	N1	C11	C10	-4.62(15)	C19	C20	C15	C16	-0.66(15)
C20	N1	C12	C13	29.43(13)	C19	C5	C6	C7	177.95(10)
C20	C15	C14	C13	-28.11(14)	C19	C18	C17	C16	-0.78(17)
C20	C15	C16	C17	0.76(16)	C12	N1	C20	C15	2.25(15)
C11	N1	C20	C15	-174.39(10)	C12	N1	C20	C19	-178.05(9)
C11	N1	C20	C19	5.31(15)	C12	N1	C11	O3	0.08(15)
C11	N1	C12	C13	-153.67(9)	C12	N1	C11	C10	178.62(9)
C11	C10	C5	C6	-177.97(9)	C1	O1	C7	C6	4.08(15)
C11	C10	C5	C19	3.20(15)	C1	O1	C7	C8	-176.26(9)
C11	C10	C9	C8	178.57(9)	C17	C18	C19	C20	0.86(16)
C10	C5	C6	C7	-0.84(15)	C17	C18	C19	C5	-177.42(10)
C10	C5	C19	C20	-2.57(15)	C14	C15	C16	C17	-177.45(10)
C10	C5	C19	C18	175.70(10)	C16	C15	C14	C13	150.07(10)
C15	C20	C19	C5	178.21(9)	C3	O2	C8	C7	177.01(9)
C15	C20	C19	C18	-0.13(15)	C3	O2	C8	C9	-2.49(15)

Table 7 Hydrogen Atom Coordinates (Å×10^4) and Isotropic Displacement Parameters (Å^2×10^3) for 2014sot0019.

Atom	*x*	*y*	*z*	U(eq)
H18	4584	1451	5719	22
H6	3054	948	5127	19
H9	1787	3368	2398	19
H12A	5392	6277	2837	23
H12B	5185	4920	2091	23
H1A	1960	-1107	5418	33
H1B	862	-813	5649	33
H1C	1704	583	5839	33
H17	6275	2025	6338	24
H14A	7626	4444	4113	24
H14B	6903	6010	4066	24
H16	7295	3541	5553	22
H2A	-1533	1507	2317	35
H2B	-1622	3150	1760	35
H2C	-1338	3231	2794	35
H13A	6590	3344	2833	23
H13B	6971	5126	2618	23
H4A	800	1322	1475	38
H4B	-213	2040	902	38
H4C	-255	402	1448	38
H3	158	3610	2193	23

10-Hydroxy-11-methoxy-5,6-dihydropyrido[3,2,1-*de*]phenanthridin-8(4*H*)-one (**3.26**)

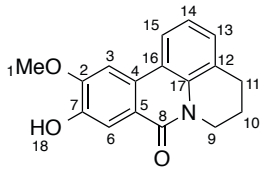

$C_{17}H_{15}NO_3$

MW: 281.31 g.mol^{-1}

To a stirred solution of **3.36** (1.870 g, 5.782 mmol, 1.0 equiv) in dried CH_2Cl_2 (250 mL), $AlCl_3$ (2.310 g, 17.35 mmol, 3.0 equiv) and ethanethiol (1.28 mL, 17.35 mmol, 3.0 equiv) were added. The reaction mixture was stirred for 2 h at rt. The initial white cloudy suspension turned successively from yellow, white to finally very pale orange. The reaction mixture was cooled with ice/salt bath, followed by quenching with ice-cold deionised water (200 mL) upon vigorous stirring. The organic solution was extracted with an aqueous HCl (1.0 M) solution (2 x 100 mL), washed with brine (2 x 100 mL), dried over anhydrous Na_2SO_4, filtered and concentrated under reduced pressure. The pale yellow crude was purified by column chromatography (silica gel, hexane/EtOAc 1:1 to 0:1) to afford **3.26** as an off-white solid (1.343 g, 4.774 mmol, 83%).

TLC Rf 0.25 (hexane/EtOAc 3:7).

MP 270–272 °C (hexane).

IR (neat) ν_{max} 3300-2700 (b), 3184 (w), 2967 (m), 1607 (s), 1567 (s), 1459 (s), 1132 (m) cm^{-1}.

^{1}H NMR (400 MHz, $CDCl_3$) δ (ppm) 9.82 (s, 1H, **18**), 8.22 (dd, *J* = 7.8, 0.9 Hz, 1H, **15**), 7.80 (s, 1H, **6**), 7.68 (s, 1H, **3**), 7.25 (dd, *J* = 7.4, 0.9 Hz, 1H, **13**), 7.16 (dd, *J* = 7.8, 7.4 Hz, 1H, **14**), 4.15-4.12 (m, 2H, **9**), 4.01 (s, 3H, **1**), 2.93 (t, *J* = 6.1 Hz, 2H, **11**), 2.00 (quin, *J* = 6.1 Hz, 2H, **10**).

^{13}C NMR (101 MHz, $CDCl_3$) δ (ppm) 159.36 (**8**), 152.54 (**2**), 147.57 (**7**), 133.27 (**17**), 128.10 (**13**), 126.80 (**5**), 125.23 (**11**), 121.46 (**14**), 121.16 (**15**), 118.85 (**4**), 118.56 (**16**), 112.04 (**6**), 104.02 (**3**), 55.94 (**1**), 42.09 (**9**), 27.46 (**11**), 20.33 (**10**).

LRMS (ESI$^+$) *m/z* 281.9 [M+H]$^+$, 563.0 [2M+H]$^+$, 584.9 [2M+Na]$^+$.

HRMS (ESI$^+$) *m/z* calcd for $C_{17}H_{16}NO_3$ [M+H]$^+$, 282.1125, found 282.1122 Da.
(ESI$^+$) *m/z* calcd for $C_{17}H_{15}NNaO_3$ [M+Na]$^+$, 304.0944, found 304.0936 Da.

Methyl 3-(benzyloxy)-6-(3-hydroxyprop-1-yn-1-yl)picolinate (**3.37**)

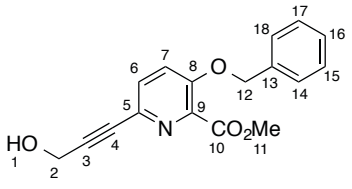

$C_{17}H_{15}NO_4$

MW: 297.31 g.mol^{-1}

Following the procedure described for the Sonogashira coupling to form compound **2.49**, acetylene **3.37** was obtained using propargyl alcohol (90 μL, 1.550 mmol, 1.0 equiv), methyl 3-benzyloxy-6-bromopicolinate **2.10** (0.500 g, 0.155 mmol, 1.0 equiv), $Pd[PPh_3]_4$ (0.090 g, 0.078 mmol, 0.05 equiv), CuI (0.030 g, 0.156 mmol, 0.1 equiv), CH_2Cl_2 (50 mL) and Et_3N (10 mL). The crude acetylene was purified by column chromatography (silica gel, hexane/EtOAc 1:1 to 2:3) to afford **3.37** as an off-white powder (0.433 g, 1.457 mmol, 94%).

TLC Rf 0.27 (hexane/EtOAc 2:3).

MP 132–134 °C (hexane).

IR (neat) ν_{max} 3379 (w), 2951 (w), 2174 (w), 1732 (s), 1564 (m), 1451 (s), 1383 (m), 1294 (s), 1270 (s), 1213 (s), 1147 (w), 1101 (s), 1042 (m) cm^{-1}.

^{1}H NMR (400 MHz, $CDCl_3$) δ (ppm) 7.49-7.27 (m, 7H, **6**, **7**, **14**, **15**, **16**, **17** & **18**), 5.22 (s, 2H, **12**), 4.48 (d, *J* = 6.4 Hz, 2H, **2**), 3.97 (s, 3H, **11**), 1.66 (t, *J* = 6.3 Hz, 1H, **1**).

^{13}C NMR (101 MHz, $CDCl_3$) δ (ppm) 164.76 (**10**), 153.62 (**8**), 140.54 (**9**), 135.49 (**5**), 134.31 (**13**), 130.29 (**6**), 128.94 (2C, **15** & **17**), 128.44 (**16**), 127.05 (2C, **14** & **18**), 121.81 (**7**), 86.99 (**3**), 84.16 (**4**), 71.04 (**12**), 52.91 (**11**), 51.86 (**2**).

LRMS (ESI$^+$) *m/z* 298.1 $[M+H]^+$.

HRMS (ESI$^+$) *m/z* calcd for $C_{17}H_{16}NO_4$ $[M+H]^+$, 298.1073, found 298.1071 Da.
(ESI$^+$) *m/z* calcd for $C_{17}H_{15}NNaO_4$ $[M+Na]^+$, 320.0893, found 320.0890 Da.

Methyl 3-(benzyloxy)-6-(4-hydroxybut-1-yn-1-yl)picolinate (**3.39**)

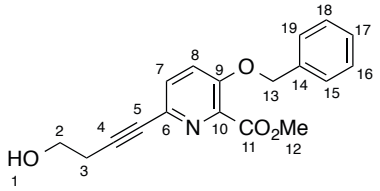

$C_{18}H_{17}NO_4$

MW: 311.34 g.mol^{-1}

Following the procedure described for the Sonogashira coupling to form compound **2.49**, acetylene **3.39** was obtained using 3-butyn-1-ol (65 µL, 0.856 mmol, 1.0 equiv), methyl 3-benzyloxy-6-bromopicolinate **2.10** (0.276 g, 0.856 mmol, 1.0 equiv), $Pd[PPh_3]_4$ (0.050 g, 0.043 mmol, 0.05 equiv), CuI (0.016 g, 0.086 mmol, 0.1 equiv), CH_2Cl_2 (12 mL) and Et_3N (6 mL). The crude acetylene was purified by column chromatography (silica gel, petroleum ether/EtOAc 1:1) to afford **3.39** as an off-white powder (0.261 g, 0.839 mmol, 98%). Spectroscopic data were consistent with those reported in literature[244]

TLC Rf 0.39 (petroleum ether/EtOAc 7:3).

MP 135–137 °C (hexane).

IR (neat) ν_{max} 3379 (s), 2951 (m), 2881 (m), 2233 (s), 1728 (s), 1562 (m), 1450 (s), 1380 (m), 1269 (s), 1207 (s), 1097 (s) cm^{-1}.

^{1}H NMR (400 MHz, $CDCl_3$) δ (ppm) 7.44-7.27 (m, 7H, **7**, **8**, **15**, **16**, **17**, **18** & **19**), 5.19 (s, 2H, **13**), 3.96 (s, 3H, **12**), 3.83 (t, *J* = 6.4 Hz, 2H, **2**), 3.06 (br s , 1H, **1**), 2.68 (t, *J* = 6.4 Hz, 2H, **3**).

^{13}C NMR (101 MHz, $CDCl_3$) δ (ppm) 164.78 (**11**), 153.17 (**9**), 139.96 (**10**), 135.50 (**6**), 135.08 (**14**), 130.14 (**7**), 128.79 (2C, **16** & **18**), 128.31 (**17**), 126.96 (2C, **15** & **19**), 121.94 (**8**), 87.36 (**4**), 80.66 (**5**), 70.90 (**13**), 60.75 (**2**), 52.77 (**12**), 23.80 (**3**).

LRMS (ESI$^+$) *m/z* 312.1 $[M+H]^+$.

HRMS (ESI$^+$) *m/z* calcd for $C_{18}H_{18}NO_4$ $[M+H]^+$, 312.1230, found 312.1228 Da.
(ESI$^+$) *m/z* calcd for $C_{18}H_{17}NNaO_4$ $[M+Na]^+$, 334.1049, found 334.1046 Da.

Methyl 3-(benzyloxy)-6-(3-((11-methoxy-8-oxo-5,6-dihydro-4*H*,8*H*-pyrido[3,2,1-*de*]phenanthridin-10-yl)oxy)prop-1-yn-1-yl)picolinate (**3.38**)

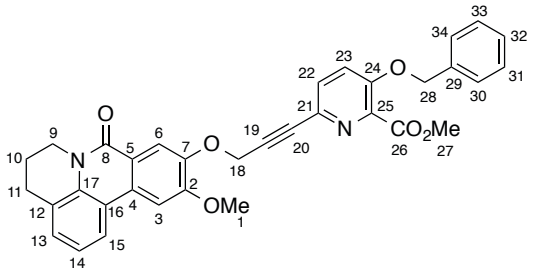

$C_{34}H_{28}N_2O_6$

MW: 560.61 g.mol^{-1}

Procedure 1: To a suspension of phenol **3.26** (0.050 g, 0.178 mmol, 1.0 equiv), acetylene **3.37** (0.053 g, 0.178 mmol, 1.0 equiv) and PPh_3 (0.047 g, 0.178 mmol, 1.0 equiv) in CH_2Cl_2 (1.0 mL), DIAD (35 μL, 0.178 mmol, 1.0 equiv) was added dropwise at 0 °C. Upon addition, the reaction mixture was warmed to rt and stirred overnight. Upon completion, the reaction mixture was quenched with an aqueous NaOH (0.5 M) solution (1 mL) and extracted with CH_2Cl_2. The combined organic solution was washed with an aqueous NaOH (0.5 M) solution (1 mL), H_2O (1 mL) and brine (1 mL), dried over anhydrous Na_2SO_4, filtered and concentrated under reduced pressure. The crude product was purified by column chromatography (silica gel, hexane/EtOAc 1:4) to afford **3.38** as white solid (0.051 g, 0.091 mmol, 51%).

TLC Rf 0.55 (hexane/EtOAc 1:4).

MP 225–227 °C (hexane).

IR (neat) ν_{max} 2947 (w), 2160 (w), 2040 (w), 1732 (s), 1632 (s), 1612 (s), 1589 (s), 1516 (s), 1454 (s), 1384 (s), 1335 (w), 1304 (s), 1265 (s), 1207 (s), 1130 (m), 1099 (s) cm^{-1}.

^{1}H NMR (400 MHz, $CDCl_3$) δ (ppm) 8.10 (s, 1H, **6**), 8.00 (d, *J* = 8.1 Hz, 1H, **15**), 7.62 (s, 1H, **3**), 7.52 (d, *J* = 8.7 Hz, 1H, **13**), 7.46-7.26 (m, 7H, **22**, **23**, **30**, **31**, **32**, **33** & **34**), 7.23-7.15 (m, 1H, **14**), 5.20 (s, 2H, **28**), 5.12 (s, 2H, **18**), 4.31 (t, *J* = 8.0 Hz, 2H, **9**), 4.08 (s, 3H, **27**), 3.95 (s, 3H, **1**), 3.02 (t, *J* = 6.1 Hz, 2H, **11**), 2.14 (quin, *J* = 5.9 Hz, 2H, **10**).

^{13}C NMR (101 MHz, $CDCl_3$) δ (ppm) 164.73 (**26**), 160.71 (**8**), 153.74 (**24**), 153.71 (**2**), 147.93 (**7**), 140.33 (**25**), 135.49 (**17**), 134.38 (**5**), 134.06 (**29**), 130.96 (**22**), 129.35 (**4**), 128.91 (2C, **31** & **33**), 128.88 (**13**), 128.41 (**32**), 127.03 (2C, **30** & **34**), 125.81 (**12**), 121.88 (**14**), 121.71 (**15**), 120.93 (**23**), 119.46 (**21**), 119.02 (**16**), 111.04 (**6**), 103.28 (**3**), 86.07 (**19**), 83.04 (**20**), 70.98 (**28**), 57.50 (**18**), 56.27 (**1**), 52.88 (**27**), 42.94 (**9**), 28.43 (**11**), 20.97 (**10**).

LRMS (ESI$^+$) *m/z* 561.2 $[M+H]^+$.

HRMS (ESI$^+$) *m/z* calcd for $C_{34}H_{29}N_2O_6$ $[M+H]^+$, 561.2020, found 561.2029 Da.
(ESI$^+$) *m/z* calcd for $C_{34}H_{28}N_2NaO_6$ $[M+Na]^+$, 583.1840, found 583.1845 Da.

Procedure 2: Following the procedure described for the Sonogashira coupling to form compound **2.49**, acetylene **3.38** was obtained using terminal alkyne **3.41** (0.400 g, 1.253 mmol, 1.0 equiv), methyl 3-benzyloxy-6-bromopicolinate **2.10** (0.444 g, 1.378 mmol, 1.1 equiv), $Pd[PPh_3]_4$ (0.145 g, 0.125 mmol, 0.1 equiv), CuI (0.048 g, 0.251 mmol, 0.2 equiv), THF (16 mL), Et_3N (6 mL) and dry DMF (3 mL). The crude acetylene was purified by column chromatography (silica gel, CH_2Cl_2/MeOH 98:2 to 9:1) to afford **3.38** as white solid (0.674 g, 1.203 mmol, 96%). Spectroscopic data were consistent with **3.38** obtained by Mitsunobu reaction.

TLC Rf 0.23 (CH_2Cl_2/MeOH 98:2).

MP 225–227 °C (hexane).

IR (neat) ν_{max} 2944 (w), 2237 (w), 1731 (m), 1633 (s), 1610 (s), 1588 (s), 1515 (m), 1469 (m), 1446 (m), 1386 (m), 1337 (w), 1308 (s), 1267 (s), 1206 (m), 1132 (w), 1098(m) cm^{-1}.

^{1}H NMR (400 MHz, $CDCl_3$) δ (ppm) 8.09 (s, 1H, **6**), 7.99 (d, *J* = 7.8 Hz, 1H, **15**), 7.60 (s, 1H, **3**), 7.53 (d, *J* = 8.8 Hz, 1H, **13**), 7.44-7.27 (m, 7H, **22**, **23**, **30**, **31**, **32**, **33** & **34**), 7.20 (t, *J* = 7.6 Hz, 1H, **14**), 5.20 (s, 2H, **28**), 5.11 (s, 2H, **18**), 4.31 (t, *J* = 5.0 Hz, 2H, **9**), 4.08 (s, 3H, **27**), 3.96 (s, 3H, **1**), 3.02 (t, *J* = 6.0 Hz, 2H, **11**), 2.14 (quin, *J* = 6.6 Hz, 2H, **10**).

^{13}C NMR (101 MHz, $CDCl_3$) δ (ppm) 164.73 (**26**), 160.66 (**8**), 153.71(**24**), 153.69 (**2**), 147.91 (**7**), 140.37 (**25**), 135.50 (**17**), 134.35 (**5**), 134.06 (**29**), 130.91 (**22**), 129.31 (**4**), 128.88 (2C, **31**+**33**), 128.84 (**13**), 128.39 (**32**), 127.02 (2C, **30**+**34**), 125.77 (**12**), 121.85 (**14**), 121.71 (**15**), 120.89 (**23**), 119.43 (**21**), 118.98 (**16**), 111.04 (**6**), 103.28 (**3**), 86.06 (**19**), 83.07 (**20**), 70.96 (**28**), 57.47 (**18**), 56.23 (**1**), 52.83 (**27**), 42.89 (**9**), 28.40 (**11**), 20.94 (**10**).

LRMS (ESI$^+$) *m/z* 561.3 $[M+H]^+$.

HRMS (ESI$^+$) *m/z* calcd for $C_{34}H_{29}N_2O_6$ $[M+H]^+$, 561.2020, found 561.2029 Da.
(ESI$^+$) *m/z* calcd for $C_{34}H_{28}N_2NaO_6$ $[M+Na]^+$, 583.1840, found 583.1845 Da.

11-Methoxy-10-(prop-2-yn-1-yloxy)-5,6-dihydro-4*H*,8*H*-pyrido[3,2,1-*de*]phenanthridin-8-one (**3.41**)

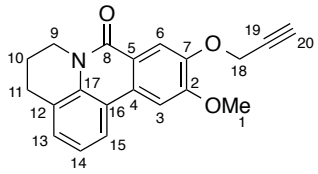

$C_{20}H_{17}NO_3$

MW: 319.36 g.mol^{-1}

To a suspension of phenol **3.26** (0.360 g, 1.280 mmol, 1.0 equiv) in dry DMF (6.4 mL) was added propargyl bromide (285 μL of a 80% wt. solution in toluene, 2.560 mmol, 2.0 equiv) and anhydrous K_2CO_3 (0.226 g, 1.920 mmol, 1.5 equiv). The reaction mixture was stirred for 4 h at rt. The yellow suspension turned to a dark and off-white cloudy solution successively. Upon completion, the reaction mixture was dissolved in EtOAc (10 mL), washed with an aqueous NaOH (5%) solution (15 mL), brine (15 mL), dried over anhydrous Na_2SO_4, filtered and concentrated under reduced pressure. The pale yellow crude was purified by column chromatography (silica gel, EtOAc/hexane 7:3 to 1:0) to afford **3.41** as white solid (0.336 g, 1.052 mol, 82%).

TLC Rf 0.44 (hexane/EtOAc 3:7).

MP 213–214 °C (hexane).

IR (neat) ν_{max} 3306 (w), 2953 (m), 2227 (m), 1630 (s), 1610 (s), 1587 (s), 1516 (s), 1470 (m), 1385 (s), 1334 (m), 1308 (m), 1268 (m), 1242 (m), 1205 (m), 1110 (m) cm^{-1}.

^{1}H NMR (500 MHz, $CDCl_3$) δ (ppm) 8.08 (s, 1H, **6**), 8.00 (d, *J* = 7.2 Hz, 1H, **15**), 7.62 (s, 1H, **3**), 7.29-7.26 (m, 1H, **13**), 7.20 (t, *J* = 8.0 Hz, 1H, **14**), 4.92 (d, *J* = 2.4 Hz, 2H, **18**), 4.36-4.30 (m, 2H, **9**), 4.08 (s, 3H, **1**), 3.02 (t, *J* = 6.2 Hz, 2H, **11**), 2.56 (t, *J* = 2.4 Hz, 1H, **20**), 2.14 (quin, *J* = 6.1 Hz, 2H, **10**).

^{13}C NMR (126 MHz, $CDCl_3$) δ (ppm) 160.74 (**8**), 153.66 (**2**), 147.70 (**7**), 134.40 (**17**), 129.35 (**4**), 128.92 (**13**), 125.85 (**12**), 121.91 (**15**), 120.92 (**14**), 119.45 (**16**), 119.03 (**5**), 110.95 (**6**), 103.26 (**3**), 77.89 (**19**), 76.54 (**20**), 56.80 (**18**), 56.28 (**1**), 42.92 (**9**), 28.44 (**11**), 20.97 (**10**).

LRMS (ESI$^+$) *m/z* 320.2 [M+H]$^+$, 639.3 [2M+H]$^+$, 661.3 [2M+Na]$^+$.

HRMS (ESI$^+$) *m/z* calcd for $C_{20}H_{17}NNaO_3$ [M+Na]$^+$, 342.1101, found 342.1107 Da.

3-Hydroxy-6-(3-((11-methoxy-8-oxo-5,6-dihydro-4*H*,8*H*-pyrido[3,2,1-*de*]phenanthridin-10-yl)oxy)propyl)picolinaldehyde oxime (**3.24**)

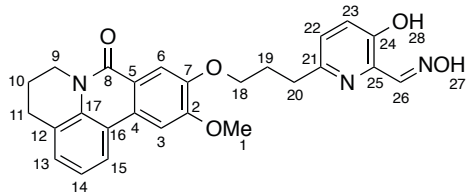

$C_{26}H_{25}N_3O_5$

MW: 459.50 g.mol^{-1}

Oxime **3.24** was obtained according to general procedures D, E, F and G using for procedure D **3.38** (0.100 g, 0.178 mmol, 1.0 equiv), $Pd(OH)_2/C$ (20% wt. with 50% moisture, 0.050 g, 0.036 mmol, 0.2 equiv) and MeOH (18 mL). The presence of the desired phenolic alkane was supported by TLC and LRMS (ESI$^+$, *m/z* 475.3 $[M+H]^+$). After drying *in vacuo*, the crude product was subjected to procedure E using 2,6-lutidine (59 μL, 0.506 mmol, 3.0 equiv), TBSOTf (116 μL, 0.506 mmol, 3.0 equiv) in CH_2Cl_2 (8.5 mL). The presence of the desired silylether was supported by TLC and LRMS (ESI$^+$, *m/z* 589.6 $[M+H]^+$). After drying *in vacuo*, the crude material was subjected to procedure F using DIBAL-H (507 μL of a 1.0 M solution in CH_2Cl_2, 0.507 mmol, 3.0 equiv) in CH_2Cl_2 (8.5 mL). The presence of the desired aldehyde was supported by TLC and LRMS (ESI$^+$, *m/z* 445.2 $[M+H]^+$). After drying *in vacuo*, the crude product was subjected to procedure G using hydroxylamine hydrochloride (0.018 g, 0.254 mmol, 1.5 equiv) and CH_3CO_2Na (0.021 g, 0.254 mmol, 1.5 equiv) in EtOH (3.4 mL). The crude was purified by column chromatography (silica gel, CH_2Cl_2/MeOH 98:2) to afford **3.24** as white solid (0.002 g, 0.004 mol, 4% over 4 steps).

TLC Rf 0.40 (CH_2Cl_2/MeOH 9:1).

^{1}H NMR (500 MHz, $CDCl_3$) δ (ppm) 8.82 (br s, 1H, **26**), 7.99 (d, *J* = 7.2 Hz, 1H, **15**), 7.88 (s, 1H, **3**), 7.57 (s, 1H, **13**), 7.55-7.47 (m, 1H, **6**), 7.33-7.26 (m, 2H, **22** & **23**), 7.19 (t, *J* = 7.9 Hz, 1H, **14**), 4.30 (t, *J* = 5.7 Hz, 2H, **18**), 4.26 (t, *J* = 4.6 Hz, 2H, **9**), 4.02 (s, 3H, **1**), 3.45-3.44 (m, 1H, **28**), 3.25-3.17 (m, 2H, **20**), 3.01 (t, *J* = 6.0 Hz, 2H, **11**), 2.44-2.38 (m, 2H, **19**), 2.13 (quin, *J* = 6.5 Hz, 2H, **10**).

LRMS (ESI$^+$) *m/z* 460.3 $[M+H]^+$.

HRMS (ESI$^+$) *m/z* calcd for $C_{26}H_{26}N_3O_5$ $[M+H]^+$, 460.1867, found 460.1869 Da.

A.4 Molecular dynamic simulations

Molecular dynamics simulations were carried out using GROMACS 4.5.6[330] and the Amber99sb forcefield.[331] The topological description of each molecule was built using acpype and the general amber force field.[332] The hAChE-VX complex in the conformation obtained from flexible dockings together with crystal water molecules and the different molecules, was immersed in a periodic water box of cubic shape with a minimal distance of 10 Å to any edge and periodic boundary conditions. The box was solvated using the TIP3P solvation model and chloride and sodium counter ions were added to neutralize the simulation system. After energy minimization using a 500-step steepest decent method, the system was subjected to equilibration at 1 bar for 50 ps under the conditions of position restraints for heavy atoms. The solvent, the counter ions, and the protein were coupled separately to a temperature bath at 300 K. The Lennard-Jones interactions were cut off at 1.4 nm. The long-range electrostatic interactions were handled using particle-mesh Ewald method for determining long-range electrostatics (9 Å cutoff). Temperature was set to 300 K and was kept constant using a Berendsen thermostat (with a coupling time constant of 0.1 ps).[333] Pressure with a reference value of 1 bar was controlled by a Berendsen barostat (with a coupling time constant of 1 ps and a compressibility of 4.5 x 10^5 bar). Full MD simulation was performed for 5 ns at 300 K, using 2 femtosecond timesteps. All bond lengths were constrained using the LINCS algorithm allowing an integration step of 2 fs.[334] Coordinates were saved every 250 steps (every 0.5 ps).

A.5 Flexible dockings

Dockings have been performed using autodock vina[335] and by preparing the system in PyMOL (Schrödinger) using the plug-in developed by Daniel Seeliger (http://wwwuser.gwdg.de/~dseelig/adplugin.html). VX-*h*AChE was constructed from the apo form (pdb code 4EY4) by homology to the VX-*m*AChE structure (pdb code 2Y2U), keeping in the active site all the usually conserved water molecules. Residues in the gorge (Tyr72, Asp74, Trp86, Tyr124, Ser125, Trp286, Tyr337, Phe338, Tyr341) have been chosen as flexible, along with the ethyl group of VX. A docking box of 60 x 60 x 60 Å was chosen, centered at the bottom of the gorge between Tyr124 and Trp86. Ligands were built and optimized from SMILEs string using Phenix elbow.[336] The default parameter set of Autodock vina was used to generate 10 docking poses per molecule.

Examples of dockings:

Hybrid reactivators	Side view
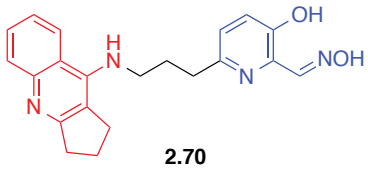 **2.70**	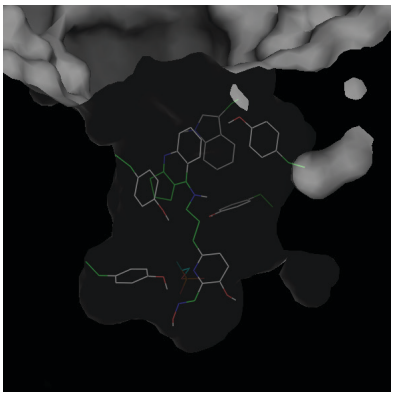
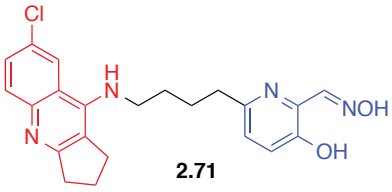 **2.71**	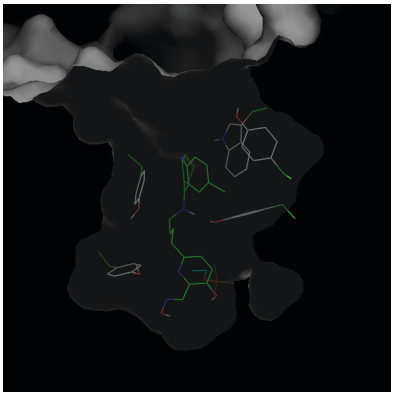
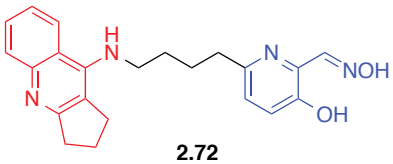 **2.72**	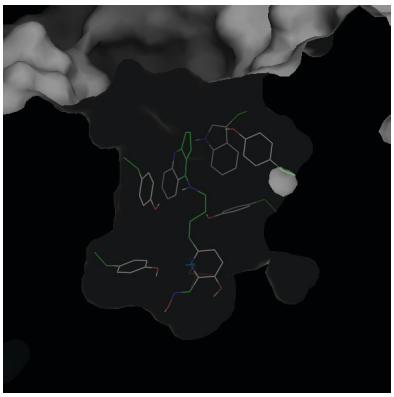
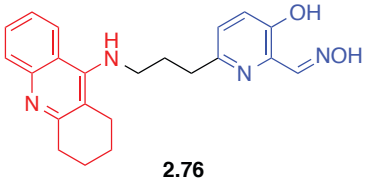 **2.76**	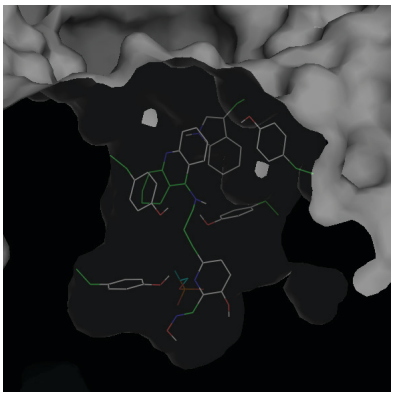

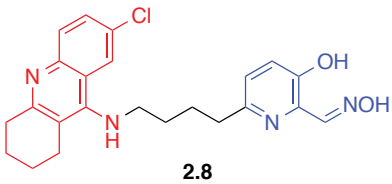

2.8

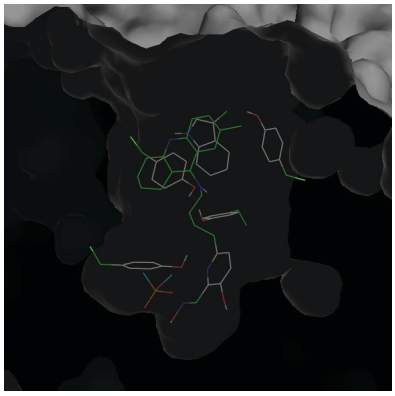

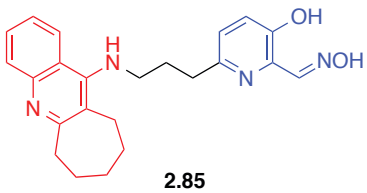

2.85

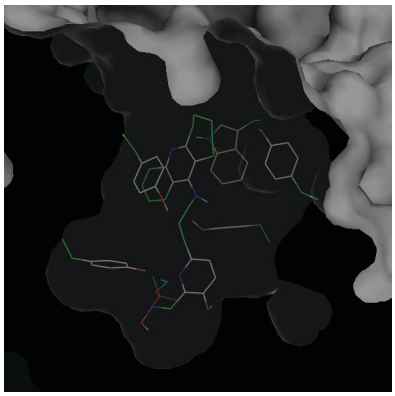

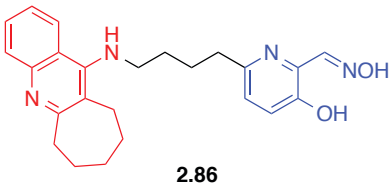

2.86

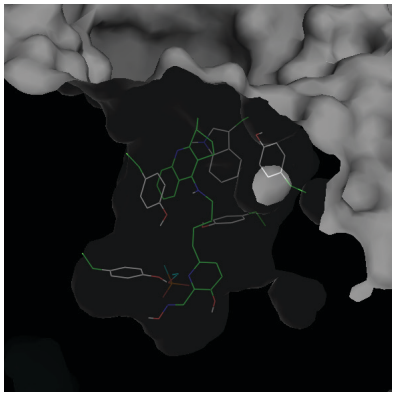

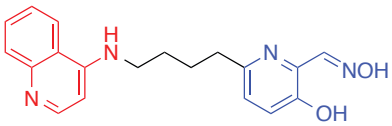

3.1

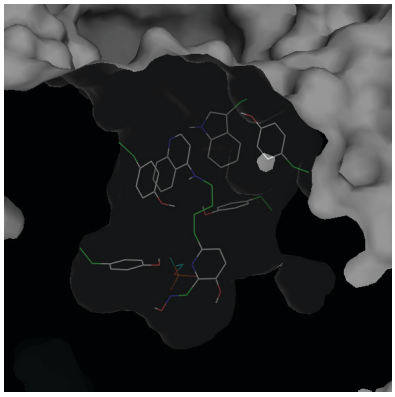

A.6 IC_{50} measurements

Recombinant *h*AChE was produced and purified as previously described.[335] Oximes were dissolved in MeOH to make 5- or 10- mM stock solution. Recombinant *h*AChE activity was measured by spectrophotometry (absorbance at 412 nm) in the presence of various concentrations of oximes in 1 mL Ellman's buffer (phosphate 0.1 M, pH 7.4, 0.1% BSA, 5% MeOH, 0.5 mM DTNB, 25 °C). Measurements were performed at least in duplicate for each concentration tested. The concentration of oxime producing 50% of enzyme inhibition was determined by non-linear fitting using ProFit (Quantumsoft) using the standard IC_{50} equation:

$$\%Activity = 100\frac{IC_{50}}{(IC_{50} + [Ox])}$$

IC_{50} curves

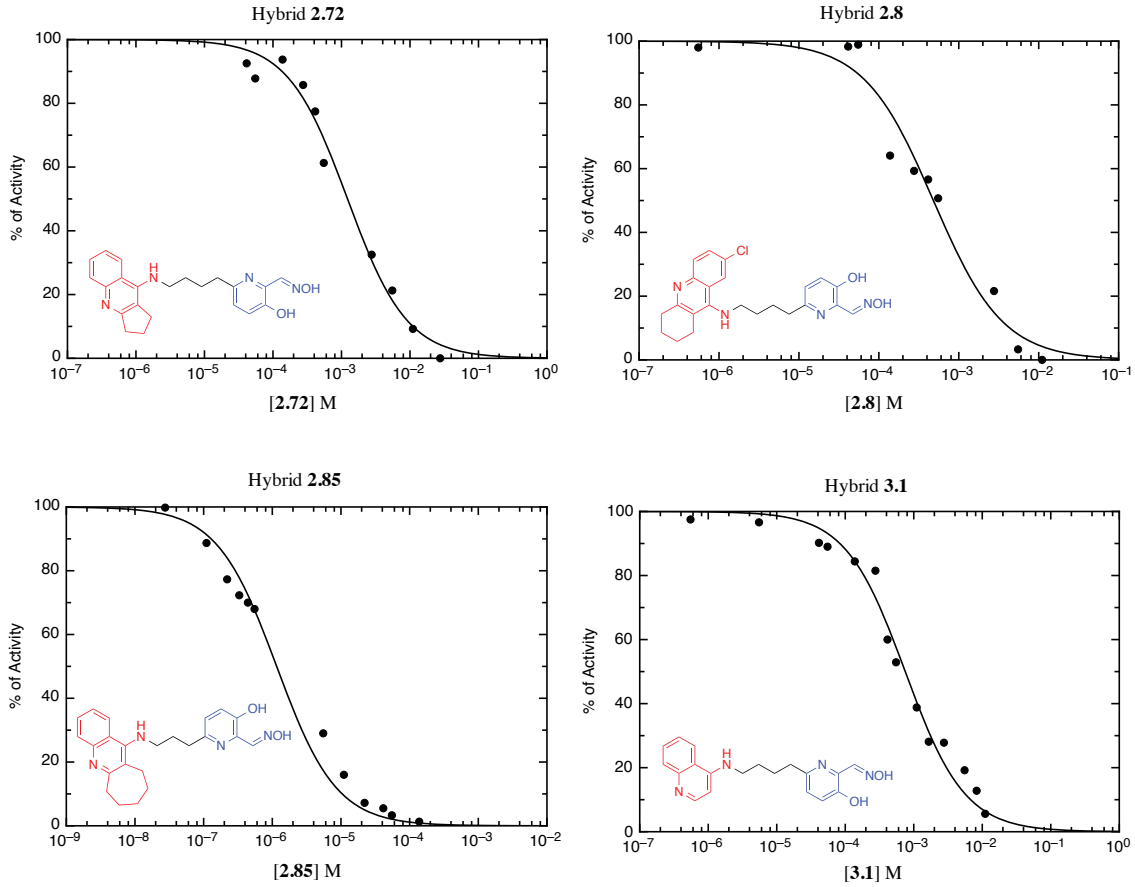

A.7 Inhibition of *h*AChE

VX, Sarin, and Tabun were from DGA maîtrise NRBC (Vert le Petit, France). Ethyl paraoxon was purchased from Sigma-Aldrich. Stock solution of OPNA were 5 mM in isopropanol. The inhibition of 120 µM *h*AChE is realised with a 10-fold excess of OPNAs and was performed in tris buffer (20 mM, pH 7.4, 0.1% BSA) at 25 °C. After incubating for 20 min, inhibited *h*AChE was desalted on PD-10 column (GE Healthcare).

A.8 Reactivation of OPNA-inhibited *h*AChE

Hlö-7 was from DGA maîtrise NRBC (Vert le Petit, France), HI-6 from Pharmacie Centrale des Armées (Orléans, France) and obidoxime was from CRSSA (Lyon, France; synthesized by Bernard Desiré). OPNA-inhibited *h*AChE was incubated at 37 °C with at least 5 concentrations of oxime in phosphate buffer (0.1 M, pH 7.4, 0.1% BSA). Every solution containing the different concentrations of oxime were transferred to 1 mL cuvettes at time intervals ranging from 1 to 10 minutes depending on the reactivation rate for measurement of *h*AChE activity using 1 mM acetylthiocholine in Ellman's buffer (phosphate 0.1 M, pH 7.4, 0.1% BSA, 0.5 mM DTNB, 25 °C). The enzyme activity in the control remained constant during the experiment. The percentage of reactivated enzyme ($\%E_{react}$) was calculated as the ratio of the recovered enzyme activity and activity in the control. The apparent reactivation rate k_{obs} for each oxime concentration, the dissociation constant K_D of inhibited enzyme-oxime complex (E-POx) and the maximal reactivation rate constant k_r, were calculated by non-linear fit with ProFit (Quantumsoft) using the standard oxime concentration-dependent reactivation equation derived from the following figure:

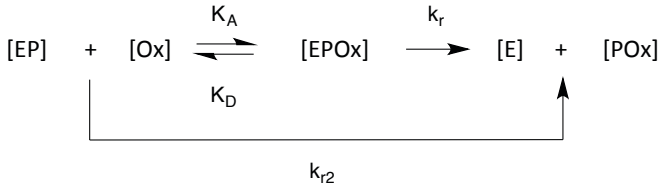

$$\%Activity = 100.(1 - e^{-k_{obs}t})$$

$$k_{obs} = \frac{k_r.[Ox]}{K_D + [Ox]}$$

Reactivation curves

Hybrid **2.72**

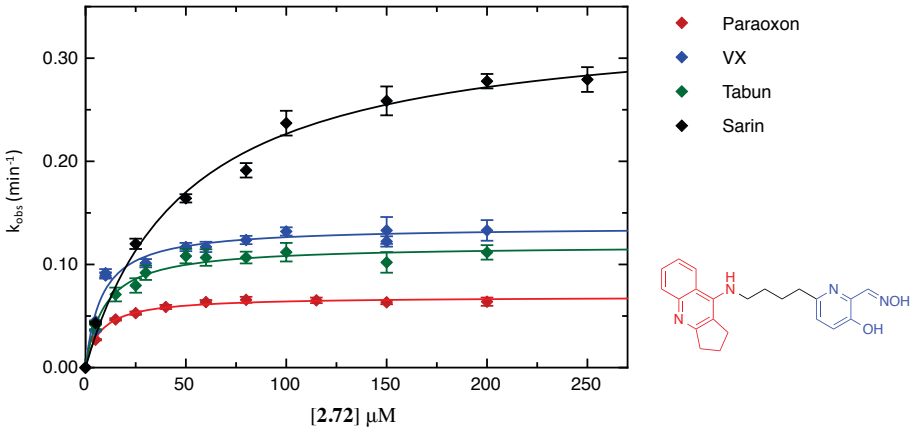

Hybrid **2.8**

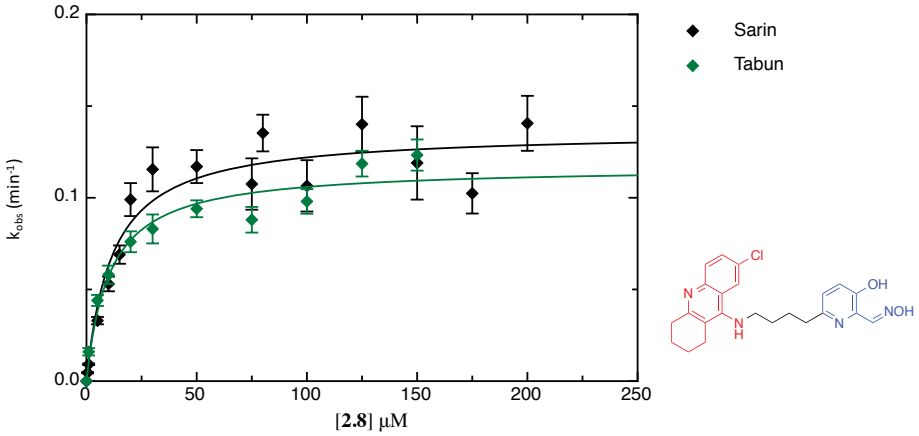

Hybrid **2.85**

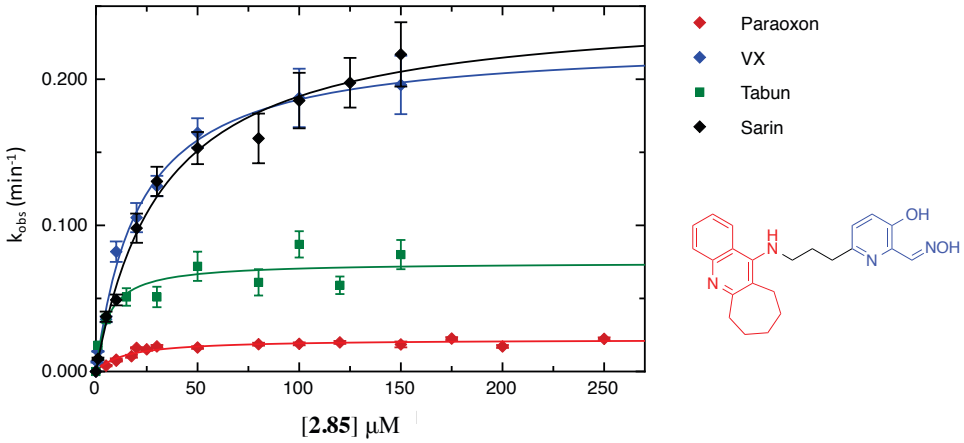

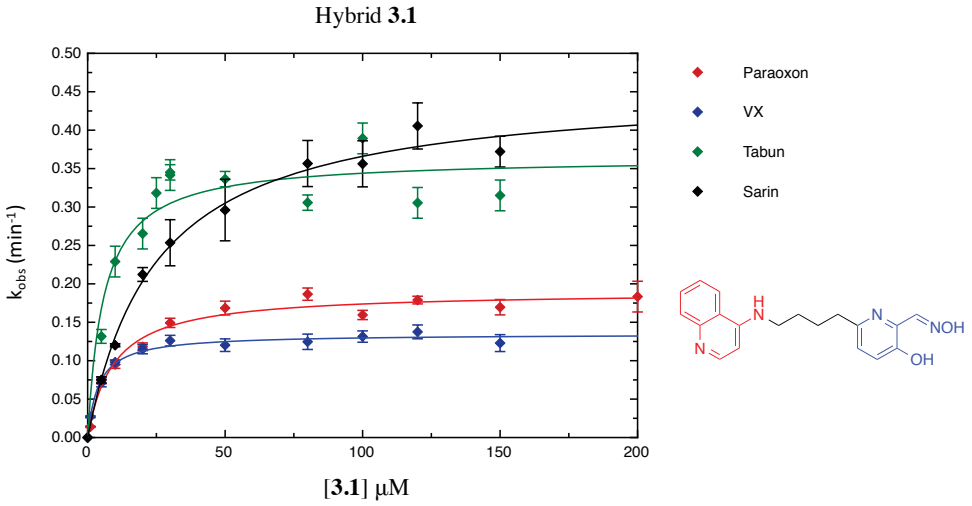

A.9 Pharmacokinetics on mice

A.9.1 Standard reactivation curves

Plasma was isolated from erythrocytes by centrifugation at 3000 *g* for 10 min. Endogenous cholinesterases from plasma were then heat-inactivated at 56 °C for 30 min. VX-inhibited *h*AChE was incubated for 30 min at 37 °C in presence of different concentrations of oximes diluted in plasma (0, 1, 5, 10, 50, 100, 150 and 250 µM). A volume of 7 µL of heated plasma containing oxime was mixed with the same volume of VX-inhibited *h*AChE solution in sodium-phosphate buffer (0.1 M, pH 7.4, 0.1% BSA) and incubated 30 min at 37 °C to reactivate *h*AChE. An incubation of 30 min was empirically chosen to obtain full reactivation at the highest oxime concentration tested. 10-µL aliquots of each sample were transferred to cuvettes containing 1 mM acetylthiocholine in 1 mL Ellman's buffer (sodium-phosphate 0.1 M, pH 7.4, 0.1% BSA, 0.5 mM DTNB, 25 °C) for measurement of resulting *h*AChE activity at 412 nm. The enzyme activity in the control (uninhibited enzyme + oxime) remained constant during the experiment. The percentage of reactivated enzyme (%E_{react}) was calculated as the ratio of the recovered VX-inhibited *h*AChE activity and HI-6 reactivated *h*AChE activity, knowing that maximal reactivation (i.e. %E_{react} = 100%) was achieved by incubating VX-inhibited *h*AChE with 200 µM HI-6 diluted in heated plasma. Three independent experiments were carried out for each oxime and results are presented as mean values ± SEM.

Standard curves were fitted with ProFit (Quantumsoft) using a standard asymptotical/exponential time-dependent reactivation equation giving $\%E_{react}$ in function of the oxime concentration ([Ox]): $\%E_{react} = 100.\left(1 - e^{k.[Ox].t}\right)$

where k is an apparent bimolecular rate constant ($\mu M^{-1}min^{-1}$) and t = 30 min for these series of experiment.

A.9.2 Blood samples

Mice were anesthetized by isoflurane gas and kept anesthetized during shaving. Mice hind limbs were shaved with a 3 min-long application of a commercial depilatory cream. The day of the experiment, mice received intraperitoneal injection of oxime (50 mg kg^{-1}). At various times (0, 2, 5, 10, 15, 30, 60 and 180 minutes after oxime injection for 2-PAM, and other oximes and 0, 5, 15, 30, 60 and 180 minutes for HI-6), the saphenous vein was drilled with a needle, about 15 µL of blood was collected with an heparinized capillary tube and put in a collection tube containing 2 µL of heparine. Blood collection was carried out and the exact volume of collected blood of each sample was determined in order to calculate the dilution factor due to the heparine. Next, plasma was isolated from erythrocytes by centrifugation at 3000 *g* for 10 min. Plasma samples were then treated as previously described to obtain the percentage of reactivated enzyme ($\%E_{react}$). t_{max} corresponds to the time when the curve reachs $\%E_{react}$. To fit the curves a two-compartment kinetic model was used. The area under the plasma percentage of reactivation-time curve (AUC) was calculated using the trapezoidal rule. The area under the first moment curve (AUMC) was determined using a plot of plasma percentage of reactivation times time versus time and calculation of its area under the curve calculated by the trapezoidal rule. Mean residence time (MRT) was calculated as the ratio of AUMC to AUC

A.10 Irritancy assays

A.10.1 Materials

Reagents for the TRPA1 assay were from Sigma-Aldrich unless stated. Gibco Hank's balanced salts solution was from Fisher Scientific (Loughborough, UK). The HEK Photoscreen TRPA1 cell line (AX-004-PCL) was obtained from PerkinElmer Life and Analytical Sciences (Waltham, MA, USA).

A.10.2 Cell culture

HEK TRPA1 cells were grown in 150 cm^2 flasks (Corning Inc., NY, USA) at 37 °C (5% CO_2 – 95% air) in culture medium (Earle's modification of Eagle's medium (EMEM) supplemented with fetal bovine serum (10% v/v); penicillin and streptomycin (100 $units.mL^{-1}$ and 100 $\mu g.mL^{-1}$, respectively), L-glutamine (2 mM) and G418 (0.4 $mg.mL^{-1}$)). At 80-90% confluency, the cells were passaged at split ratios of 1:4 to 1:18 for continued growth in new flasks, or for sowing into poly-D-lysine (PDL)-coated 96-well black Biocoat cell culture plates (BD Biosciences, Bedford, MA, USA) for Ca^{2+} assays. Cells were washed with Ca^{2+}- and Mg^{2+}-free Dulbecco's phosphate buffered saline (DPBS, 12 mL) and detached using a solution of trypsin/$EDTA(Na)_4$ in DPBS for 5 min at 37 °C. Detached cells were collected by centrifugation (95 *g* for 5 min at 20 °C) and the resulting pellet was resuspended in culture medium. Cells were counted and cell viability determined using trypan blue. The cells were sown into PDL-coated plates at a density of 12,500 viable cells per well and were grown for 48 h prior to use. Cells at passage numbers 14-20 were used.

A.10.3 TRPA1 agonism

HEK TRPA1 cells were loaded with a Ca^{2+} fluorophore using a Calcium 5 assay kit (Molecular Devices Ltd., Berkshire, UK). Loading buffer containing the Ca^{2+} fluorophore was prepared by supplementing every 10 mL of the proprietary loading buffer with assay buffer (5 mL) comprising a 1:1 v/v mixture of EMEM and HBSS (buffered to pH 7.4 with 20 mM HEPES). Cells in the black PDL-coated 96-well plates were loaded in preparation for the assay by removal of the EMEM and addition of the loading buffer (90 µL) to each well. The cells were then incubated for 30 min at 37 °C in a humidified atmosphere of 5%–95% air. Acridine analogue stocks of 4 mM were prepared in assay buffer. Subsequently, serial dilutions of these

stocks were prepared in standard 96-well culture plates (Costar brand, Corning Inc.) to provide a semi-log dilution series from 0 to 378 μM. *trans*-cinnamaldehyde was employed as an internal standard control (as it is a specific TRPA1 agonist). It was serially diluted to provide a semi-log dilution series from 0 to 4 mM.

Cellular fluorescence, indicative of activation of the TRPA1 ion channel (as determined by the influx of Ca^{2+} into the cell via this channel), was measured at 1 s intervals before and after addition of the agonist solutions (30 μL) using a FlexStation 3 (Molecular Devices Inc., Sunnyvale, CA, USA). The cells were exposed to molecules **4.1**, **2.59**, **2.22.3** and **2.60** at concentrations from 0 to 94.5 μM and from 0 to 1 mM for *trans*-cinnamaldehyde in a semi-log progression. Fluorescence from formation of the Calcium-5-Ca^{2+} complex formed intracellularly, after agonist-induced activation of the TRPA1 ion channel, was measured using excitation wavelength 485 nM and emission wavelength 525 nm. Baseline fluorescence data were collected for 15 s prior to addition of the agonist solutions and the response followed for a further 45 s.

A.10.4 Data analysis

Fluorescence emission data (fluorescence intensity versus time) were captured from the FlexStation 3 using SoftMax Pro software v. 5.4.1 (Molecular Devices Inc., 1992-2010) on a Dell Optiplex 960 PC workstation. The area under the time-response curve was calculated for the entire recording and imported into GraphPad Prism v. 6 (GraphPad Software Inc., San Diego, CA, USA) for nonlinear curve fitting. Raw concentration-response data were fitted with a four parameter logistic equation: $Y = Bottom + (Top - Bottom)/(1 + 10((Log\ EC_{50} - X) \times Slope)$, where X = logarithm of concentration and Y = response. The EC_{50} and 95% confidence interval (C.I.) were obtained were appropriate.

Appendix

α-Trifluoromethyl oximes were synthesised *one-pot* from the corresponding methyl ester.

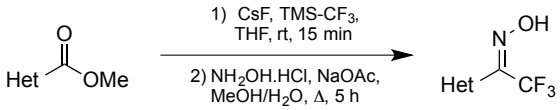

Entry	Starting material	Structure	Yields
1	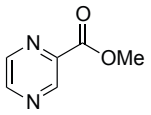	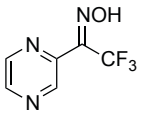	36%
2	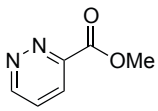	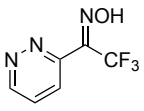	30%
3	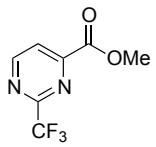	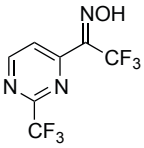	30%

New heterocyclic aldoximes were synthesised from the corresponding aldehyde.

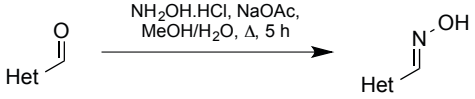

Entry	Starting material	Structure	Yields	Entry	Starting material	Structure	Yields
1	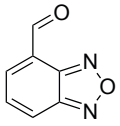	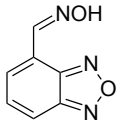	86%	3	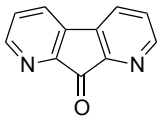	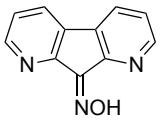	58%
2	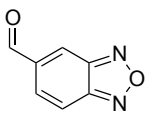	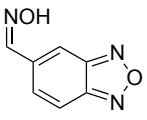	87%	4	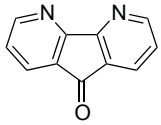	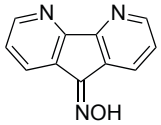	57%

In vitro evaluation for VX-*h*AChE.

Structure of α-nucleophiles	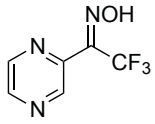	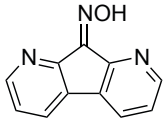	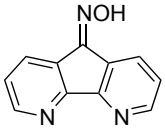
IC_{50} range	~ mM	~ mM	~ mM
Reactivation rate	0.1%/min @ 100 μM 0.3%/min @ 500 μM	0.06%/min @ 100 μM	0.08%/min @ 100 μM
pKa	7.99 ± 0.21	Out of Range	Out of Range

Structure of α-nucleophiles	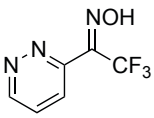	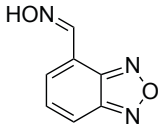	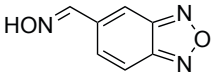
IC_{50} range	~ mM	~ mM	~ mM
Reactivation rate	0.1%/min @ 100 μM	0.1%/min @ 100 μM	0.08%/min @ 100 μM
pKa	7.61 ± 0.16	Out of Range	Out of Range

References

(1) De Clermont, P. *Carbohydr. Res.* **1854**, *39*, 338.

(2) De Clermont, P. *Ann. Chem. Phys.* **1855**, *44*, 330.

(3) Petroianu, G. a. *Pharmazie* **2008**, *63* (4), 325.

(4) Holmstedt, B. In *Handbuch Der Expermentellen Pharmakologie*; 1963; Vol. Erganzungs, pp 165–181.

(5) Lange, W.; Krueger, G. V. *Chem. Ber.* **1932**, *65B*, 1253.

(6) Tucker, J. B. *War of Nerves: Chemical Warfare From World War I to Al-Qaeda.*, Pantheon B.; 2006.

(7) Fukuto, T. R. *Environ. Health Perspect.* **1990**, *87*, 245.

(8) Costa, L. G. *Clin. Chim. Acta* **2006**, *366* (1-2), 1.

(9) Eleršek, T.; Filipi, M. *Natl. Inst. Biol. - Slov.* **2011**, *12*, 243.

(10) Eddleston, M.; Karalliedde, L.; Buckley, N.; Fernando, R.; Hutchinson, G.; Isbister, G.; Konradsen, F.; Murray, D.; Piola, J. C.; Senanayake, N.; Sheriff, R.; Singh, S.; Siwach, S. B.; Smit, L. *The Lancet* **2002**, *360*, 1163.

(11) Bardin, P. G. *Arch. Intern. Med.* **1944**, *154*, 1433.

(12) Sogorb, M. a.; Vilanova, E.; Carrera, V. *Toxicol. Lett.* **2004**, *151* (1), 219.

(13) Worek, F.; Koller, M.; Thiermann, H.; Szinicz, L. *Toxicology* **2005**, *214* (3), 182.

(14) Eddleston, M.; Buckley, N. A.; Eyer, P.; Dawson, A. H. *The Lancet* **2008**, *371*, 597.

(15) Delfino, R. T.; Ribeiro, T. S.; Figueroa-Villar, J. D. *J. Braz. Chem. Soc.* **2009**, *20* (3), 407.

(16) Romano, J.; Lukey, B.; Salem, H. *Chemical warfare agents: chemistry, pharmacology, toxicology, and therapeutics*; 2008.

(17) Degenhardt, C. E. A. M.; Van Den Berg, G. R.; De Jong, L. P. A.; Benschop, H. P. *J. Am. Chem. Soc.* **1986**, *108*, 8290.

(18) Krejcova, G.; Kuca, K.; Sevelova, L. *Def. Sci. J.* **2005**, *55* (2), 105.

(19) Maynard, R. L. *Chemical Warfare Agents - Toxicology and Treatment*, 2nd ed.; John Wiley & Sons Ltd: West Sussex, 2007.

(20) Toy, R. J. T. *Medical Aspects of Chemical and Biological Warfare - Textbook of Military Medicine*; Sidell, F. R., Takafuji, E. T., Franz, D. R., Eds.; US Army: Washington D.C., 1997.

(21) Fusek, J.; Bajgar, J.; Kassa, J.; Hajek, P.; Slizova, D.; Krs, O. *Differences in the action of G- and V-agents Central and peripheral nervous system: effects of highly toxic organophosphates and their antidotes*; 2009.

(22) Watson, A.; Opresko, D.; Young, R.; Hauschild, V.; King, J.; Bakshi, K. In *Handbook of Toxicology of Chemical Warfare Agents*; Academic Press Inc: London, 2009.

(23) Takafuji, E. T.; Kok, A. B. *Medical Aspects of Chemical and Biological Warfare - Textbook of Military Medicine*; Sidell, F. R., Takafuji, E. T., Franz, D. R., Eds.; US Army: Washington D.C., 1997.

(24) Macilwain, C. Study proves Iraq used nerve gas. *Nature*, 1993, *363*, 3.

(25) Nagao, M.; Takatori, T.; Matsuda, Y.; Nakajima, M.; Iwase, H.; Iwadate, K. *Toxicol. Appl. Pharmacol.* **1997**, *144* (1), 198.

(26) Yanagisawa, N.; Morita, H.; Nakajima, T. *J. Neurol. Sci.* **2006**, *249* (1), 76.

(27) Yokoyama, K. *Neurotoxicology* **2007**, *28* (2), 364.

(28) The Technical Secretariat of the Organization for the Prohibition of Chemical Weapons. *Convention on the Prohibition of the Development, Production, Stockpiling and Use of Chemical Weapons and on Their Destruction*; The Hague, Netherlands, 1993.

(29) The Technical Secretariat of the Organization for the Prohibition of Chemical Weapons. Global Campaign to Destroy Chemical Weapons Passes 60 Percent Mark, 2010, http://www.opcw.org/nc/.

(30) Casida, J. E.; Quistad, G. B. *Chem. Biol. Interact.* **2005**, *157-158*, 277.

(31) Quinn, D. M. *Chem. Rev.* **1987**, *87* (5), 955.

(32) Lockridge, O.; Masson, P. *Neurotoxicology* **2000**, *21* (1-2), 113.

(33) Masson, P.; Carletti, E.; Nachon, F. *Protein Pept. Lett.* **2009**, *16* (10), 1215.

(34) Darvesh, S.; Hopkins, D. a; Geula, C. *Nat. Rev. Neurosci.* **2003**, *4* (2), 131.

(35) Lockridge, O.; Duysen, E. G.; Masson, P. In *Anticholinesterase Pesticides*; Satoh, T., Gupta, R. C., Eds.; John Wiley & Sons, Inc.: Hoboken, NJ, USA, 2010; pp 25–41.

(36) Vellom, D. C.; Radić, Z.; Li, Y.; Pickering, N. A.; Camp, S.; Taylor, P. *Biochemistry* **1993**, *32* (1), 12.

(37) Masson, P.; Froment, M. T.; Gillon, E.; Nachon, F.; Lockridge, O.; Schopfer, L. M. *Biochim. Biophys. Acta - Proteins Proteomics* **2007**, *1774* (1), 16.

(38) Masson, P.; Froment, M. T.; Fortier, P. L.; Visicchio, J. E.; Bartels, C. F.; Lockridge, O. *Biochim. Biophys. Acta - Protein Struct. Mol. Enzymol.* **1998**, *1387* (1-2), 41.

(39) Mack, A.; Robitzki, A. *Prog. Neurobiol.* **2000**, *60* (6), 607.

(40) Taylor, P. *Goodman & Gilman's The Pharmacological Basis of Therapeutics*, 13th Ed.; Brunton, L. L., Chabner, B., Knollman, B., Eds.; McGraw-Hill: New York, 2011.

(41) Kovarik, Z.; Katalinić, M.; Šinko, G.; Binder, J.; Holas, O.; Jung, Y. S.; Musilova, L.; Jun, D.; Kuča, K. *Chem. Biol. Interact.* **2010**, *187* (1-3), 167.

(42) Grisaru, D.; Sternfeld, M.; Eldor, A.; Glick, D.; Soreq, H. *Eur. J. Biochem.* **1999**, *264* (3), 672.

(43) Van der Kloot, W.; Molgó, J.; Cameron, R.; Colasante, C. *J. Physiol.* **2002**, *541* (2), 385.

(44) Soreq, H.; Seidman, S. *Nat. Rev. Neurosci.* **2001**, *2* (4), 294.

(45) Ollis, D. L.; Carr, P. D. *Protein Pept. Lett.* **2009**, *16* (10), 1137.

(46) Perrier, A. L.; Massoulié, J.; Krejci, E. *Neuron* **2002**, *33* (2), 275.

(47) MacPhee-Quigley, K.; Taylor, P.; Taylor, S. *J. Biol. Chem.* **1985**, *260* (22), 12185.

(48) Schumacher, M.; Camp, S.; Maulet, Y.; Newton, M.; MacPhee-Quigley, K.; Taylor, S. S.; Friedmann, T.; Taylor, P. *Nature* **1986**, *319*, 407.

(49) Soreq, H.; Ben-Aziz, R.; Prody, C. A.; Seidman, S.; Gnatt, A.; Neville, L.; Lieman-Hurwitz, J.; Lev-Lehman, E.; Ginzberg, D.; Lipidot-Lifson, Y. *Proc. Natl. Acad. Sci. U. S. A.* **1990**, *87* (24), 9688.

(50) Sussman, J. L.; Harel, M.; Frolow, F.; Oefner, C.; Goldmant, A.; Toker, L.; Silman, I. *Science* **1991**, *253*, 872.

(51) Kryger, G.; Harel, M.; Giles, K.; Toker, L.; Velan, B.; Lazar, a.; Kronman, C.; Barak, D.; Ariel, N.; Shafferman, a.; Silman, I.; Sussman, J. L. *Acta Crystallogr. Sect. D Biol. Crystallogr.* **2000**, *56* (11), 1385.

(52) Nicolet, Y.; Lockridge, O.; Masson, P.; Fontecilla-Camps, J. C.; Nachon, F. *J. Biol. Chem.* **2003**, *278* (42),

41141.

(53) Marchot, P.; Ravelli, R. B.; Raves, M. L.; Bourne, Y.; Vellom, D. C.; Kanter, J.; Camp, S.; Sussman, J. L.; Taylor, P. *Protein Sci.* **1996**, *5* (4), 672.

(54) Bourne, Y.; Radić, Z.; Sulzenbacher, G.; Kim, E.; Taylor, P.; Marchot, P. *J. Biol. Chem.* **2006**, *281* (39), 29256.

(55) Harel, M.; Kryger, G.; Rosenberry, T. L.; Mallender, W. D.; Lewis, T.; Fletcher, R. J.; Guss, J. M.; Silman, I.; Sussman, J. L. *Protein Sci.* **2000**, *9* (6), 1063.

(56) Radic, Z.; Pickering, N. A.; Vellom, D. C.; Camp, S.; Taylor, P. *Biochemistry* **1993**, *32* (45), 12074.

(57) Mallender, W. D.; Szegletes, T.; Rosenberry, T. L. *Biochemistry* **2000**, *39* (26), 7753.

(58) Taylor, P.; Lappi, S. *Biochemistry* **1975**, *14* (9), 1989.

(59) Barak, D.; Kronman, C.; Ordentlich, A.; Ariel, N.; Bromberg, A.; Marcus, D.; Lazar, A.; Velan, B.; Shafferman, A. *J. Biol. Chem.* **1994**, *269* (9), 6296.

(60) Barak, D.; Ordentlich, A.; Bromberg, A.; Kronman, C.; Marcus, D.; Lazar, A.; Ariel, N.; Velan, B.; Shafferman, A. *Biochemistry* **1995**, *34* (47), 15444.

(61) Bourne, Y.; Kolb, H. C.; Radić, Z.; Sharpless, K. B.; Taylor, P.; Marchot, P. *Proc. Natl. Acad. Sci. U. S. A.* **2004**, *101* (6), 1449.

(62) Bourne, Y.; Taylor, P.; Radić, Z.; Marchot, P. *EMBO J.* **2003**, *22* (1), 1.

(63) Masson, P.; Nachon, F.; Lockridge, O. *Chem. Biol. Interact.* **2010**, *187*, 157.

(64) Johnson, J. L.; Cusack, B.; Davies, M. P.; Fauq, A.; Rosenberry, T. L. *Biochemistry* **2003**, *42* (18), 5438.

(65) Colletier, J.-P.; Fournier, D.; Greenblatt, H. M.; Stojan, J.; Sussman, J. L.; Zaccai, G.; Silman, I.; Weik, M. *EMBO J.* **2006**, *25* (12), 2746.

(66) Axelsen, P. H.; Harel, M.; Silman, I.; Sussman, J. L. *Protein Sci.* **1994**, *3* (2), 188.

(67) Shafferman, A.; Velan, B.; Ordentlich, A.; Kronman, C.; Grosfeld, H.; Leitner, M.; Flashner, Y.; Cohen, S.; Barak, D.; Ariel, N. *EMBO J.* **1992**, *11* (10), 3561.

(68) Ma, J. C.; Dougherty, D. A. *Chem. Rev.* **1997**, *97*, 1303.

(69) Wandhammer, M.; Carletti, E.; Van Der Schans, M.; Gillon, E.; Nicolet, Y.; Masson, P.; Goeldner, M.; Noort, D.; Nachon, F. *J. Biol. Chem.* **2011**, *286* (19), 16783.

(70) Taylor, P.; Radic, Z. *Annu. Rev. Pharmacol. Toxicol.* **1994**, 281.

(71) Jokanovic, M. *Toxicology* **2001**, *166* (3), 139.

(72) Abbott, N. J.; Rönnbäck, L.; Hansson, E. *Nat. Rev. Neurosci.* **2006**, *7* (1), 41.

(73) Jokanovic, M.; Prostran, M. *Curr. Med. Chem.* **2009**, *16* (17), 2177.

(74) Millard, C. B.; Koellner, G.; Ordentlich, A.; Shafferman, A.; Silman, I.; Sussman, J. L. *J. Am. Chem. Soc.* **1999**, *121* (42), 9883.

(75) Carletti, E.; Colletier, J.-P.; Dupeux, F.; Trovaslet, M.; Masson, P.; Nachon, F. *J. Med. Chem.* **2010**, *53* (10), 4002.

(76) Sanson, B.; Nachon, F.; Colletier, J.-P.; Froment, M.-T.; Toker, L.; Greenblatt, H. M.; Sussman, J. L.; Ashani, Y.; Masson, P.; Silman, I.; Weik, M. *J. Med. Chem.* **2009**, *52* (23), 7593.

(77) Worek, F.; Diepold, C.; Eyer, P. *Arch. Toxicol.* **1999**, *73* (1), 7.

(78) Trovaslet-Leroy, M.; Musilova, L.; Renault, F.; Brazzolotto, X.; Misik, J.; Novotny, L.; Froment, M.-T.; Gillon,

E.; Loiodice, M.; Verdier, L.; Masson, P.; Rochu, D.; Jun, D.; Nachon, F. *Toxicol. Lett.* **2011**, *206* (1), 14.

(79) Ordentlich, A.; Kronman, C.; Barak, D.; Stein, D.; Ariel, N.; Marcus, D.; Velan, B.; Shafferman, A. *FEBS Lett.* **1993**, *334* (2), 215.

(80) Segall, Y.; Waysbort, D.; Barak, D.; Ariel, N.; Doctor, B. P.; Grunwald, J.; Ashani, Y. *Biochemistry* **1993**, *32* (49), 13441.

(81) Worek, F.; Thiermann, H.; Szinicz, L. *Arch. Toxicol.* **2004**, *78* (4), 212.

(82) Shafferman, A.; Ordentlich, A.; Barak, D.; Stein, D.; Ariel, N.; Velan, B. *Biochem. J.* **1996**, *318*, 833.

(83) Nachon, F.; Asojo, O. a.; Borgstahl, G. E. O.; Masson, P.; Lockridge, O. *Biochemistry* **2005**, *44* (4), 1154.

(84) Aurbek, N.; Thiermann, H.; Szinicz, L.; Eyer, P.; Worek, F. *Toxicology* **2006**, *224* (1-2), 91.

(85) Li, H.; Schopfer, L. M.; Nachon, F.; Froment, M. T.; Masson, P.; Lockridge, O. *Toxicol. Sci.* **2007**, *100* (1), 136.

(86) Marrs, T. C. *Chemical Warfare Agents- Toxicology and Treatment*, 2nd Ed.; Marrs, T. C., Maynard, R. L., Sidell, F. R., Eds.; John Wiley & Sons Ltd: West Sussex, 2007.

(87) Vale, J. A. *Toxicol. Lett.* **1998**, *102-103*, 649.

(88) Senanayake, N.; Karalliedde, L. *N. Engl. J. Med.* **1987**, *316* (13), 761.

(89) Benslama, A.; Moutaouakkil, S.; Charra, B.; Menebhi, L. *Ann. Fr. Anesth. Reanim.* **2004**, *23* (4), 353.

(90) Sevim, S.; Aktekin, M.; Dogu, O.; Ozturk, H.; Ertas, M. *Can. J. Neurol. Sci.* **2003**, *30* (1), 75.

(91) Moretto, a; Lotti, M. *J. Neurol. Neurosurg. Psychiatry* **1998**, *64* (4), 463.

(92) Golomb, B. A. *Proc. Natl. Acad. Sci. U. S. A.* **2008**, *105* (11), 4295.

(93) Maxwell, D. M.; Brecht, K. M.; Doctor, B. P.; Wolfe, A. D. *J. Pharmacol. Exp. Ther.* **1993**, *264* (3), 1085.

(94) Amourette, C.; Lamproglou, I.; Barbier, L.; Fauquette, W.; Zoppe, A.; Viret, R.; Diserbo, M. *Behav. Brain Res.* **2009**, *203* (2), 207.

(95) van Helden, H. P. M.; Joosen, M. J. A.; Philippens, I. H. C. *Toxicol. Lett.* **2011**, *206* (1), 35.

(96) Masson, P. *Toxicol. Lett.* **2011**, *206* (1), 5.

(97) Albuquerque, E. X.; Pereira, E. F. R.; Aracava, Y.; Fawcett, W. P.; Oliveira, M.; Randall, W. R.; Hamilton, T. A.; Kan, R. K.; Romano, J. A.; Adler, M. *Proc. Natl. Acad. Sci. U. S. A.* **2006**, *103* (35), 13220.

(98) Lallement, G.; Baille, V.; Baubichon, D.; Carpentier, P.; Collombet, J. M.; Filliat, P.; Foquin, A.; Four, E.; Masqueliez, C.; Testylier, G.; Tonduli, L.; Dorandeu, F. *Neurotoxicology* **2002**, *23* (1), 1.

(99) Kassa, J.; Bajgar, J.; Kuča, K.; Musílek, K.; Karasová, J. *Interdiscip. Toxicol.* **2008**, *1* (1), 18.

(100) Wang, Y.; Wei, Y.; Oguntayo, S.; Doctor, B. P.; Nambiar, M. P. *Chem. Biol. Interact.* **2013**, *203* (1), 120.

(101) Gunosewoyo, H.; Tipparaju, S. K.; Pieroni, M.; Wang, Y.; Doctor, B. P.; Nambiar, M. P.; Kozikowski, A. P. *Bioorganic Med. Chem. Lett.* **2013**, *23* (5), 1544.

(102) Nachon, F.; Brazzolotto, X.; Trovaslet, M.; Masson, P. *Chem. Biol. Interact.* **2013**, *206* (3), 536.

(103) Wolfe, A. D.; Rusha, R. S.; Doctora, B. P.; Koplovitz, I.; Jones, D. *Fundam. Appl. Toxicol.* **1987**, *9* (2), 266.

(104) Ashani, Y.; Pistinner, S. *Toxicol. Sci.* **2004**, *77* (2), 358.

(105) Kronman, C.; Cohen, O.; Mazor, O.; Ordentlich, A.; Raveh, L.; Velan, B.; Shafferman, A. *Chem. Biol. Interact.* **2010**, *187* (1-3), 253.

(106) Casida, J. E.; Quistad, G. B. *Chem. Res. Toxicol.* **2004**, *17* (8), 983.

(107) Lenz, D. E.; Yeung, D.; Smith, J. R.; Sweeney, R. E.; Lumley, L. a.; Cerasoli, D. M. *Toxicology* **2007**, *233* (1-3 SPEC. ISS.), 31.

(108) Saxena, A.; Luo, C.; Doctor, B. P. *Protein Expr. Purif.* **2008**, *61* (2), 191.

(109) Geyer, B. C.; Kannan, L.; Garnaud, P.-E.; Broomfield, C. A.; Cadieux, C. L.; Cherni, I.; Hodgins, S. M.; Kasten, S. A.; Kelley, K.; Kilbourne, J.; Oliver, Z. P.; Otto, T. C.; Puffenberger, I.; Reeves, T. E.; Robbins, N.; Woods, R. R.; Soreq, H.; Lenz, D. E.; Cerasoli, D. M.; Mor, T. S. *Proc. Natl. Acad. Sci. U. S. A.* **2010**, *107* (47), 20251.

(110) Huang, Y.-J.; Huang, Y.; Baldassarre, H.; Wang, B.; Lazaris, A.; Leduc, M.; Bilodeau, A. S.; Bellemare, A.; Côté, M.; Herskovits, P.; Touati, M.; Turcotte, C.; Valeanu, L.; Lemée, N.; Wilgus, H.; Bégin, I.; Bhatia, B.; Rao, K.; Neveu, N.; Brochu, E.; Pierson, J.; Hockley, D. K.; Cerasoli, D. M.; Lenz, D. E.; Karatzas, C. N.; Langermann, S. *Proc. Natl. Acad. Sci. U. S. A.* **2007**, *104* (34), 13603.

(111) Taylor, P.; Kovarik, Z.; Reiner, E.; Radić, Z. *Toxicology* **2007**, *233* (1-3), 70.

(112) Kovarik, Z.; Radić, Z.; Berman, H. A.; Taylor, P. *Toxicology* **2007**, *233* (1-3 SPEC. ISS.), 79.

(113) diTargiani, R. C.; Chandrasekaran, L.; Belinskaya, T.; Saxena, A. *Chem. Biol. Interact.* **2010**, *187* (1-3), 349.

(114) Bigley, A. N.; Raushel, F. M. *Biochim. Biophys. Acta - Proteins Proteomics* **2013**, *1834* (1), 443.

(115) Masson, P.; Josse, D.; Lockridge, O.; Viguié, N.; Taupin, C.; Buhler, C. *J. Physiol. Paris* **1998**, *92* (5-6), 357.

(116) Rochu, D.; Chabrière, E.; Masson, P. *Toxicology* **2007**, *233* (1-3 SPEC. ISS.), 47.

(117) Valiyaveettil, M.; Alamneh, Y.; Rezk, P.; Biggemann, L.; Perkins, M. W.; Sciuto, A. M.; Doctor, B. P.; Nambiar, M. P. *Biochem. Pharmacol.* **2011**, *81* (6), 800.

(118) Masson, P.; Nachon, F.; Broomfield, C. A.; Lenz, D. E.; Verdier, L.; Schopfer, L. M.; Lockridge, O. *Chem. Biol. Interact.* **2008**, *175* (1-3), 273.

(119) Nachon, F.; Carletti, E.; Wandhammer, M.; Nicolet, Y.; Schopfer, L. M.; Masson, P.; Lockridge, O. *Biochem. J.* **2011**, *434* (1), 73.

(120) Bismuth, C. *Réanimation Urgences* **1993**, *2* (6), 625.

(121) Jokanović, M.; Stojiljković, M. P. *Eur. J. Pharmacol.* **2006**, *553* (1-3), 10.

(122) Johnson, D. D.; Stewart, W. C. *Can. J. Physiol. Pharmacol.* **1970**, *48* (9), 625.

(123) Marrs, T. C. *Toxicol. Rev.* **2003**, *22* (2), 75.

(124) Bajgar, J.; Fusek, J.; Kuca, K.; Bartosova, L.; Jun, D. *Mini-Rev. Med. Chem.* **2007**, *7* (5), 461.

(125) Rousseau, J. M.; Besse Bardot, I.; Franck, L.; Libert, N.; Lallement, G.; Clair, P. *Ann. Fr. Anesth. Reanim.* **2009**, *28* (5), 482.

(126) Antonijevic, B.; Stojiljkovic, M. P. *Clin. Med. Res.* **2007**, *5* (1), 71.

(127) Mercey, G.; Verdelet, T.; Renou, J.; Kliachyna, M.; Baati, R.; Nachon, F.; Jean, L.; Renard, P.-Y. *Acc. Chem. Res.* **2012**, *45* (5), 756.

(128) Worek, F.; Eyer, P.; Aurbek, N.; Szinicz, L.; Thiermann, H. *Toxicol. Appl. Pharmacol.* **2007**, *219* (2-3), 226.

(129) Worek, F.; Thiermann, H.; Szinicz, L.; Eyer, P. *Biochem. Pharmacol.* **2004**, *68* (11), 2237.

(130) Wilson, I. B. *J. Biol. Chem.* **1951**, *190*, 111.

(131) Wilson, I. B. *J. Am. Chem. Soc.* **1953**, *75*, 4628.

(132) Edwards, J. O.; Pearson, R. G. *J. Am. Chem. Soc.* **1962**, *84* (1), 16.

(133) Childs, A. F.; Davies, D. R.; Green, A. L.; Rutland, J. P. *Br. J. Pharmacol. Chemother.* **1955**, *10* (4), 462.

(134) Wilson, I. B.; Ginsburg, S. *Biochim. Biophys. Acta* **1955**, *18*, 168.

(135) Namba, T. *J. Am. Med. Assoc.* **1958**, *166* (15), 1834.

(136) Hobbiger, F. *Br. J. Pharmacol. Chemother.* **1957**, *12* (4), 438.

(137) Hobbiger, F.; O'Sullivan, D. G.; Sadler, P. W. *Nature* **1958**, *182* (4648), 1498.

(138) Wilson, I.; Ginsburg, S. *Biochem. Pharmacol.* **1959**, *1*, 200.

(139) Clement, J. G. *Toxicol. Sci.* **1981**, *1* (2), 193.

(140) Musilek, K.; Holas, O.; Misik, J.; Pohanka, M.; Novotny, L.; Dohnal, V.; Opletalova, V.; Kuca, K. *ChemMedChem* **2010**, *5* (2), 247.

(141) Lüttringhaus, A.; Hagedorn, I. *Arzneim. Forsch.* **1964**, *14*, 1.

(142) Hagedorn, I.; Gundel, W. H.; Schoene, K. *Arzneim. Forsch.* **1969**, *19*, 603.

(143) Löffler, M. Quartäre Salze von Pyridin-2,4-dialdoxim als Gegenmittel für Organophosphat-Vergiftungen., University of Freiburg, Germany, 1986.

(144) Terrier, F.; Rodriguez-Dafonte, P.; Le Guével, E.; Moutiers, G. *Org. Biomol. Chem.* **2006**, *4* (23), 4352.

(145) Hörnberg, A.; Artursson, E.; Wärme, R.; Pang, Y.-P.; Ekström, F. *Biochem. Pharmacol.* **2010**, *79* (3), 507.

(146) Ekström, F.; Åstot, C.; Pang, Y. *Clin. Pharmacol. Ther.* **2007**, *82*, 282.

(147) Ekström, F.; Hörnberg, A.; Artursson, E.; Hammarström, L. G.; Schneider, G.; Pang, Y. P. *PLoS One* **2009**, *4* (6).

(148) Ekström, F.; Pang, Y. P.; Boman, M.; Artursson, E.; Akfur, C.; Börjegren, S. *Biochem. Pharmacol.* **2006**, *72* (5), 597.

(149) Worek, F.; Wille, T.; Koller, M.; Thiermann, H. *Biochem. Pharmacol.* **2012**, *83* (12), 1700.

(150) Carletti, E.; Aurbek, N.; Gillon, E.; Loiodice, M.; Nicolet, Y.; Fontecilla-Camps, J.-C.; Masson, P.; Thiermann, H.; Nachon, F.; Worek, F. *Biochem. J.* **2009**, *421* (1), 97.

(151) Kassa, J. *J. Toxicol. Clin. Toxicol.* **2002**, *40* (6), 803.

(152) Kassa, J.; Karasová, J. Ž.; Šepsová, V.; Bajgar, J. *J. Appl. Biomed.* **2011**, *9* (4), 225.

(153) Kassa, J.; Karasova, J. Z.; Caisberger, F.; Musilek, K.; Kuca, K.; Jung, Y.-S. *J. Enzyme Inhib. Med. Chem.* **2010**, *25* (4), 480.

(154) Busker, R. W.; Zijlstra, J. J.; van der Wiel, H. J.; Melchers, B. P.; van Helden, H. P. *Toxicology* **1991**, *69* (3), 331.

(155) Hamilton, M. G.; Lundy, P. M. *Arch. Toxicol.* **1989**, *63*, 144.

(156) Øydvin, O. K.; Tansø, R.; Aas, P. *Eur. J. Pharmacol.* **2005**, *516* (3), 227.

(157) Becker, G.; Kawan, A.; Gutzeit, D.; Worek, F.; Szinicz, L. *Arch. Toxicol.* **2007**, *81* (6), 415.

(158) Bartosova, L.; Kuca, K.; Kunesova, G.; Jun, D. *Neurotox. Res.* **2006**, *9* (4), 291.

(159) Lorke, D. E.; Kalasz, H.; Petroianu, G. A.; Tekes, K. *Curr. Med. Chem.* **2008**, *15* (8), 743.

(160) Sakurada, K.; Matsubara, K.; Shimizu, K.; Shiono, H.; Seto, Y.; Tsuge, K.; Yoshino, M.; Sakai, I.; Mukoyama, H.; Takatori, T. *Neurochem. Res.* **2003**, *28* (9), 1401.

(161) Cassel, G.; Karlsson, L.; Waara, L.; Ang, K. W.; Göransson-Nyberg, A. *Eur. J. Pharmacol.* **1997**, *332* (1), 43.

(162) Petroianu, G. A.; Lorke, D. E.; Hasan, M. Y.; Adem, A.; Sheen, R.; Nurulain, S. M.; Kalasz, H. *J. Appl. Toxicol.* **2007**, *27* (4), 350.

(163) Worek, F.; Kirchner, T.; Szinicz, L. *Toxicology* **1995**, *95* (1-3), 123.

(164) Worek, F.; Eyer, P.; Kiderlen, D.; Thiermann, H.; Szinicz, L. *Arch. Toxicol.* **2000**, *74* (1), 21.

(165) Leader, H.; Vincze, A.; Manisterski, B.; Rothschild, N.; Dosoretz, C.; Ashani, Y. *Biochem. Pharmacol.* **1999**, *58* (3), 503.

(166) Ashani, Y.; Bhattacharjee, A. K.; Leader, H.; Saxena, A.; Doctor, B. P. *Biochem. Pharmacol.* **2003**, *66* (2), 191.

(167) Herkenhoff, S.; Szinicz, L.; Rastogi, V. K.; Cheng, T. C.; DeFrank, J. J.; Worek, F. *Arch. Toxicol.* **2004**, *78* (6), 338.

(168) Ashani, Y.; Leader, H.; Rothschild, N.; Dosoretz, C. *Biochem. Pharmacol.* **1998**, *55* (2), 159.

(169) Kiderlen, D.; Eyer, P.; Worek, F. *Biochem. Pharmacol.* **2005**, *69* (12), 1853.

(170) Stenzel, J.; Worek, F.; Eyer, P. *Biochem. Pharmacol.* **2007**, *74* (9), 1390.

(171) Sharma, R.; Gupta, B.; Singh, N.; Acharya, J. R.; Musilek, K.; Kuca, K.; Ghosh, K. K. *Mini-Rev. Med. Chem.* **2015**, *15*, 58.

(172) Hobbiger, F.; Pitman, M.; Sadler, P. W. *Biochem. J.* **1960**, *75*, 363.

(173) Hoskovcová, M.; Halámek, E.; Kobliha, Z.; Tusarová, I. *Toxicol. Mech. Methods* **2010**, *20* (5), 223.

(174) Ohta, H.; Ohmori, T.; Suzuki, S.; Ikegaya, H.; Sakurada, K.; Takatori, T. *Pharm. Res.* **2006**, *23* (12), 2827.

(175) Musilek, K.; Kucera, J.; Jun, D.; Dohnal, V.; Opletalova, V.; Kuca, K. *Bioorganic Med. Chem.* **2008**, *16* (17), 8218.

(176) Bharate, S. B.; Guo, L.; Reeves, T. E.; Cerasoli, D. M.; Thompson, C. M. *Bioorganic Med. Chem. Lett.* **2009**, *19* (17), 5101.

(177) Acharya, J.; Rana, H.; Aditya Kapil, V.; Kaushik, M. P. *Med. Chem. Res.* **2013**, *22* (3), 1277.

(178) Chambers, J. E.; Chambers, H. W.; Meek, E. C.; Pringle, R. B. *Chem. Biol. Interact.* **2013**, *203* (1), 135.

(179) Ginsburg, S.; Wilson, I. B. *J. Am. Chem. Soc.* **1957**, *79* (1933), 481.

(180) Kuca, K.; Picha, J.; Cabal, J.; Liska, F. *J. Appl. Biomed.* **2004**, *2*, 51.

(181) Salvador, R. L.; Saucier, M.; Simon, D.; Goyer, R. *J. Med. Chem.* **1972**, *15* (6), 646.

(182) Bedford, C. D.; Harris, R. N.; Howd, R. a.; Miller, A.; Nolen, H. W.; Kenley, R. a. *J. Med. Chem.* **1984**, *27* (11), 1431.

(183) Goff, D. A.; Koolpe, G. A.; Kelson, A. B.; Vu, H. M.; Taylor, D. L.; Bedford, C. D.; Harris, R. N.; Mussalam, H. A.; Koplovitz, I. *J. Med. Chem.* **1991**, *34* (4), 1363.

(184) Koolpe, G. A.; Lovejoy, S. M.; Goff, D. A.; Lin, K. Y.; Leung, D. S.; Bedford, C. D.; Harris, R. N.; Musallam, H. A.; Koplovitz, I. *J. Med. Chem.* **1991**, *34* (4), 1368.

(185) Musilek, K.; Komloova, M.; Holas, O.; Horova, A.; Pohanka, M.; Gunn-Moore, F.; Dohnal, V.; Dolezal, M.; Kuca, K. *Bioorganic Med. Chem.* **2011**, *19* (2), 754.

(186) Musilek, K.; Holas, O.; Hambalek, J.; Kuca, K.; Jun, D.; Dohnal, V.; Dolezal, M. *Lett. Org. Chem.* **2006**, *3* (11), 831.

(187) Musilek, K.; Holas, O.; Kuca, K.; Jun, D.; Dohnal, V.; Dolezal, M. *Bioorg. Med. Chem. Lett.* **2006**, *16* (21),

5673.

(188) Chennamaneni, S. R.; Vobalaboina, V.; Garlapati, A. *Bioorg. Med. Chem. Lett.* **2005**, *15* (12), 3076.

(189) Rao Chennamaneni, S.; Vobalaboina, V.; Garlapati, A. *Bioorganic Med. Chem. Lett.* **2006**, *16* (8), 2134.

(190) Kassa, J.; Kuca, K.; Karasova, J.; Musilek, K. *Mini-Rev. Med. Chem.* **2008**, *8* (11), 1134.

(191) Cabal, J.; Kuca, K.; Kassa, J. *Basic Clin. Pharmacol. Toxicol.* **2004**, *95* (2), 81.

(192) Pang, Y.-P.; Kollmeyer, T. M.; Hong, F.; Lee, J.-C.; Hammond, P. I.; Haugabouk, S. P.; Brimijoin, S. *Chem. Biol.* **2003**, *10* (6), 491.

(193) Kuca, K.; Jun, D.; Kim, T.-H.; Cabal, J.; Jung, Y.-S. *Bull. Korean Chem. Soc.* **2006**, *27* (3), 395.

(194) Kuca, K.; Cabal, J.; Jung, Y. S.; Musilek, K.; Soukup, O.; Jun, D.; Pohanka, M.; Musilova, L.; Karasová, J.; Novotný, L.; Hrabinova, M. *Basic Clin. Pharmacol. Toxicol.* **2009**, *105* (3), 207.

(195) Worek, F.; Bierwisch, A.; Wille, T.; Koller, M.; Thiermann, H. *Toxicol. Lett.* **2012**, *212* (1), 29.

(196) Acharya, J.; Dubey, D. K.; Raza, S. K. *Toxicol. Vitr.* **2010**, *24* (6), 1797.

(197) Musilek, K.; Holas, O.; Kuca, K.; Jun, D.; Dohnal, V.; Dolezal, M. *J. Enzyme Inhib. Med. Chem.* **2007**, *22* (4), 425.

(198) Acharya, J.; Rana, H.; Kaushik, M. P. *Eur. J. Med. Chem.* **2011**, *46* (9), 3926.

(199) Karade, H. N.; Valiveti, A. K.; Acharya, J.; Kaushik, M. P. *Bioorg. Med. Chem.* **2014**, *22* (9), 2684.

(200) Musílek, K.; Kuča, K.; Jun, D.; Doležal, M. *J. Appl. Biomed.* **2007**, *5*, 25.

(201) Musilek, K.; Holas, O.; Kuca, K.; Jun, D.; Dohnal, V.; Opletalova, V.; Dolezal, M. *J. Enzyme Inhib. Med. Chem.* **2008**, *23* (1), 70.

(202) Musilek, K.; Holas, O.; Jun, D.; Dohnal, V.; Gunn-Moore, F.; Opletalova, V.; Dolezal, M.; Kuca, K. *Bioorganic Med. Chem.* **2007**, *15* (21), 6733.

(203) Musilek, K.; Holas, O.; Kuca, K.; Jun, D.; Dohnal, V.; Opletalova, V.; Dolezal, M. *Bioorganic Med. Chem. Lett.* **2007**, *17* (11), 3172.

(204) Kuca, K.; Cabal, J.; Musilek, K.; Jun, D.; Bajgar, J. *J. Appl. Toxicol.* **2005**, *25* (6), 491.

(205) Kassa, J.; Karasova, J. Z.; Pavlikova, R.; Musilek, K.; Kuca, K.; Bajgar, J.; Jung, Y.-S. *Toxicol. Mech. Methods* **2011**, *21* (3), 241.

(206) Kassa, J.; Žďárová Karasová, J.; Krejčiová, M. *J. Appl. Biomed.* **2012**, *11* (1), 7.

(207) Kassa, J.; Karasova, J. Z.; Sepsova, V.; Caisberger, F. *Basic Clin. Pharmacol. Toxicol.* **2011**, *109* (1), 30.

(208) Kassa, J.; Karasová, J. Ž.; Pavlíková, R.; Caisberger, F.; Bajgar, J. *Acta Medica Cordoba.* **2012**, *55* (1), 27.

(209) Chen, Y. *Neurotoxicology* **2012**, *33* (3), 391.

(210) Langer, K.; Anhorn, M. G.; Steinhauser, I.; Dreis, S.; Celebi, D.; Schrickel, N.; Faust, S.; Vogel, V. *Int. J. Pharm.* **2008**, *347* (1-2), 109.

(211) Wagner, S.; Kufleitner, J.; Zensi, A.; Dadparvar, M.; Wien, S.; Bungert, J.; Vogel, T.; Worek, F.; Kreuter, J.; von Briesen, H. *PLoS One* **2010**, *5* (12), e14213.

(212) Jeong, H. C.; Kang, N. S.; Park, N.-J.; Yum, E. K.; Jung, Y.-S. *Bioorg. Med. Chem. Lett.* **2009**, *19* (4), 1214.

(213) Jeong, H. C.; Park, N.-J.; Chae, C. H.; Musilek, K.; Kassa, J.; Kuca, K.; Jung, Y.-S. *Bioorg. Med. Chem.* **2009**, *17* (17), 6213.

(214) Timperley, C. M.; Banks, R. E.; Young, I. M.; Haszeldine, R. N. *J. Fluor. Chem.* **2011**, *132* (8), 541.

(215) Heldman, E.; Ashani, Y.; Raveh, L.; Rachaman, E. S. *Carbohydr. Res.* **1986**, *151*, 337.

(216) Garcia, G. E.; Campbell, A. J.; Olson, J.; Moorad-Doctor, D.; Morthole, V. I. *Chem. Biol. Interact.* **2010**, *187* (1-3), 199.

(217) Bhonsle, J. B.; Causey, R.; Oyler, B. L.; Bartolucci, C.; Lamba, D.; Pesaresi, A.; Bhamare, N. K.; Soojhawon, I.; Garcia, G. E. *Chem. Biol. Interact.* **2013**, *203* (1), 129.

(218) Odžak, R.; Čalić, M.; Hrenar, T.; Primožič, I.; Kovarik, Z. *Toxicology* **2007**, *233* (1-3 SPEC. ISS.), 85.

(219) Odžak, R.; Oršulić, M.; Tomić, S. *Toxicology* **2007**, *233* (1-3), 227.

(220) Bodor, N.; Shek, E.; Higuchi, T. *J. Med. Chem.* **1976**, *19* (1), 102.

(221) Prokai, L.; Prokai-Tatrai, K.; Bodor, N. *Med. Res. Rev.* **2000**, *20* (5), 367.

(222) Prokai-Tatrai, K.; Kim, H.-S.; Prokai, L. *Open Med. Chem. J.* **2008**, *2*, 97.

(223) DeMar, J. C.; Clarkson, E. D.; Ratcliffe, R. H.; Campbell, A. J.; Thangavelu, S. G.; Herdman, C. A.; Leader, H.; Schulz, S. M.; Marek, E.; Medynets, M. A.; Ku, T. C.; Evans, S. A.; Khan, F. A.; Owens, R. R.; Nambiar, M. P.; Gordon, R. K. *Chem. Biol. Interact.* **2010**, *187* (1-3), 191.

(224) Worek, F.; Thiermann, H. *Chem. Biol. Interact.* **2011**, *194* (2-3), 91.

(225) Shih, T.-M.; Skovira, J. W.; O'Donnell, J. C.; McDonough, J. H. *Toxicol. Mech. Methods* **2009**, *19* (6-7), 386.

(226) Shih, T.-M.; Skovira, J. W.; O'Donnell, J. C.; McDonough, J. H. *Adv. Stud. Biol.* **2009**, *1*, 155.

(227) Skovira, J. W.; O'Donnell, J. C.; Koplovitz, I.; Kan, R. K.; McDonough, J. H.; Shih, T.-M. *Chem. Biol. Interact.* **2010**, *187* (1-3), 318.

(228) Degorre, F.; Kiffer, D.; Terrier, F. *J. Med. Chem.* **1988**, *31* (4), 757.

(229) Sit, R. K.; Radić, Z.; Gerardi, V.; Zhang, L.; Garcia, E.; Katalinić, M.; Amitai, G.; Kovarik, Z.; Fokin, V. V; Sharpless, K. B.; Taylor, P. *J. Biol. Chem.* **2011**, *286* (22), 19422.

(230) Radić, Z.; Sit, R. K.; Kovarik, Z.; Berend, S.; Garcia, E.; Zhang, L.; Amitai, G.; Green, C.; Radić, B.; Fokin, V. V; Sharpless, K. B.; Taylor, P. *J. Biol. Chem.* **2012**, *287* (15), 11798.

(231) Radić, Z.; Sit, R. K.; Garcia, E.; Zhang, L.; Berend, S.; Kovarik, Z.; Amitai, G.; Fokin, V. V.; Barry Sharpless, K.; Taylor, P. *Chem. Biol. Interact.* **2013**, *203* (1), 67.

(232) Kalisiak, J.; Ralph, E. C.; Zhang, J.; Cashman, J. R. *J. Med. Chem.* **2011**, *54* (9), 3319.

(233) Jencks, W.; Carriuolo, J. *J. Am. Chem. Soc.* **1960**, *82* (55), 1778.

(234) Kalisiak, J.; Ralph, E. C.; Cashman, J. R. *J. Med. Chem.* **2012**, *55* (1), 465.

(235) Ribeiro, T. S.; Prates, A.; Alves, S. R.; Oliveira-Silva, J. J.; Riehl, C. A. S.; Figueroa-Villar, J. D. *J. Braz. Chem. Soc.* **2012**, *23* (7), 1216.

(236) Kovarik, Z.; MačEk, N.; Sit, R. K.; Radić, Z.; Fokin, V. V.; Barry Sharpless, K.; Taylor, P. *Chem. Biol. Interact.* **2013**, *203* (1), 77.

(237) de Koning, M. C.; van Grol, M.; Noort, D. *Toxicol. Lett.* **2011**, *206* (1), 54.

(238) Louise-Leriche, L.; Paunescu, E.; Saint-André, G.; Baati, R.; Romieu, A.; Wagner, A.; Renard, P.-Y. *Chem. Eur. J.* **2010**, *16* (11), 3510.

(239) Saint-André, G.; Kliachyna, M.; Kodepelly, S.; Louise-Leriche, L.; Gillon, E.; Renard, P.-Y.; Nachon, F.; Baati, R.; Wagner, A. *Tetrahedron* **2011**, *67* (34), 6352.

(240) Hayashi, I.; Ogihara, K.; Shimizu, K. *Bull. Chem. Soc. Jpn.* **1983**, *56* (8), 2432.

(241) Mercey, G.; Verdelet, T.; Saint-andré, G.; Gillon, E.; Wagner, A. *Chem. Commun.* **2011**, *47*, 5295.

(242) Mercey, G.; Renou, J.; Verdelet, T.; Kliachyna, M.; Baati, R.; Gillon, E.; Arboléas, M.; Loiodice, M.; Nachon, F.; Jean, L.; Renard, P.-Y. *J. Med. Chem.* **2012**, *55* (23), 10791.

(243) Renou, J.; Mercey, G.; Verdelet, T.; Paunescu, E.; Gillon, E.; Arboléas, M.; Loiodice, M.; Kliachyna, M.; Baati, R.; Nachon, F.; Jean, L.; Renard, P.-Y. *Chem. Biol. Interact.* **2013**, *203*, 81.

(244) Renou, J.; Loiodice, M.; Arboléas, M.; Baati, R.; Jean, L.; Nachon, F.; Renard, P.-Y. *Chem. Commun.* **2014**, *50* (30), 3947.

(245) Kliachyna, M.; Santoni, G.; Nussbaum, V.; Renou, J.; Sanson, B.; Colletier, J.-P.; Arboléas, M.; Loiodice, M.; Weik, M.; Jean, L.; Renard, P.-Y.; Nachon, F.; Baati, R. *Eur. J. Med. Chem.* **2014**, *78*, 455.

(246) Gregor, V. E.; Emmerling, M. R.; Lee, C.; Moore, C. J. *Bioorg. Med. Chem. Lett.* **1992**, *2* (8), 861.

(247) Summers, W. K.; Majovski, L. V.; Marsh, G. M.; Tachiki, K.; Kling, A. *N. Engl. J. Med.* **1986**, *315* (20), 1241.

(248) Giacobini, E. In *Cognitive Enhancing Drugs*; Buccafusco, J., Ed.; Milestones in Drug Therapy MDT; Birkhäuser Basel, 2004; pp 11–36.

(249) Shaw, F.; Bentley, G. *Aust. J. Exp. Biol. Med. Sci.* **1953**, *31* (6), 573.

(250) Patocka, J.; Jun, D.; Kuca, K. *Curr. Drug Metab.* **2008**, *9* (4), 332.

(251) Recanatini, M.; Cavalli, A.; Belluti, F.; Piazzi, L.; Rampa, A.; Bisi, A.; Gobbi, S.; Valenti, P.; Andrisano, V.; Bartolini, M.; Cavrini, V. *J. Med. Chem.* **2000**, *43*, 2007.

(252) Giudice, M. Del; Borioni, A.; Mustazza, C.; Gatta, F.; Meneguz, A.; Volpe, M. *Farmaco* **1996**, *51* (11), 693.

(253) Wlodeck, S. T.; Antosiewicz, J.; Mccammon, J. A.; Strratsma, T. P.; Gilson, M. K.; Briggs, J. M.; Humblet, C.; Sussman, J. L. *Biopolymers* **1996**, *38*, 109.

(254) Pohanka, M.; Kuca, K.; Kassa, J. *Neuro Endocrinol. Lett.* **2008**, *29* (5), 755.

(255) Korabecny, J.; Musilek, K.; Holas, O.; Binder, J.; Zemek, F.; Marek, J.; Pohanka, M.; Opletalova, V.; Dohnal, V.; Kuca, K. *Bioorg. Med. Chem. Lett.* **2010**, *20*, 6093.

(256) Korabecny, J.; Musilek, K.; Holas, O.; Nepovimova, E.; Jun, D.; Zemek, F.; Opletalova, V.; Patocka, J.; Dohnal, V.; Nachon, F.; Hroudova, J.; Fisar, Z.; Kuca, K. *Molecules* **2010**, *15* (12), 8804.

(257) Korabecny, J.; Musilek, K.; Zemek, F.; Horova, A.; Holas, O.; Nepovimova, E.; Opletalova, V.; Hroudova, J.; Fisar, Z.; Jung, Y.-S.; Kuca, K. *Bioorg. Med. Chem. Lett.* **2011**, *21* (21), 6563.

(258) Shutske, G.; Pierrat, F.; Kapples, K.; Cornfeldt, M.; Szewczak, M.; Huger, F.; Bores, G.; Haroutunian, V.; Davis, K. L. *J. Med. Chem.* **1989**, *32*, 1805.

(259) Kuca, K.; Jun, D.; Musilek, K. *Mini-Rev. Med. Chem.* **2006**, *6* (3), 269.

(260) Korabecny, J.; Holas, O.; Musilek, K.; Pohanka, M.; Opletalova, V.; Dohnal, V.; Kuca, K. *Lett. Org. Chem.* **2010**, *7*, 327.

(261) Colletier, J. P.; Sanson, B.; Nachon, F.; Gabellieri, E.; Fattorusso, C.; Campiani, G.; Weik, M. *J. Am. Chem. Soc.* **2006**, *128* (14), 4526.

(262) Mercey, G.; Verdelet, T.; Saint-André, G.; Gillon, E.; Wagner, A.; Baati, R.; Jean, L.; Nachon, F.; Renard, P.-Y. *Chem. Commun.* **2011**, *47* (18), 5295.

(263) Xiong, X.-D.; Chen, W.-X.; Kuang, Y.-Y.; Chen, F.-E. *Org. Prep. Proced. Int.* **2009**, *41* (5), 423.

(264) Li, D.; Shi, F.; Guo, S.; Deng, Y. *Tetrahedron Lett.* **2005**, *46* (4), 671.

(265) Liu, X.-Y.; Che, C.-M. *Angew. Chemie Int. Ed.* **2008**, *47* (20), 3805.

(266) Ge, Y.-S.; Tai, S.-X.; Xu, Z.-Q.; Lai, L.; Tian, F.-F.; Li, D.-W.; Jiang, F.-L.; Liu, Y.; Gao, Z.-N. *Langmuir* **2012**, *28* (14), 5913.

(267) Gaspar, B.; Carreira, E. M. *Angew. Chemie Int. Ed.* **2008**, *47* (31), 5758.

(268) Abdel-Magid, A. F.; Carson, K. G.; Harris, B. D.; Maryanoff, C. A.; Shah, R. D. *J. Org. Chem.* **1996**, *61* (11), 3849.

(269) Cheval, N. P.; Dikova, A.; Blanc, A.; Weibel, J.-M.; Pale, P. *Chem. Eur. J.* **2013**, *19* (27), 8765.

(270) Smith, W. B.; Ho, O. C. *J. Org. Chem.* **1990**, *55* (8), 2543.

(271) Spivey, A. C.; Shukla, L.; Hayler, J. F. *Org. Lett.* **2007**, *9* (5), 891.

(272) Chen, J.; Kampf, J. W.; McNeil, A. J. *Langmuir* **2010**, *26* (16), 13076.

(273) Manetsch, R.; Krasiński, A.; Radić, Z.; Raushel, J.; Taylor, P.; Sharpless, K. B.; Kolb, H. C. *J. Am. Chem. Soc.* **2004**, *126* (40), 12809.

(274) Muci, A.; Buchwald, S. *Cross-Coupling React.* **2002**, *219* (topics in current chemistry), 131.

(275) Hartwig, J. F. *Nature* **2008**, *455* (7211), 314.

(276) Huang, X.; Anderson, K. W.; Zim, D.; Jiang, L.; Klapars, A.; Buchwald, S. L. *J. Am. Chem. Soc.* **2003**, *125* (22), 6653.

(277) Shen, Q.; Shekhar, S.; Stambuli, J. P.; Hartwig, J. F. *Angew. Chemie - Int. Ed.* **2005**, *44* (9), 1371.

(278) Butini, S.; Campiani, G.; Borriello, M.; Gemma, S.; Panico, A.; Persico, M.; Catalanotti, B.; Ros, S.; Brindisi, M.; Agnusdei, M.; Fiorini, I.; Nacci, V.; Novellino, E.; Belinskaya, T.; Saxena, A.; Fattorusso, C. *J. Med. Chem.* **2008**, *51* (11), 3154.

(279) Ma, M.; Mehta, J.; Williams, L. D.; Carlier, P. R. *Tetrahedron Lett.* **2011**, *52* (8), 916.

(280) Ronco, C.; Jean, L.; Outaabout, H.; Renard, P.-Y. *Eur. J. Org. Chem.* **2011**, *2011* (2), 302.

(281) Fors, B. P.; Watson, D. A.; Biscoe, M. R.; Buchwald, S. L. *J. Am. Chem. Soc.* **2008**, *130* (41), 13552.

(282) Kochi, A.; Eckroat, T. J.; Green, K. D.; Mayhoub, A. S.; Lim, M. H.; Garneau-Tsodikova, S. *Chem. Sci.* **2013**, *4* (11), 4137.

(283) Romero, A.; Cacabelos, R.; Oset-Gasque, M. J.; Samadi, A.; Marco-Contelles, J. *Bioorg. Med. Chem. Lett.* **2013**, *23* (7), 1916.

(284) Chao, X.; He, X.; Yang, Y.; Zhou, X.; Jin, M.; Liu, S.; Cheng, Z.; Liu, P.; Wang, Y.; Yu, J.; Tan, Y.; Huang, Y.; Qin, J.; Rapposelli, S.; Pi, R. *Bioorg. Med. Chem. Lett.* **2012**, *22* (20), 6498.

(285) Fernández-Bachiller, M. I.; Pérez, C.; González-Muñoz, G. C.; Conde, S.; López, M. G.; Villarroya, M.; García, A. G.; Rodríguez-Franco, M. I. *J. Med. Chem.* **2010**, *53* (13), 4927.

(286) Wang, Y.; Wang, F.; Yu, J.-P.; Jiang, F.-C.; Guan, X.-L.; Wang, C.-M.; Li, L.; Cao, H.; Li, M.-X.; Chen, J.-G. *Bioorg. Med. Chem.* **2012**, *20* (21), 6513.

(287) Hopkins, A. L. *Nat. Chem. Biol.* **2008**, *4* (11), 682.

(288) Cavalli, A.; Bolognesi, M. L.; Minarini, A.; Rosini, M.; Tumiatti, V.; Recanatini, M.; Melchiorre, C. *J. Med. Chem.* **2008**, *51* (3), 347.

(289) Zalesskiy, S. S.; Ananikov, V. P. *Organometallics* **2012**, *31* (6), 2302.

(290) Wolfe, J. P.; Wagaw, S.; Buchwald, S. L. *J. Am. Chem. Soc.* **1996**, *118* (30), 7215.

(291) Driver, M. S.; Hartwig, J. F. *J. Am. Chem. Soc.* **1996**, *118* (30), 7217.

(292) Poondra, R. R.; Turner, N. J. *Org. Lett.* **2005**, *7* (5), 863.

(293) Tundel, R. E.; Anderson, K. W.; Buchwald, S. L. *J. Org. Chem.* **2006**, *71*, 430.

(294) Wang, Y.; Chen, C.; Zhang, S.; Lou, Z.; Su, X.; Wen, L.; Li, M. *Org. Lett.* **2013**, *15* (18), 4794.

(295) Elangovan, A.; Wang, Y.-H.; Ho, T.-I. *Org. Lett.* **2003**, *5* (11), 1841.

(296) Rommel, M.; Ernst, A.; Koert, U. *Eur. J. Org. Chem.* **2007**, *2007* (26), 4408.

(297) Brown, L. J.; Spurr, I. B.; Kemp, S. C.; Camp, N. P.; Gibson, K. R.; Brown, R. C. D. *Org. Lett.* **2008**, *10* (12), 2489.

(298) Da Silva, G. *Environ. Sci. Technol.* **2013**, *47* (14), 7766.

(299) Cross, R. M.; Maignan, J. R.; Mutka, T. S.; Luong, L.; Sargent, J.; Kyle, D. E.; Manetsch, R. *J. Med. Chem.* **2011**, *9*, 4399.

(300) de Sousa, J.; Brown, R. C. D.; Baati, R. *Eur. J. Org. Chem.* **2014**, *2014* (16), 3468.

(301) Meerow, A.; Snijman, D. Springer-Verlag: Berlin, 1998; pp 83–110.

(302) Bastida, J.; Lavila, R.; Viladomat, F. *The alkaloids, chemistry and biology*; Elsevier: Amsterdam, 2006; Vol. 63.

(303) Sweeney, J. E.; Puttfarcken, P. A.; Coyle, J. T. *Pharmacol. Biochem. Behav.* **1989**, *34* (1), 129.

(304) Thomsen, T.; Kewitz, H. *Life Sci.* **1990**, *46* (21), 1553.

(305) Thomsen, T.; Zendeh, B.; Fischer, J. P.; Kewitz, H. *Biochem. Pharmacol.* **1991**, *41* (1), 139.

(306) López, S.; Bastida, J.; Viladomat, F.; Codina, C. *Life Sci.* **2002**, *71* (21), 2521.

(307) Isoni, V. Asymmetric synthesis of bioactive alkaloids from Amaryllidaceae, University of Southampton, 2013.

(308) Wang, X.; Leow, D.; Yu, J.-Q. *J. Am. Chem. Soc.* **2011**, *133* (35), 13864.

(309) Karthikeyan, J.; Cheng, C. H. *Angew. Chemie - Int. Ed.* **2011**, *50* (42), 9880.

(310) Yeung, C. S.; Zhao, X.; Borduas, N.; Dong, V. M. *Chem. Sci.* **2010**, *1* (3), 331.

(311) Ridley, C. P.; Reddy, M. V. R.; Rocha, G.; Bushman, F. D.; Faulkner, D. J. *Bioorg. Med. Chem.* **2002**, *10* (10), 3285.

(312) Raach, A.; Reiser, O. *J. Prakt. Chemie* **2000**, *342* (6), 605.

(313) Dalcanale, E.; Montanari, F. *J. Org. Chem.* **1986**, *51* (4), 567.

(314) Harayama, T.; Shibaike, K. *Heterocycles* **1998**, *49* (1), 191.

(315) Harayama, T.; Sato, T.; Hori, A.; Abe, H.; Takeuchi, Y. *Heterocycles* **2005**, *66* (1), 527.

(316) Amatore, C.; Jutand, A. *Acc. Chem. Res.* **2000**, *33* (5), 314.

(317) Amatore, C.; Bensalem, S.; Ghalem, S.; Jutand, A. *J. Organomet. Chem.* **2004**, *689* (24 SPEC. ISS.), 4642.

(318) Banwell, M. G.; Flynn, B. L.; Stewart, S. G. *J. Org. Chem.* **1998**, *63* (24), 9139.

(319) Bryant, H. U.; Cullinan, G. J.; Dodge, J. A. Benzothiophene compounds, compositions and methods. US005981570A, 1999.

(320) Ellman, G. L. *Arch. Biochem. Biophys.* **1959**, *82* (1), 70.

(321) Ellman, G. L.; Courtney, K. D.; Andres, V.; Featherstone, R. M. *Biochem. Pharmacol.* **1961**, *7* (2), 88.

(322) Carlier, P. R.; Chow, E. S.; Han, Y.; Liu, J.; El Yazal, J.; Pang, Y. P. *J. Med. Chem.* **1999**, *42* (20), 4225.

(323) Silman, I.; Sussman, J. L. *Curr. Opin. Pharmacol.* **2005**, *5*, 293.

(324) Lindsay, C. D.; Green, C.; Bird, M.; Jones, J. T. A.; Riches, J. R.; Mckee, K. K.; Sandford, M. S.; Wakefield, D. A.; Timperley, C. M. *R. Soc. Open Sci.* **2015**, *2*, 1.

(325) Armarego, W. L. F.; Chai, C. L. L. *Purification of Laboratory Chemicals*; Elsevier, 2003.

(326) Battenberg, O. A.; Nodwell, M. B.; Sieber, S. A. *J. Org. Chem.* **2011**, *76* (15), 6075.

(327) Cross, R. M.; Maignan, J. R.; Mutka, T. S.; Luong, L.; Sargent, J.; Kyle, D. E.; Manetsch, R. *J. Med. Chem.* **2011**, *9*, 4399.

(328) Molander, G. A.; Cadoret, F. *Tetrahedron Lett.* **2011**, *52* (17), 2199.

(329) Beugelmans, R.; Roussi, G.; González Zamora, E.; Carbonnelle, A.-C. *Tetrahedron* **1999**, *55* (16), 5089.

(330) Hess, B.; Kutzner, C.; van der Spoel, D.; Lindhal, E. *J. Med. Theory Comput.* **2008**, *4*, 435.

(331) Hornak, V.; Abel, R.; Okur, A.; Strockbine, B.; Roitberg, A.; Simmerling, C. *Proteins* **2006**, *65* (3), 712.

(332) Wang, J.; Wolf, R. M.; Caldwell, J. W.; Kollman, P. A.; Case, D. A. *J. Comput. Chem.* **2004**, *25* (9), 1157.

(333) Berendsen, H. J. C.; Postma, J. P. M.; van Gunsteren, W. F.; DiNola, A.; Haak, J. R. *J. Chem. Phys.* **1984**, *81* (8), 3684.

(334) Hess, B.; Bekker, H.; Berendsen, H. J. C.; Fraaije, J. G. E. M. *J. Comput. Chem.* **1997**, *18* (12), 1463.

(335) Carletti, E.; Li, H.; Li, B.; Ekström, F.; Nicolet, Y.; Loiodice, M.; Gillon, E.; Froment, M. T.; Lockridge, O.; Schopfer, L. M.; Masson, P.; Nachon, F. *J. Am. Chem. Soc.* **2008**, *130* (47), 16011.

(336) Adams, P. D.; Afonine, P. V; Bunkóczi, G.; Chen, V. B.; Davis, I. W.; Echols, N.; Headd, J. J.; Hung, L.-W.; Kapral, G. J.; Grosse-Kunstleve, R. W.; McCoy, A. J.; Moriarty, N. W.; Oeffner, R.; Read, R. J.; Richardson, D. C.; Richardson, J. S.; Terwilliger, T. C.; Zwart, P. H. *Acta Crystallogr. D. Biol. Crystallogr.* **2010**, *66*, 213.

Julien Alain Albino de Sousa

DESIGN, SYNTHESIS AND BIOLOGICAL EVALUATION OF NOVEL UNCHARGED BIFUNCTIONAL HYBRID REACTIVATORS FOR ORGANOPHOSPHORUS NERVE AGENT-INHIBITED HUMAN ACETYLCHOLINESTERASE

ABSTRACT

Remediation of both acute and chronic intoxications by organophosphorus nerve agents, both chemical warfare agents and pesticides, continues to be a challenge of paramount importance. These manmade poisons act as covalent and irreversible inhibitors of acetylcholinesterase, a key enzyme mostly located in the nervous system, through phosphylation of its active site. The phosphylated active site residues do not undergo spontaneous hydrolysis. However, hydrolysis can be achieved through the use of strong nucleophiles (also called acetylcholinesterase reactivators) able to enter the buried active site of the protein. Our research is based on the rational design of hybrid structures containing two key elements: a neutral reactivator to restore the enzyme activity, and a peripheral site ligand giving selectivity by targeted binding to a site at the entrance of the enzyme active site gorge. A library of novel reactivators based on acridine, quinoline and original oxoassoanine analogues was synthesised, evaluated and is herein described. Delightfully, most of these hybrids proved to be equally or more potent than the drugs currently in use. Outstandingly, we have discovered the first broad-spectrum reactivator that outperformed all known reactivators (standard and lead compounds) for both chemical warfare agent and pesticide intoxications.

Key words: reactivators, acetylcholinesterase, hybrids, oximes, organophosphorus nerve agents.

RESUME

Ce projet à caractère dual civil et militaire vise à développer de nouvelles contre-mesures médicales d'urgences hautement efficaces en cas d'intoxications accidentelles ou volontaires aux organophosphorés toxiques (gaz de combat et pesticides). Ces poisons agissent comme des inhibiteurs irréversibles de l'acétylcholinestérase, enzyme clé principalement localisé dans notre système nerveux, par phosphorylation du site actif enzymatique. Cependant, l'hydrolyse de ce site actif phosphorylé peut avoir lieu par le biais d'un nucléophile puissant capable de pénétrer jusqu'au site actif de la protéine. Notre recherche réside sur l'élaboration de molécules hybrides possédant deux systèmes clés : une partie réactivatrice neutre capable de restaurer l'activité enzymatique et un ligand du site périphérique capable de vectoriser la structure hybride à l'entrée du site actif. Une librairie de nouveaux hybrides bifonctionnels a ainsi été synthétisée, évaluée et décrite dans ces travaux de thèse. L'ensemble de ces hybrides démontre une activité égale ou supérieure à celle des réactivateurs de référence. Nous avons même découvert le premier hybride universel surpassant l'activité de réactivation des antidotes actuellement commercialisés pour des intoxications aux gaz de combat et aux pesticides.

Mots-clés : réactivateurs, acétylcholinestérase, hybrides, oximes, neurotoxiques organophosphorés.